KU Leuven

Biomedical Sciences Group

Faculty of Pharmaceutical Sciences

Department of Pharmaceutical and Pharmacological Sciences

Laboratory for Pharmaceutical Analysis

COMBINING ADVANCED LC-MS TECHNIQUES AND *IN VIVO* MODELS FOR THE HOLISTIC ASSESSMENT OF THE ELECTROCHEMICAL DEGRADATION OF EMERGING MICROPOLLUTANTS

Rafael TEIXEIRA DOS REIS

Jury:

Promoter:	Prof. Deirdre Cabooter
Co-promoter:	Prof. Peter de Witte
Chair:	Prof. Ann Van Schepdael
Jury members:	Prof. Raf Dewil
	Prof. Peter Verwilst
	Prof. Frederic Lynen
	Prof. François Lestremau

Dissertation presented in partial fulfilment of the requirements for the degree of Doctor in Pharmaceutical Sciences

July 2024

Acknowledgements

As I near the finish line of this PhD journey, it's time to express my gratitude to those who have supported me along the way.

First, I would like to express my thanks to my promoter Prof. Deirdre Cabooter for giving me the opportunity to embark on my doctoral studies in the Pharmaceutical Analysis lab. Thank you for your supervision, constant availability and guidance in scientific research. I am also grateful to my co-promoter Prof. Peter de Witte for all the help during the preparation of my scientific articles and for the relevant scientific discussions. I want to thank Prof. Ann Van Schepdael for your help concerning the PhD-related matters and for being the chair of the jury.

I extend my appreciations to the jury members, Prof. Raf Dewil, Prof. Peter Verwilst, Prof. Frederic Lynen and Prof. François Lestremau, for being part of my thesis Examining Committee. Thank you for reading my PhD thesis and for all your suggestions to improve the manuscript.

This PhD project was part of the InnovEOX consortium, comprising 15 PhD candidates funded by the Marie Skłodowska-Curie Actions. I am grateful to everyone involved in the consortium for the collaborative work, training opportunities, scientific discussions, and enjoyable moments we shared. I hope our paths will cross again in the future.

This PhD research was primarily conducted at the lab for Pharmaceutical Analysis, where I had the pleasure of meeting many people throughout my time there. I want to thank everyone who contributed to creating a pleasant working environment. Special thanks to Soraya and Marie for the research collaboration and tireless efforts in instrument troubleshooting. I am also deeply grateful to Kris for his calm composure, assistance in troubleshooting, and endless patience in unclogging the numerous viper tips blocked in the valves. I also want to thank the Biomedical Discovery Lab for the guidance in handling *in vivo* embryos.

My research journey included research secondments at the University of Patras (Greece) and at Watchfrog in Paris.

Acknowledgements

I would like to thank Patras team for their warm welcome and for providing me with a better insight into the electrochemical/engineering work, as well as Greek culture, food and landscape. Ευχαριστώ πολύ!

Je tiens à exprimer ma plus profonde gratitude à la l'équipe Watchfrog, dont le soutien et la collaboration ont été essentiels sur la partie toxicologie de cette thèse. Travailler avec des embryons dans un cadre à la fois avancé et éthique a été une expérience enrichissante. Je remercie particulièrement David et Andrew pour leurs précieux conseils et leur aide tout au long de ce projet.

Gostaria de expressar a minha profunda gratidão a todos aqueles que, de alguma forma ou de outra, contribuíram para a realização desta tese.

Aos meus amigos, por me proporcionarem momentos de descontração, diversão e alegria, essenciais para manter o equilíbrio e serenidade durante todo este processo.

Aos meus irmãos, pelo apoio incondicional que sempre demonstraram, mesmo à distância.

À minha família, por todo o carinho e apoio que me motivaram a seguir em frente.

A mi novia, por su amor, cariño, apoyo incondicional y su paciencia durante el período más difícil de mi tesis. ¡Muchas gracias por todo!

Finalmente, dedico esta tese aos meus pais, por todos os seus esforços e sacrifícios ao longo de todos estes anos, sem os quais esta aventura não seria possível.

To everyone who crossed my path during this journey and contributed to this work in any way:

Thank you very much / Merci beaucoup / Heel erg bedankt / Muito obrigado!

"All truths are easy to understand once they are discovered;
the point is to discover them."
Galileo Galilei

Research Summary

Since the Industrial Revolution, water has served as a critical indicator of human activity and its environmental impact. As industrial activities intensified, urbanization followed, leading to an increase in domestic sewage and runoff from urban areas. The advent of new chemicals designed to improve the quality of life, began appearing in water bodies, often in trace amounts but with potentially significant effects on both human health and the environment. These contaminants are known as emerging micropollutants (EMs), whose behavior and fate are currently unknown. Water treatment is a primary strategy for removing EMs from water and it is expected to become even more critical in addressing the increasing water scarcity caused by climate change and the need for water reuse. Most of these compounds are persistent organic pollutants, resistant to conventional treatments, necessitating advanced remediation technologies for their removal.

Electrochemical advanced oxidation processes (eAOPs) rely on the *in situ* production of highly reactive hydroxyl radicals (•OH), which non-selectively react with most organics, enabling the degradation of a wide range of recalcitrant compounds. However, these processes typically do not completely mineralize organic compounds, leading to the formation of numerous transformation products (TPs). While the removal of organic micropollutants during water treatment receives considerable attention, the formation of TPs is often overlooked when evaluating treatment efficiency. Nevertheless, there is a growing concern that some of the generated TPs may be as toxic or even more toxic than the parent compounds. Therefore, a comprehensive chemical and biological characterization of these TPs is necessary before implementing eAOPs in real-life applications. This PhD project focused on the extensive study of TPs resulting from the electrochemical degradation of EMs, using advanced and reliable chemical and biological tools.

The non-selective nature of radical species generates a vast array of TPs with a wide range of polarities. Consequently, powerful analytical techniques are necessary to separate and analyze the constituents of degraded samples. A detailed comparison was made between an in-house developed two-dimensional liquid chromatography (2D-LC) setup and a commercially available 2D-LC instrument. This comparison considered experimental differences as well as general factors such as cost, flexibility, and ease of operation. Different strategies to address mobile phase incompatibility between highly orthogonal separation mechanisms were also evaluated. This detailed comparison provided analysts with insights into the capacities and performance of available setups, considering the specific needs of their samples, their experience and skills, and the budget for instrumentation.

To assess the efficiency and safety of eAOPs, two environmentally relevant endocrine disrupting chemicals (EDCs) were selected as study models: 17α-ethinylestradiol (EE2) and diclofenac (DCF). EE2, a synthetic steroidal estrogen, and DCF, a non-steroidal anti-inflammatory drug (NSAID), have been included in the first Watch List of the Water Framework Directive (WFD, EU Directive 2000/60/EC, EU Implementing Decision 2015/495).

The efficiency of the electrochemical degradation of EE2 was evaluated by comparing the analytically determined EE2 concentration, through a validated UHPLC-QTOF-MS method, with the hormonal equivalent, measured by a reliable transgenic medaka strain. A high correlation was observed between the degradation kinetics of EE2 and the reduction in sample estrogenicity. However, the detection of estrogenic activity in the final degraded samples suggested that estrogenicity was not completely eradicated, even though EE2 was no longer detectable by analytical methods.

For the first time, it was revealed that DCF has thyroid-disrupting properties in amphibians. As the electrochemical degradation of DCF was carried out, the DCF degradation kinetics and the toxicity evolution were not correlated. An observed increase in toxicity indicated potential risks associated with the incomplete removal of EMs by eAOPs due to the production of TPs possessing a higher toxicity than the original compound. More importantly, the first-time discovery of toxic TPs with a different mode of action than the parent compound highlighted the potential of eAOPs to extensively degrade pollutants and introduce new toxic moieties in the molecular structure of the resulting TPs, which poses a significant environmental risk.

The primary conclusion of this PhD thesis is that the radical transformation of organic pollutants by eAOPs can generate TPs with unpredictable chemical and biological characteristics, potentially posing risks to non-target organisms. This emphasizes the need for comprehensive and reliable chemical and biological tools to assess the efficiency and safety of these innovative remediation technologies. Future studies on new remediation technologies should use a multidisciplinary approach to ensure that the advantages of advanced oxidative treatments in degrading pollutants do not outweigh the unintended and potentially harmful consequences for the environment and public health.

Samenvatting

De Industriële Revolutie markeerde een belangrijk keerpunt in menselijke activiteit en milieueffecten, waarbij water een cruciale indicator werd van deze veranderingen. Industriële activiteiten en verstedelijking hebben geleid tot een toename van huishoudelijk afvalwater en stedelijke afvoer, wat een verscheidenheid aan verontreinigende stoffen in water heeft geïntroduceerd. Onder deze stoffen bevinden zich opkomende micropolluenten (OMP's), waaronder nieuwe chemicaliën die zijn ontworpen om de levenskwaliteit te verbeteren, maar in lage concentraties in water voorkomen en mogelijk zowel de menselijke gezondheid als het milieu beïnvloeden. Waterzuivering is essentieel om deze verontreinigende stoffen te verwijderen, vooral nu watertekorten en de noodzaak om water te hergebruiken dringender zijn door de klimaatverandering. Veel van deze verbindingen zijn persistente organische stoffen die bestand zijn tegen conventionele behandelingen, waardoor geavanceerde technologieën nodig zijn voor hun effectieve verwijdering.

Dergelijke geavanceerde technologieën zijn elektrochemische geavanceerde oxidatie-processen (eAOP's), die *in situ* zeer reactieve hydroxylradicalen (•OH) genereren. Deze radicalen reageren niet-selectief met een breed scala aan organische verbindingen en vergemakkelijken hun afbraak. eAOP's mineraliseren organische verbindingen echter vaak onvolledig, wat leidt tot de vorming van talrijke transformatieproducten (TP's). De vorming van deze TP's, waarvan sommige net zo toxisch of zelfs toxischer kunnen zijn dan de oorspronkelijke verbindingen, is een toenemend probleem. Daarom is een uitgebreide chemische en biologische karakterisering van TP's noodzakelijk voordat eAOP's op grote schaal kunnen worden geïmplementeerd.

Dit doctoraatsonderzoek richtte zich op de uitgebreide studie van TP's die ontstaan bij de elektrochemische afbraak van EM's, met behulp van geavanceerde en betrouwbare chemische en biologische hulpmiddelen. Gezien de niet-selectieve aard van radicalen, wordt een groot aantal TP's met verschillende polariteiten gegenereerd, waardoor krachtige analytische technieken nodig zijn voor hun scheiding en analyse. Een gedetailleerde vergelijking werd gemaakt tussen een in-huis ontwikkelde tweedimensionale vloeistof-chromatografie (2D-LC) opstelling en een commercieel beschikbaar 2D-LC instrument. Deze vergelijking hield rekening met experimentele verschillen, kosten, flexibiliteit en gebruiks-gemak, en verschaft analisten inzicht in de mogelijkheden en prestaties van beschikbare opstellingen op basis van hun specifieke behoefte, ervaring en budget.

Om de efficiëntie en veiligheid van eAOP's te evalueren, werden twee relevante hormoon-ontregelende chemicaliën (EDC's) geselecteerd als studiemodel: 17α-ethinylestradiol (EE2)

en diclofenac (DCF). EE2, een synthetisch steroïdaal oestrogeen, en DCF, een niet-steroïdale ontstekingsremmer (NSAID), staan op de eerste Watch List van de Kaderrichtlijn Water (WFD, EU Richtlijn 2000/60/EC, EU Uitvoeringsbesluit 2015/495).

De efficiëntie van de elektrochemische afbraak van EE2 werd beoordeeld door de analytisch bepaalde EE2-concentratie, bepaald met een gevalideerde UHPLC-QTOF-MS methode, te vergelijken met het hormonale equivalent, gemeten met een betrouwbare transgene medaka-stam. Er werd een hoge correlatie gevonden tussen de afbraakkinetiek van EE2 en de vermindering in oestrogeniteit van het staal. De detectie van oestrogene activiteit in de uiteindelijk afgebroken stalen toonde echter dat de oestrogeniteit niet volledig werd geëlimineerd, ook al was EE2 niet langer detecteerbaar door analytische methoden.

Voor het eerst werd aangetoond dat DCF schildklier ontregelende eigenschappen heeft bij amfibieën. Tijdens de elektrochemische afbraak van DCF waren de afbraakkinetiek en de evolutie van de toxiciteit niet gecorreleerd, met een waargenomen toename in toxiciteit die mogelijke risico's suggereert gepaard aan de onvolledige verwijdering van EM's door eAOP's. Deze toename in toxiciteit was te wijten aan de productie van TP's met een hogere toxiciteit dan DCF, en sommige TP's vertoonden andere werkingsmechanismen dan de oorspronkelijke verbinding, wat aanzienlijke milieurisico's met zich meebrengt.

De belangrijkste conclusie van dit doctoraat is dat de radicale transformatie van organische verontreinigende stoffen door eAOP's, TP's kan genereren met onvoorspelbare chemische en biologische kenmerken, wat mogelijk risico's oplevert voor het milieu. Dit benadrukt de noodzaak aan uitgebreide en betrouwbare chemische en biologische hulpmiddelen om de efficiëntie en veiligheid van deze innovatieve technologieën te beoordelen. Toekomstige studies naar nieuwe verwijderingstechnologieën zullen een multidisciplinaire benadering moeten hanteren om ervoor te zorgen dat de voordelen van geavanceerde oxidatieve behandelingen bij het afbreken van verontreinigende stoffen niet worden overschaduwd door onbedoelde en mogelijk schadelijke gevolgen voor het milieu en de volksgezondheid.

Table of Contents

Acknowledgements i

Research Summary iii

Samenvatting v

List of Abbreviations ix

List of Symbols xiv

CHAPTER 1

General Introduction 1

1.1. Emerging micropollutants 3

1.1.1. Source, transportation & fate of emerging micropollutants 4

1.1.2. Regulations 5

1.1.3. Remediation technologies 6

1.2. Transformation products 10

1.2.1. Ecotoxicological concerns 10

1.2.2. Identification and prioritization of transformation products 11

1.3. Environmental risk assessment 13

1.3.1. Ecotoxicological assessment 14

1.3.2. Methodologies for ecotoxicological testing 15

1.3.3. Chemical assessment 21

CHAPTER 2

Research Objectives 37

CHAPTER 3

Detailed comparison of in-house developed and commercially available heart-cutting and selective comprehensive two-dimensional liquid chromatography systems 43

3.1. Introduction 45
3.2. Materials & methods.....49
3.3. Results & discussion 55
3.4. Conclusion 70

CHAPTER 4

Electrochemical degradation of 17α-ethinylestradiol: Transformation products, degradation pathways and *in vivo* assessment of estrogenic activity.....73

4.1. Introduction 75
4.2. Materials & methods.....78
4.3. Results & discussion 82
4.4. Conclusions.....110

CHAPTER 5

Electrochemical degradation of diclofenac generates unexpected thyroidogenic transformation products: Implications for environmental risk assessment.....113

5.1. Introduction 115
5.2. Materials & Methods.....118
5.3. Results & Discussion.....124
5.4. Conclusions.....152

CHAPTER 6

General Discussion & Perspectives.....155

Supporting Information.....173

References.....199

List of Abbreviations

^{1}D	First dimension
1D-LC	One-dimensional liquid chromatography
^{2}D	Second dimension
2D-LC	Two-dimensional liquid chromatography
3Rs	Replacement, reduction, refinement
ACN	Acetonitrile
ADME	Absorption, distribution, metabolism, excretion
AF	Ammonium formate
AO	Anodic oxidation
AOP	Advanced oxidation process
APCI	Atmospheric pressure chemical ionization
API	Atmospheric pressure ionization
APPI	Atmospheric pressure photoionization
ASM	Active solvent modulation
AUC	Aera under the curve
BDD	Boron-doped diamond
BEQ	Bioanalytical equivalent
CAD	Charged aerosol detector
CCS	Collision cross-section
CEC	**C**ontaminants of emerging concern
ChgH	Choriogenin H
CID	Collision-induced dissociation
COD	Chemical oxygen demand
DAD	Diode array detector
DBE	Double bond equivalent
DBP	Disinfection by-product
DCF	Diclofenac
DCF-$^{13}C_6$	Diclofenac-$^{13}C_6$
DF	Dilution factor
DMPO	5,5-Dimethyl-1-pyrroline N-oxide
DMSO	Dimethyl sulfoxide
DOM	Dissolved organic matter
E1	Estrone
E2	17β-estradiol
eAOP	Electrochemical advanced oxidation process
EC	Effective concentration
EC50	Median effective concentration

ECB	European Chemicals Bureau
ECp	Effective concentration for p% of the maximum effect
ED50	Median effective dose
EDA	Effect-driven approach
EDC	Endocrine-disrupting chemical
EE2	17α-ethinylestradiol
EE2-$^{13}C_2$	17α-ethinylestradiol-$^{13}C_2$
EEQ	17β-estradiol equivalent concentration
EF	Electro-Fenton
eGFP	Enhanced green fluorescent protein
EIC	Extracted ion chromatogram
ELSD	Evaporative light scattering detector
EM	Emerging micropollutant
EMA	European Medicines Agency
EPR	Electron paramagnetic resonance
ER	Estrogen receptor
ERA	Environmental risk assessment
ESI	Electrospray ionization
EtOH	Ethanol
EU	European Union
FA	Formic acid
FET	Fish embryo toxicity test
FT-ICR	Fourier-transform ion cyclotron resonance
FWHM	Full width at half maximum
GC	Gas chromatography
GFP	Green fluorescent protein
H_2O_2	Hydrogen peroxide
HCD	High-energy collision-induced dissociation
HEq	Hormonal equivalent
HILIC	Hydrophilic interaction liquid chromatography
HPLC	High-performance liquid chromatography
HPT	Hypothalamic-pituitary-thyroid
HQ	Hazard quotient
HR	High resistance flow capillary
HRMS	High resolution mass spectrometry
$HO_2^{\cdot}$	Hydroperoxyl
IC	Industrial chemical
ID	Internal diameter
IEC	Ion exchange chromatography
ILMM	In-line mixing modulation

IMS	Ion mobility spectrometry
IS	Internal standard
IT	Ion trap
JW	Jet weaver
LBD	Ligand-binding domain
LC	Liquid chromatography
LC-HRMS	Liquid chromatography-high resolution mass spectrometry
LC-LC	Heart-cutting two-dimensional liquid chromatography
LC × LC	Comprehensive two-dimensional liquid chromatography
LC-MS	Liquid chromatography-mass spectrometry
LOD	Limit of detection
LOAEL	Lowest observed adverse effects level
LLOQ	Lower limit of quantification
LR	Low resistance flow capillary
Luc	Luciferase
m/z	Mass-to-charge ratio
MALDI	Matrix-assisted laser desorption/ionisation
MCE	Mineralization current efficiency
MCT	Multicolumn thermostat
ME	Matrix effect
MEC	Measured environmental concentration
MeOH	Methanol
MFE	Molecular feature extraction
mLC-LC	Multiple heart-cutting two-dimensional liquid chromatography
MoA	Mode of action
MS	Mass spectrometry
MS^1	Precursor ion
MS^2	Product ion
MS222	Tricaine methanesulfonate
MS^n	Multi-stage fragmentation
MS/MS	Tandem mass spectrometry
MSI	Metabolomics standards initiative
NAM	New approach methodology
NMR	Nuclear magnetic resonance
NOAEL	No adverse effects level
NPLC	Normal-phase liquid chromatography
NSAID	Non-steroidal anti-inflammatory drug
NTS	Non-target screening
•OH	Hydroxyl radical
$O_2^{-\bullet}$	Superoxide anion

O_3	Ozone
OECD	Organisation for Economic Co-operation and Development
PC	Parent compound
PCP	Personal care product
PEF	Photoelectro-Fenton
PNEC	Predicted no effect concentration
PRK	Pressure release kit
QC	Quality control
QLIT	Quadrupole linear ion trap
QQQ	Triple quadrupole
QSAR	Quantitative structure-activity relationship
REACTIV	Rapid estrogen activity *in vivo* assay
REF	Relative enrichment factor
REP	Relative potency
RI	Retention index
ROS	Reactive oxygen species
RPLC	Reversed-phase liquid chromatography
RSD	Relative standard deviation
RT	Retention time
S/N	Signal-to-noise ratio
SE	Sonoelectrochemistry
SEC	Size-exclusion chromatography
SEM	Standard error of the mean
SH	Steroid hormone
SL	Sample loop
sLC × LC	Two-dimensional liquid chromatography
SI	Supporting information
$SO_4^{\bullet-}$	Sulfate radical
SRM	Selected reaction monitoring
T3	Triiodothyronine
T4	Thyroxine
TEQ	Toxic equivalent concentration
TH	Thyroid hormone
TH/bZIP	Thyroid hormone promoter / basic leucine zipper
TOC	Total organic carbon
TOF	Time-of-flight
TP	Transformation product
TR	Thyroid receptor
TTR	Transthyretin
UHPLC	Ultra high-performance liquid chromatography

ULOQ	Upper limit of quantification
US EPA	United States Environmental Protection Agency
UV	Ultraviolet
WFD	Water Framework Directive
WL	Watch List
WWTP	Wastewater treatment plant
XETA	Xenopus eleutheroembryonic thyroid assay
YES	Yeast estrogen screen

List of Symbols

°C	Degree Celsius
j	Current density (mA/cm^2)
k_{app}	Apparent rate constant
Log K_{ow}	Octanol-water partition coefficient
LogD	Octanol-water distribution coefficient
M	Molar
mW	Milliwatt
n_c	Peak capacity
nm	Nanometer
R^2	Regression coefficient
t	Time (min)
V1	Switching valve 1
V2	Switching valve 2
V3	Switching valve 3
v/v%	volume/volume%
Δppm	Mass deviation
λ	Number of times a sample loop is flushed
Ω/cm	Resistivity

CHAPTER 1

General Introduction



Around 3000 B.C., significant silver deposits were mined in Anatolia (now Turkey). During this time, silver extraction methods were basic, often resulting in the unintentional extraction of lead, a byproduct then deemed inconsequential and frequently discarded. Unbeknownst to the local population, this process resulted in environmental contamination with this heavy metal. As lead is a persistent environmental contaminant, it would have gradually infiltrated the local ecosystems through the water sources in the region. Crops irrigated with this contaminated water would have accumulated lead, a process known as bioaccumulation, and this would extend to the livestock that consumed these crops. Consequently, lead entered the food chain, affecting the local population reliant on these resources. At the time, the clinical understanding of lead poisoning was nonexistent. The exposure symptoms, which include chronic fatigue, abdominal pain, and neurological changes like irritability and cognitive impairment, would have been mysterious and perplexing to contemporary observers. With continuous exposure, these symptoms would intensify over generations, owing to the bioaccumulative nature of lead. Prenatal exposure would also have been a concern, as lead can cross the placental barrier. The ancient Anatolian population, lacking scientific knowledge, might have interpreted these health issues as supernatural in origin. The irony lies in the fact that their valuable resource, silver, was indirectly contributing to these health and environmental problems. It was not until recent times, with advancements in scientific techniques and archaeological methodologies, that the full scope of this environmental issue was understood. Modern research, involving analysis of skeletal remains and soil samples from that period, has revealed high levels of lead, corroborating the hypothesis of environmental lead contamination and its impacts. This historical instance is one of the first instances of emerging micropollutants and underscores the critical need for awareness of the environmental impact of human activities. (Historical instance based on [1–4]).

1.1. Emerging micropollutants

Emerging micropollutants (EMs) are defined as “chemicals or materials characterized by a perceived, potential, or real threat to human health or the environment or by a lack of published health standards” [5]. They include various synthetic or naturally occurring chemical and biological substances and are typically present in the environment at trace levels ranging from nanograms to micrograms per liter (ng/L - µg/L). EMs, also commonly referred to as contaminants of emerging concern (CECs), are increasingly recognized for their persistent, bioaccumulative properties and widespread impact on urban water systems worldwide. The term “emerging” refers to their insufficient monitoring and increasing concerns regarding their potential impact on human health and the environment [6,7]. A contaminant might also be

classified as "emerging" due to the identification of a novel source or a newly recognized route of human exposure [5].

EMs include pharmaceuticals, personal care products (PCPs), pesticides, steroid hormones (SH), industrial chemicals (ICs), harmful nanomaterials, microplastics and heavy metals (**Fig. 1.1**).

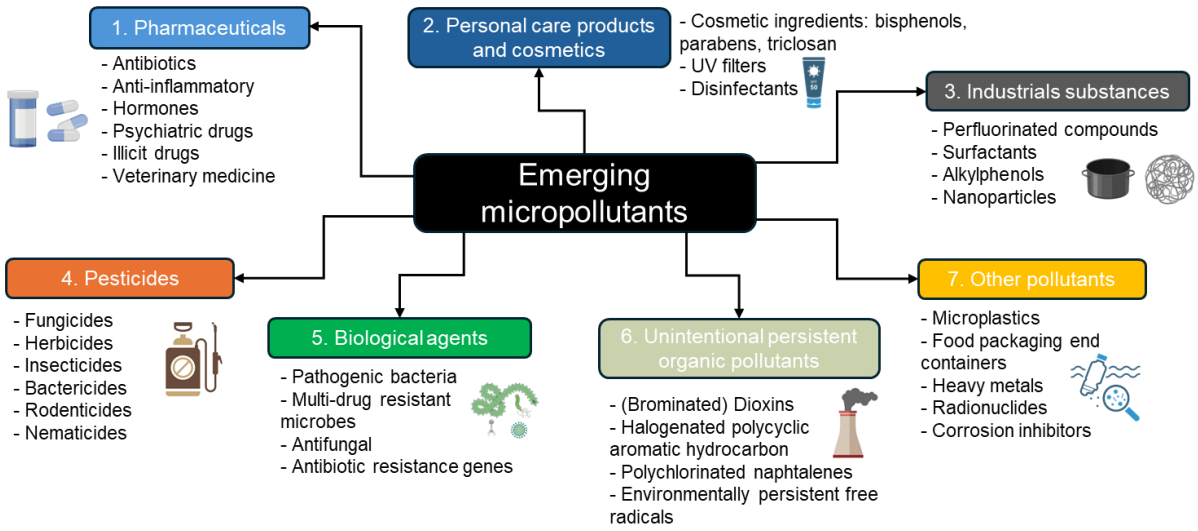

Figure 1.1 – Different types of EMs in urban water systems.

1.1.1. Source, transportation & fate of emerging micropollutants

EMs originate from a wide array of sources and have been detected in a variety of water bodies including groundwater, surface water, wastewater and drinking water [7,8]. These pollutants enter water bodies through several channels (**Fig. 1.2**): surface runoff, groundwater flow, direct discharges from distinct sources, atmospheric deposition and precipitation, leading to their accumulation in aquatic habitats [7,9]. Pharmaceuticals find their way into the environment via wastewater treatment plants (WWTPs), agriculture, human waste excretion, disposal of unused or expired drugs, veterinary medications in animal waste, industrial manufacturing processes and emissions from hospital and healthcare establishments [10,11]. PCPs are commonly discharged into wastewater through shower runoff [12], from where they can enter surface water bodies. Pesticides, mainly herbicides, typically reach groundwaters through leaching from agricultural sites [13,14].

The behavior and ultimate fate of EMs in water is influenced by numerous factors, including the physicochemical characteristics of the EM, environmental conditions, the nature of the water bodies they infiltrate and the presence of other micropollutants, adding complexity to understanding their impact [12,15]. Furthermore, the persistence of EMs often hinders their decomposition, resulting in their extended presence in aquatic environments [16]. Once

present in aquatic ecosystems, EMs can undergo various transformations such as biodegradation, photodegradation, hydrolysis, and may even convert into more harmful forms [13].

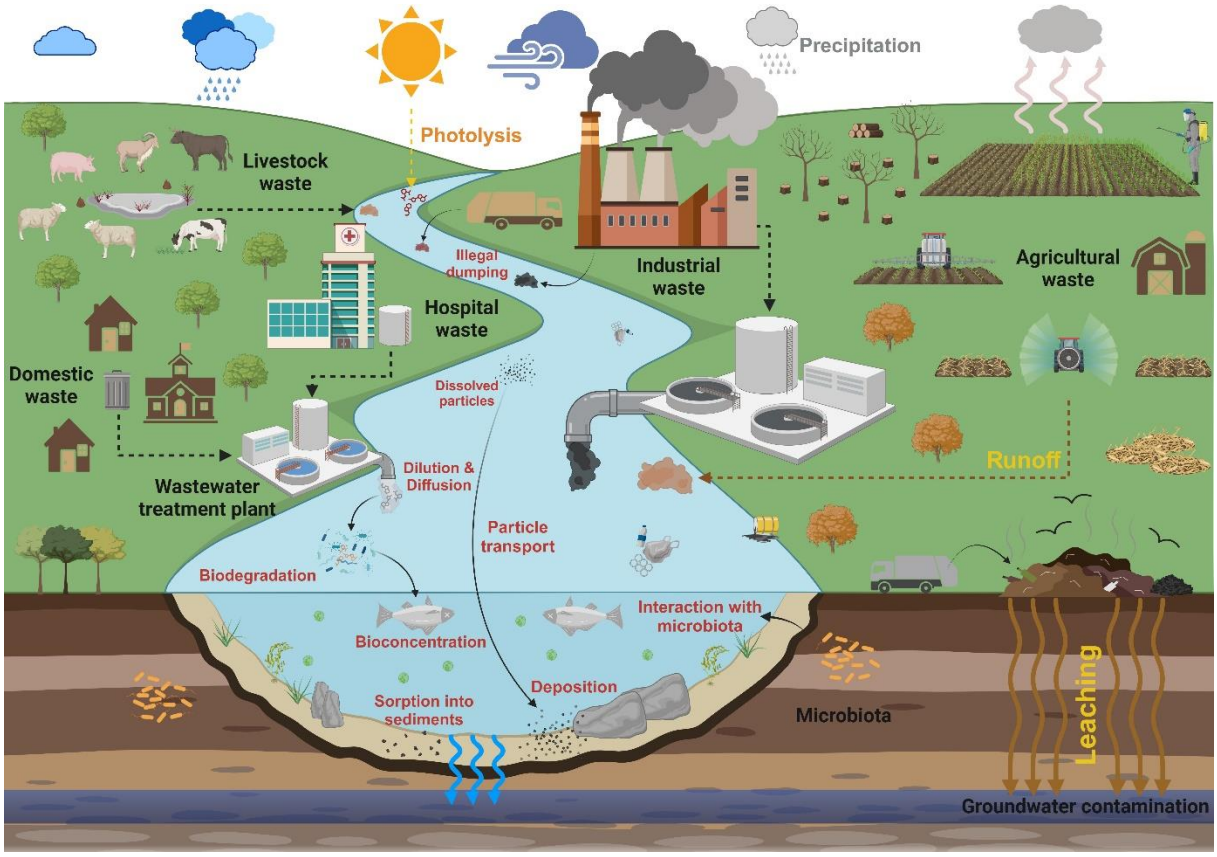

Figure 1.2 – Sources, transportation and the fate of EMs in the environment. Image created with BioRender.com.

1.1.2. Regulations

Access to clean water is a fundamental human necessity and a valuable asset, hence the new European Water Policy is designed to “get polluted waters clean again, and ensure clean waters are kept clean”. The current approach to water management in Europe is shaped by the Water Framework Directive (WFD) of 2000, which sets forth principles for safeguarding European waters [17]. The WFD categorizes chemicals into two principal groups of priority substances [18]. The "Black list" comprises dangerous priority substances that are persistent, highly toxic, or prone to bioaccumulation. The "Grey list" includes priority substances that pose a considerable environmental risk. The identification of these substances is based on either individual chemicals or groups of chemicals, or by the type of industrial sector.

Presently, Europe is encouraging industries to innovate and reduce or eliminate the discharge of priority substances in their wastewater. This includes environmental protection, the adoption

of "green chemistry" principles, the use of renewable resources, efficient water management through wastewater recycling, and addressing health concerns [18]. As a result, effluent treatment has emerged as a critical concern for the industrial sector.

In 2013, a mechanism known as the Watch List (WL) was introduced to better identify substances of significant concern [19]. The WL under the WFD is a strategic initiative by the EU to better manage and understand the impact of emerging pollutants in water bodies [19]. It serves to identify substances of potential concern, mandates targeted monitoring for data collection on these substances across Member States, and aids in risk assessment [20]. The insights gained from this process inform policy development, particularly concerning the regulation of priority substances to protect aquatic environments [19]. Additionally, the WL enables adaptive management of water quality, allowing the EU to respond effectively to new scientific findings and environmental challenges [19]. In this regard, Member States must conduct annual monitoring of the listed substances for a duration of up to four years [20]. The WL was initially established in 2015 and has since been updated in 2018, 2020, and most recently in 2022 [21].

The first WL under the Water Framework Directive (WFD, EU Directive 2000/60/EC, EU Implementing Decision 2015/495) included 10 individual or groups of substances to monitor [19]. Among these were three steroidal estrogens: 17α-ethinylestradiol (EE2), 17β-estradiol (E2) and estrone (E1), along with the non-steroidal anti-inflammatory drug (NSAID) diclofenac. The 4th WL updated in 2022 includes guanylurea, a transformation product (TP) of metformin, highlighting the necessity for additional EU-wide monitoring data of TPs in surface waters [21]. This step could be crucial for the potential incorporation of further TPs into the list of substances that require regular monitoring in aquatic environments.

1.1.3. Remediation technologies

As WWTP effluents are major sources of EMs [12,15,16], it is imperative to remove these micropollutants from polluted wastewater to mitigate their detrimental impacts on both human health and the environment. Considering that the majority of EMs are both novel and complex, mitigating their discharge poses challenges for wastewater treatment methods [22]. Therefore, there is a need to develop advanced and effective removal strategies.

1.1.3.1. Conventional wastewater treatment

Several physical, chemical and biological technologies have been developed for the treatment of municipal water, such as flotation, precipitation, oxidation, carbon adsorption, ion exchange, membrane filtration, biodegradation and phytoremediation [18]. Generally, the treatment of

wastewater consists of 5 successive steps [18], as depicted in **Fig. 1.3**: (1) preliminary treatment or pre-treatment; (2) primary treatment; (3) secondary treatment or purification; (4) tertiary or final treatment; and (5) sludge treatment.

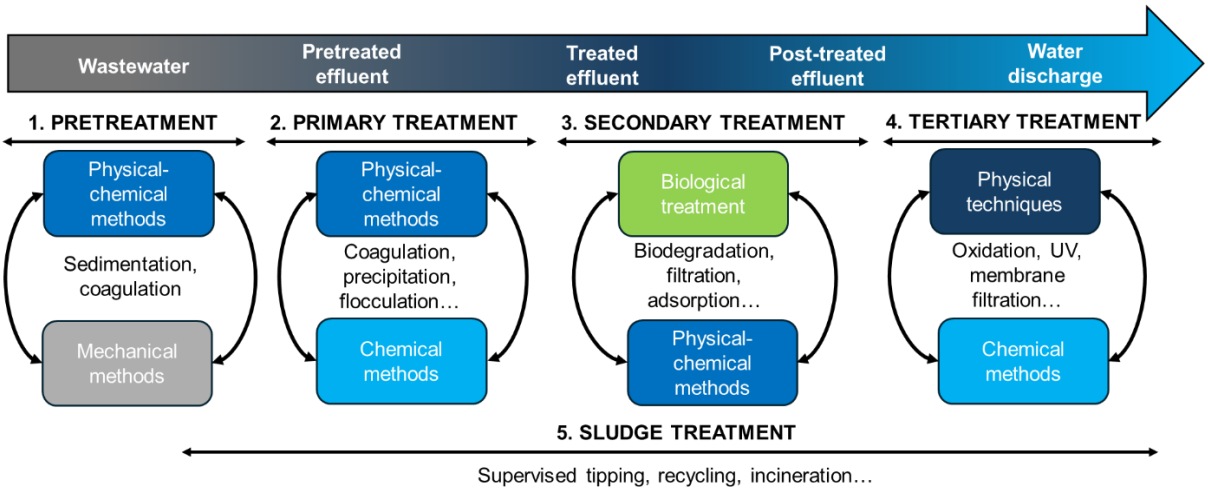

Figure 1.3 – Main processes of wastewater treatment. Adapted from [18].

The choice of treatment method is influenced by the specific characteristics of the wastewater. Each method presents unique challenges, including considerations of cost, feasibility, efficiency, practicality, reliability, environmental impact, local regulations, sludge production, operational complexity, pre-treatment needs, and the potential generation of toxic by-products [18]. Despite the variety of available treatment processes, only a few are commonly employed in WWTPs due to technological and economic constraints [18].

Conventional physicochemical and biological methods are commonly used to remove pollutants from effluents [22]. Nonetheless, the presence of EMs in treated effluents indicates the inefficacy of these treatment methods in eliminating these substances from wastewaters [23]. The limited effectiveness of biological (secondary) wastewater treatment in removing EMs is due to their complex structures and low concentrations, which hinder easy breakdown [15]. These compounds are often designed to resist degradation, and microorganisms in secondary treatments may not possess the enzymes needed to degrade newer and more complex pollutants [16,24]. Additionally, micropollutants can bind to solids or accumulate in microbial biomass [25]. Interference from other wastewater compounds, particulary antibiotics and heavy metals, can also inhibit microbial activity [16,26].

Ultraviolet (UV) irradiation is a widely adopted tertiary treatment process in WWTPs and involves the photo-transformation of organic pollutants using high-energy UV light [23]. The effectiveness of UV treatment is limited to only a select few organic pollutants, with the majority exhibiting low removal rates (often <20%) [27,28]. To enhance the removal of EMs and meet

emerging environmental standards, conventional WWTPs hence need to be upgraded by integrating additional tertiary treatment technologies, such as advanced oxidation processes.

1.1.3.2. Advanced oxidation processes

Advanced oxidation processes (AOPs) generate reactive radicals with a high oxidizing power for the elimination of compounds in wastewater that are non-biodegradable, persistent, and chemically stable [29]. AOPs include a range of methods, such as heterogeneous and homogeneous photocatalysis, Fenton and Fenton-like reactions, ozonation, plasma-based AOP, and the use of ultrasound, microwaves, and γ-irradiation, in addition to electrochemical techniques [30,31]. AOPs aim to transform contaminants into simpler, less harmful, or more easily biodegradable forms, through either full mineralization or the formation of oxidized intermediates [32]. As a result, they are considered one of the most suitable methods for improving the breakdown of EMs [30].

Free radicals are potent oxidizing agents with at least one unpaired electron. Examples include the hydroxyl (•OH), superoxide anion ($O_2^{-\bullet}$), hydroperoxyl ($HO_2^{\bullet}$), sulfate ($SO_4^{\bullet-}$), and alkoxy radical (RO•). Among these, •OH is particularly noteworthy for its non-selective oxidation, high oxidation potential (E_0 = 2.80 eV), and capacity to react with a broad spectrum of pollutants [33]. Due to its unstable nature and very short life time, •OH is only produced *in situ* through the application of different methods, such as the use of oxidizing agents (*e.g.*, ozone, hydrogen peroxide), irradiation (*e.g.*, ultraviolet, ultrasound, gamma ray/electron beam), and catalysts (e.g. transition metal ions, semiconductors) [34]. However, these methods require adding additional reagents and/or are inefficient in generating radicals [35], which can make these techniques unfeasible from a chemical and toxicological point of view.

1.1.3.2.1. Electrochemical advanced oxidation processes

In recent years, significant developments in electrochemical advanced oxidation processes (eAOPs) have occurred [36,37]. eAOPs offer numerous benefits to address pollution, primarily because they utilize electrons, which are clean reagents [37]. Additional benefits include their high energy efficiency, the capability for automated operation, the ease of use due to their straightforward equipment, the possibility to be powered by a renewable energy source and the safe operation under gentle conditions such as ambient temperature and pressure [30]. Furthermore, eAOPs are highly versatile, suitable for treating a wide range of effluent concentrations with a chemical oxygen demand (COD) from 0.1 to 100 g/L [37].

Leading techniques within eAOPs include anodic oxidation (AO), electro-Fenton (EF), photoelectro-Fenton (PEF), and sonoelectrochemistry (SE), with AO being the most sought-after technique [37]. AO is characterized as an electrochemical process capable of oxidizing

and degrading pollutants in wastewater through either direct oxidation on the anode's surface, a mediated oxidative process, or a combination of both [38]. The oxidative process starts at the anode and can be considered as either heterogeneous or homogeneous oxidation [39] (**Fig. 1.4**).

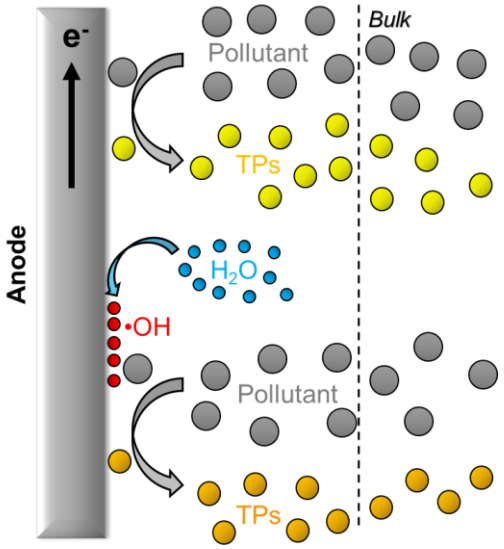

Figure 1.4 – Schematic representation of a generic anodic oxidation (AO) process. TPs: transformation products. Adapted from [23].

Heterogeneous oxidation of EMs takes place when these pollutants undergo direct oxidation at the electrode's surface. The process begins with the transportation of the pollutant from the bulk of the sample to the electrode surface, where it adsorbs. Following this, a direct electrochemical reaction occurs, involving the transfer of an electron to the pollutant. Subsequently, the transformed products undergo a desorption process, after which they are released back into the bulk of the media.

Homogeneous oxidation of EMs occurs in the main body of the media, through interaction of pollutants with oxidants that are generated at the anode surface. These oxidants originate from components within the bulk solution and are created through heterogeneous oxidation of water or other ions that are introduced in the media to enhance the production of oxidants.

When species undergo direct oxidation at the anode surface, reactive radicals are created that subsequently merge to form stable oxidants. Anions like sulfate, phosphate, and carbonate contribute to the generation of these radicals [37]. The formation of electrochemical •OH predominantly occurs in the initial stages of water oxidation. Due to the brief lifespan of •OH, the oxidation of pollutants predominantly takes place near the anode surface [23]. Although •OH [40–42] is the main produced radical, $O_2^{\bullet-}$, $HO_2^{\bullet}$, sulfate radicals ($SO_4^{\bullet-}$), peroxyl radicals (ROO•), organic radicals (R•), nitric oxide ($NO^{\bullet}$) and nitrogen dioxide ($NO^{2\bullet}$) may also be generated, depending on electrochemical conditions such as applied potential, solution pH, and the presence of specific electrolytes or substrates [34,40–43]. Less potent oxidants like

hydrogen peroxide (H_2O_2), which result from the dimerization of hydroxyl radicals, and ozone (O_3) formed by water discharge at the anode surface, may also play a role in breaking down pollutants [23]. Nevertheless, the primary factor driving the degradation process is the interaction between the pollutants and the anode surface [23]. Consequently, the efficiency of AO processes is intrinsically linked to the diffusion of pollutants from the bulk liquid to the anode surface or its nearby vicinity [44].

Selecting the right electrode is critical in designing an AO system for wastewater treatment. In this context, there is a notable preference for boron doped diamond (BDD) as the anode [23]. BDD has an exceptionally wide oxygen overpotential range [45], allowing to operate within the potential range required for water decomposition [44].

Unlike other advanced oxidation treatments, eAOPs do not depend on external reagents for their operation. However, for these processes to be efficient, the solution must have a high enough conductivity to facilitate effective electron transfer. Sodium sulphate (Na_2SO_4) is predominantly selected as a supportive electrolyte due to its inert and neutral characteristics [23], essential to prevent interference in measurements that might arise from pH fluctuations or secondary chemical reactions within the medium [46].

1.2. Transformation products

While there is an increasing understanding of the presence, behavior, and risks associated with EMs in the environment, their transformation products (TPs) have long been overlooked. However, since a few years, TPs have started to receive more scientific scrutiny [47,48]. Recent research has confirmed their widespread presence in the environment and raised questions about their toxicity, bioaccumulation, and environmental stability [47].

TPs can be categorized into three types according to their origin: those formed through biological processes, those emerging from non-biological (abiotic) processes, and those produced by engineered systems, such as advanced water treatment technologies [49]. This thesis primarily focuses on TPs created by engineered systems.

1.2.1. Ecotoxicological concerns

The environmental behavior of many TPs differs from that of their parent compounds (PCs) [47]. Generally, oxidative treatment yields more polar TPs, which increases environmental mobility in comparison to the PC [49,50]. However, despite being less susceptible to bioaccumulation and exerting toxic effects, the higher mobility can still negatively impact the environment [49].

Nevertheless, the major concern is the generation of TPs that are equally or more toxic than the PCs, which can occur for several reasons [49,51]. Firstly, the toxicophore of the PC might still be present in the TP, leading to a similar toxic effect. Secondly, the transformation process can lead to the cleavage of polar or charged functional groups of the PC, enhancing its hydrophobicity. This makes the resulting TPs more prone to accumulate at the site of action and potentially increases its toxicity, particularly for compounds with similar toxic modes of action (MoA). Thirdly, the transformation process might result in a TP with a different toxicophore leading to a different MoA than the PC.

1.2.2. Identification and prioritization of transformation products

Within eAOPs, the high *in situ* generation of non-selective reactive species such as •OH and $SO_4^{\bullet-}$ can result in the generation of a diverse array of TPs through different degradation pathways. As identifying all TPs is labor-intensive or even unfeasible, prioritizing the most relevant TPs is necessary. This can be done by two main approaches (**Fig. 1.5**): the exposure-driven approach and the effect-directed analysis (EDA) [49].

The exposure-driven approach is the most common method and involves isolating and identifying TPs, followed by assessments of their toxicity or environmental fate. In cases where the chemical structure of a TP can be determined, it may be synthesized to evaluate its biological impact. However, isolating and identifying relevant TPs can be challenging, posing a disadvantage to this approach. Additionally, available analytical methods may not be sensitive or selective enough to detect or distinguish between closely related TPs.

The EDA employs a tiered system to analyze the toxicity of TPs. In EDA, treated samples are taken over time and subjected to chemical analysis to determine the transformation kinetics of the PC. Simultaneously, by using a carefully chosen battery of bioassays the evolution of the toxicity is monitored throughout the degradation process, progressing from untreated samples to treated ones. Generally, the selection of bioassays is dependent on the MoA of the PC tested. In the initial stage, the EDA offers insights into whether the toxicity levels are increasing or decreasing throughout the transformation process, thereby indicating the potential formation of toxic TPs. This determination can be made by assessing whether the observed changes in toxicity can be entirely attributed to the reduction in concentration of the PC. If there is no noticeable disparity between the degradation kinetics of the PC and the kinetics of toxicity, it can be deduced that toxic TPs have not been generated, removing the need for additional experiments.

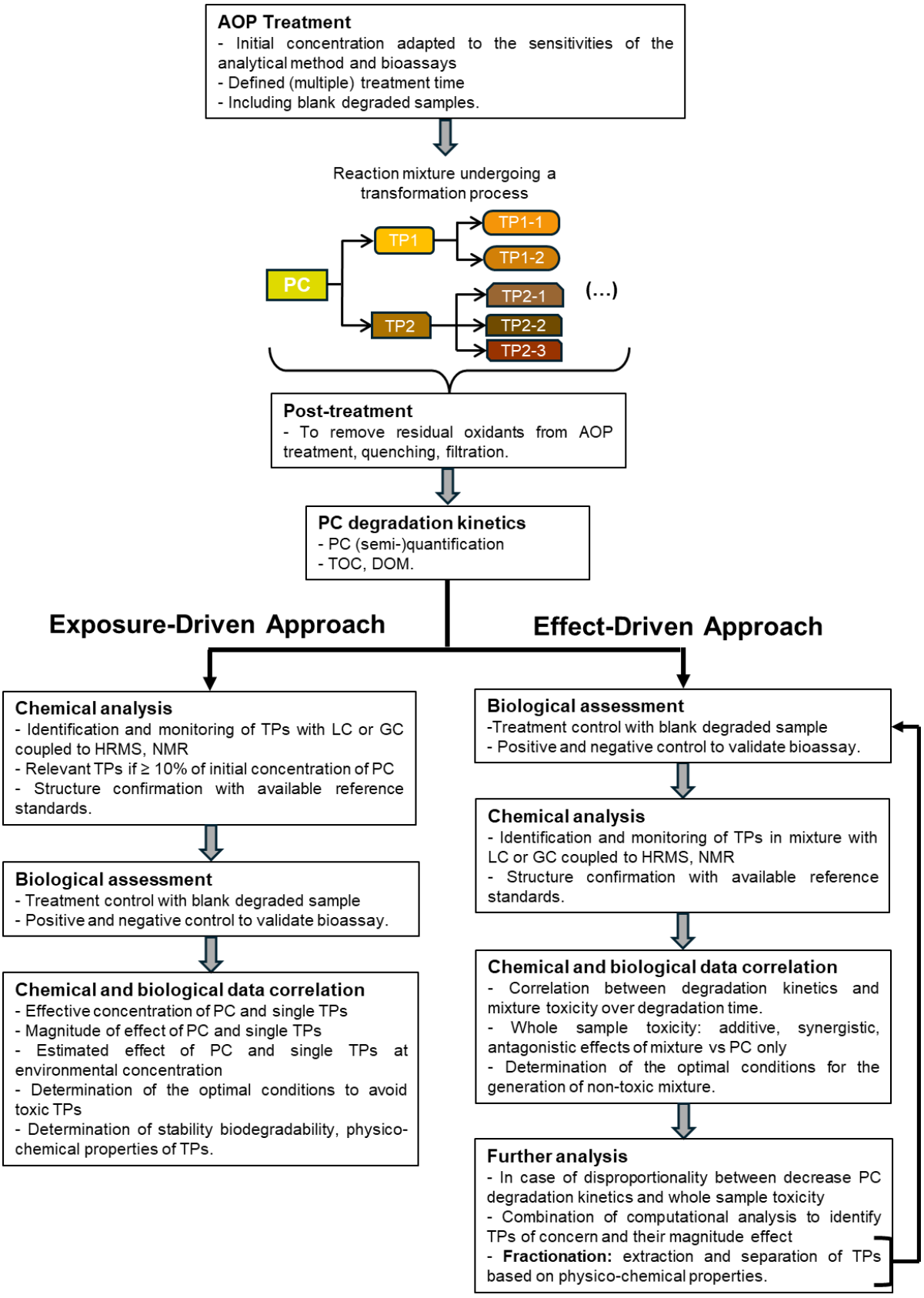

Figure 1.5 – Exposure and effect driven approaches for the identification of TPs in engineering systems. AOP: advanced oxidation process; PC: parent compound; TPs: transformation products; TOC: total organic carbon; DOM: dissolved organic matter; LC: liquid chromatography; GC: gas chromatography; HRMS: high resolution mass spectrometry; NMR: nuclear mass resonance. Based on [49,52].

If significant discrepancies are observed between the rates of PC degradation and the evolution of toxicity, further investigations are required to identify and characterize the TPs that contribute to the overall toxicity of the reaction mixture. In this case, the reaction mixture is subjected to preparative fractionation based on hydrophobicity, followed by testing the toxicity of each fraction using appropriate bioassays. This process aims to determine whether the observed increase in toxicity is due to a rise in hydrophobicity or the formation of specifically acting or inherently more toxic TPs. If the toxicity increase correlates with the hydrophobicity of the tested fractions, the toxicity of the TPs can be attributed to an enhanced bioaccumulation potential. Under these circumstances, the toxicity of the isolated compounds can be estimated using existing methods based on the octanol-water partition coefficient (Log K_{ow}).

Conversely, if the second-tier analysis reveals the formation of specifically acting or inherently more toxic TPs, evidenced by higher toxicity in fractions with lower hydrophobicity, then a more comprehensive analysis is warranted to characterize these TPs. In some instances, it may be possible to conclusively identify the most toxic TP by correlating the temporal changes in the concentration of individual TPs with the variations in toxicity. An addition is the use of multispecies modelling to predict toxicity of the identified TPs based on *in silico* tools.

A key strength of EDA is its ability to investigate the toxicity of mixtures. However, it may not facilitate the identification of specific molecules causing effects, thereby missing certain details. A notable challenge with this approach is ensuring that no component of the sample is missed during fractionation, a task complicated by the likelihood that several TPs will have closely related properties. Furthermore, EDA requires comprehensive chemical and biological assessments that are resource-intensive and demand significant labor and time.

1.3. Environmental risk assessment

Environmental risk assessment (ERA) is a structured process for evaluating the potential effects of chemicals, processes or activities on the global environment [53]. Its goal is to identify and quantify risks posed by environmental hazards to ecosystems, wildlife, and human health [54,55]. In Europe, a pharmaceutical must undergo an ERA process if its predicted concentration in the environment is more than 10 ng/L [54]. Additionally, ecotoxicological testing is mandatory if a drug impacts the reproduction of vertebrates or lower animals at concentrations below 10 ng/L [55]. Moreover, when micropollutants degrade in the environment or by engineered processes, they may form persistent and toxic TPs, which should also be accounted for in the ERA of the parent compounds [49].

1.3.1. Ecotoxicological assessment

Historically, toxicity tests primarily focused on mortality as the main endpoint. However, in more recent times, toxicity assessments have shifted towards evaluating sub-lethal endpoints, including growth, reproductive function, morphology, lifespan, and even behavior [53]. Contemporary ecotoxicological methods assess the effects of low and environmentally realistic concentrations of chemicals over extended periods, aiming to identify non-lethal alterations in physiological functions of organisms. This shift has led to the introduction of important concepts like the median effective concentration (EC50) and dose (ED50). In addition to EC50, other key metrics have been established, such as the No Adverse Effects Level (NOAEL), which is the maximum tested amount of a chemical that does not cause harm to the test organisms and the Lowest Observed Adverse Effects Level (LOAEL), which is the smallest amount of a contaminant that has been observed to cause harmful changes in the organism being studied. The definitions of exposure duration are not fixed and can vary widely. Typically, acute tests last 1–4 days, sub-acute tests up to 28 days, sub-chronic up to 90 days, and chronic over 90 days [56]. In experimental settings, however, the duration of the bioassays is often linked to the life cycle of the test species.

Hazard assessment is a key element of risk assessment, particularly in aquatic environments. The basics of risk assessment related to the aquatic environment are universal in that they compare the exposure (a part) of the ecosystem to a chemical with the sensitivity of the ecosystem for this chemical [57]. Exposure levels are typically represented by the Predicted Environmental Concentration (PEC) or Measured Environmental Concentration (MEC), which can be determined through field monitoring or estimated using environmental models.

Ecosystem sensitivity, on the other hand, is often indicated by the Predicted No Effect Concentration (PNEC) that represents the concentration below which an unacceptable effect most likely will not occur, and is widely used for risk assessment and in environmental policy and regulation [58]. To assess the potential risk for the environment, the Hazard Quotient (HQ) is widely recognized and employed in aquatic risk assessment models for the purposes of screening and identifying hazards [53]. HQ is defined as the ratio of the potential exposure to a substance to the level at which no adverse effect is expected [55]. It is calculated by dividing the MEC in a given environment by the PNEC. An HQ above 1.0 indicates an increased likelihood of a toxicological response to a chemical.

In complex samples, the effective concentration (EC) for p% of the maximum effect, (ECp) is usually expressed in terms of the relative enrichment factor (REF) or dilution factor [59]. This approach, however, can be challenging to convey to regulatory bodies and difficult to align with water quality standards, especially since a lower ECp value indicates higher toxicity [59].

For toxicants that act through receptor-mediated mechanisms, an alternative method of reporting toxicity data is the concept of toxic equivalent concentration (TEQ) or bioanalytical equivalent (BEQ). BEQs of mixtures are widely used to reflect the potential threat of pollutants in the environment and can be obtained by bioassays or using chemical analysis combined with relative potencies (REPs) [60]. A widely accepted use of the BEQ concept is in measuring sample estrogenic activity, typically expressed as 17β-estradiol equivalent concentrations (EEQ) [59,61]. Numerous studies have found a strong correlation between EEQ values obtained through bioassays and those calculated from analytically determined concentrations of estrogenic chemicals, taking into account their known REPs [62–64]. The consistency between calculated and measured EEQ is mainly due to the limited variety of potent estrogenic substances that predominantly influence the overall estrogenic effect, including natural and synthetic hormones and certain xenoestrogens [59]. Bioassays that measure BEQs of other receptor mediated effects are being developed and implemented to assess water quality and toxicity [60,65].

1.3.2. Methodologies for ecotoxicological testing

(Eco)toxicological testing involves methodologies that expose biological entities to an environmental medium to assess the impacts of chemical stressors at various levels of biological organization, from molecules to ecosystems (**Fig. 1.6**). These tests encompass a broad spectrum, including *in vitro* assessments of sub-organismal responses, *in vivo* studies on ecosystem impacts, effect-based methods, standard toxicity tests, bioassays, biomarkers, and experiments in micro- and mesocosms [66].

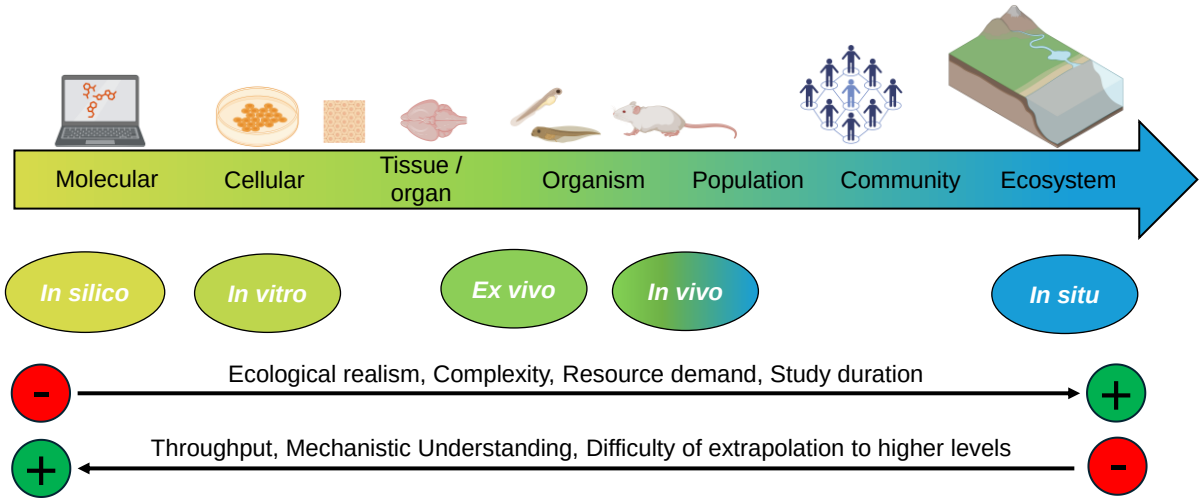

Figure 1.6 – Levels of biological organization and tools in support of chemical ecological assessment. Adapted from [67].

Incorporating ecotoxicity tests which measure biological effects into monitoring strategies can moreover i) offer a more holistic and accurate evaluation of how aquatic organisms are affected by chemical stressors, ii) aid in the elucidation of the mechanisms leading to negative impacts on aquatic ecosystems, and iii) serve as an early-warning system to enable preemptive actions [66].

Traditional approaches to ecotoxicological assessment have heavily relied on *in vivo* models. However, these animal-based tests present significant challenges, including high costs, lengthy durations, and the requirement for rigorous ethical oversight. Consequently, there is a substantial demand for alternative models that offer more cost-effective and expedited solutions [68]. Moreover, in alignment with the principles of Replacement, Reduction, and Refinement (3Rs), considerable efforts are being made to minimize animal experimentation and enhance animal welfare, ultimately striving towards the complete substitution of animal tests with alternative scientific methodologies [69].

In pursuit of these goals, new approach methodologies (NAMs) have emerged as innovative alternatives. NAMs are described as “any technology, methodology, approach, or combination that can provide information on chemical hazard and risk assessment to avoid the use of animal testing” [70]. These novel methodologies are capable of providing information on molecular alterations, disturbances at the molecular/cellular level, toxicokinetics, toxico-dynamics, and the mechanisms behind toxicity, rather than measuring apical endpoints that are assessed *in vivo* [71]. NAMs are highly promising in enhancing the efficiency of screening tests for regulatory decision-making purposes and offer the additional advantage of decreasing dependency on more resource-heavy studies that require the use of many animals [72]. Currently, there are three main categories of toxicity models in environmental research, i.e., *in silico*, *in vivo*, and *in vitro* models.

1.3.2.1. *In silico*

Computational tools are increasingly recognized as NAMs that have the capacity to accelerate the process of toxicological evaluation [67]. Their benefits include the ability to rapidly process and analyze data, cost-effectiveness and simplicity. Presently, computational strategies serve as alternatives or enhancements of traditional *in vitro* and *in vivo* tests. Currently available *in silico* models primarily fall into two categories [73]. Ligand-based *in silico* models, such as Quantitative Structure-Activity Relationship (QSAR) models, predict activity by using molecular fingerprints and descriptors [74]. These models are developed using advanced algorithms that correlate molecular structures or distinct structural motifs with specific physicochemical properties or biological activities, based on the properties of known chemicals [75].

Examples of widely used tools in ecotoxicology are the OECD QSAR Toolbox, the US EPA TEST and ECOSAR software, and the European Chemicals Bureau (ECB) Toxtree software

tool [76,77]. However, their effectiveness is largely dependent on the availability of high-quality data for model training [78]. A notable limitation is the assessment of chemical mixtures, which present a particular challenge as potential additive or synergistic effects are often not accounted for [79].

Target Structure-Based *in silico* tools use the three-dimensional structure of the biological target, such as a protein, to identify and optimize potential ligands. Among these, molecular docking is widely utilized to simulate the binding configuration of small ligands to their respective protein targets [80,81]. Usually, docking can be accomplished through a two-step process: initially by exploring different conformations of the ligand within the protein's active site, followed by evaluating these conformations using a scoring function [81]. The goal is for the sampling algorithms to accurately replicate the experimentally observed binding mode, and for the scoring function to assign it the highest rank among all generated conformations [81]. In recent years, numerous studies have emphasized the utility of molecular docking to predict the biological consequences of endocrine disrupting chemicals (EDCs) [82]. The endocrine signaling pathways are well conserved across vertebrates [83], which can facilitate the extrapolation of molecular docking results to a wide range of species, including humans. This conservation allows researchers to use molecular docking to assess how EDCs might interfere with hormonal receptors, enzymes, transporter and other specific targets. The limitations of molecular docking include inaccuracies due to simplified algorithmic models, assumptions of rigidity in target and ligand structures, and often-oversimplified scoring functions that fail to capture complex physicochemical interactions [81]. Moreover, the challenge of accurately modeling receptor flexibility remains. Docking predictions require experimental validation to confirm their hypotheses, and the computational resources needed for extensive simulations can be substantial [73,84]. Additionally, the predictive accuracy for novel compounds may be limited by the chemical diversity represented in the training data of the scoring functions [85].

1.3.2.2. *In vitro*

In vitro assays employ either cell cultures, subcellular systems from organisms, or genetically modified bacteria [66]. Often, these assays use cells that have been genetically engineered to incorporate a specific receptor (such as those found in humans or other mammals) and a reporter gene that produces a detectable signal, like a fluorescent protein or an enzyme (β-galactosidase or luciferase) [86]. The ideal outcome is for the assay's detected response, such as fluorescence intensity or enzyme activity, to reflect the level of chemical interaction with the receptor [86]. Thus, *in vitro* bioassays can provide insights into toxicity mechanisms and aid in predicting the effects of substances on living organisms [66]. Moreover *in vitro* assays can also be used for the assessment of acute toxicity.

The *Vibrio fischeri* Bioluminescent Assay (Microtox®) for example is widely employed to assess the detoxification efficiency of treated wastewater [87]. It is an effective tool to assess overall acute non-specific toxicity due to its high sensitivity, ease of use, and rapidity [88].
In vitro models used in toxicity testing have diverse advantages, such as the use of a lower number of animals, reduced price of animal maintenance, small amount of chemicals needed for testing, short times, and increase in throughput for evaluating large number of chemicals and their metabolism [73,89]. The main disadvantage of *in vitro* bioassays is the extrapolation to higher biological levels. This is largely due to the absence of comprehensive toxicokinetic mechanisms in the *in vitro* setting, which are not typically replicated in these simplified models [67]. In addition, receptor binding assays would likely not be able to capture responses from life stages when an organism would be more susceptible to the effects of an EDC [67].

1.3.2.3. *In vivo*

In vivo toxicity models employ whole organisms, integrating the complete spectrum of physiological responses and biochemical interactions potentially overlooked by *in vitro* or *in silico* approaches [66,90]. This comprehensive approach enables the detailed assessment of detrimental effects across multiple biological tiers, including molecular, cellular, tissue, organ, and systemic [91].
Bioassays employing organisms at their early life stages are increasingly developed, especially those within aquatic ecosystems. These assays, employing eleuthero-embryonic life stages, offer three primary benefits over conventional *in vivo* methods [67]. Firstly, the eleuthero-embryos used are typically a few millimeters in length, facilitating their accommodation in six-well plates. This represents a significant logistical improvement over traditional methods that require juvenile or adult stages. Secondly, early-life stage assays can be completed much faster, with exposure durations ranging from 24 to 96 hours, in stark contrast to the 21 days or more required by conventional *in vivo* assays. Thirdly, the assays are ethically advantageous, as the eleuthero-embryonic stages of fish or amphibians, despite being hatched, still depend on the yolk supplied by the mother and do not feed independently. According to European regulations, these eleuthero-embryonic stages do not qualify as protected life stages, and their utilization hence aligns with the 3Rs principles [92].
An example of an *in vivo* model is *Danio rerio* or zebrafish, a small tropical freshwater fish. The strength of this *in vivo* model relies on its high genetic, physiologic and pharmacologic homology to humans [93,94]. Since its discovery as a suitable lab animal in the 1960s, *Danio rerio* evolved into a powerful model for biological, environmental and pharmaceutical studies, as biological pathways to the targets of exposure are largely common across different animal phyla [94]. The external development of eggs facilitates the monitoring of physiological changes throughout the transparent embryo and larvae stages [95].

This process is instrumental in evaluating environmental safety, as it enables the observation of phenotypic alterations in exposed fish. Developmental toxicity assays using zebrafish embryos have been recognized as an effective intermediate model that combines the advantages of *in vitro* and *in vivo* methodologies, enabling high-throughput applications [95]. The fish embryo toxicity test (FET; OECD TG 236) aligns with a significant portion of the regulatory standards for simplified *in vivo* models [96]. Moreover, zebrafish embryos are suitable for extensive toxicity screenings, including high-throughput and high-content analyses, evidenced by numerous studies that have explored endpoints such as mortality, morphometric evaluations, developmental toxicity, immunotoxicity, neurotoxicity, cardiotoxicity, and neuro-behavioral assays [95,97].

Japanese medaka fish (*Oryzias latipes*) is another *in vivo* model that has been used for over 60 years for toxicity testing. These small fish present a rapid screening method to predict toxicity, and are easy to handle and maintain in a laboratory [98]. Medaka fish is an attractive model for the assessment of endocrine disruption, particularly estrogenic activity [99]. The *vitellogenin* (egg yolk precursor protein) and *choriogenin* (egg envelope protein) genes are inducible in response to estrogen exposure in the low ng/L and are widely used as biomarker for exposure to estrogenic chemicals in aquatic ecotoxicology [100].

Finally, the African clawed frog (*Xenopus laevis)* is an attractive *in vivo* model due to its rapid development, versatility and well-understood endocrine physiology [101,102]. Anurans have long been employed as bioindicators to determine the toxicity of aquatic pollutants, leveraging their sensitivity to waterborne contaminants through dermal, respiratory, and ingestion pathways [103]. More recently, they are considered to be the primary model organism for identifying substances that interfere with the hypothalamic-pituitary-thyroid (HPT) endocrine axis [104].

Amphibians serve as effective models for studying thyroid function due to the fact that their metamorphosis is regulated by thyroid hormones (THs), which parallels the perinatal development observed in birds and mammals [105]. Specifically, the role of triiodothyronine (T3) in anuran metamorphosis is universally recognized as the catalyst and key regulator of frog metamorphosis [106]. These changes include a range of quantifiable endpoints, such as the resorption of tails and gills, growth of fore- and hindlimbs, and the remodeling of the intestines, central nervous system, respiratory system, cranial cartilages and skin [107]. Therefore, deviations in these developmental stages during metamorphosis can indicate disruptions within the hypothalamic-pituitary-thyroid (HPT) axis.

Since the early 1980s, transgenic animals, which possess foreign DNA from an external source intentionally incorporated into their genome, have been produced across a diverse range of species, including mammals, birds, amphibians, fish, and invertebrates [100]. Zebrafish, medaka fish and Xenopus laevis are widely used models in biological research for

transgenesis, offering several advantages such as efficient transgenesis techniques and a tolerance for genetic manipulation [108].

With transgenic technology, a reporter gene is attached to a regulatory sequence of another gene of interest in DNA or RNA experiments to determine if the target gene is being expressed. This technology is particularly useful to assess endocrine disruption by enabling the visualization and quantification of gene expression changes directly linked to the activity of hormone-responsive promoters [103]. This allows the direct and sensitive detection of endocrine-disrupting effects at the molecular level, revealing even subtle alterations in hormonal signaling pathways. Reporter genes are chosen for their easily identifiable and measurable characteristics, allowing the quantification of gene expression visually or through biochemical assays [100]. Usually, reporter genes are placed downstream of the promoter of the inserted transgene [100]. The most common reporter genes used in transgenic models are luciferase (Luc) and green fluorescent protein (GFP), with the latter being more prominent due to its stability and strong fluorescent emission [100,109].

As shown in **Fig. 1.7**, the underlying principle of this transgenic technology involves connecting a hormone-responsive promoter to the green fluorescent protein (GFP) gene. As a result, a fluorescent signal is generated in proportion to the activation of the promoter and the amount of hormone present in the tissue. Therefore, exposure of the transgenic model to an EDC or bioactive TP induces the activation of an inducible promoter that triggers expression of the reporter (e.g. GFP). The influence on the corresponding endocrine axis can then be deduced. Transgenic fish and amphibian models offer the advantages of both *in vitro* and *in vivo* models for chemical testing, providing rapid, sensitive, and repeatable screening options that are cost-effective compared to mammalian models [100,110]. They enable detailed toxicodynamic and toxicokinetic studies by allowing the assessment of chemical uptake, distribution, metabolism, clearance and accumulation, alongside targeted analyses of biological effects.

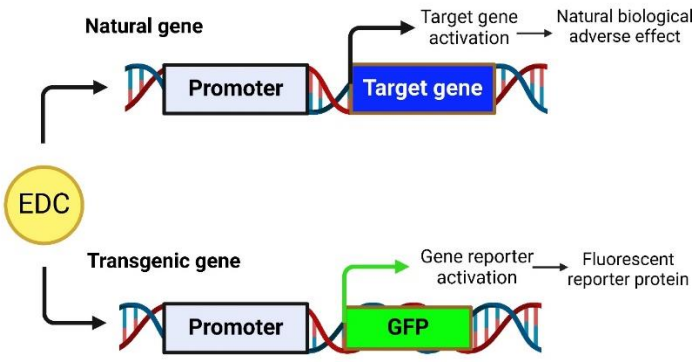

Figure 1.7 – Fluorescence reveals the natural reaction of the organisms. EDC: endocrine disrupting compound. GFP: green fluorescent protein. Image created with BioRender.com.

Furthermore, these models enable the identification and observation of tissues sensitive to chemical exposure in early life, as well as monitoring the long-term impacts on those specific tissues later in life [67]. Transgenic fish can also serve as valuable tools for examining the interactions of various chemicals, whether individually or in combinations, within the organism [100]. This approach enables the assessment of how sequential exposures influence various bodily tissues and allows for the study of the impact of real-world chemical mixtures, such as treated effluent discharges, on development and health. However, challenges such as model validation, life stage-dependent effects, and differences in sensitivity need to be addressed to fully realize their potential in standardized chemical testing and regulatory guidelines [67,110].

1.3.3. Chemical assessment

The evaluation of environmental contamination demands ongoing advancements in analytical instruments and methodologies to ensure the swift detection and accurate quantification of potentially harmful substances. Chemical analysis is crucial in assessing the TPs of EMs, due to its ability to elucidate their chemical characteristics and reactivity. By identifying and characterizing these TPs, it becomes feasible to assess their hazards, including toxicity, environmental persistence, and bioaccumulation potential.

1.3.3.1. Separation techniques

Since the late 1980s, liquid chromatography–mass spectrometry (LC-MS) has become the main analytical method for environmental monitoring. LC-MS presents several benefits for analyzing polar contaminants, including the capacity of analyzing a broad range of chemicals and the low overall time required for analysis [111].

1.3.3.1.1. Basic principles

In LC, a sample is introduced into a column that is packed with small, often porous particles. These particles are coated with a stationary phase on their porous surfaces. A solvent, known as the mobile phase, is forced through the column at high pressure and carries the sample components with it. Different interactions between the sample components, the stationary and the mobile phase, cause the analytes in the sample to move through the column at different speeds, based on their physicochemical properties. As a result, the sample components are separated and sequentially eluted from the column. The end of the column is connected to a detector, which records the compound signals as they are eluted. Advanced computer software then analyzes the detector signal, converting it into a chromatogram wherein peaks represent

the distribution of compounds as they leave the column. The area under the curve (AUC) of the peaks is proportional to the amount of each substance present in the sample.
Numerous laboratory studies use either classical high performance liquid chromatography (HPLC) or the more recent ultra-high performance liquid chromatography (UHPLC) for the analysis of TPs or EMs [112]. The major advantage of UHPLC is the use of smaller particle sizes (≤ 2 µm) over classical HPLC (between 3 and 5 µm) [113]. The smaller particles improve peak resolution within a shorter retention time (RT) and higher analytical sensitivity [113].

1.3.3.1.2. Retention mechanisms

Depending on the physicochemical properties of the analytes, a suitable surface chemistry for the sorbent particles can be selected. Generally, the separation of molecules is accomplished either by the size of the analytes or through different types of molecular interactions [114]. These include electrostatic interactions, van der Waals forces and dipole-dipole interactions. LC column types are distinguished by their separation modes, including normal-phase (NP) LC, reversed-phase (RP) LC, hydrophilic interaction liquid chromatography (HILIC), size-exclusion chromatography (SEC), and ion-exchange chromatography (IEC) [114]. Among these, RPLC columns are notably predominant, representing over 90% of all HPLC separations, and extensively used in environmental sciences [115].
Within RPLC, the most frequently used stationary phases are silica particles with bonded octyl (C8) or octadecyl (C18) chains conferring the hydrophobicity of the stationary phase. The mobile phase applied in RPLC typically consists of water, often buffered, and a water-miscible organic modifier like methanol or acetonitrile [116]. In RPLC, the retention of solutes increases with their hydrophobicity, the hydrophobicity of the stationary phase, and the polarity of the mobile phase. Separation occurs through partitioning, where analyte molecules fully dissolve into the bonded phase, and adsorption, taking place at the interface between the bonded phase and the solvent [115].
HILIC is an alternative LC mode to separate polar compounds. Similar to normal phase liquid chromatography (NPLC), HILIC columns have a polar stationary phase, *e.g.*, silica, amino or cyano, while the mobile phase is similar to those employed in RPLC, however, containing a much larger amount of organic modifier [117]. HILIC can also be used to analyze charged substances [117]. The underlying separation mechanism is not fully comprehended yet, and depends on the structure of the analyte and the physicochemical characteristics of both the stationary and mobile phases. The prevailing theory suggests that the primary factor influencing retention is the analyte's partitioning between the mobile phase and a partially immobilized layer of water on the stationary phase [118]. In HILIC, the selectivity and retention of compounds are primarily influenced by modifying the type and proportion of organic solvent,

adjusting the type and concentration of buffer, and changing the pH [117]. Generally, an increase in the fraction of organic solvent leads to greater retention of polar substances.
The pH impacts retention by affecting the ionization state of both the stationary phase and analytes. An ionized analyte, being more hydrophilic than its neutral counterpart, tends to exhibit stronger retention on HILIC columns. Furthermore, buffered mobile phases are often used to minimize electrostatic interactions between the analyte and the silanol groups on the stationary phase, and to enhance or reduce ion-exchange or ion exclusion interactions [118].

1.3.3.2. Two-dimensional liquid chromatography

In environmental analysis, conventional one-dimensional liquid chromatography (1D-LC) methods often lack sufficient separation power due to the complexity and heterogeneity of the analyzed matrices [119]. Therefore, the use of two-dimensional liquid chromatography (2D-LC) is a powerful tool to consider, especially when coupled to mass spectrometry (MS). 2D-LC leverages two distinct separation mechanisms to analyze a single sample, significantly enhancing the separation power [120]. Initially, the sample is introduced into a first column, or first dimension (^{1}D), where separation occurs. Subsequently, selected fractions from the ^{1}D effluent are transferred to a second dimension (^{2}D) for further separation. This process allows to resolve compounds that were not adequately separated using the ^{1}D retention mechanism alone. The enhanced separation efficiency of 2D-LC is often expressed in terms of peak capacity (n_c), where the peak capacity of the 2D-LC separation is calculated as the product of the peak capacities of the individual dimensions. However, in practice, several correction factors must be applied to account for orthogonality and undersampling, which is the loss of resolution of analytes obtained from the ^{1}D due to the recombination of those analytes during the sampling process (e.g., in a sample loop) [120].
In 2D-LC, orthogonality between the ^{1}D and ^{2}D is crucial. Orthogonality implies that the two employed separation mechanisms operate independently and exhibit unique retention behaviors, offering different selectivities [121]. However, true orthogonality is technically difficult to achieve, as orthogonality depends on the separation mechanisms, the properties of the solutes and the separation conditions. Due to their complementary selectivity, RPLC and HILIC are often considered for 2D-LC separations [117]. However, a significant challenge arises from the fact that the high-organic mobile phases used in HILIC exhibit strong elution in RPLC, and conversely, mobile phases with high water contents common in RPLC are strong eluents in HILIC. This poses significant difficulties especially for online HILIC×RPLC or RPLC×HILIC configurations with direct fraction transfer from the ^{1}D to the ^{2}D through a switching valve interface and can result in reduced resolution, peak asymmetry, and even split peaks in the ^{2}D [122].

1.3.3.2.1. Types of two-dimensional liquid chromatography

2D-LC can be categorized into various types based on several criteria [123]: (i) the method of transferring effluent from the ^{1}D to the ^{2}D which distinguishes online and offline modes; and (ii) the number of fractions from the ^{1}D effluent that are transferred to the ^{2}D, leading to further classification into (multiple) heart-cutting (LC–LC) and comprehensive (LC × LC) 2D-LC.

In offline 2D-LC, fractions derived from the ^{1}D effluent are collected offline and subsequently introduced into the ^{2}D. This approach offers certain advantages, including straightforward instrumentation, flexibility in sample handling between the two-dimensional analyses, and the potential for slower separations in the ^{2}D [124]. Drawbacks include prolonged analysis times, challenges in automation, and the risk of losses and contamination during fraction collection [124]. Online applications involve the automatic collection and real-time transfer of fractions from the ^{1}D to the ^{2}D through a modulator, typically a valve, connecting both dimensions [125]. Furthermore, 2D-LC can be categorized into LC–LC and LC × LC based on how fractions are transferred to the ^{2}D. A visual representation of these techniques and their hybrid implementations is depicted in **Fig. 1.8**.

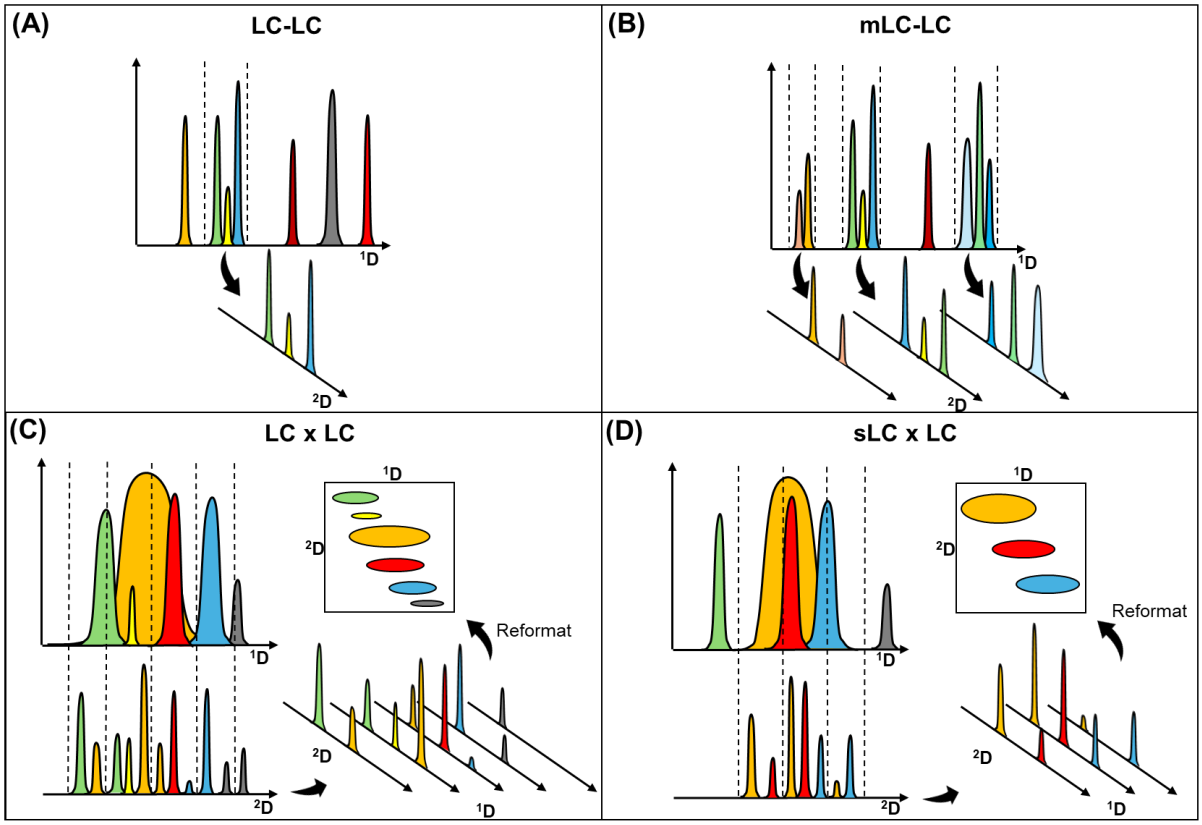

Figure 1.8 – Schematic representations of the various 2D-LC techniques and hybrid implementations, including **(A)** heart-cutting (LC–LC), **(B)** multiple heart-cutting two-dimensional liquid chromatography (mLC–LC), **(C)** comprehensive (LC × LC), and **(D)** selective comprehensive (sLC × LC) methods. Based on [126,127].

In LC–LC, a single fraction is collected and introduced into the ^{2}D. This approach enables the resolution of target compounds that co-elute in ^{1}D. Importantly, the analysis time in the ^{2}D is independent of the ^{1}D run time, allowing the use of longer ^{2}D columns and extended ^{2}D gradients with durations exceeding the ^{1}D sampling time, enhancing separation efficiency. A notable drawback of this technique is the loss of information for the peaks in the ^{1}D effluent that are not collected, as they cannot be analyzed while the gradient is still progressing in the ^{2}D [120]. Conversely, in LC × LC mode, the entire effluent from the ^{1}D is transferred and analyzed in the ^{2}D to maximize the information acquired from complex samples. In this mode, high-frequency sampling during the transfer to the ^{2}D is necessary to ensure the preservation of the separation achieved in the ^{1}D. This requirement leads to typical LC × LC operations characterized by reduced flows in the ^{1}D, and fast gradients, shorter columns, and elevated flow rates in the ^{2}D [123]. This configuration ensures that each cycle in the ^{2}D corresponds to the collection time of the ^{1}D effluent. Compared to LC–LC, LC × LC enables the acquisition of more comprehensive details about the composition of a sample. However, this additional information often introduces complexity to the instrumentation and may result in a potential loss of data from the ^{1}D separation due to undersampling. Additionally, in most cases, a ^{2}D flow splitting system is required as the high flow rates essential for ^{2}D separation are not compatible with coupling to MS [123].

To overcome the challenges posed by these methods, hybrid approaches have been introduced. Among these, multiple heart-cutting 2D-LC (mLC–LC) is an attractive alternative to LC–LC. This method allows to collect and preserve different fractions of the ^{1}D effluent simultaneously, even as one fraction undergoes analysis in the ^{2}D [120]. The various fractions from ^{1}D are stored in loops connected through additional valves, necessitating a complex arrangement of valves [120]. Specifically, one valve facilitates the connection between the ^{1}D and ^{2}D phases, while two other valves house the loops for storing the ^{1}D fractions until they are analyzed in the ^{2}D column.

In 2012, Groskreutz et al. introduced a hybrid approach that bridges the gap between LC–LC and LC × LC, known as selective comprehensive 2D-LC (sLC × LC) [128]. This technique enhances the analysis by modulating a targeted peak from the ^{1}D into multiple fractions, which are then individually injected into the ^{2}D column. A key advantage of sLC × LC over traditional heart-cutting methods is its ability to capture detailed information from specific regions of interest within the ^{1}D peak. By transferring the entire volume of a ^{1}D target peak to the ^{2}D, it ensures a comprehensive transfer of information, thereby minimizing the potential for data loss [120]. Moreover, sLC × LC offers the benefit of separating the timing of ^{1}D separations from the analysis of the fractions in the ^{2}D, allowing for rapid separations in the ^{1}D with precise sampling of the peak fractions. This precise fractionation helps to avoid the remixing effect that can occur when multiple peaks are present within the same ^{1}D fraction due to undersampling

[128]. While the setup for sLC × LC is more complex, it is noteworthy that similar equipment can be utilized for both sLC × LC and mLC–LC, despite the differences in their implementation.

1.3.3.2.2. Modulations strategies

Efforts to achieve maximal orthogonality between the two separation dimensions often give rise to compatibility issues such as solvent mismatch. To address these challenges, various modulations strategies and interfaces have been developed, rendering online 2D-LC one of the most adaptable and versatile techniques available. Among the various interfaces available, electronically controlled switching valves are commonly preferred [126]. For a successful transfer of fractions from the ^{1}D to the ^{2}D, valves are typically connected to sampling loops, trapping columns, or parallel columns [129]. Sampling loops are most frequently employed due to their simplicity [130]. The choice of the loop size is critical, as it dictates the volume of ^{1}D effluent collected and transferred to the ^{2}D column. Employing sampling loops larger than necessary for the ^{1}D fraction can enhance the ^{2}D separation efficiency as the excess loop volume, not filled by the ^{1}D fraction, gets filled with the mobile phase from the ^{2}D, diluting the transferred fraction with a solvent compatible with the ^{2}D phase [131]. Additionally, the impact of the parabolic flow profile of the sample in the loop, must be considered. To counteract the potential loss of ^{1}D effluent due to this effect, it is advised to ensure the volume of the ^{1}D fraction collected does not surpass two-thirds of the loop volume [132].

When modifications are made to the fractions between the ^{1}D and the ^{2}D, beyond merely collecting ^{1}D fractions, this process is known as "active modulation." Various techniques for active modulation exist, including the use of stationary-phase-assisted modulation, vacuum-evaporation modulation, or active-solvent modulation (ASM). The ASM method, introduced by Stoll et al., stands out as a particularly innovative approach [133]. This valve-based strategy facilitates the dilution of the ^{1}D solvent with a weak solvent by incorporating a parallel flow through an ASM capillary before the sample is reintroduced into the ^{2}D [133]. An advantage of this method is that it allows high quality 2D-LC separations with a fast ^{2}D re-equilibration [133].

1.3.3.3. Mass spectrometry

Mass spectrometry (MS) is a predominant analytical tool in environmental analysis due to its high sensitivity, selectivity, mass accuracy and high-throughput. The principle of MS involves the creation of ions from the sample molecules in a gas phase. These ions are then distinguished and measured based on their mass-to-charge ratio (m/z), with their detection signal reflecting their relative abundance. Essentially, a mass spectrometer comprises the ion source, where sample molecules are ionized into gas-phase ions, the mass analyzer, which separates the ions based on their m/z, and the detector, where the ions are ultimately detected.

1.3.3.3.1. Ionization sources

The initial step in MS involves transforming the target analytes from their liquid or solid state into ionized species in the gas phase. Various ionization methods exist, each offering unique benefits and suitability for particular applications. The selection of the ionization technique can greatly influence the outcome of the MS analysis, affecting analytical method parameters such as the lower limit of detection and the linear dynamic range. Most notable for the environmental analyses in this thesis are atmospheric pressure ionization (API). The ionization mechanisms occurring in API sources are of low energy, leading to minimal in-source fragmentation which helps to identify the molecular mass of the analyte. These "soft-ionization" techniques generate spectral data rich in molecular or protonated molecule information. API can be realized by electrospray ionization (ESI), atmospheric pressure chemical ionization (APCI), and atmospheric pressure photoionization (APPI), among which ESI is the most widely used in LC-MS [134]. The selection of a specific ionization source is primarily influenced by the polarity and size of the target compounds (**Fig. 1.9**).

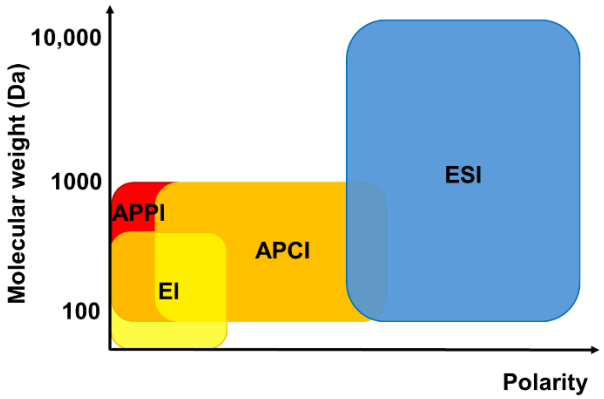

Figure 1.9 – Ionization range of different ion sources as a function of compound polarity and molecular weight. Adapted from [135].

APPI and APCI are predominantly used for ionizing small, relatively nonpolar molecules, which tend to be poorly ionized with ESI [136]. ESI is preferred for ionizing substances with moderate to high polarity across a larger range of molecular weight, covering a vast array of pharmaceuticals and proteins. Fundamentally, the ionization process in ESI and APCI adheres to acid-base principles [136]. In positive mode (ESI+ or APCI+), molecules primarily undergo protonation to form $[M+H]^+$ ions with an m/z value of (M+1). Conversely, in negative mode (ESI- or APCI-), ions are formed through deprotonation to yield $[M–H]^–$ with an m/z value of (M–1). Additionally, the formation of adducts such as $[M+Na]^+$, $[M+K]^+$, and $[M+NH_4]^+$ in ESI+, and $[M+Cl]^–$ and $[M+CH_3COO]^–$ in ESI-, is also possible depending on the additive used. Although API sources generate minimal in-source fragmentation, they are significantly challenged by matrix effects (MEs). These effects, which can suppress or enhance signals during ionization, occur due to the co-elution of analytes with endogenous compounds in the sample [137].

The impact of these matrix effects varies widely among compounds and is notably more pronounced with ESI as opposed to APCI, and to a lesser extent, APPI [138]. This can be attributed to the fact that in APPI, the ionization of analytes is influenced by their ionization energy rather than their proton affinity [137]. One of the main strategies to address matrix effects is the use of isotopically labeled standards which act as internal standards, closely mimicking the chemical and physical properties of the analytes of interest. This approach ensures that any signal suppression or enhancement experienced by the analyte during the ionization process is equally reflected in the behavior of the isotopically labeled standard [138].

1.3.3.3.2. Mass analyzers

Commonly employed mass analyzers include the quadrupole, ion trap (IT), time-of-flight (TOF), Orbitrap and Fourier-transform ion cyclotron resonance (FT-ICR) [139]. These mass analyzers can be hyphenated with a quadrupole to enhance their selectivity and sensitivity [140]. TOF detectors are often combined with a quadrupole (Q-TOF), a configuration prominent in environmental analysis for integrating both qualitative and quantitative capabilities [139,141]. Q-TOF instruments offer high mass resolution and high scan speed, making them ideal for analyzing environmental samples [142]. A concise summary of commercially available MS used with LC is provided in **Table 1.1**.

Triple quadrupole (QQQ) or quadrupole linear ion trap (QLIT) mass spectrometers (MS) offer superior sensitivity when the third quadrupole operates in linear ion trap mode [143]. These devices are utilized in tandem MS (MS/MS) to isolate the molecular ion of the target compound in the initial stage of the mass analyzer and achieve selective precursor-product ion transitions, through selected reaction monitoring (SRM) [144]. The second quadrupole functions as a collision cell, differing from the first one by fragmenting a precursor ion and focusing the resulting product ions into the third quadrupole. While both QQQ and QLIT instruments boast a broad linear dynamic range, spanning at least three orders of magnitude, QQQ instruments are generally 10–20 times more sensitive than IT when operated in SRM mode [144]. Although IT instruments are less commonly used for quantitative analyses, they offer several benefits over QQQ instruments: they are more compact, less expensive, and capable of trapping and accumulating ions to enhance the signal-to-noise ratio [144,145]. Furthermore, IT devices can perform multi-stage fragmentation (MS^n) analyses, a feature particularly useful for identifying TPs by allowing to propose fragmentation pathways, which might not be as discernible in the product ion spectra of QQQ instruments [112]. MS instruments that incorporate QQQ and, to a lesser extent, QLIT, are known for their high sensitivity and selectivity but are limited by operating at unit resolution [140]. Moreover, QQQ provides a diminished sensitivity in full-scan mode, which constrains their capacity to effectively detect unknown substances [140].

Table 1.1 – Comparison of commercial mass analyzers in LC-MS instruments. The presented figures represent commonly achievable values on commercially available instruments. Values are highly dependent on experimental setup and the specific instrument and should be considered an estimate only. Based on [140,147].

Detector	Mass resolution	Mass accuracy (ppm)	Scan Rate	MS/MS	Dynamic range	Advantages	Limitations
Triple quadrupole	Unit resolution	100 - 1000	Moderate	MS^2	10^7	- High selectivity and sensitivity in SRM mode	- Low sensitivity in full-scan mode
Ion trap	1000-2000	100 - 500	Fast	MS^n	10^{3-4}	- Moderate to high sensitivity in full-scan mode - Moderate sensitivity in SRM mode	- Limited capacity for ion storage
TOF	10.000-50.000	<2 - 10	Fast	MS^2	10^5	- Compatible with fast UHPLC - High sensitivity in full-scan mode	- Less sensitive than QQQ for quantitative purposes - Not able to perform MS^n
Orbitrap	7500-480.000	<5	Moderate	MS^n	10^{3-4}	- Moderate to high sensitivity in full-scan mode - Large space charge capacity	- Not fully UHPLC compatible at high resolution
FT-ICR	100.000-1.000.000	<2	Slow	MS^n	10^{3-4}	- Very high mass resolution power - Sensitivity in full scan mode	- Not compatible with fast UHPLC separation - Very expensive

Legend: MS/MS: tandem mass spectrometry, MS^2: two-stage fragmentation, MS^n: multi-stage fragmentation (n> 2), SRM: selected reaction monitoring, UHPLC: ultra-high performance liquid chromatography, QQQ: triple quadrupole, FT-ICR: Fourier-transform ion cyclotron resonance mass spectrometry.

In high resolution mass spectrometry (HRMS), full spectral scans are obtained across the entire chromatographic run with high mass-resolving capacity. This resolving power, critical for distinguishing closely adjacent mass peaks, is quantified by the ratio between the m/z of the measured ion and the full width at half maximum (FWHM) [146]. To achieve near-baseline resolution between two neighboring mass peaks, their mass difference should be at least double the FWHM value [146]. Therefore, enhancing the resolving power in HRMS is crucial, as it improves the ability to differentiate target ions from both background noise and naturally occurring substances, thereby decreasing the likelihood of encountering (partially) unresolved analytes because of interference from isobaric ions [139].

The significance of high mass resolution is that it enables more accurate and precise mass (m/z) measurements, thus enhancing identification capabilities beyond those achievable with unit-resolution mass spectrometry. The uncertainty in mass measurement, which includes both mass accuracy (the average mass error) and mass precision (standard deviation on the mass error), is determined by calculating the relative (ppm) or absolute (mDa) difference between the experimentally measured accurate mass and the theoretically calculated exact mass of an analyte [146,148]. Accuracy and precision in mass measurements are critical for the reliable determination of accurate masses, and identifying the various sources of mass measurement uncertainty can lead to significant improvements.

While precise mass accuracy may facilitate the prediction of a molecule's formula, it provides limited structural information. Consequently, it becomes necessary to gather further data, such as fragmentation spectra, to gain insight into the molecule's structure. The fragmentation spectra of an ion contain extensive structural information as they reflect the relative bond energies and the structures of both the precursor ion and the resulting product ions [147]. Collision-induced dissociation (CID) involves the activation of a precursor ion through collision with a neutral gas, leading to its fragmentation into various product ions [147]. This fragmentation can be carried out in the collision cell of a quadrupole or within an ion trap, using low collision energies [139]. Another prevalent form of fragmentation is high-energy collision-induced dissociation (HCD), which takes place in the HCD cell of an Orbitrap instrument. Despite the availability of different fragmentation techniques, CID is widely documented in literature and remains the most commonly reported fragmentation method in databases [147].

1.3.3.3. Data analysis

HRMS has enabled the extensive characterization of environmental samples, allowing to detect hundreds to thousands of features in a single sample across wide mass and dynamic ranges. However, it has led to a relatively new challenge: managing the large volume of generated data.

Although chromatographic separation helps to reduce the complexity of samples and improve the sensitivity and specificity of detection, data analysis strategies are nevertheless required to identify unknown substances. Targeted analysis, suspect screening, and nontarget screening (NTS) are chemical analysis approaches that cover a progressively wider range of analytes [112,140,149]. **Fig. 1.10** provides a detailed comparison of these distinct screening methodologies.

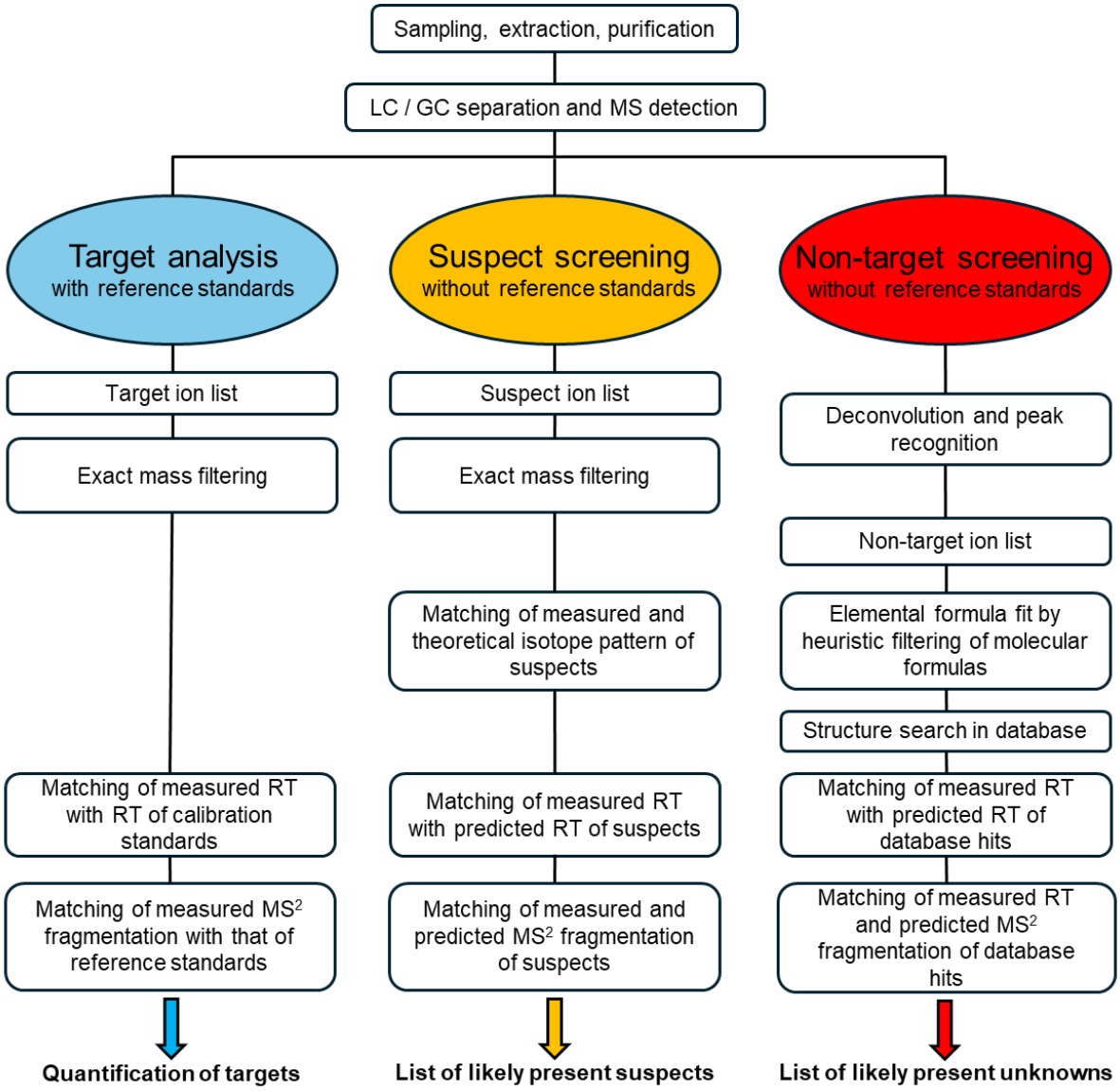

Figure 1.10 – Comparison of systematic approaches for (i) quantitative analysis of targets using reference standards, (ii) screening of suspected compounds without reference standards, and (iii) non-targeted screening for unknown substances in environmental samples utilizing LC-high resolution (tandem) mass spectrometry. LC: liquid chromatography GC: gas chromatography; MS: mass spectrometry; MS^2: two-stage fragmentation. Adapted from [140].

In target analysis, reference standards are used to produce precise, authentic but finite data, including chromatographic RT, quasi-molecular ions (i.e., MS^1 or precursor ions), and

fragmentation spectra (i.e., MS^2 or product ions) [149,150]. This data is then matched against features in the observed mass spectrum. According to the European Union's Decision 2002/657/EC, the confirmation of compound identification through HRMS requires matching a precursor ion and a significant product ion, or two significant product ions [150].

Suspect screening does not rely on reference standards for identification and quantification. This is particularly relevant as reference standards are often unavailable for EMs and especially TPs [149]. However, it is necessary to have specific information about the compounds' molecular formula and structure beforehand. This information aids in creating a suspect ion list with identification references based on theoretical monoisotopic masses, isotopic patterns, chromatographic retention indexes (RIs), and MS^2 spectra available in public databases. *In silico* tools for the prediction of chromatographic RT through RIs or MS^2 fragmentation simulation can also be used. Moreover, molecules containing halogens like chlorine (Cl) and bromine (Br) facilitate the chemical formula attribution due to their distinctive isotopic patterns. The reference data of the suspect list is then compared with the recorded multidimensional data to identify positive matches.

Non-target screening (NTS) focuses on investigating the multidimensional data without a priori chemical information [112]. This requires utilizing the monitored data efficiently to systematically exclude molecular structures of potential candidates that do not match, easing the tentative identification of unknown compounds [150]. Once HRMS data have been recorded and processed, each precisely measured ion (and/or its elemental formula determined by heuristic rules) is compared to available chemical databases such as PubChem, ChemSpider, Metlin, and MassBank for potential matches [150]. The chromatographic RT and fragmentation patterns of all candidates, whether from public data or predicted, are then compared against the recorded data to seek evidence for identification.

Suspect screening can be seen as a method within NTS for rapidly identifying known organic pollutants from an unknown standpoint, referred to as "Known Unknowns” [151]. From this angle, employing a data-mining strategy that leverages the molecular features of known pollutants is advantageous for managing the complexities of multidimensional data in the search for "Unknown Unknowns" [150].

However, it is important to acknowledge that the risk of misidentification in NTS is significant for several reasons. Firstly, isomers are frequently found among TPs, and distinguishing them can be challenging, particularly when they exhibit similar fragmentation patterns or when they are not effectively separated [152]. Secondly, the detection of specific analytes may be obstructed by interfering substances, although the enhanced resolution offered by modern HRMS has somewhat mitigated this problem [150,152]. Thirdly, it is possible that a compound in the sample is not detected by HRMS, because the compound can get lost at any stage of the analytical process or may not ionize as expected [153,154].

Consequently, it is crucial to thoroughly validate the entire process by employing a variety of reference standards and conducting a comparative analysis based on the suspected compounds' predicted physicochemical properties to reduce the likelihood of false negatives [155]. Moreover, establishing a cohesive analytical workflow that integrates sample preparation, data collection, pre-processing, quality assurance and control, data-mining, and structural elucidation is also critical [150]. Such a workflow should be well-adjusted to ensure a focus on the appropriate range of analytes, collect extensive chemical information, and prioritize key chemical features.

Drawing from the guidelines set by the Metabolomics Standards Initiative (MSI), a tailored confidence level system for NTS in environmental analysis has been suggested and broadly accepted [156]. This system categorizes structure elucidation into five levels of confidence (**Fig. 1.11**): confirmed structure (Level 1), probable structure (Level 2), tentative candidate (Level 3), unequivocal molecular formula (Level 4), and exact mass only (Level 5).

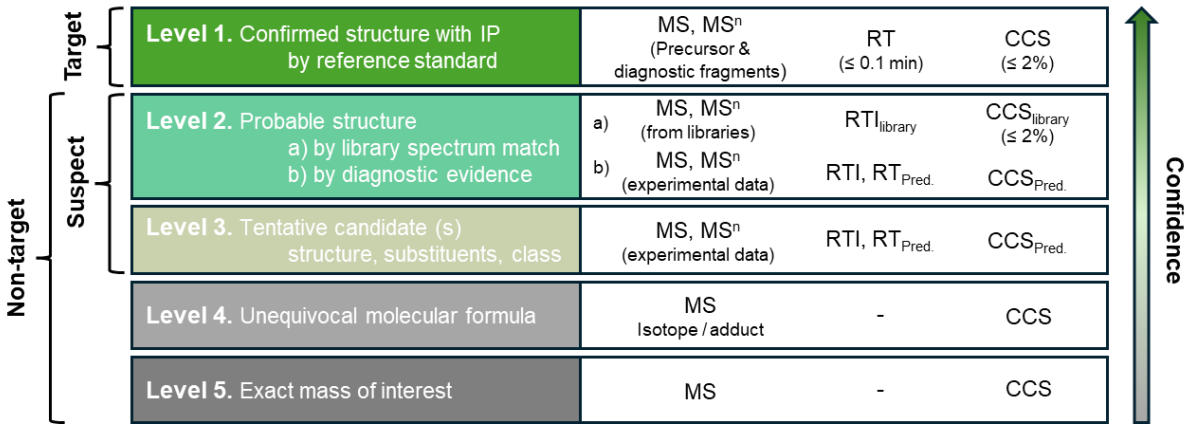

Figure 1.11 – Identification confidence levels in high resolution mass spectrometric analysis. MS: accurate mass of the precursor ion, MS^n: accurate mass of the fragment ions, RT: retention time; RTI: retention time indexing systems; CCS: collision cross-section; sub index library: value in available library; sub index Pred: obtained value with a predictive models applied. Adapted from [157].

Level 1 is the structural confirmation by matching MS^1, MS^2, and RT to an authentic reference standard. Level 2 implies a high probability of the exact structure, identified either through matching with literature or library spectra where the link between spectrum and structure is clear (Level 2a), or supported by specific MS^2 fragmentation patterns, ionization characteristics, or information about the parent compound (Level 2b). Level 3 indicates potential structures but lacks information for a definitive identification, such as for positional isomers. Levels 4 and 5 confirm only the elemental composition and the measured m/z value, respectively. An enhanced communication system that incorporates RI and collision cross-section (CCS) data has recently been introduced [157]. This new layer of information offers

additional structural insights that can help distinguish between isomeric structures, potentially elevating the confidence level of identifications.

CHAPTER 2

Research Objectives



Agriculture, industry and domestic activities around the world are releasing a multitude of potentially toxic emerging micropollutants (EMs), mainly through wastewater, leading to an increasing occurrence of contaminants in aquatic environments. Consequently, wastewater treatment is needed to remove these micropollutants and ensure the safety and cleanliness of water for both human consumption and ecological health. Among the various remediation technologies, electrochemical advanced oxidation processes (eAOPs) stand out for their efficiency in generating potent oxidants. However, the emergence of transformation products (TPs) through these processes, whose chemical and biological properties are largely unknown, underscores the need for a holistic chemical and toxicological assessment. These complementary evaluations are crucial to ensure the safety of using such technologies in water treatment applications.

The overarching goal of this doctoral thesis is to thoroughly assess the generation and impact of TPs from key EMs by adopting an effect-driven approach (EDA). This entails a comprehensive examination from electrochemical degradation efficiency to structure elucidation of the generated TPs and respective toxicological assessments, aimed at determining the safety and efficacy of eAOPs in water treatment. The specific objectives of this PhD thesis are as follows:

i. Technological advancement in analyzing EMs and their respective TPs

The detection and identification of EMs and their TPs is challenging due to the vast number of mostly unknown compounds, their often-low concentrations and the complexity of the matrices in which they are present. There is hence a need to develop robust, comprehensive analytical techniques that allow the analysis of a large variety of molecules generated during wastewater treatment. **Chapter 3** presents a comparative analysis between an in-house developed heart-cutting 2D-LC setup and a commercially available 2D-LC system. This comparison is aimed at addressing the complexity of samples treated by eAOPs by optimizing the analysis of 28 representative pharmaceuticals and pesticides with a broad range in polarity. The setups are compared in terms of cost of the systems, flexibility, ease of implementation, and robustness.

ii. Chemical and biological assessment of TPs generated by eAOPs

Currently, there is a substantial knowledge gap in understanding the reaction mechanisms that yield TPs during eAOPs, leading to challenges in predicting their molecular configurations.

Furthermore, it is crucial to address the significant knowledge gap regarding the toxic effects of TPs, particularly their potential to be as hazardous, if not more, than the original compounds. The second part of the thesis therefore focuses on the electrochemical degradation of two environmentally relevant endocrine-disrupting chemicals (EDCs), particularly in the structure elucidation of the formed TPs by LC-HRMS and their endocrine-disrupting assessment using *in vivo* transgenic models. **Chapter 4** describes the electrochemical degradation of 17α-ethinylestradiol (EE2), a powerful synthetic steroidal estrogen that is capable of inducing sex changes in fish at very low concentrations, and therefore introduced in the first Watch List. This chapter evaluates the degradation efficiency and the estrogenic activity of TPs by correlating the analytically measured EE2 concentrations with the sample hormonal equivalent determined through the estrogenic bioassays. **Chapter 5** explores the electrochemical decomposition of diclofenac (DCF), a prevalent non-steroidal anti-inflammatory drug (NSAID), also listed in the first Watch List. Classified as an EDC with multiple MoAs, the investigation extends to examine whether the electrochemically degraded TPs exhibit thyroid activity and aims to provide more insights into the environmental risk assessment of TPs generated by engineered processes.

CHAPTER 3

Detailed comparison of in-house developed and commercially available heart-cutting and selective comprehensive two-dimensional liquid chromatography systems

In-house 2D-LC

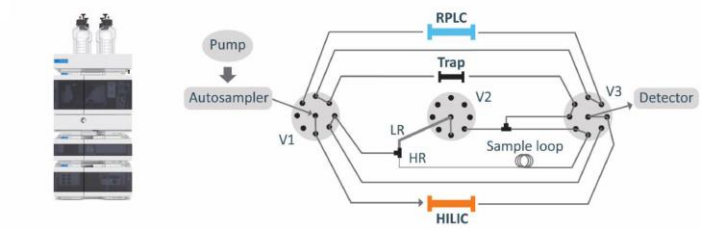

VS

Commercial 2D-LC

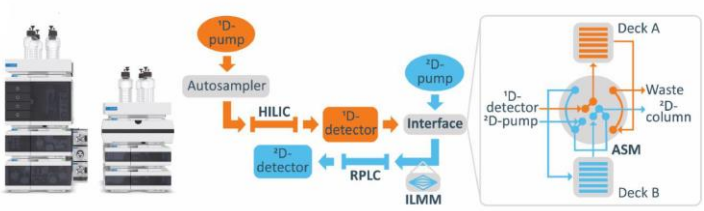

Based on: M. Pardon‡, R. Reis‡, P. de Witte, S. Chapel, D. Cabooter, *Detailed comparison of in-house developed and commercially available heart-cutting and selective comprehensive two-dimensional liquid chromatography systems*, Journal of Chromatography A, 1713 (2024) 464565.

‡authors contributed equally

3.1. Introduction

Complex samples, containing a large number of compounds with diverse physicochemical properties, are increasingly encountered in various research fields, including environmental [119,158], food [123,159], (bio-)pharmaceutical analysis [160], proteomics [161,162], metabolomics [163,164] and lipidomics [127,165,166]. The characterization of these complex samples remains extremely challenging, due to the high separation power required for their adequate analysis [167].

To improve the separation power in liquid chromatography (LC), several strategies have been proposed, including the use of small particle packed columns operated at ultra-high pressure (UHPLC) [168], core-shell particles [169], monolithic stationary phases [170] and improvements in LC-mass spectrometry (LC-MS) instruments [171]. However, despite the impressive improvement in separation efficiency and peak capacity these developments offer, they are often still inadequate for very complex samples [122]. In such cases, two-dimensional liquid chromatography (2D-LC) can provide a solution. In 2D-LC, (part of or the entire) effluent of a first separation dimension (^{1}D) column, typically containing unresolved peaks, is sent to a second-dimension (^{2}D) column for further separation [122]. When the separation mechanisms in both dimensions are sufficiently different or *orthogonal*, this results in an increased peak capacity [163,167,172]. Online 2D-LC approaches, wherein the ^{1}D-effluent is automatically sent to the ^{2}D using one or multiple switching valves equipped with sampling loops, are mostly used, because of the better reproducibility, reduced sample contamination and faster operation. On the other hand, offline approaches wherein the ^{1}D-effluent is temporarily collected offline before reinjection into the ^{2}D-column are typically less complex than online approaches, however, at the cost of being more time-consuming, less repeatable, and with an increased risk of sample contamination [173].

As explained in the general introduction (**Chapter 1**), two main modes of 2D-LC exist: full comprehensive (LC × LC) and heart-cutting (LC-LC) 2D-LC. Variations of these two modes are also possible, including multiple heart-cutting 2D-LC (mLC-LC) and selective comprehensive 2D-LC (sLC × LC), which samples specific regions of the ^{1}D-separation in a comprehensive manner [120]. The key advantage of sLC × LC is its ability to break the link between the timescales of the ^{1}D- and ^{2}D-separations, allowing to address practical challenges related to undersampling and solvent incompatibility. This advantage shows similarities to those derived from the offline 2D-LC approach, without the major drawbacks [128].

To achieve the highest possible resolving power for a 2D-LC method, the combined LC modes need to be complementary. This can be obtained by selecting different stationary and mobile phases in both dimensions. An important problem encountered when combining different separation mechanisms is their typical mobile phase incompatibility [132,174].

An example is the combination of hydrophilic interaction liquid chromatography (HILIC) and reversed-phase LC (RPLC), a useful combination for the analysis of samples containing compounds with a broad variety in polarity, as encountered in environmental, pharmaceutical and natural product analysis, metabolomics and proteomics [175–180]. The challenge for this specific combination is the opposite elution strength of their mobile phases [179]. In HILIC, the mobile phase typically contains a high percentage of acetonitrile (ACN), which is a strong eluent in RPLC. Together with the effect of a much larger injection volume compared to one-dimensional LC (1D-LC), the transfer of large ACN-rich fractions from ^{1}D-HILIC can negatively impact the peak shapes obtained in ^{2}D-RPLC [132,176,181].

If HILIC is used in the second dimension, the same problem arises, now caused by the large water-rich fractions transferred from ^{1}D-RPLC. This may result in band broadening, peak distortion, and/or analyte breakthrough, affecting the ^{2}D-separation by decreasing both the peak capacity and peak intensity [132,176]. Different strategies to deal with this mobile phase incompatibility have recently been explored [125,129,182]. In general, these include strategies to modify the composition and/or the volume of the fractions transferred from the first to the second dimension using either flow splitting [183–186], in-line mixing modulation (ILMM) [187], on-line dilution (with trapping columns [176,188,189] or sample loops/capillaries [179,190–192]), and solvent evaporation [193,194].

Despite these complications, the essential concepts of LC-LC and LC × LC were already introduced in the 1970s [165,195]. However, the number of publications involving 2D-LC only started to increase in the 1990s [196], and have seen a surge in the past decade [160]. An important factor in this increasing popularity is the transition from in-house developed 2D-LC instruments, originally used to investigate and improve the technology, to commercially available 2D-LC systems, offering a wide range of applications in a relatively straightforward way, making this technique accessible to less experienced users [120].

Commercially available 2D-LC systems can typically be used in various configurations, including single LC-LC, multiple LC-LC (mLC-LC), sLC × LC, and LC × LC, due to the presence of valves containing multiple sample loops. To deal with the mobile-phase incompatibility, different solutions are available. One example, called active solvent modulation (ASM), is a valve-based approach using a bypass capillary to dilute the ^{1}D-effluent with a weak solvent (compared to the ^{2}D-column) prior to transfer to the ^{2}D-column. The dilution solvent is provided by the same pump as used for the ^{2}D-separation, making this a relatively simple approach to implement in a 2D-LC setup. The dilution factor (DF) results from the split ratio between the ASM bypass capillary and the valve containing the sample loops (‘deck’), and depends on the backpressures generated by the flow path through the ASM bypass capillary and the flow path through the deck (**Fig. 3.1**). The DF can be changed by changing the dimensions of the ASM bypass capillary [133].

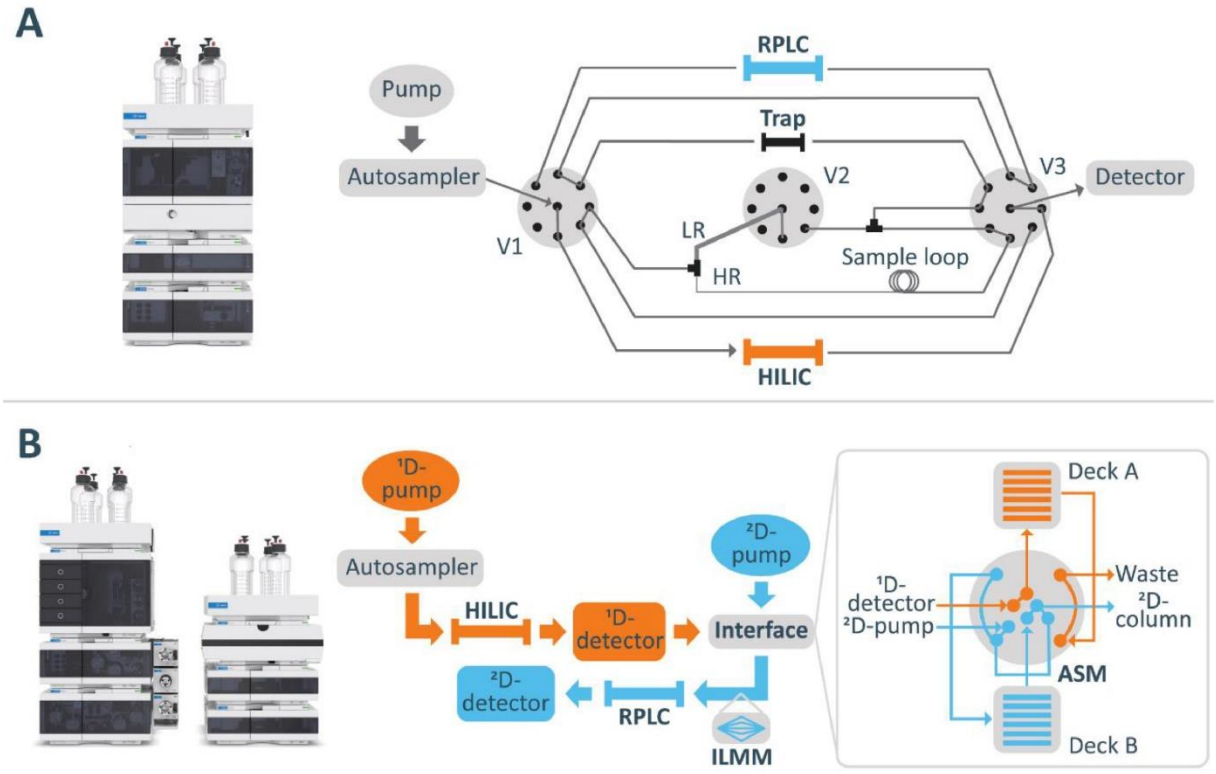

Figure 3.1 – Overview of the in-house developed (**A**) (V: valve, HR/LR: high/low restriction capillary) and the commercial (**B**) 2D-LC setup (ASM: Active Solvent Modulation, ILLM: In-line mixing modulation). (Images taken from Agilent Technologies [197,198]).

Despite the increasing popularity of these commercial 2D-LC solutions, 2D-LC separations can also be performed on simpler, in-house modified 1D-LC systems. As an example, our research group developed an LC-LC setup that combines HILIC in ^{1}D with RPLC in ^{2}D, allowing to analyze polar and non-polar compounds within a single chromatographic run, using a single quaternary pump [176]. In this approach, HILIC and RPLC columns are combined using high-pressure switching valves that allow redirecting unretained non-polar compounds eluting from the HILIC column to a sample loop. To address the mobile phase incompatibility between both separation modes, an innovative mixing unit is used to dilute the ^{1}D-effluent in the sample loop before performing the ^{2}D-separation. This dilution process is based on a similar mechanism as the ASM approach. The mixing unit is assembled by interconnecting two restriction capillaries of different dimensions using three high-pressure switching valves and two T-pieces (**Fig. 3.1**). The sample loop is connected in series with a restriction capillary characterized by a high backpressure, which, in turn, is interconnected in parallel with a restriction capillary with a significantly lower backpressure. By applying a highly aqueous mobile phase through both restriction capillaries, the highly organic mobile phase containing the non-polar compounds in the sample loop is diluted to achieve a mobile phase composition suitable for the subsequent RPLC analysis.

To ensure this dilution can be achieved at a sufficiently high flow rate, the non-polar compounds are first sent to a short RPLC trap column with a low backpressure after dilution. Subsequently, the trap column is connected to the RPLC column for analysis. This setup was shown to be capable of separating a mixture of common pharmaceuticals with a wide range in polarity (LogD values between -5.75 and 4.22) with satisfactory recoveries (between 82% and 99%) and repeatability [176]. Since only one pump is used for the entire operation, the separation can moreover be visualized in a single chromatogram, hence no specialized 2D-LC software is required. However, the setup in its current form only allows single heart-cutting 2D-LC analysis.

This study aims to investigate for the first time the capabilities of the in-house developed 2D-LC setup in-depth and compare it with a commercial 2D-LC system for a more complex sample of 28 pharmaceuticals and pesticides with a wide polarity range, as typically encountered in environmental analysis. Special attention is paid to the optimization of the different modulation mechanisms of both systems, especially regarding the different strategies to deal with the mobile phase incompatibility between HILIC and RPLC. On-line dilution on the commercial 2D-LC system is obtained via ASM and compared to the approach using restriction capillaries and a trap column in the in-house developed setup. For the commercial instrument, both LC-LC and sLC × LC are considered, while the in-house developed setup is only operated in LC-LC. An alternative approach to deal with the mobile phase incompatibility, called in-line mixing modulation (ILMM), is also considered for the commercial instrument [187]. ILLM is achieved by installing a commercially available in-line mixer (Jet Weaver, JW) in front of the ^{2}D-column (**Fig. 3.1**). JWs are normally installed after the LC pump head and used to homogenize mobile phases with different strengths and viscosities. They contain a three-dimensional multichannel flow path that distributes the flow at its inlet into multiple partial flows and recombines them again at the outlet. In ILLM, the DF can be changed by using a combination of JWs of various volumes [176,187]. A recent publication compared the performance of ILMM (using JWs with volumes of 35, 100 and 380 µL) to ASM (DF of 5) in various 2D-LC setups. In general, for larger ^{1}D-fractions, ASM was not sufficient to deal with the mobile phase incompatibility in each setup, while ILMM did improve the ^{2}D-peak shapes when larger JW mixer volumes were used for larger fractions, even in a higher solvent incompatibility scenario (higher transfer volume) in the LC × LC mode [187].

The two set-ups considered in this chapter are evaluated based on obtained peak shapes, peak widths and recoveries, as these are important parameters for an accurate quantification of compounds of interest in real samples, in addition to differences in analysis time. A more general comparison is also made based on the cost of the systems, their flexibility, ease of implementation, and robustness. Since both set-ups use components from the same vendor, any bias in terms of performance and cost price is moreover excluded.

3.2. Materials & methods

3.2.1. Chemicals

Caffeine, progesterone, pipamperone, bezafibrate, atenolol, metolachlor, (4)-nonylphenol, and ketoprofen were obtained from Sigma-Aldrich (Diegem, Belgium), sulfamethoxazole from Roche (Mannheim, Germany), ibuprofen and lidocaine from Certa (Braine-l'Alleud, Belgium), lorazepam from Fagron (Waregem, Belgium), amitrole from J&K Scientific (Marbach, Germany), and propranolol, paracetamol, diclofenac, diazepam, and carbamazepine from Alpha Pharma (Zwevegem, Belgium). Paroxetine, trimethoprim, iopromide, venlafaxine, codeine, cilostazol, imipramine, ticlopidine, oxazepam, and escitalopram were available in the lab as USP reference standards. The solvents used to prepare sample stock solutions and mobile phases were: acetonitrile (ACN, HPLC and MS grade) from Sigma-Aldrich and VWR (Leuven, Belgium), water (H_2O, MS grade) from VWR, ethanol (EtOH, absolute, analytical reagent grade) from Fisher Chemical (Loughborough, UK), and methanol (MeOH, HPLC grade) from Thermo Fisher Scientific. Formic acid (FA, 99% for LC-MS) was from VWR and ammonium formate (AF, ≥ 99.995%) was from Sigma-Aldrich. Ultra-pure H_2O (conductivity = 0.1 µS/cm, pH 6.00) was produced in the lab using a Milli-Q gradient purification system from Millipore (Bedford, MA, USA).

3.2.2. Sample preparation

The sample evaluated in this study contained 28 compounds with a wide variety in polarity, as typically encountered in environmental analysis. All compounds, their sample solvents, concentrations in stock and working solutions and predicted log D values at pH 3.0 (calculated using Marvin Sketch software version 23.10, ChemAxon (https://www.chemaxon.com)) are shown in **Table S3.1** in the Supporting Information (SI). Sample stock solutions of all compounds were prepared in concentrations between 2 and 20 mg/mL, depending on the solubility of the compounds. Working solutions were made by mixing appropriate volumes of the different compounds and adding H_2O and ACN to obtain a total sample volume of 5 mL with compound concentrations of 10-400 µg/mL in 10:90 H_2O:ACN (v/v%), to ensure enough sample volume for all experiments on both 2D-LC instruments. These concentrations were selected to acquire compound peaks with comparable heights at a detection wavelength of 254 nm. For the recovery determination, an additional sample was prepared containing only

the 15 non-polar compounds (compounds 14-28 in **Table S3.1**), with the same concentrations and solvent composition as in the above mixture. All samples were stored in the fridge (4°C).

3.2.3. Instrumentation

An schematic overview of both systems is shown in **Fig. 3.1**.

3.2.3.1. In-house developed 2D-LC setup

The in-house developed 2D-LC setup consisted of an Infinity 1290 system from Agilent Technologies (Waldbronn, Germany) equipped with a 1290 quaternary pump, a 1290 autosampler with a maximum injection volume of 20 µL and a 1290 DAD detector with a 1.0 µL flow cell and a path length of 10 mm. The system was additionally equipped with three 9-port/8-position ultra-high-pressure valves (valves 1, 2 and 3, max. pressure of 1200 bar) from Agilent Technologies. NanoViper tubings (inner diameters ranging from 50 to 150 µm) from Thermo Scientific (Germering, Germany) or stainless steel tubing (diameter: 170 µm) from Agilent Technologies with the shortest possible length were used to establish connections between the pump, valves, columns and detector. The dwell volume of the quaternary pump was 550 µL. To collect the non-polar compounds eluting from the HILIC column, Rheodyne sample loops with volumes of 100, 50, and 33 µL, along with VICI Valco T-pieces featuring a bore size of 0.25 mm, were acquired from Sigma-Aldrich. Sample loops were connected in series with zero-dead volume unions to obtain the desired volume. Agilent MassHunter Workstation (version 10.0, Agilent Technologies) was used to operate the system, control the valve configurations and acquire and analyze data.

3.2.3.2. Commercial 2D-LC setup

The commercial 2D-LC system was a 1290 Agilent Infinity II 2D-LC system from Agilent Technologies, equipped with two 1290 high-pressure binary pumps, a 1290 autosampler with a maximum injection volume of 20 µL, a Multicolumn Thermostat (MCT) column oven and two diode array detectors (DAD) with a 1.0 µL flow cell and a path length of 10 mm. The first and second dimensions were interfaced by a 10-port/4-position ASM valve (configured in backflush mode) from Agilent Technologies, connected via two 1.9 µL transfer capillaries (170 × 0.12 mm) to two 14-port/2-position deck valves carrying either one sample loop with a volume of 180 µL (1870 × 0.35 mm) for the LC-LC experiments, or six sample loops with a volume of 40

µL each (420 × 0.35 mm) for the sLC × LC experiments. The transfer volume, resulting from the time difference between the peak detection in the ^{1}D-DAD and the arrival in the sample loop, which needs to be considered for a correct sampling of the ^{1}D-effluent, was determined experimentally to be 15 µL. The dwell volumes were 180 µL and 90 µL (deck loop volume excluded) in ^{1}D and ^{2}D, respectively.

Experiments were carried out without the pressure release kit (PRK) between the ^{1}D-DAD and the ASM valve, which is normally used to minimize baseline disturbances arising from the 2D-LC valves switching, since the use of this PRK can lead to a reduced ^{2}D-recovery, as discussed in [50]. For experiments without PRK, the ^{1}D-detector was removed as well, in order to protect the flow cell, as recommended by the manufacturer. Stainless steel capillaries of different dimensions from Agilent Technologies were used to obtain different DFs, as shown in **Table 3.1** [199]. A JW with a volume of 100 µL from Agilent Technologies was also considered. Agilent OpenLab CDS Chemstation edition (Rev. C.01.10 [287]) software and Agilent 1290 Infinity 2D-LC software add-on (version A.01.04 [036]) were used to operate the system, control the valves and acquire data. Data were analyzed using Agilent 1290 Infinity 2D-LC software and Microsoft Excel.

Table 3.1 – ASM/dilution factors (DF) obtained using ASM capillaries with different dimensions for a sample loop (SL) of 180 and 40 µL.

ASM capillary			ASM DF	
Length (mm)	**Inner diameter (mm)**	**Volume (µL)**	**180 µL SL**	**40 µL SL**
85	0.12	0.96	5	5
150	0.17	3.40	11	10
1247	0.35	119.91	22	21
420	0.35	40.39	64	61

3.2.4. General Methodology

Separations on both setups were performed with the following mobile phases: (A) 98:2 H_2O:ACN (with AF dissolved in the H_2O-phase and adjusted to pH 3 using FA, to obtain a concentration of 2 mM AF in the H_2O:ACN mixture), (B) 2:98 H_2O:ACN (with AF dissolved in the H_2O-phase and adjusted to pH 3 using FA, to obtain a concentration of 2 mM AF in the H_2O:ACN mixture), (C) 0.1% FA in H_2O, (D) 0.1% FA in ACN. All mobile phases were degassed with helium prior to use.

For the ^{1}D-separation, an Acquity BEH HILIC column (1.0 × 150 mm; 1.7 µm) from Waters (Wexford, Ireland) was used in both setups. The ^{1}D-injection volume was 0.5 µL. For the in-house developed setup, the mobile phase was varied as follows: 1/99 – 5/95 – 1/99 – 1/99 (v/v) A/B in 0 – 20 – 20.92 – 30 min at a flow rate of 0.09 mL/min. For the commercial system, an additional isocratic step was added to the gradient program to account for the lower dwell volume of the binary pump. This resulted in the following gradient program: 1/99 – 1/99 – 5/95 – 1/99 – 1/99 (v/v%) A/B in 0 – 3.56 – 23.56 – 24.48 – 30 min.

The unretained non-polar compounds on the ^{1}D-HILIC column were sampled and collected in sample loops using switching valves. The different strategies to circumvent the solvent incompatibility of the two dimensions are discussed in **section 3.2.5**.

In the second dimension, the separation was carried out on a Zorbax Eclipse Plus C_{18} column (3.0 × 50 mm; 1.8 µm) from Agilent Technologies in both setups. For the commercial setup, the separation was carried out with the following gradient conditions: 98/2 – 5/95 – 98/2 – 98/2 (v/v%) C/D in 0 - 3.51 - 3.81 - 4.74 min at a flow rate of 0.8 mL/min. For the in-house built setup, a Cortecs Phenyl RP trap column (3.0 × 3 mm; 2.7 µm, Waters) was used in combination with the RPLC column (see **section 3.2.5**). In order to maintain the same gradient slope on both setups, the gradient time for the RPLC separation on the in-house built setup was increased in comparison with the commercial setup. Therefore, the mobile phase was varied using the following gradient conditions: 98/2 – 5/95 – 98/2 – 98/2 (v/v%) C/D in 0 – 4.32 – 4.7 - 8 min at a flow rate of 0.8 mL/min.

The detection wavelength was set at 254 nm in both dimensions with an acquisition rate of 20 Hz. The column oven temperature was not controlled in ^{1}D (room temperature) and was set to 30°C in ^{2}D of the commercial system.

3.2.5. Interface: ^{1}D-fraction transfer and dilution strategies

The transfer of the ^{1}D-fractions to the ^{2}D-column and the strategy to overcome the mobile phase incompatibility between HILIC and RPLC differed between both systems, as illustrated in **Fig. 3.1**.

3.2.5.1. In-house developed 2D-LC setup: restriction capillaries

On the in-house developed 2D-LC setup, the sample was only analyzed in LC-LC. **Fig. 3.2** represents the sequential operation procedure used for this setup.

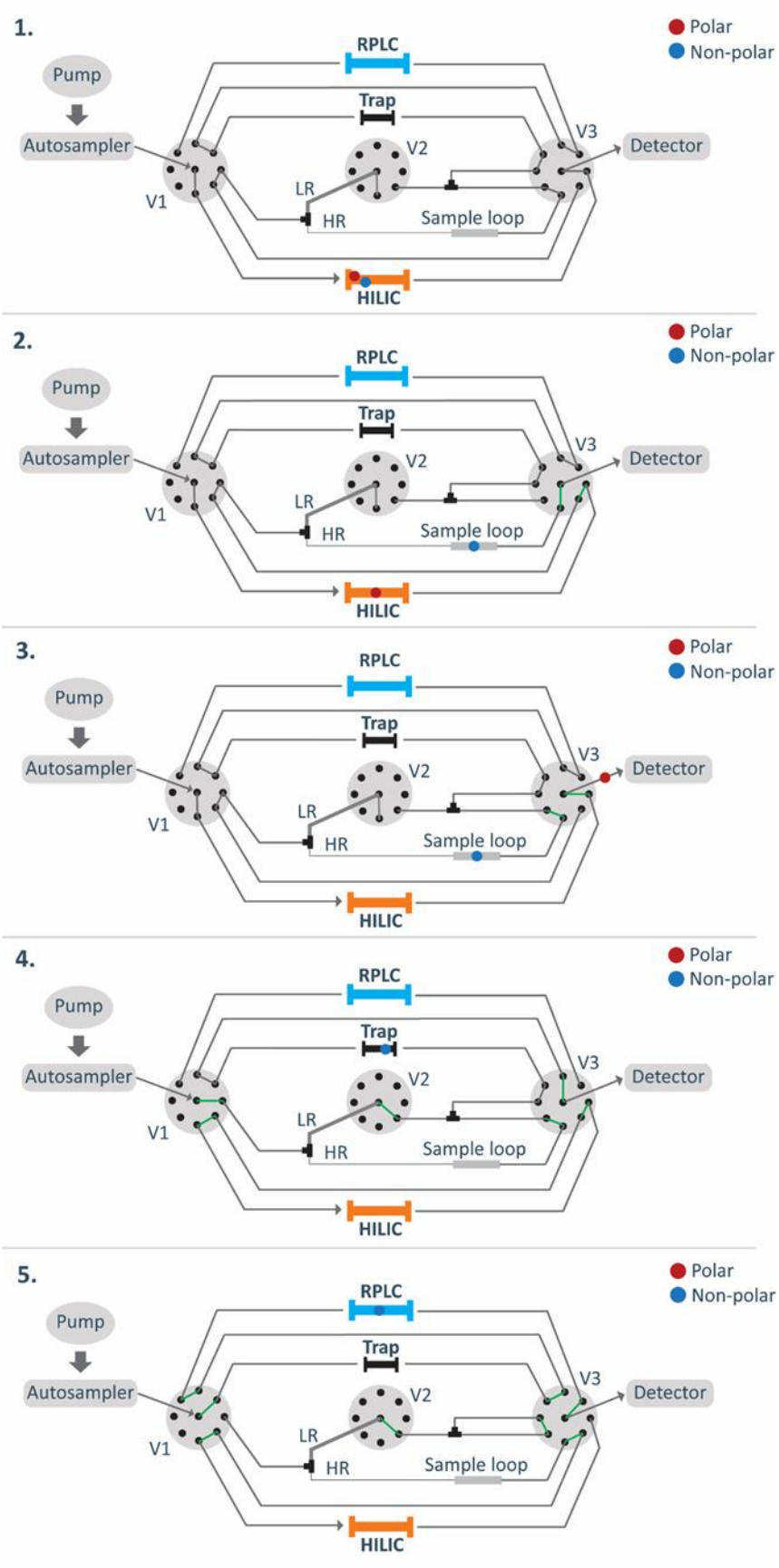

Figure 3.2 – Sequential operation procedure of the in-house developed setup. Red dots (•) represent polar compounds, blue dots (•) the non-polar compounds.

After injection in the ^{1}D (**Fig. 3.2, step 1**), the unretained non-polar compounds were diverted to the sample loop just after eluting from the HILIC column, by switching the configuration of valve 3 (**Fig. 3.2, step 2**). Once the non-polar compounds were collected in the sample loop, valve 3 was switched back to its original position (**Fig. 3.2, step 3**) to direct the separated polar compounds from the HILIC column to the detector. Then, the configuration of the three valves was changed to dilute the solvent containing the non-polar compounds in the sample loop with aqueous mobile phase C (0.1% FA in H_2O) and direct the non-polar compounds towards the RP trap column (**Fig. 3.2, step 4**). To deal with the solvent incompatibility, the mixing unit developed by Loos et al was used [176]. This mixing unit consisted of two restriction capillaries with different flow resistances: a high flow resistance capillary (HR, 50 µm × 350 mm) and a low flow resistance capillary (LR, 150 µm × 250 mm), resulting in a DF of ~74.

These restriction capillaries were interconnected by two T-pieces creating two parallel flow paths. The different flow resistances of the LR and HR capillaries allowed diluting the ACN-rich ^{1}D-effluent containing the unretained non-polar compounds. To speed up the dilution, a flow rate of 3 mL/min was applied. The dilution allowed trapping the non-polar compounds on the trap column. To ensure all non-polar compounds were transferred to the trap column, the sample loop was flushed at least 1.2 times. After the dilution step, the configuration of valves 1 and 3 was changed to direct the non-polar compounds from the trap column to the RP analytical column in backflush mode (**Fig. 3.2, step 5**).

3.2.5.2. Commercial 2D-LC setup: active solvent modulation

In contrast to the in-house developed system, the commercial 2D-LC system offers the possibility to carry out LC-LC, sLC × LC, and even LC × LC experiments. For this comparison study, both LC-LC and sLC × LC modes were considered. For LC-LC, operations with no ASM and ASM with different DFs were evaluated. These DFs were obtained using ASM capillaries of different dimensions [50]. **Table 3.1** shows the DFs obtained for a sample loop of 180 µL or 40 µL, using different ASM capillaries. For sLC × LC, both no ASM and a DF of 10 were used, as this was the optimal DF in a comparable sLC × LC setup [199]. For the experiments with ASM, the same gradient conditions as for those without ASM were applied, including an additional isocratic step (ASM phase) programmed before the start of the gradient, during which the on-line dilution occurred. For the ASM process, the duration of this isocratic step depended on the DF and on the number of times the sample loop was flushed (λ). An ASM phase duration of λ= 0.5, and a backflush sample loop unloading configuration were considered optimal for a DF of 10 in a previous study, and were therefore applied in this study as well [199]. For both the LC-LC and sLC × LC mode, ILMM using a JW with a volume of 100 µL from Agilent Technologies (installed between the ASM valve and the ^{2}D-column) was also

evaluated with and without ASM. The re-equilibration time was adapted for each experimental setup, to keep a similar equilibration, based on the total ^{2}D-dwell time.

3.2.6. Calculations

Recoveries were determined by comparing the area under the curve for the peaks in the 2D-LC configuration ($AUC_{2D\text{-}LC}$) with the areas under the curve when the working solution was injected directly into the RPLC column ($AUC_{1D\text{-}RPLC}$) under the same conditions as for the ^{2}D-separation, as shown in **Eq. 3.1**:

$$\boldsymbol{Recovery}\ (\%) = \frac{(\boldsymbol{AUC_{2D-LC}})}{(\boldsymbol{AUC_{1D-RPLC}})}\ .\mathbf{100}\% \qquad (\mathbf{3.1})$$

3.3. Results & discussion

3.3.1. First dimension: HILIC

To achieve a high degree of comparability, the ^{1}D-HILIC conditions were kept similar between the in-house developed system and the commercial system (an isocratic hold was added to the commercial system to account for the different dwell volumes). In **Fig. 3.3A1** and **A2**, the resulting HILIC separations obtained on both setups are shown. All 13 polar compounds were well-separated, highlighting the benefits of adding a HILIC column to the setup when both very polar and non-polar compounds need to be analyzed in a sample.

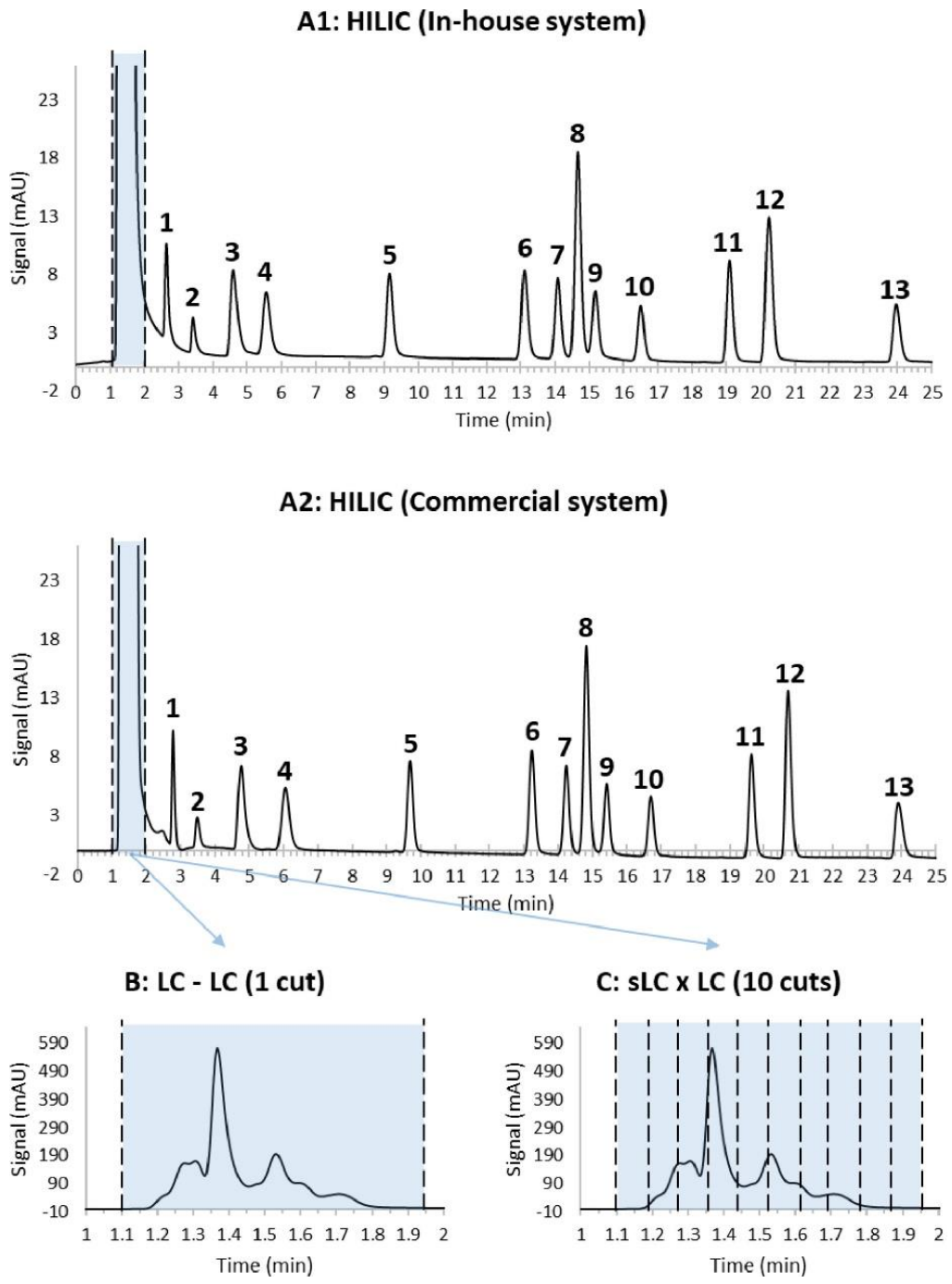

Figure 3.3 – [1]D-HILIC chromatogram and the selected sampling range for transfer to the [2]D-RPLC column. **A1**: Full [1]D-HILIC separation on the in-house system. **A2**: Full [1]D-HILIC separation on the commercial system **B**: Sampling range for heartcutting mode (LC–LC) (same for in-house developed and commercial setup). **C**: Sampling range for selective comprehensive mode (sLC × LC) on commercial setup.

The non-polar compounds were unretained on the [1]D-HILIC column and eluted in a range between 1.1 and 1.95 min on both systems. This unretained fraction was sampled in heart-cutting mode on the in-house developed and commercial setup (**Fig. 3.3B**), and additionally in selective comprehensive mode on the commercial 2D-LC set-up (**Fig. 3.3C**).

3.3.2. Second dimension: RPLC

3.3.2.1. In-house developed system: LC–LC

One of the strategies to overcome solvent mismatch involves diluting the ^{1}D-effluent with a weak solvent prior to injection on the ^{2}D column. In order to prevent peak distortion and any loss of compounds, it is crucial to thoroughly evaluate the appropriate dilution conditions.

Previous work on the in-house developed setup for a sample of comparable complexity in terms of polarity demonstrated that a DF of 50 was insufficient to adequately dilute and trap the sample plug containing the non-polar compounds on the RPLC trap column [176]. Higher DFs of 74 and 97 resulted in adequate trapping and subsequent satisfactory peak shapes and recoveries of the non-polar compounds on the RPLC column. However, a DF of 97 increased the total analysis time, as the time required to transfer the non-polar compounds from the sample loop to the RPLC trap column increased. Therefore, in this study, a DF of 74 was selected as a trade-off between compound recovery and total analysis time.

As shown in **Fig. 3.3**, the non-polar compounds eluted in a range between 1.1 and 1.95 min on the ^{1}D-HILIC column. Considering the flow rate on the HILIC column was 0.09 mL/min, this resulted in a plug volume of 76.5 µL to be transferred to the RPLC column. Due to the parabolic flow profile of the plug in the sample loop, it is recommended that the volume occupied by the collected ^{1}D-fraction should not exceed two-thirds of the loop volume, to avoid losing compounds during transfer [132,200,201]. To investigate the effect of sample loop volume and filling on the obtained recoveries, sample loops with volumes of 100 µL and 150 µL were considered. Additionally, a sample loop volume of 183 µL was also considered, as this was closest to the sample loop volume of the commercial setup (note that the sample loops of the commercial setup cannot be used on the in-house developed setup, due to different fittings). These sample loop volumes hence resulted in sample loop fillings of 77, 51, and 42%, respectively. Furthermore, to ensure all non-polar compounds were adequately transferred from the sample loop to the trap column, the sample loops were flushed either 1.2 or 1.5 times, cfr. prior optimizations [176]. **Fig. 3.4** shows the chromatogram obtained by directly injecting the non-polar compounds on the RPLC column, used for the calculation of the recoveries in LC-LC, while the values obtained for the corresponding peak widths can be found in **Table S3.2**.

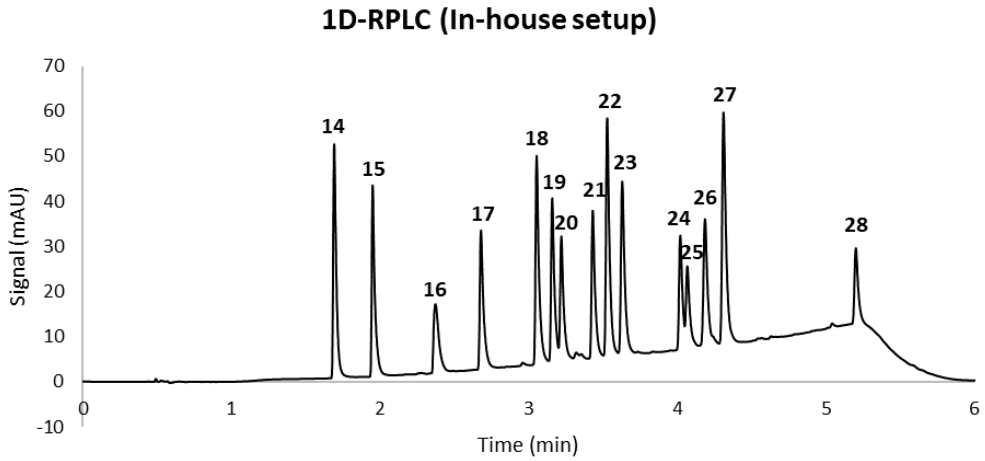

Figure 3.4 – 1D-RPLC chromatogram obtained by directly injecting the non-polar compounds on the RPLC column on the in-house developed setup for recovery determination (compound numbers correspond to the compounds in **Table S3.1**).

Fig. 3.5 shows the separation of the non-polar compounds on the RPLC column (^{2}D) using the in-house developed setup, for a sample loop volume of 183 µL and a flush time of 1.2. **Table S3.3** in the SI furthermore shows the obtained recoveries and peak widths on the RPLC column in LC-LC, for the different sample loop volumes and flush times.

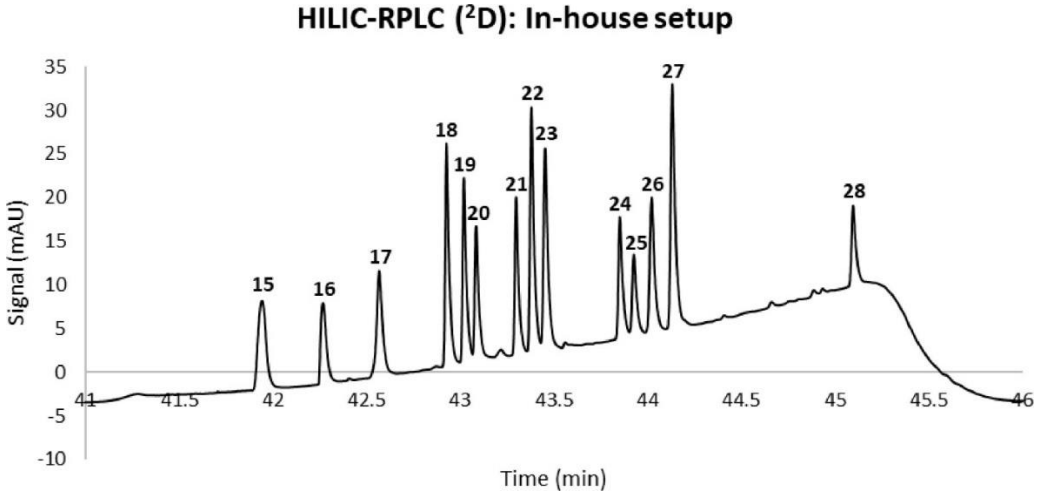

Figure 3.5 – ^{2}D-chromatogram obtained in HILIC-RPLC setup on the in-house 2D-LC system, using a sample loop volume of 183 µL and a sample loop flush time of 1.2.

As can be observed from **Table S3.3**, the first eluting compound on the RPLC column (paracetamol, compound 14) was not retrieved under any of the tested conditions. Likely, the employed dilution conditions were insufficient to adequately retain paracetamol on the trap column, hence losing it for subsequent analysis on the RPLC column. Moreover, peak broadening occurred for caffeine (compound 15), ticlopidine (compound 16), and sulfamethoxazole (compound 17), regardless of the sample loop volume and rinsing times applied. Nevertheless, satisfactory recoveries (between 90 and 110%) were obtained for all compounds across all tested conditions, with the exception of caffeine for the 183 µL sample loop rinsed 1.5 times, however, still resulting in a recovery of 78%. This is because caffeine, which is relatively polar, is probably (partly) flushed out of the trap column when using a high dilution volume. Both larger sample loop volumes and longer flush times increased the volume required to dilute the non-polar compounds in the sample loop. As shown in **Table 3.2,** a higher dilution volume also increased the duration of the dilution step (since the same flow rate was applied for dilution in all cases).

Table 3.2 – Dilution volume and total analysis time for each sample loop size and flush time.

Sample loop volume (µL)	**100**		**150**		**183**	
Flush time	**1.2**	**1.5**	**1.2**	**1.5**	**1.2**	**1.5**
Dilution volume (mL)	8.88	11.10	13.32	16.65	16.25	20.31
Total analysis time (min)	45	46	47	48	48	49

However, since the short trap column (with low backpressure) allowed applying a high flow rate of 3.0 mL/min during dilution, this increase in dilution time was relatively modest, increasing the total analysis time from 45 min for a sample loop volume of 100 µL and a flush time of 1.2x, to 49 min for a sample loop volume of 183 µL and a flush time of 1.5x. **Fig. 3.6** shows the separation of all 28 compounds in a single chromatographic run, achieved by employing a 183 µL sample loop and flush time of 1.2x. The results demonstrate that the percentage of sample loop filling did not significantly influence the recovery of the non-polar compounds, indicating a high percentage loop filling (77%) can effectively accommodate the ^{1}D-effluent. A high percentage of sample loop filling moreover allows using relatively small sample loops, reducing the need for excessive dilution volumes and thus overall analysis times. The latter is, however, not too problematic when high flow rates can be applied during dilution. This was the case here, where a trap column with a low backpressure was used in between the sample loop and the analytical column.

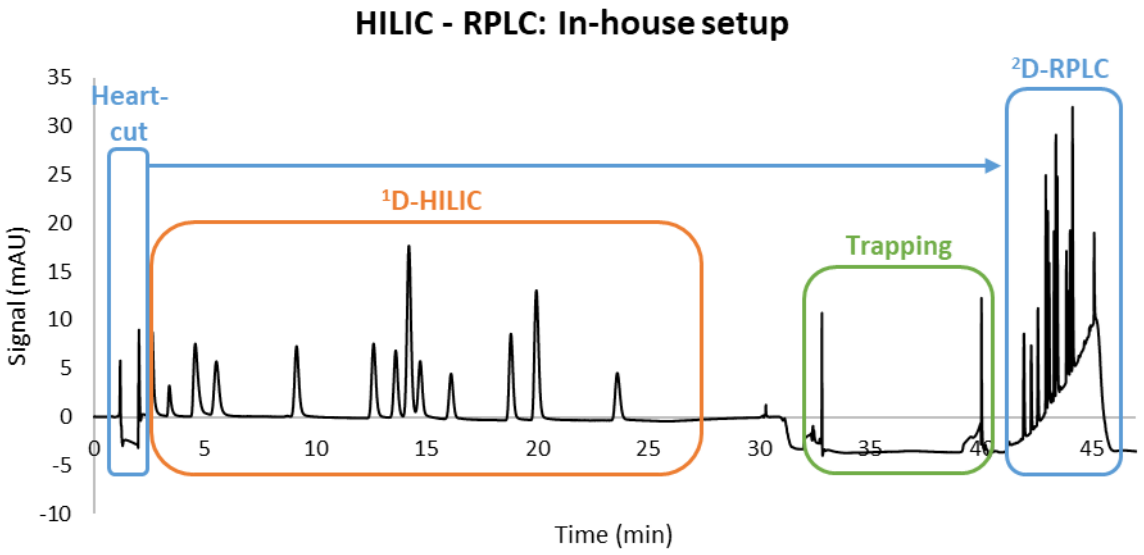

Figure 3.6 – Separation of all 28 compounds on the in-house developed set-up. The unretained non-polar pharmaceuticals eluting in the void of the HILIC column are transferred and separated in the ^{2}D. Sample loop size: 183 µL. Loop flushing volume: 1.2-fold. Total analysis time: 48 min.

Overall, the in-house developed setup allowed a satisfactory separation of all compounds except one (paracetamol), with acceptable recoveries between 90 and 110% (in most cases even between 95 and 105%) in a total analysis time of minimum 45 min, whereby all separated compounds could be visualized in a single chromatogram (for an example see **Fig. 3.6**).

3.3.2.2. Commercial system: LC–LC

To compare the commercial 2D-LC setup with the in-house developed setup, the LC-LC approach was considered first because this is essentially the same operational principle as for the in-house developed setup. The main differences with the in-house developed setup are that two pumps are used instead of one (allowing ^{1}D and ^{2}D to be operated simultaneously) and the use of ASM to deal with the mobile phase incompatibility. As for the in-house developed setup, the transferred fraction volume was 76.5 µL, therefore a sample loop filling of 43% was obtained in the 180 µL sample loop that was available on the setup. The LC-LC approach was carried out without and with ASM, with a sample loop flushing of λ= 0.5 and a sample loop unloading configuration in backflush mode. **Fig. 3.7** shows the chromatogram obtained by directly injecting the non-polar compounds on the RPLC column, used for the calculation of the recoveries in LC-LC.

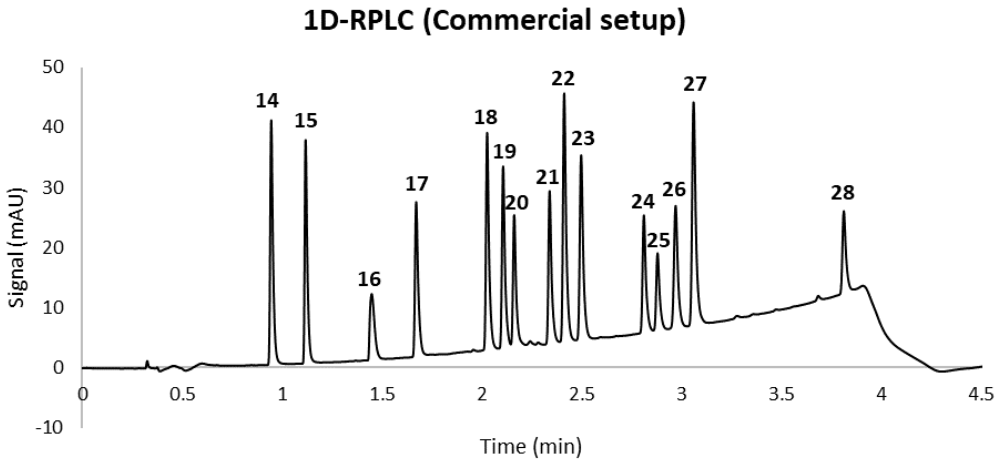

Figure 3.7 – 1D-RPLC chromatogram obtained by directly injecting the non-polar compounds on the RPLC column on the commercial setup for recovery determination (compound numbers correspond to the compounds in **Table S3.1**).

The corresponding peak widths are given in **Table S3.4** in the SI. In **Fig. 3.8A**, the results for the ^{2}D-RPLC separation obtained without ASM are shown. All peaks showed broadening, and severe breakthrough (highlighted by an asterisk) was observed for the earlier eluting compounds (14-23, as specified in **Table S3.1** in the SI) due to the high percentage of ACN in the sample, resulting in poor retention for all compounds.

In **Fig. 3.8B**, the results obtained with ASM using a DF of 22, are shown. Other DFs (5 – 64) were tested as well, as shown in **Fig. 3.9**. In **Table S3.5** in the SI, all values regarding the obtained recoveries and peak widths are shown. A DF of 22 gave the best peak shapes while keeping the analysis time minimal, as illustrated in **Fig. 3.8B**. Note that this DF is lower than the optimal DF used in the in-house developed setup, since the non-polar compounds were immediately sent to the analytical column in the commercial setup, which had a higher retention capacity compared to the trap column in the in-house developed setup. The later eluting compounds (18-28) displayed sharper peak shapes compared to the same conditions without ASM. However, earlier eluting compounds (15-17) still showed some peak broadening, while the first eluting compound (compound 14, paracetamol) was missing from the chromatogram (indicated by an arrow in **Fig. 3.8B**), very similar to what was observed for the in-house developed setup. Recoveries were slightly worse compared to the in-house developed setup and ranged between 85 and 113% for a DF of 22. Diluting the ^{1}D-fraction with the starting gradient composition of the ^{2}D-mobile phase (2:98 ACN:H_2O) during the ASM phase, hence significantly improved the peak shapes, especially for the later eluting compounds, due to a better focusing effect at the column inlet upon injection.

These improved peak shapes, however, came at the cost of an increased ^{2}D-analysis time, due to the extra time required for on-line dilution (0.6 min for a DF of 5, 1.22 min for a DF of 11, 2.5 min for a DF of 22 and 7 min for a DF of 64), resulting in a total analysis time of 5.52 min for a DF of 5, 6.14 min for a DF of 11, 7.42 min for a DF of 22 and 12.12 min for a DF of 64. For the early eluting compounds, the resulting mobile phase composition after dilution remained too strong and the volume of the fraction too large, therefore still causing poor peak shapes, even after dilution. Especially for the first compound, for which the sample plug was so large and the resulting analyte band too broad to result in a visible peak in the ^{2}D-chromatogram. A combination of ILMM and ASM was therefore assessed next, as shown in **Fig. 3.10** and **Table S3.6** in the SI.

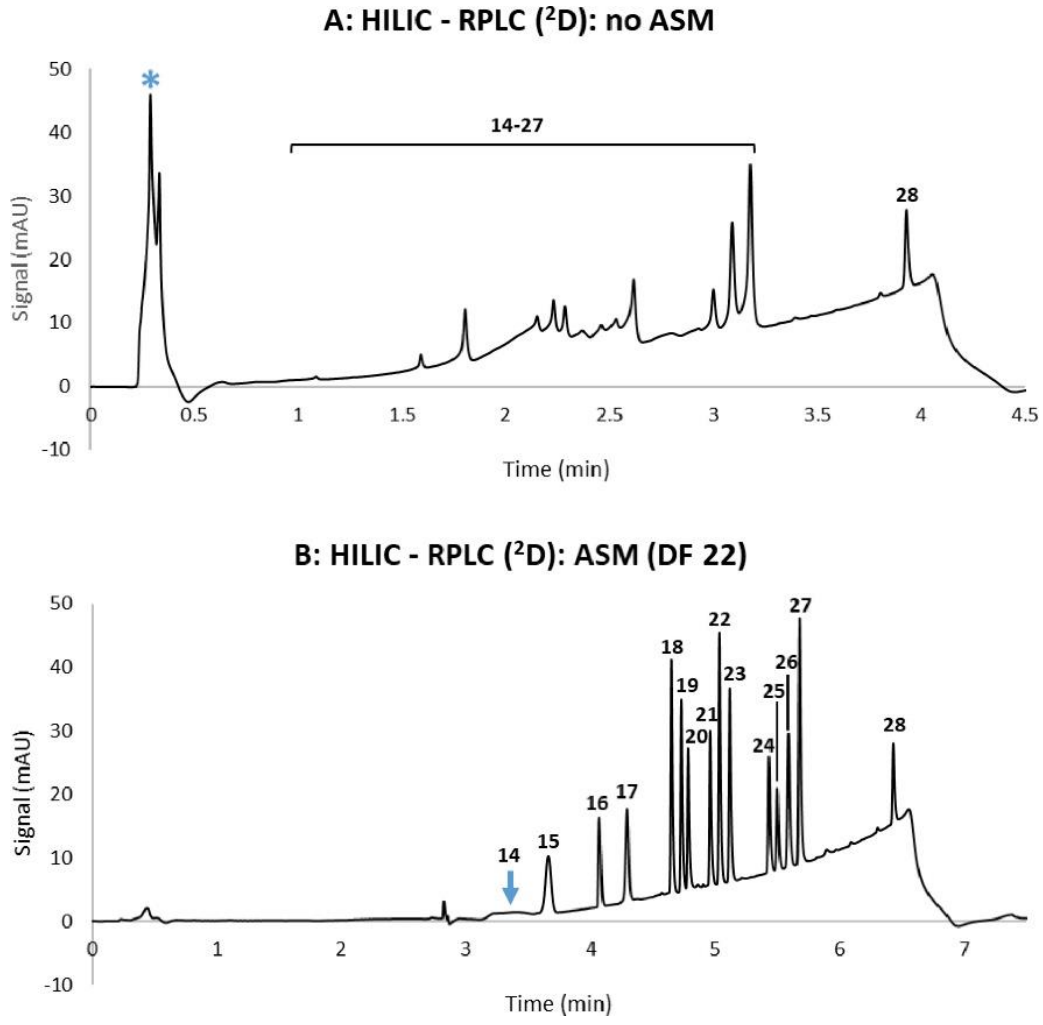

Figure 3.8 – Comparison of ^{2}D-chromatograms obtained with/without ASM in HILIC-RPLC setup on commercial 2D-LC system. **A**: no ASM. **B**: ASM (DF 22).

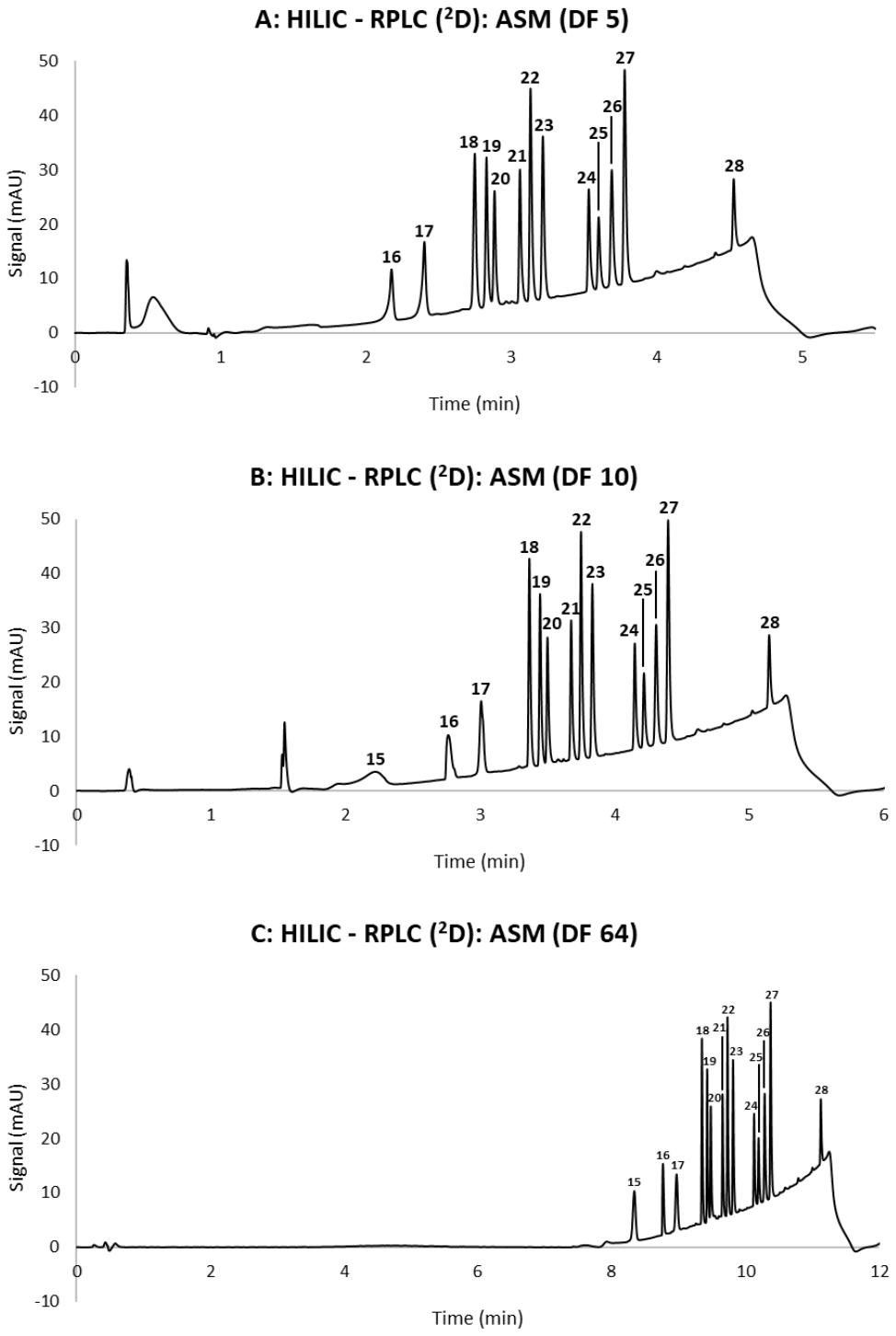

Figure 3.9 – Comparison of ^{2}D-chromatograms obtained with different dilution factors in the HILIC-RPLC setup on the commercial 2D-LC system. **A**: DF: 5, **B**: DF: 10, **C**: DF: 64 (compound numbers as in **Table S3.1**).

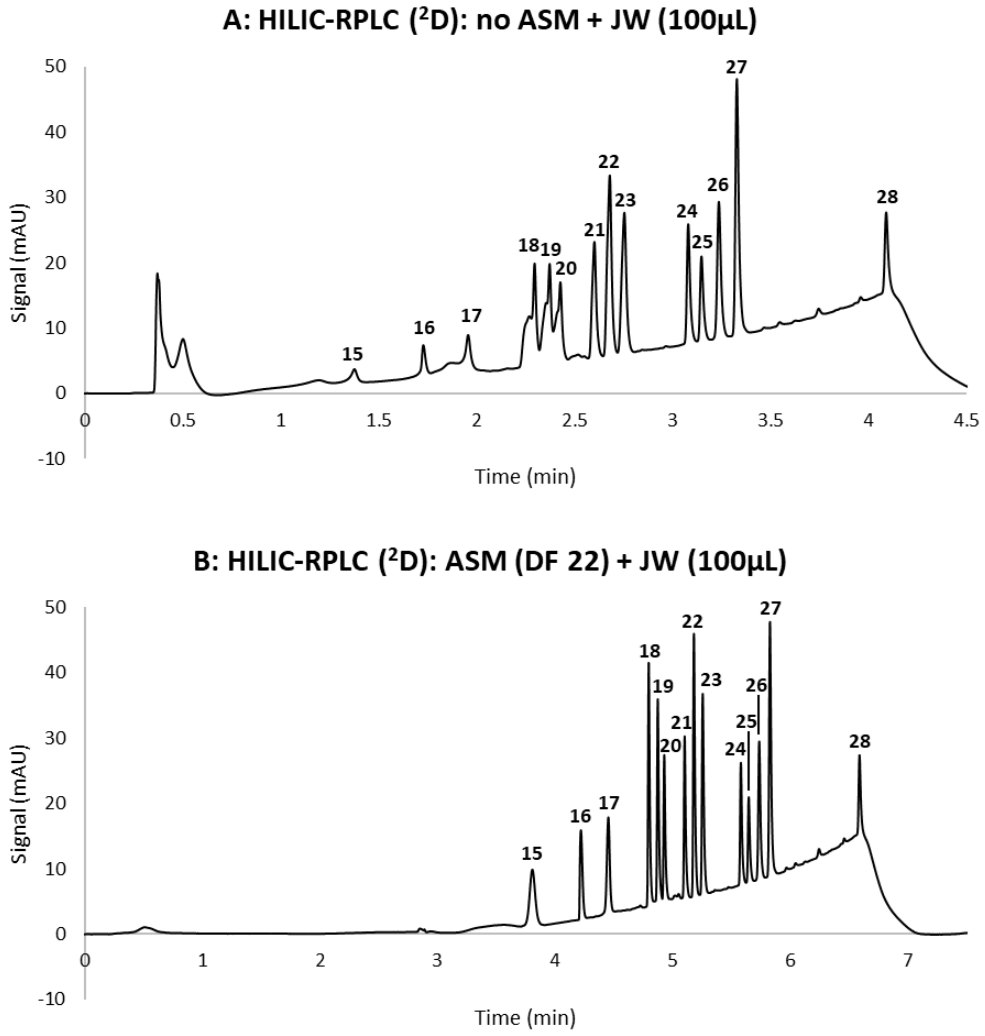

Figure 3.10 – Comparison of ^{2}D-chromatograms obtained with Jet Weaver (JW) Mixer (100 µL) with and without ASM in the HILIC-RPLC setup on the commercial 2D-LC system. **A**: no ASM. **B**: DF of 22 (compound numbers correspond to the compounds in **Table S3.1**).

The peak shapes obtained when using a JW without ASM already improved compared to the results obtained without ASM (**Fig. 3.10A** vs **Fig. 3.8A**). However, the combination of a JW and ASM was not better compared to using solely ASM (**Fig. 3.10B** vs **Fig. 3.8B**), most likely due to the large volume of the ^{1}D-fraction (76.5 µL) compared to the volume of the JW (100 µL), insufficient to create adequate mixing and dilution. Overall, these results demonstrate that diluting the mobile phase of the transferred fraction before directing it to the second dimension is a good approach to tackle the mobile phase incompatibility between HILIC and RPLC, as was also demonstrated with the in-house set-up.

A great advantage of the commercial system is that the ^{1}D- and ^{2}D-separations are carried out almost simultaneously, since the ^{2}D-separation can immediately start once the ^{1}D-fraction has been collected, resulting in a shorter total analysis time: 30 min for the commercial setup (time of the ^{1}D-HILIC separation) versus 45 min for the in-house setup (^{1}D-HILIC separation followed by trapping and ^{2}D-RPLC separation). On the other hand, for the in-house setup, the entire separation is shown in a sequential manner in the same chromatogram, which facilitates the integration and interpretation of the results. Overall, the results obtained on both setups are still not optimal, mainly for the earlier eluting compounds that suffered more from the incompatibility issue. Therefore, it was investigated whether this could be improved by carrying out an sLC × LC experiment.

3.3.2.3. Commercial system: sLC × LC

Due to the presence of the two decks containing multiple sample loops, the commercial system can also be used for sLC × LC experiments, in addition to the other 2D-LC modes.

The sLC × LC cuts resulted in 10 transferred fractions of 7.65 µL each, therefore a sample loop filling of 19% was obtained for the 40 µL sample loops. Reducing the volume of the transferred ^{1}D-fractions is a possible strategy to further reduce the negative effects on the ^{2}D-peak shapes when dealing with mobile phase incompatibility problems [132]. In **Fig. 3.11A**, the results for the sLC × LC approach obtained without ASM are shown, with a sample loop flushing of λ = 0.5 and a sample loop unloading configuration in backflush mode. In **Fig. 3.11B**, the results obtained with ASM for a DF of 10 are shown. This DF was previously shown to be ideal in an sLC × LC setup under similar conditions [199]. In **Table S3.7** in the SI, all values regarding the recoveries and peak widths can be found. It is clear that, even without on-line dilution, sLC × LC gave better peak shapes compared to the LC-LC approach without ASM. This is due to the reduced volume of the transferred ^{1}D-fractions (10 transferred fractions of 7.65 µL each, compared to one transferred fraction of 76.5 µL in the LC-LC mode). Additionally, the filling percentage of the sample loops was also lower, resulting in additional in-loop dilution of the sample plug with the ^{2}D-mobile phase, improving the ^{2}D-peak shapes further [199].

With ASM, the results were even better, and the first compound (14) was now better focused on the ^{2}D-column and therefore visible in the chromatogram, as opposed to the LC-LC method. Despite these improved peak shapes, the total sLC × LC analysis time (56 min) was much longer than that of the commercial LC-LC method (30 min) and the LC-LC method on the in-house developed setup (45 min). The reason is that the total sLC × LC analysis time is the sum of the analysis time of each cut (5 min) and the time needed to flush the capillaries in the decks (which is always programmed into the analysis by the software, and is equal to the time of one ^{2}D-cycle).

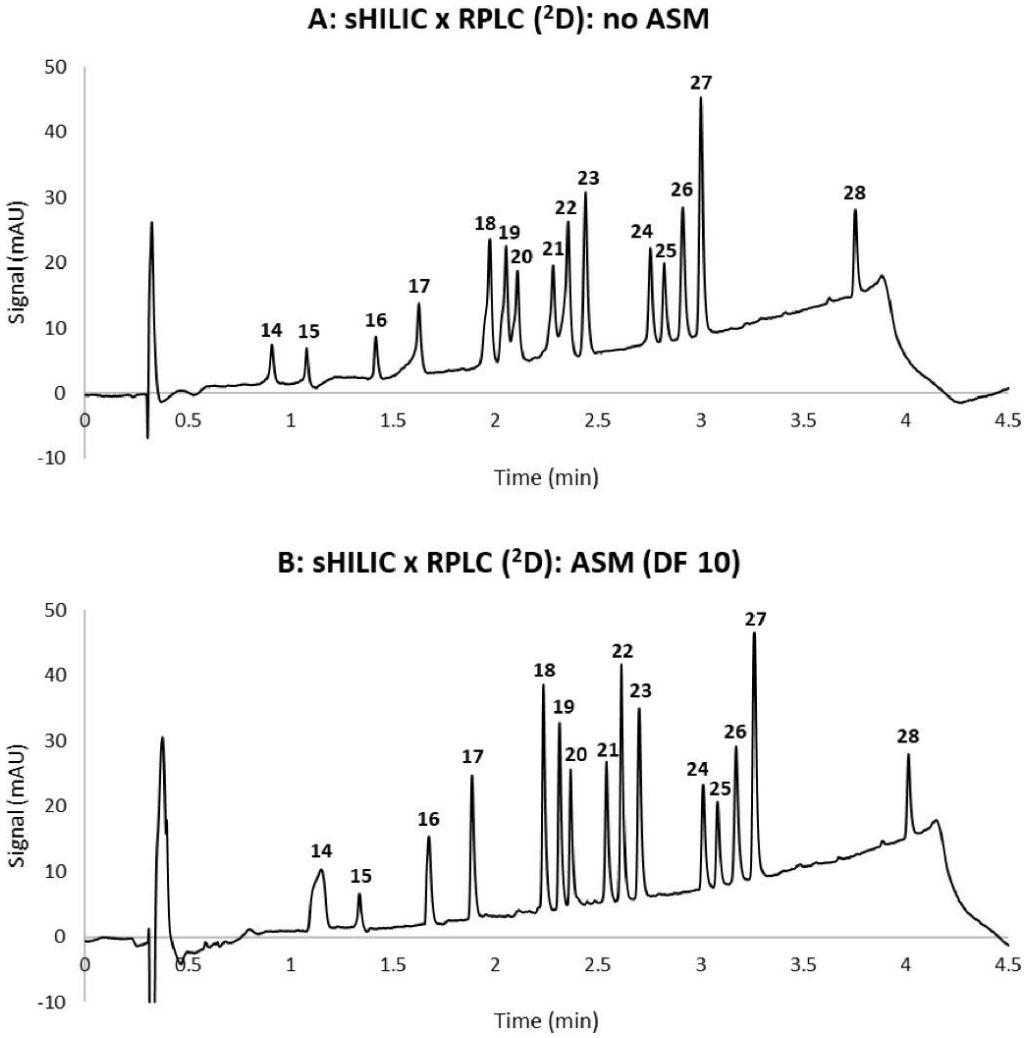

Figure 3.11 – Comparison of ^{2}D-chromatograms obtained with/without ASM in sHILIC × RPLC setup on commercial 2D-LC system. **A**: no ASM. **B**: ASM (DF 10). Both chromatograms show the sum of the cuts taken from the first dimension for each condition.

Overall, it seems that a tradeoff needs to be made between minimizing analysis time and achieving the best peak shapes for early eluting compounds. Even though the first compound was now focused and visible on the ^{2}D-column, the peak shapes and recoveries of the first two eluting compounds were still not optimal. For caffeine, the recovery was even substantially lower than for the in-house and commercial LC-LC methods. Several possibilities could be considered to further improve these [199], including changing the dilution solvent to 100% H_2O (using a different stationary phase which can operate at 100% H_2O in the second dimension). However, in this study, the dilution solvent was already 98% H_2O, therefore the additional benefit would probably be minimal. Another option would be to increase the retention factor of the early eluting compounds by selecting a different stationary phase, however, at the risk of changing the separation selectivity. ILMM using the JW either with or without ASM was assessed as well, as shown in **Fig. 3.12**.

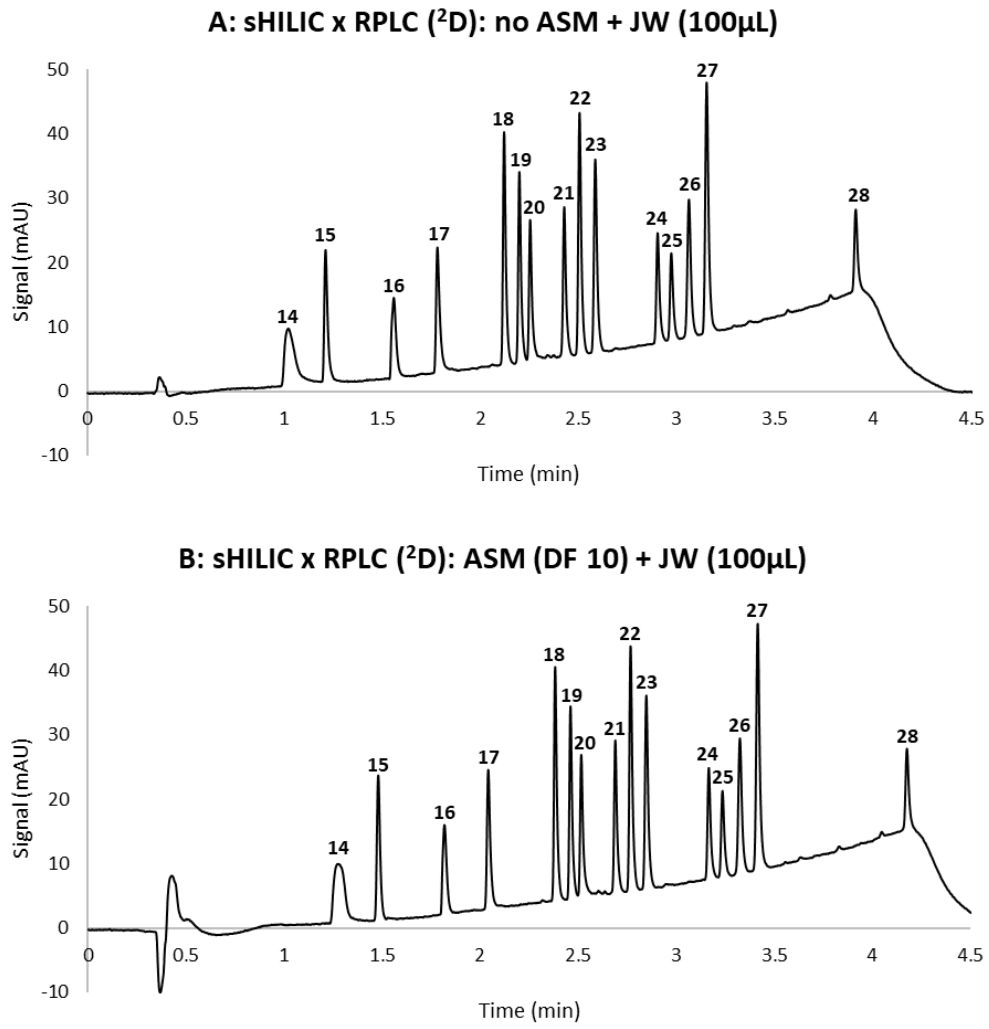

Figure 3.12 – Comparison of ^{2}D-chromatograms obtained with/without Jet Weaver (JW) mixer (100 µL) on the sHILIC × RPLC setup on the commercial 2D-LC system. **A:** no ASM. **B:** ASM (DF 10). Both chromatograms show the sum of the cuts taken from the first dimension for each condition (compound numbers correspond to the compounds in **Table S3.1**).

Both approaches resulted in somewhat better peak shapes compared to the optimized ASM conditions for the first two eluting compounds, while their ^{2}D-recoveries were significantly improved (slightly more for the JW in combination with ASM), as shown in **Table S3.8** in the SI. It has been shown before that the performance of ILMM can be better than ASM alone, depending on the volume of the transferred fraction and that of the JW used, since the multichannel flow path enables a more effective homogenization of ^{1}D-fractions, thus allowing the analytes to be more focused [187].

An improvement was only observed when adding the JW in the sLC × LC mode compared to the LC – LC mode, since much smaller fraction volumes were used in sLC × LC, while the fraction volume in LC-LC was rather of the same order of magnitude as that of the JW. Overall, the volume of the JW versus that of the transferred fractions is an important parameter in the method optimization, and increasing the JW volume for LC-LC setups with larger fractions might improve the ^{2}D-peak shapes even more. Additionally, the impact of the JW on the total analysis time was limited: using no ASM and the JW required 4.87 min per cut, resulting in a total analysis time of 55 min, only ASM (DF 10) required 5 min per cut, resulting in a total analysis time of 56 min, while the combination of ASM and JW required 5.1 min per cut, resulting in a total analysis time of 57.5 min.

3.3.3. General differences between the in-house developed and the commercial 2D-LC system

In addition to the experimentally determined differences in peak shapes and analysis time, some other general facts need to be considered in this comparison. One of the most important differences is the cost price of both systems: the commercial system is significantly more expensive than the in-house developed setup (list price for commercial setup: 213.000 Euro (2 binary high-pressure pumps, 2 DAD, 1 vialsampler, 2D-LC interface and software) versus 113.000 Euro for the in-house developed setup (1 quaternary high-pressure pump, 1 DAD, 1 vialsampler, 2D-LC interface and software). This is mainly due to the need for two pumps and two detectors, while the in-house system uses a (cheaper) quaternary pump to supply the mobile phases for both dimensions. Both separation dimensions are carried out sequentially in the in-house developed setup, while both separation dimensions are carried out simultaneously in the commercial setup, necessitating the use of two separate pumps. The latter approach has the advantage that the second dimension separation can already be initiated while the first dimension separation is still ongoing, which saves time and makes LC × LC (and sLC × LC) possible. These 2D-LC modes, however, generate a more complex output (multiple ^{2}D-chromatograms, which need to be summed up in the case of sLC × LC or aligned to generate a contour plot in LC × LC). Such software needs to be purchased separately (additional price of 2D-LC add-on and Image LCxLC software: 25.000 Euro), further increasing the cost of the commercial system. For the 2D-LC interface, both setups require 3 additional valves leading to a similar cost price (list price: 26.000 Euro). However, to perform ASM, the commercial setup requires an additional valve head with a list price of around 9.000 Euro. Additionally, since the commercial system can simultaneously perform the ^{1}D- and ^{2}D-separations, this implies that two detectors are required for LC-LC and sLC × LC experiments,

which is not problematic if DADs are used (except in terms of an increased cost price). If a destructive detector such as a mass spectrometer, evaporative light scattering detector (ELSD) or charged aerosol detector (CAD) is used, the experiments need to be carried out twice if information about both dimensions is required, whereby in each run a different dimension is coupled to the detector. This will increase the total analysis time significantly. When performing LC × LC experiments, this is not an issue, since the entire first dimension is also sent to the second, so only the ^{2}D-column needs to be connected to a detector.

Overall, the possibility of performing LC × LC experiments, which is usually needed for the analysis of very complex samples, is a main advantage of the commercial system. An LC × LC setup can also be lab-made, however, this requires two pumps and is most likely not as robust and user-friendly as the commercial options. This implies that the commercial system can easily be used for many different types of samples with different degrees of complexity, depending on the analytical goal (LC-LC, sLC × LC or LC × LC).

In terms of instrument operation, an in-house 2D-LC system can be built up from an existing 1D-LC system by adding the required switching valves, capillaries, columns, and sample loops, thus providing adaptability to specific analytical goals, and making it interesting for more innovative or complicated 2D-LC research. This, however, requires sufficient knowledge of LC systems and can therefore be less straightforward for beginning practitioners. On the other hand, the commercial system is bought as a whole, which makes it less inviting to make changes to the standard setup, although the latter is still possible (***e.g.,*** introducing a JW for ILMM or further customizing the ASM capillaries). Generally, the commercial system is easier for less experienced users, and more routine applications. In addition, the specialized 2D-LC software developed for these systems makes setting up 2D-LC experiments more straightforward. In comparison, when using an in-house setup, there is no need for (expensive) specialized software, but it is necessary to manually configure the method, which is more time-consuming, and carefully monitor the chromatographic run.

When dealing with the mobile phase incompatibility, the commercial system has some advantages. Since multiple sample loops are available, smaller transferred fractions and required DFs are possible, which overall results in better ^{2}D-peak shapes. It is perfectly possible to add additional sample loops to the in-house developed system as well, to accommodate multiple smaller fraction volumes. However, this would require the introduction of two more switching valves, thus increasing the price, bulkiness, and complexity of the system.

Finally, the commercial systems are very robust and provide highly reproducible 2D-LC experiments, while the in-house system is more fragile and technical problems can occur more easily when the setup is less well understood. In the commercial system, the delay time is also significantly reduced.

3.4. Conclusion

The goal of this study was to make a comparison between an in-house developed 2D-LC setup and a commercially available 2D-LC instrument, based on experimental differences, in addition to more general differences, including cost price, flexibility, and ease of operation. The different strategies to deal with the mobile phase incompatibility between HILIC and RPLC was investigated as well in detail on both setups.

For the commercial 2D-LC instrument, the strategy used was ASM and ILMM, while for the in-house developed setup, a combination of restriction capillaries and a trap column was used. Using a sample of 28 compounds with a large polarity range, peak shapes and recoveries of the ^{2}D-chromatograms were compared for both setups, as these are important parameters for an adequate quantification of compounds of interest in real applications. For early eluting and hence very polar compounds, the sLC × LC approach, currently only possible on the commercial 2D-LC instrument, resulted in the best peak shapes and recoveries, however, at the cost of an increased total analysis time of 56 min. The ILMM-approach performed slightly better compared to ASM, as demonstrated before [187]. For later eluting compounds, there were no significant differences between the instruments in terms of peak shapes and recoveries. In this case, the most advantageous setup in terms of analysis time was the LC-LC approach on the commercial instrument (total analysis time of 30 min versus 45 min on the in-house developed system), since the ^{1}D- and ^{2}D-separation could be carried out simultaneously.

On the other hand, in terms of total cost, the in-house developed setup was the least expensive, with a list price that was almost half that of the commercial setup. In general, depending on the analytical goal (single heart-cut versus full-comprehensive 2D-LC), an in-house developed system can be satisfactory for the analysis of specific target compounds/samples. For more complex problems and flexibility, it can be interesting to purchase a more specialized commercial 2D-LC instrument.

Finally, this study focused on the comparison of two systems from the same vendor, as these were available in our lab and made the comparison in terms of cost price more straightforward. Systems from other vendors are of course also available, and could provide additional capabilities in terms of column switching and strategies to modify the composition of the fractions transferred between both dimensions. Investigating and comparing the possibilities of such systems could provide directions for future research. Additionally, this study focused on a very particular sample, representative for typical environmental analyses. Other sample types, containing an even wider variety of compound classes, could shed further light on the capabilities of in-house versus commercially available systems.

The main purpose of this study was to encourage analysts to explore the capabilities of the systems available in their labs and select the most appropriate set-up (in-house built versus commercially available), depending on the particular needs of their samples, their own experience and skills, and the available budget.

CHAPTER 4

Electrochemical degradation of 17α-ethinylestradiol: Transformation products, degradation pathways and *in vivo* assessment of estrogenic activity

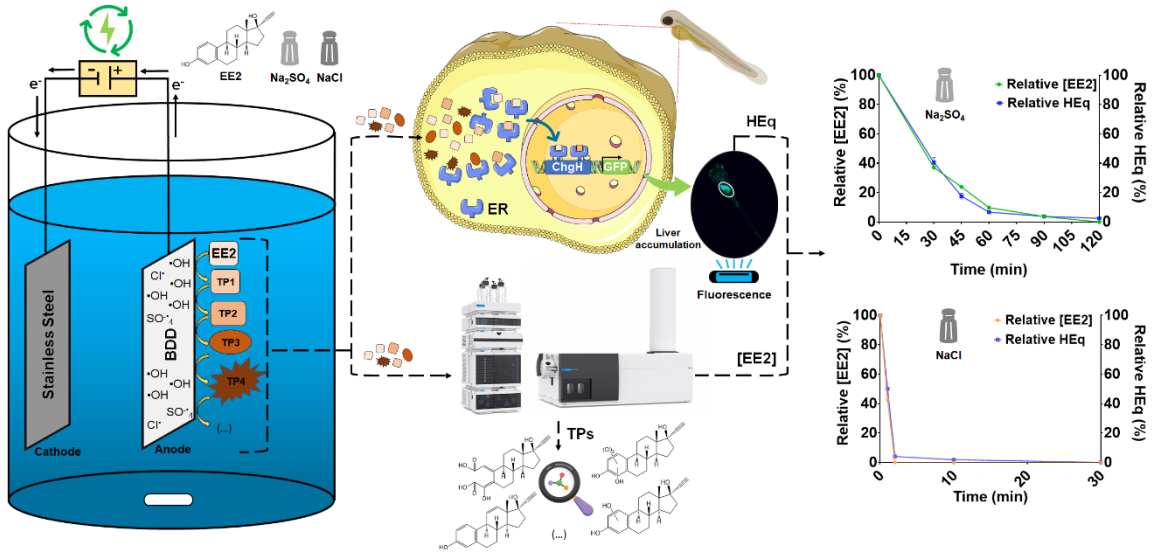

Adapted from: Rafael Reis, Rebecca Dhawle, David Du Pasquier, Andrew J. Tindall, Zacharias Frontistis, Dionissios Mantzavinos, Peter de Witte, Deirdre Cabooter, *Electrochemical degradation of 17α-ethinylestradiol: Transformation products, degradation pathways and in vivo assessment of estrogenic activity*. Environment International, 176 (2023) 107992.

4.1. Introduction

In recent decades, the presence of endocrine disrupting compounds (EDCs) in surface and groundwater has become a global problem since these compounds pose a serious threat to both aquatic organisms and human health [202]. One of the main EDCs in the environment is 17α-ethinylestradiol (EE2), a synthetic derivative of the natural hormone 17β-estradiol (E2) that is widely present in oral contraceptive pills. In addition, it is also extensively used in livestock and aquaculture to promote growth and to prevent and treat reproductive disorders [203–205]. As shown in **Fig. 4.1**, the chemical structure of EE2 has the same backbone as common steroid hormones. It possesses four fused rings, more specifically, three cyclohexane rings (designated as the A-, B- and C-rings) and one cyclopentane ring (classified as the D-ring). EE2 possesses a phenolic A-ring and a hydroxyl group on position 17, similar to E2. It differs with the addition of an ethinyl group on position 17.

EE2 has become an environmental concern due to its physicochemical properties and biological effects: its half-life in lake water can be up to 108 days, classifying it persistent in surface and groundwaters [206]. The compound's hydrophobic nature and low volatility make it prone to absorption by organic matter, concentration in sediment, and bioaccumulation in biota [8,203,207]. Compared to its natural counterpart, the binding affinity of EE2 to the estrogen receptor (ER) is up to two times higher in humans [208,209] and up to five times higher in fish [203,210–212]. Its physiological effect is mediated through interaction with the ligand-binding domain (LBD) of the ER [213]. Receptor interaction is mediated by means of a combination of specific hydrogen bonds, mainly via the phenol group located on the A-ring [214].

EE2, like many other EDCs, is discharged into urban sewage networks by human activities [215]. The treatment of urban wastewater is, therefore, crucial to reduce the effects of these molecules in the environment. Conventional wastewater treatment plants (WWTPs) are, however, largely ineffective in removing several EDCs from wastewater [216,217]. More effective and specific treatments are, therefore, urgently needed. Advanced oxidation processes (AOPs) are a class of water treatment technologies that involve the production of highly reactive hydroxyl radicals (•OH) for the oxidation of organic pollutants in water [218]. AOPs include ozonation, photocatalysis, Fenton and Fenton-like processes [30]. Previous studies have shown the potential of these processes to remove EE2 [219–225]. Currently, there is also an interest in the development of electrochemical AOPs (eAOP) that are chemical-free, operate at ambient temperature and pressure, and can be powered by green energy sources [30].

The boron-doped diamond (BDD) electrode is highly suited for the electrochemical oxidation of organic contaminants in the aquatic environment due to its physical and chemical properties [226]. The main advantage of this type of anode is the high generation efficiency of •OH at its surface [227]. Many different supporting electrolytes are used in eAOPs, such as sodium sulfate (Na_2SO_4), sodium chloride (NaCl), sodium perchlorate ($NaClO_4$) and sodium nitrate ($NaNO_3$). Both Na_2SO_4 and NaCl are widely used as supporting electrolytes, the former due to the high stability of sulfate ions and its low electrode corrosion rates [228], the latter due to its high organic removal efficiency owing to the production of several active chlorine species [229]. Moreover, chloride (Cl^-) and sulfate (SO_4^{2-}) ions are extensively present in groundwater, municipal and industrial wastewater [230–232]. Therefore, it is of utmost importance to study the role of these ions in electrochemical processes. Previous studies have demonstrated the potential of BDD electrochemical oxidation for the efficient degradation of EE2 in water [233–235]. These degradation processes can, however, result in transformation products (TPs) that can preserve the biological activity of the original molecule. Frontistis et al. (2011) detected a persistent estrogenicity in degraded samples after complete EE2 removal by BDD electrochemical oxidation using the yeast estrogen screen (YES). However, no TPs were described. In addition, although *in vitro* assays such as the YES assay are capable of detecting estrogen receptor agonists and antagonists, they are not designed to replace *in vivo* tests on whole water samples, which are needed to identify all possible modes of action leading to endocrine disruption and involving multiple organs and tissues. Consequently, a more comprehensive analysis of eAOP degraded water samples from a chemical and endocrine disruption point-of-view is needed before these techniques can be employed in real-life.

Japanese medaka fish (*Oryzias latipes*) have been used for over 60 years for toxicity testing. These small fish are useful vertebrate models that are aquatic ecosystem sentinels, present a rapid screening method to predict toxicity, and are easy to handle and maintain in a laboratory [98]. Transgenic medaka fish, such as transgenic choriogenin H-green fluorescent protein (ChgH-GFP) medaka fish, have been developed for the detection of estrogenic active compounds at trace levels and for the quantification of hormonal equivalence [236–239]. This *in vivo* model contains the green fluorescence protein (GFP) gene that is controlled by the regulatory sequence of the estrogen responsive gene choriogenin H (ChgH). The ChgH promoter is activated in response to estrogen active compounds at trace levels [239] and is inducible in a concentration dependent manner [240]. This *in vivo* model is capable of detecting disruption of the estrogenic axis by environmentally relevant chemicals [237,239] and is hence a valuable tool for the estrogenic assessment of whole water samples. It is currently evaluated by the Organization for Economic Cooperation and Development (OECD) for publication as an international test guideline as the Rapid Estrogen ACTivity In Vivo (REACTIV) assay.

Since the estrogen signaling pathway is highly conserved across vertebrates [241], *in vivo* vertebrate models can play a critical role in assessing the estrogenic activity of EDCs and their potential risks on human health.

The identification of TPs formed during degradation processes can be challenging due to their large numbers, mostly unknown structures, often low concentrations and the complexity of the matrices they present themselves in, requiring highly selective and sensitive analysis techniques. The hyphenation of liquid chromatography (LC) with high-resolution mass spectrometry (HRMS) is a suitable strategy for the screening of diverse organic pollutants in the environment, including their TPs. Hybrid quadrupole time-of-flight mass spectrometry (QTOF-MS) has gained considerable attention in environmental analytical chemistry [139]. It combines a high mass resolution with a high scan speed, allowing the identification of unknown compounds by nontarget screening and by suspect screening when database information is available. LC-QTOF-MS has recently successfully been applied in the analysis of emerging pollutants and TPs generated by AOPs [242–245], as well as in effect-directed analysis [246,247].

In this work, a BDD anode was used for the electrochemical degradation of EE2. Different parameters such as electrolyte type, electrolyte concentration and electric current were first optimized to obtain the most efficient degradation of EE2. To separate, identify and quantify EE2 and its TPs, a LC-QTOF-MS method was developed and validated. The estrogenic activity of the degraded samples was evaluated with the REACTIV assay. The effects of the supporting electrolytes on the generation of different TPs and their subsequent impact on the estrogenic activity were carefully investigated and discussed. To the best of our knowledge, this is the first comprehensive chemical and endocrine activity assessment of TPs generated from eAOP using LC-HRMS and *in vivo* models. The findings of this study can help understand the mechanisms involved in the removal of EE2 and estrogenicity in water, and hence establish a theoretical basis for utilizing eAOPs in wastewater treatment.

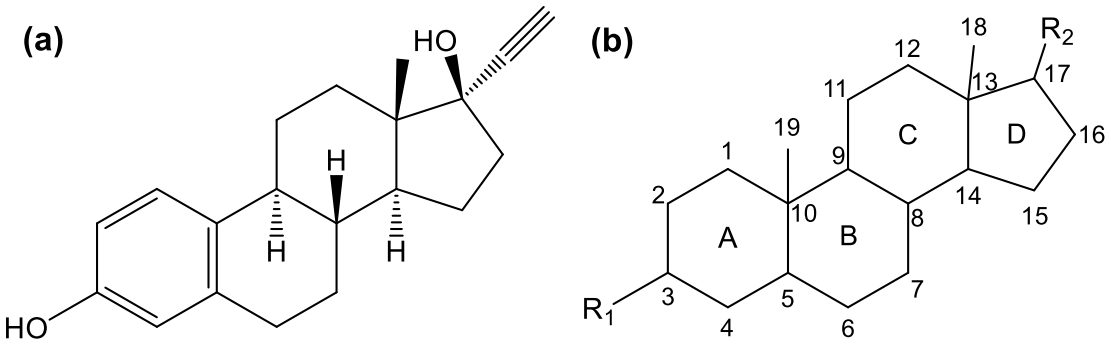

Figure 4.1 – (a) Chemical structure of EE2. (b) Chemical structure of steroids showing atom numbers and ring annotation.

4.2. Materials & methods

4.2.1. Chemicals

High purity (≥ 98%) 17α-ethinylestradiol (EE2, $C_{20}H_{24}O_2$) and 17α-ethynylestradiol-$^{13}C_2$ (EE2-$^{13}C_2$, $^{13}C_2C_{18}H_{24}O_2$) were purchased from Sigma (Steinheim, Germany) and Toronto Research Chemicals (Toronto, Canada), respectively. Extra pure (≥ 99%) anhydrous sodium sulphate (Na_2SO_4) and sodium chloride (NaCl) were bought from Merck kGaA (Darmstadt, Germany). Ultrapure water was obtained using a Milli-Q® system (18 M Ω/cm) from Merck. LC-MS-grade water and acetonitrile (ACN) were obtained from Fisher Chemicals (Loughborough, UK) and VWR chemicals (Rosny-sous-Bois, France), respectively. Ammonium fluoride (≥ 99.99%, NH_4F) and dimethyl sulfoxide (DMSO, C_2H_6OS) were obtained from Sigma. Evian mineral water was used as the biological test medium and was obtained from a local supplier.

4.2.2. UHPLC-QTOF-MS analysis

LC-HRMS analyses were carried out with an Agilent Infinity 1290 UHPLC system, equipped with a quaternary pump, an autosampler and a diode array detector (DAD) in combination with an Agilent 6530 QTOF-MS (Agilent Technologies, Waldbronn Germany). Separations were performed on a ZORBAX RRHD Eclipse Plus ® Phenyl-Hexyl column (3.0 × 100 mm; particle size: 1.8 µm, Agilent Technologies) at room temperature. Collision induced dissociation (CID) experiments were performed to obtain MS/MS fragmentation data.

Mobile phases were (A) LC-MS grade water with 1 mM ammonium fluoride and (B) LC-MS grade ACN. The separation method started with a 2-min isocratic hold at 0% B, followed by a gradient from 0% to 80% B in 10 min. The mobile phase was then kept constant at 80% B for 2 min, returned to the initial composition of 0% B in 0.1 min and kept constant at 0% B for 8 min to re-equilibrate the column. The mobile phase flow rate and the injection volume were set at 0.5 mL/min and 5 µL, respectively. Each sample was analyzed in triplicate. Ionization was performed in negative electrospray ionization mode using Dual Agilent Jet Stream Technology. The MS source was operated at a gas temperature of 300 °C, a drying gas flow rate of 8 L/min, a nebulizer pressure of 35 psi and a sheath gas temperature and flow of 350 °C and 11 L/min, respectively. The capillary voltage was set at 3500 V, the nozzle voltage at 1000 V, the fragmentor and skimmer voltage at 175 and 65 V, respectively. The QTOF-MS was operated in 2 GHz Extended Dynamic Range mode. Two reference mass compounds with m/z values of 112.9855 and 1033.9881 were constantly introduced into the ionization chamber for mass

accuracy correction. MS and MS/MS spectra were collected at 5 and 1 spectra/s, respectively. Selected compounds for CID were fragmented with nitrogen gas at 10, 20, 40 and 50 eV.

The developed UHPLC-QTOF-MS method was validated according to the international guidelines of the European Medicines Agency (EMA) [248]. The method performance for EE2 quantification was assessed through verification of method specificity, linearity, accuracy, precision, limit of detection (LOD), lower limit of quantification (LLOQ) and matrix effects (ME). EE2 working samples were prepared in LC-MS grade water. For the construction of calibration curves, 6 standard solutions with concentrations of 10, 50, 100, 500, 1000 and 5000 µg/L of EE2 were prepared. To assess the accuracy, precision and matrix effects of the method, low (20 µg/L), medium (250 µg/L) and high (2500 µg/L) level quality control (QC) samples were prepared. EE2-$^{13}C_2$ was used as the internal standard (IS) at a concentration of 500 µg/L in each sample.

The lower limit of quantification (LLOQ) was determined as the EE2 concentration for which the signal to noise ratio (S/N) was at least 10:1 and the relative standard deviation (RSD) was less than 20%. The limit of detection (LOD) was determined as the lowest concentration of EE2 for which the S/N was at least 3:1. The selectivity of the method was studied by analyzing ultrapure water and blank degraded samples (n= 6) to evaluate interferences with EE2 or the IS. These samples were spiked with EE2 at the LLOQ level and the IS and were compared with un-spiked samples. For the method to be selective, the maximum allowed difference in concentration was 20% for EE2 and 5% for the IS. Carry-over was assessed by injecting 6 water samples after the injection of one sample containing EE2 at the upper limit of quantification (ULOQ) and the IS. For carry-over to be absent, the obtained peak area had to be less than 20% of the EE2 LLOQ and 5% of the IS.

Matrix effects (MEs) were studied to evaluate possible interferences of the sample matrix with the ionization process. This was done by comparing the peak area (the area under the curve or AUC) of EE2 and the IS obtained in ultrapure water with the corresponding peak area (AUC) in non-electrolyzed samples and degraded blank samples. All samples were spiked at the low, medium and high level of QC and with the IS (n= 3). MEs were calculated as follows (**Eq. 4.1**):

$$ME\ (\%) = \frac{\left(\frac{AUC_{EE2}}{AUC_{IS}}\right)_{Sample\ with\ matrix}}{\left(\frac{AUC_{EE2}}{AUC_{IS}}\right)_{Ultrapure\ water}} \times 100\% \qquad \textbf{(Eq. 4.1)}$$

MEs were considered not-significant if the results of the samples with matrix were within ± 15% of the obtained values in ultrapure water.

Accuracy (see **Eq. 4.2**), intra- and inter-day precision (RSD) were assessed at the LLOQ and the three levels of QC. Six replicates of LLOQ and QC samples were assayed in one run for

intra-day precision. Three replicates of LLOQ and QC samples were assayed within six different days (n= 18) for inter-day precision.
The method was considered accurate and precise if the measured concentrations were within ± 15% of the nominal concentrations, except for the LLOQ which had to be within ± 20%.

$$Accuracy\ (\%) = \frac{(Measured\ concentration - Nominal\ concentration)}{Nominal\ concentration} \times 100\% \qquad \textbf{(Eq. 4.2)}$$

Dilution integrity was demonstrated by diluting a sample with a concentration of 1.6 times the ULOQ of EE2, with ultrapure water 10, 100 and 500-fold (n= 5). Both accuracy and precision were required to be within ± 15% of the nominal value.

4.2.3. Electrochemical oxidation experiments

The electrochemical oxidation of EE2 was conducted in a 100 mL glass beaker. The anode was a BDD electrode (Boron/Carbon= 1000 ppm), active on one side, from Adamant Technologies SA (La-Chaux-de-Fond, Switzerland). The cathode was a 316L grade stainless steel plate. The active area of the electrodes was 16 mA/cm^2. The electrodes were placed 2.5 cm away from each other and the solution was stirred continuously to facilitate mass transfer. The initial concentration of EE2 was 5000 µg/L, dissolved in ultrapure water. The solution was stirred for 30 min to achieve equilibrium before the start of the electrochemical oxidation. Na_2SO_4 and NaCl were assessed separately as electrolytes for the degradation experiments. The effects of different electrolyte concentrations (0.025 and 0.05 M) and applied currents (3.125, 6.25 and 12.5 mA/cm^2) were first evaluated over a total period of 2 h. For this purpose, sample aliquots of 200 µL were collected between t= 0 and t= 120 min, and analyzed.
The resulting optimal degradation conditions were subsequently used to generate degraded EE2 samples for further chemical and biological evaluation. Due to the high sample volumes required for the biological experiments (50 mL), a new experiment was conducted for each separate time point. In the presence of Na_2SO_4, samples were electrochemically degraded for t= 30, t= 45, t= 60, t= 90 and t= 120 min. In the presence of NaCl, samples were degraded for t= 1, t= 2, t= 10 and t= 30 min. For each experiment, a corresponding blank sample was generated that underwent the same eAOP process in the absence of EE2. Initial (t= 0 min) samples, with and without EE2, were collected non-electrolyzed directly from the bulk of the electrochemical cell. For each experiment, aliquots of 50 mL were collected for the estrogenic assessment while 5 mL aliquots were collected for LC-MS analysis. All samples were frozen at -20°C for storage. Prior to the LC-MS analysis, samples were thawed, filtered with

regenerated cellulose filters (< 0.22 µm) and spiked with EE2-$^{13}C_2$ at a final concentration of 500 µg/L.

4.2.4. Evaluation of estrogenic effect

Estrogenic tests were conducted in 6-well plates using newly hatched ChgH-GFP transgenic medaka larvae, at 7 days post fertilization (dpf 7). Each well contained eight larvae in a total volume of 8 mL of test medium alone, or containing control chemicals or eAOP treated EE2. Exposure time to the compound(s) was 24 h at 26°C under a 14:10 light:dark cycle. The test medium was Evian mineral water supplemented with 0.2% DMSO (v/v). After 24 h of exposure, the medium in each well was replaced by test medium and each larva was manually placed in a 96-well microplate for fluorescence quantification. To that end, larvae were illuminated with a L200/D 200W fluorescence source (Prior Scientific, Cambridge, UK) and U-F19002 GFP long-pass filters (excitation 475/40, emission 515LP, dichroic 505 nm; Olympus, Rungis, France) and imaged with a Olympus IX-73 automated inverted microscope. Images were captured with an Olympus DP74 colour camera with a 15 ms exposure time at 2x magnification and quantified with Image J Software (U.S. National Institute of Health). In order to remove background fluorescence resulting from endogenous pigments present in the larvae, a threshold intensity of 60–255 was applied to the resulting images.

Three experimental groups were considered for each estrogen test. The negative control group consisted of eleutheroembryos incubated in test medium and was used to determine the baseline fluorescence level of non-treated larvae. The positive control group consisted of larvae incubated in test medium containing 33.8, 50.6, 76.0, 114.0, 170.9 and 488 ng/L of EE2 to determine the level of fluorescence induced by EE2 in a concentration-dependent manner. The third test group consisted of larvae exposed to electrochemically oxidized aqueous solutions of EE2 diluted with test medium. This group was used to determine the fluorescence changes induced by EE2 and TPs. Three independent experiments were performed on different days and the results were pooled for each condition.

4.2.5. Data analysis and statistics

Fluorescence levels measured were processed according to the OECD guidelines for the statistical analysis of eco-toxicology experiments (OECD, 2006). GraphPad Prism version 7.00 (GraphPad Software, La Jolla, CA, USA) was used for statistical analysis and graph plotting. A D'Agostino and Pearson omnibus normality test was used to determine the distribution of

values in each of the exposure groups. A one-way ANOVA and Dunnett multi-comparison test were performed in cases wherein all groups showed a normal distribution.

A Kruskal-Wallis test with Dunn's multi-comparison test was used in cases where one or more of the compared groups did not pass the normality test. All groups were compared to the appropriate control group. Statistical significance was set at $p< 0.05$.

Data analysis for the quantification of EE2 and for the structural elucidation of TPs was performed using MassHunter and Profinder software (version 10.0, Agilent Technologies). An algorithm was used to extract and identify peaks as potential compounds, also known as "features". The parameters used for the molecular feature extraction (MFE) are given in **Table S4.1** in the Supporting Information (SI). After extraction from the obtained chromatograms, the molecular features were only considered if they met the following criteria: (i) molecular features were absent in the initial sample (t= 0 min) and in blank degraded samples, (ii) a single predicted molecular formula was obtained based on high mass accuracy (< 5 ppm), isotopic distribution and molecular formula in resemblance with EE2 ($C_{20}H_{24}O_2$) (iii) a change in intensity was observed across the length of the experiment, with respect to the IS (EE2-$^{13}C_2$). Chemical structures and MS/MS fragments were generated using ChemDraw (version 21.0, PerkinElmer, Seer Green, UK). The calculation of the exact mass and LogP values was done with MarvinSketch (version 22.19, ChemAxon Ltd, Budapest, Hungary). The TPs were classified by the identification confidence levels proposed by Schymanski et al. (2014). Briefly, level 2b was given to TPs whose experimental data matched with literature data, level 3 was attributed to positional isomers and level 4 to TPs for which MS/MS fragmentation data was unavailable or too ambiguous to propose a chemical structure. To monitor the evolution of the TPs during the electrochemical oxidation process, peak areas of the TPs were normalized with respect to the peak area of EE2-$^{13}C_2$ at the corresponding time point.

4.3. Results & discussion

4.3.1. LC-MS method validation

Typical extracted ion chromatograms of EE2 and the internal standard (IS) at 500 µg/L in ultrapure water can be found in the SI (**Fig. S4.1**). No significant interference was found between the sample matrix and the EE2 and IS signals. Based on the obtained signal to noise ratio (S/N) values and relative standard deviation (RSD), the LLOQ of EE2 was determined at 10 µg/L (S/N= 10.3, RSD 8.1%), while the LOD was determined at 3 µg/L (S/N= 3.1, RSD 17.4%). The ULOQ was set at 5000 µg/L in accordance with the initial concentration of EE2

during the electrochemical experiments and to ensure complete water solubility of this non-polar molecule (9200 µg/mL at 25°C [250]).

Linearity was determined by constructing calibration curves (n= 6) for 6 calibration standards with concentrations between the LLOQ and the ULOQ. All calibration curves demonstrated good linearity over a concentration range spanning 3 orders of magnitude with a regression coefficient (R^2) of at least 0.9970 (**Table S4.2**). For the determination of carry-over, the response of the blank samples analyzed after a ULOQ sample was less than 1% for the EE2 and for the IS. Blank degraded samples and non-electrolyzed samples were used to assess MEs. These samples were spiked with EE2 at the three levels of QC (20, 250 and 2500 µg/L) and the IS. Peak areas obtained for these samples were compared with the corresponding peak areas in ultrapure water spiked with the molecules of interest at the same concentration. **Table S4.3** shows that the obtained values ranged between 86.4 and 104.1%, indicating MEs were not-significant. Accuracy and precision results are shown in **Table S4.4** in the SI. The mean inter-day and intra-day precision were below 8.1% and 5.9%, respectively. The mean accuracy ranged between 97.0 and 106.9% for the intra-day assay and 102.3 and 110.6% for the inter-day assays. These results demonstrate the good reproducibility and reliability of the analytical method. Finally, dilution integrity was tested using a working solution with a concentration of 1.6-fold the ULOQ (8000 µg/L) and diluting this 10-, 100- and 500-fold with ultrapure water to cover the array of residual EE2 concentrations in the eAOP degraded samples. Accuracy ranged between 103.8 and 113.8% and precision ranged between 0.9 and 4.9% (**Table S4.5**). All method validation parameters hence met the validation criteria. Therefore, the developed UHPLC-QTOF-MS method was considered suitable for the quantification of EE2 in degraded samples.

4.3.2. Electrochemical degradation: optimization

Before conducting the electrochemical degradation tests, potential adsorption of EE2 on the electrodes was evaluated. To this end, aqueous solutions of EE2 (5000 µg/L) were magnetically stirred in the presence of the electrodes and electrolytes. After 30 min, sample aliquots were collected for analysis. The EE2 concentration was found to be 98.9% of the initial concentration. Consequently, EE2 adsorption on the electrodes was not considered significant. The degradation of EE2 via electrochemical oxidation on a BDD electrode occurs primarily due to •OH generated on the surface of the electrode. Besides generating •OH, the presence of Na_2SO_4 and NaCl also leads to the production of sulfate ($SO_4^{\bullet-}$) and chloride radicals ($Cl^{\bullet}$ and $Cl_2^{\bullet-}$), respectively [46,251]. Due to the distinct oxidation behavior of these radicals, it was expected that the type of electrolyte would directly affect the EE2 removal efficiency. To

optimize the removal of 5000 µg/L EE2 in 0.05 M Na_2SO_4, experiments were performed with two different current densities (j) of 6.25 mA/cm^2 and 12.5 mA/cm^2.

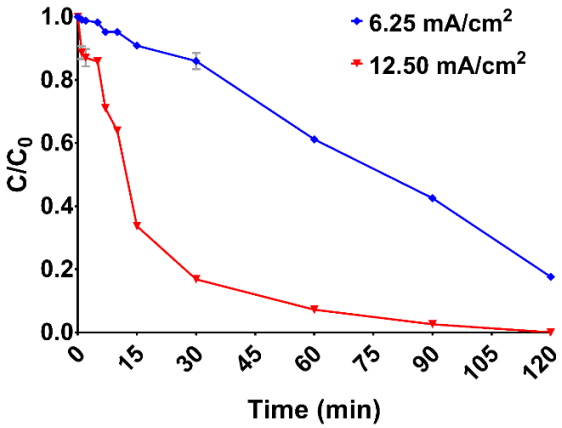

Figure 4.2 – EE2 removal at different currents in the presence of Na_2SO_4 at 0.05 M. $[EE2]_0$= 5000 µg/L; measurements performed in triplicate; mean ± standard deviation.

As shown in **Fig. 4.2**, a removal of 82.4% and more than 99.9% was achieved for a reaction time of 120 min, using 6.25 mA/cm^2 and 12.5 mA/cm^2, respectively. This is because a higher current density increases the electro-generation of •OH on the surface of the BDD, resulting in a faster removal of EE2. Assuming pseudo-first-order kinetics for the removal of EE2, the apparent rate constant (k_{app}) was calculated by plotting the logarithmic decay of EE2 versus the degradation time (data not shown). The obtained k_{app} values were 0.0117 min^{-1} and 0.0434 min^{-1} for current densities of 6.25 mA/cm^2 and 12.5 mA/cm^2, respectively. A current of 12.5 mA/cm^2 was, therefore, chosen as the optimal current density. Other studies have also shown the positive effect of an increased current density on the degradation of organic molecules [252–254].

Fig. 4.3 shows the effect of the electrolyte concentration and current density on the removal of EE2 using NaCl as the supporting electrolyte. Using 0.05 M NaCl and a current density of 12.5 mA/cm^2, EE2 was removed in less than 30 sec (data not shown). Therefore, lower electrolyte concentrations and current densities were evaluated to ensure sufficient intermediate sampling points for the subsequent chemical and biological analysis. The NaCl concentration was reduced to 0.025 M in order to decrease the number of active chlorinated species generated [229] and the current density was lowered to 6.25 mA/cm^2 and 3.125 mA/cm^2 to slow down the oxidation of EE2. Despite these changes, EE2 was still completely degraded within two minutes. In all cases, the logarithmic plot of EE2 decay versus time could not be computed due to a lack of sufficient sampling points. Keeping the current density at 3.125 mA/cm^2, the electrolyte concentration was, therefore, increased again to 0.05 M. Under these conditions, the removal of EE2 was completed in 15 min and the k_{app} value was determined to be 0.1393 min^{-1}.

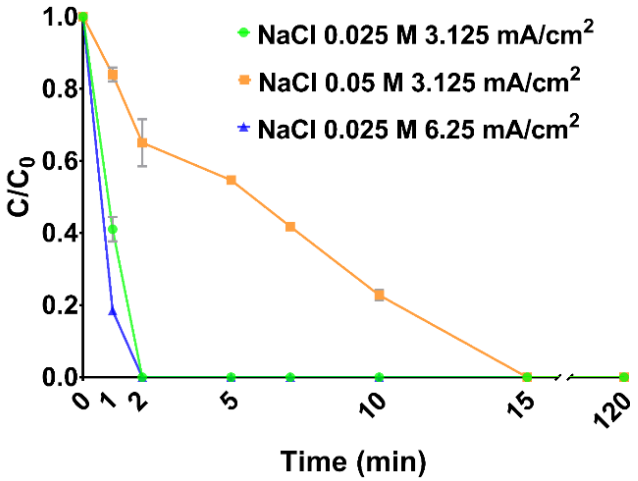

Figure 4.3 – Influence of NaCl concentration and current on the EE2 removal. $[EE2]_0$= 5000 µg/L, measurements performed in triplicate; mean ± standard deviation.

The removal of EE2 with NaCl as the supporting electrolyte instead of Na_2SO_4 was faster due to the preferential oxidation of the chloride ions (Cl^-) into free chlorine and the generation of chlorinated active species that contributed to the removal of EE2. Increasing the concentration of NaCl from 0.025 M to 0.05 M slowed down the degradation of EE2 due to the enhanced scavenging effect of Cl^- on the hydroxyl radicals (•OH). The reaction between these two species led to the formation of intermediates that further consumed •OH slowing down the removal of EE2. The effects of higher chloride concentrations on the electrochemical oxidation of organic pollutants on the surface of the BDD anodes has been reported previously by other researchers [255].

Based on the obtained removal for both electrolytes, different time points were selected for the generation of eAOP samples for an in-depth chemical and biological analysis. Due to its larger removal efficiency, the total degradation time was set to 30 min for samples to which NaCl was added, as opposed to 120 min for samples to which Na_2SO_4 was added. **Figs. S4.2** and **S4.3** show the residual concentration of EE2 and the removal rate at each time point of the electrochemical process. Likewise, EE2 was no longer detected by LC-MS after 120 min of electrochemical oxidation with Na_2SO_4 and after 2 min with NaCl.

4.3.3. Biological activity assessment

4.3.3.1. Estrogenic response

Fig. 4.4 represents a simplified diagram showing relevant features of the ChgH-GFP transgenic line.

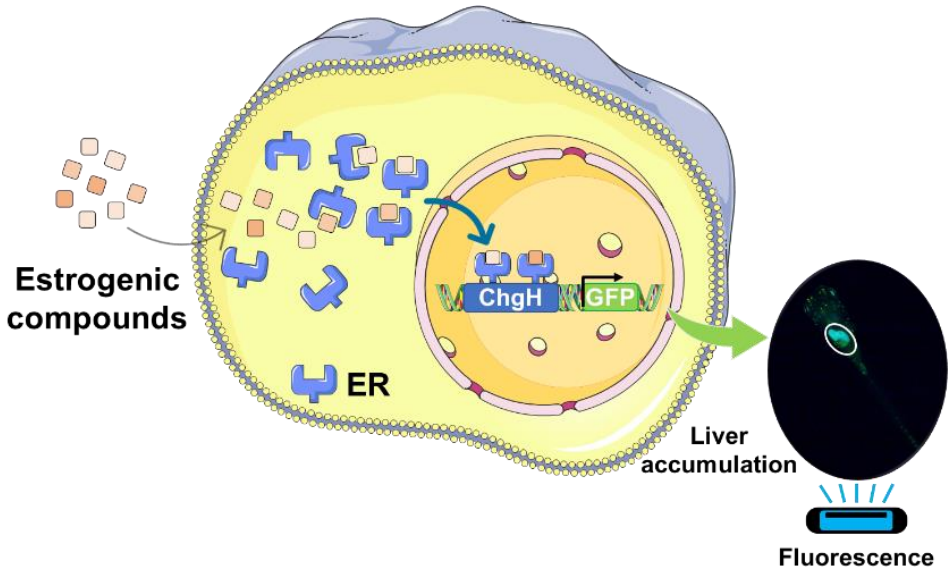

Figure 4.4 – Diagram of ChgH-GFP transgenic line.

EE2 and estrogenic active TPs interact with estrogen receptors (ER), leading to the activation of the estrogen responsive choriogenin H (ChgH) promoter. This activation promotes the production of the green fluorescence protein (GFP) that accumulates in the liver of the larvae. The amount of fluorescence relates to the amount of estrogen axis activity which is related to the presence of estrogenic compounds (EE2 and TPs) present in a sample.

Fig. 4.5 provides a visual representation of the fluorescence of a non-treated larva and the fluorescence of a larva exposed to the highest EE2 control sample (488 ng/L of EE2).

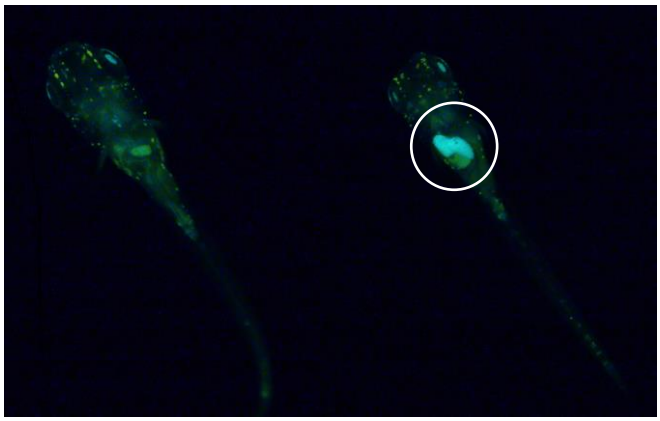

Figure 4.5 – Eleutheroembryos exposed to negative control (test medium) on the left and positive control (EE2 – 488 ng/L) on the right. The circle indicates the position of the liver where GFP is expressed.

To quantify the ChgH-GFP responsiveness to estrogenic compounds in these experiments, as demonstrated previously in other studies [237,239], the larvae were exposed to a concentration range of EE2 from 0 to 488 ng/L.

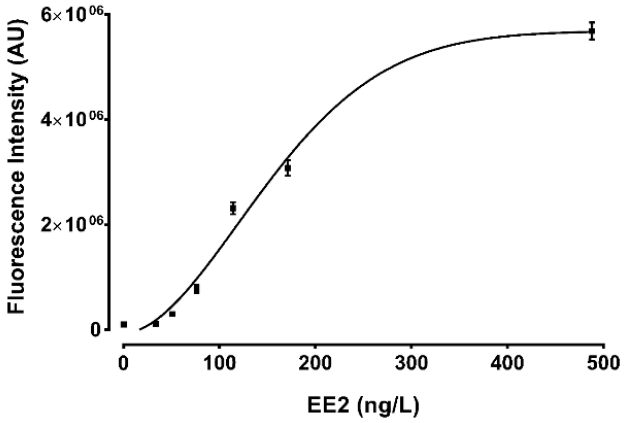

Figure 4.6 – EE2 concentration response curve constructed from the fluorescence values for the controls from all eight experiments which were performed (n= 96 for each exposure group). In comparison with the negative control (0 ng/L EE2), the ChgH-GFP response was statistically different at 76 ng/L and higher concentrations of EE2 ($p < 0.001$). Squares and error bars represent mean and standard error of the mean, respectively. AU: arbitrary units.

Fig. 4.6 shows the concentration response curve constructed using the mean fluorescence obtained when the data from the negative and positive control groups from all experiments were combined. It can be observed that an increasing concentration of EE2 led to higher levels of fluorescence in a concentration dependent manner. Under these experimental conditions, the ChgH-GFP response started to plateau at 170 ng/L reaching its saturation level at roughly 488 ng/L. In comparison with the negative controls, statistical significance was observed from a concentration of 76 ng/L EE2 onwards. This indicates that the current assay is slightly more sensitive than the assay reported by Kurauchi et al. (2005) where GFP induction was detected at a concentration of 100 ng/L for the same duration of exposure [239]. The significance level at these trace levels demonstrates the high sensitivity of this ChgH-GFP line, making it suitable for the monitoring of environmental samples.

4.3.3.2. Evolution of estrogenic activity

The overarching goal of the applied eAOP was to reduce the overall sample estrogenicity by oxidizing EE2 into biologically inert compounds. Different rates of degradation were obtained depending on the type of electrolyte used for the eAOP (**Figs. S4.2** and **S4.3**). Moreover, there was a possibility that different generated radicals with a distinct oxidizing power, would generate different TPs conferring a different biological activity to the degraded samples.

Prior to the estrogenic assessment of the EE2 degraded samples, the estrogenic activity of blank degraded samples was tested to verify the influence of the respective matrices on the ER. While the blank sample at t= 0 min containing NaCl was not toxic, acute toxicity occurred

for samples at all time points that were degraded in the presence of NaCl. All medaka larvae exposed to these samples were dead after 24 h of exposure (data not shown). It is assumed that the oxidation of Cl ions at the BDD anode gives rise to active chlorine species such as Cl_2, HClO, and ClO^-, that contribute to the oxidation of organic compounds [256,257]. However, due to the high oxidation capacity of the BDD anode, the aforementioned chlorine species can be further oxidized into chlorate and perchlorate ions [257], which are toxic to living organisms [258,259]. The formation and accumulation of these chlorine derivatives may be the cause of the observed acute toxicity. When samples were diluted 2-fold with test medium before exposure to the medaka larvae, no signs of toxicity were observed after 24 h of exposure. **Figs. S4.4** and **S4.5** show the estrogenic activity of the blank degraded samples diluted 2-fold with test medium. The level of fluorescence of all blank samples showed no statistical significance when compared to the negative control, indicating no interaction between the matrix of the samples and the ER.

Despite the efficient removal of EE2 observed in **section 4.3.2.**, the residual EE2 concentration was still too high for a proper estrogenic evaluation, as it exceeded the saturation level (488 ng/L EE2) in the 2-fold diluted samples (data not shown). To address this, a series of dilutions were tested prior to the estrogenic assessment. Each dilution was evaluated through three individual estrogenic tests, and the results are shown in **Figs. S4.6-S4.9**. These figures show the fluorescence signals of the exposed larvae in the three test groups. Besides negative and positive controls, the fluorescence signals obtained for the initial and degraded samples are shown. The concentration response curve derived from the fluorescence means of the positive control samples was used for the calculation of the hormonal equivalent (HEq). The HEq represents the overall estrogenic activity of the degraded sample and is expressed in ng/L of EE2 in a control sample. This estrogenic activity is caused not only by non-degraded EE2 left in the sample but also by TPs that preserve the estrogenic activity.

For a proper HEq calculation, degraded samples were only considered if the mean of fluorescence was above the significance level ($p< 0.05$) and below the fluorescence saturation level (EE2 at 488 ng/L). Extrapolated values were then multiplied with the dilution factor (DF). The relative EE2 concentration (**Eq. 4.3**) and relative HEq (**Eq. 4.4**) were calculated as follows:

$$Relative\ [EE2]\ (\%) = \frac{[EE2]_{t= x\ min}}{[EE2]_0} \times 100\% \qquad \textbf{(Eq. 4.3)}$$

$$Relative\ HEq\ (\%) = \frac{HEq_{t= x\ min} \times DF}{HEq_0 \times DF} \times 100\% \qquad \textbf{(Eq. 4.4)}$$

The EE2 concentration and HEq were normalized to the EE2 concentration and HEq of the corresponding initial sample (t= 0 min, HEq_0 and $[EE2]_0$ in **Eqs. 4.3** and **4.4**) and compared with each other at the corresponding time point. Values below 0.1% were not considered due

to the lower sensitivity of the LC-QTOF-MS method in comparison with the estrogenic test, as the LOD of the LC-MS method (3 µg/L) was nearly 0.1% of the initial concentration of EE2 for the eAOP experiments (5000 µg/L). **Figs. 4.7** and **4.8** show the time-dependent decrease of the relative EE2 concentration and HEq of the degraded samples with Na_2SO_4 and NaCl, respectively.

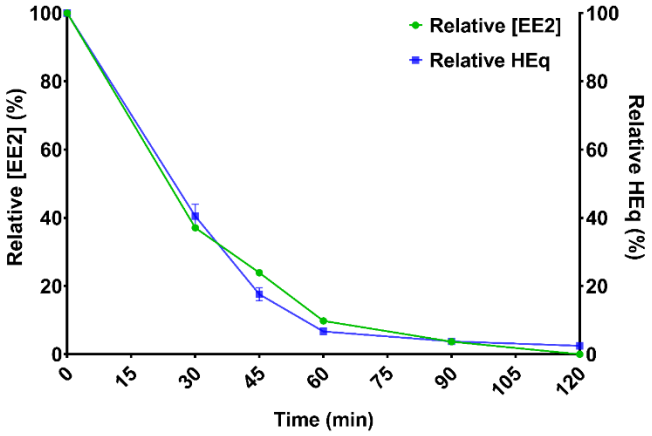

Figure 4.7 – Comparison between relative EE2 concentration (primary axis) and relative HEq (secondary axis) of samples degraded in the presence of Na_2SO_4. EE2 quantification was performed in triplicate. HEq value was calculated from the pooling of 3 estrogenic tests. Results are expressed in mean ± 95% confidence interval [upper limit - lower limit].

As can be seen in **Fig. 4.7**, during the course of the electrochemical oxidation performed in the presence on Na_2SO_4, a good correlation between the removal of EE2 and the decrease of the estrogenic activity was observed, indicating that the estrogenic activity was primarily caused by the residual EE2 in the samples. There were, however, small deviations. At t= 30 min, the HEq was slightly higher than the EE2 concentration. This relation was inverted at t= 45 min and t= 60 min. It could be hypothesized that an anti-estrogenic effect lowered the response to EE2. The cause for this anti-estrogenic effect is, however, unclear. One hypothesis is the formation of antagonist compounds that compete with EE2 on the ER binding site at these time points. Another hypothesis is a possible interference of the degraded samples via another mode of action, affecting the estrogen axis of the ChgH-GFP medaka larvae. These small differences could, however, also be the result of the variability of the biological measurements, suggesting no real difference between the relative EE2 concentration and HEq. From t= 90 min until the end of the eAOP experiment, the HEq was higher than the EE2 concentration, indicating a total removal of the estrogenic activity was not achieved (**Fig. S4.7**). This might be attributable to estrogenic active TPs that were generated during the electrochemical process.

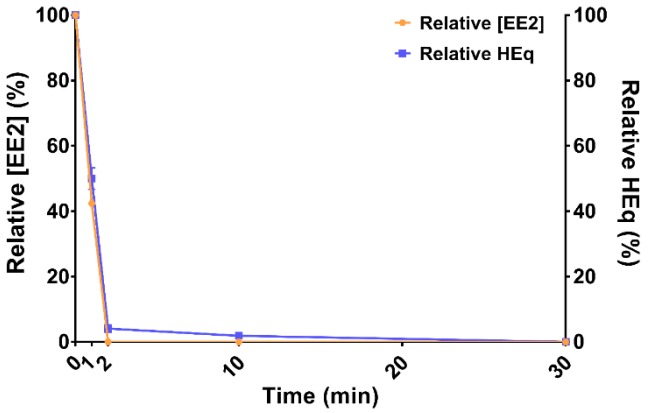

Figure 4.8 – Comparison between relative EE2 concentration (primary axis) and relative HEq (secondary axis) of samples degraded in the presence of NaCl. EE2 quantification was performed in triplicate. HEq value was calculated from the pooling of 3 estrogenic tests. Results are expressed in mean ± 95% confidence interval [upper limit - lower limit].

As illustrated in **Fig. 4.8**, the removal of EE2 in the presence of NaCl also resulted in a substantial decrease of estrogenicity. However, it is also apparent that the relative HEq of the degraded samples remained slightly but consistently higher than the relative EE2 concentration, despite the continuous reduction of the overall estrogenic activity throughout the duration of the electrochemical process. This again could be due to the variability of the biological measurements. However, the generation of TPs that conserve the biological properties of the precursor molecule cannot be excluded. Moreover, a statistically significant induction of fluorescence ($p< 0.05$) was found at the end of the electrochemical process (t= 30 min) (**Fig. S4.9**), revealing that estrogenic activity was not completely eradicated.

4.3.4. Identification and monitoring of transformation products

Previous studies have demonstrated that an alteration of the phenolic moiety at the A-ring efficiently reduces the estrogenicity of EE2 degraded samples. Nevertheless, it is presumed that some TPs formed during eAOP might still conserve the phenol group of the A-ring, retaining estrogenic activity. To obtain a better understanding of the effect of these TPs on the estrogenic activity, the primary TPs of EE2 formed during the electrochemical degradation process were investigated and identified via UHPLC-QTOF-MS using a non-targeted approach. The most relevant TPs were tentatively identified based on their accurate mass (m/z), isotopic pattern, MS/MS fragmentation data and confirmation with literature data. Following the extraction of molecular features, a structural elucidation workflow was used to tentatively identify the generated TPs, as depicted in **Fig. 4.9**.

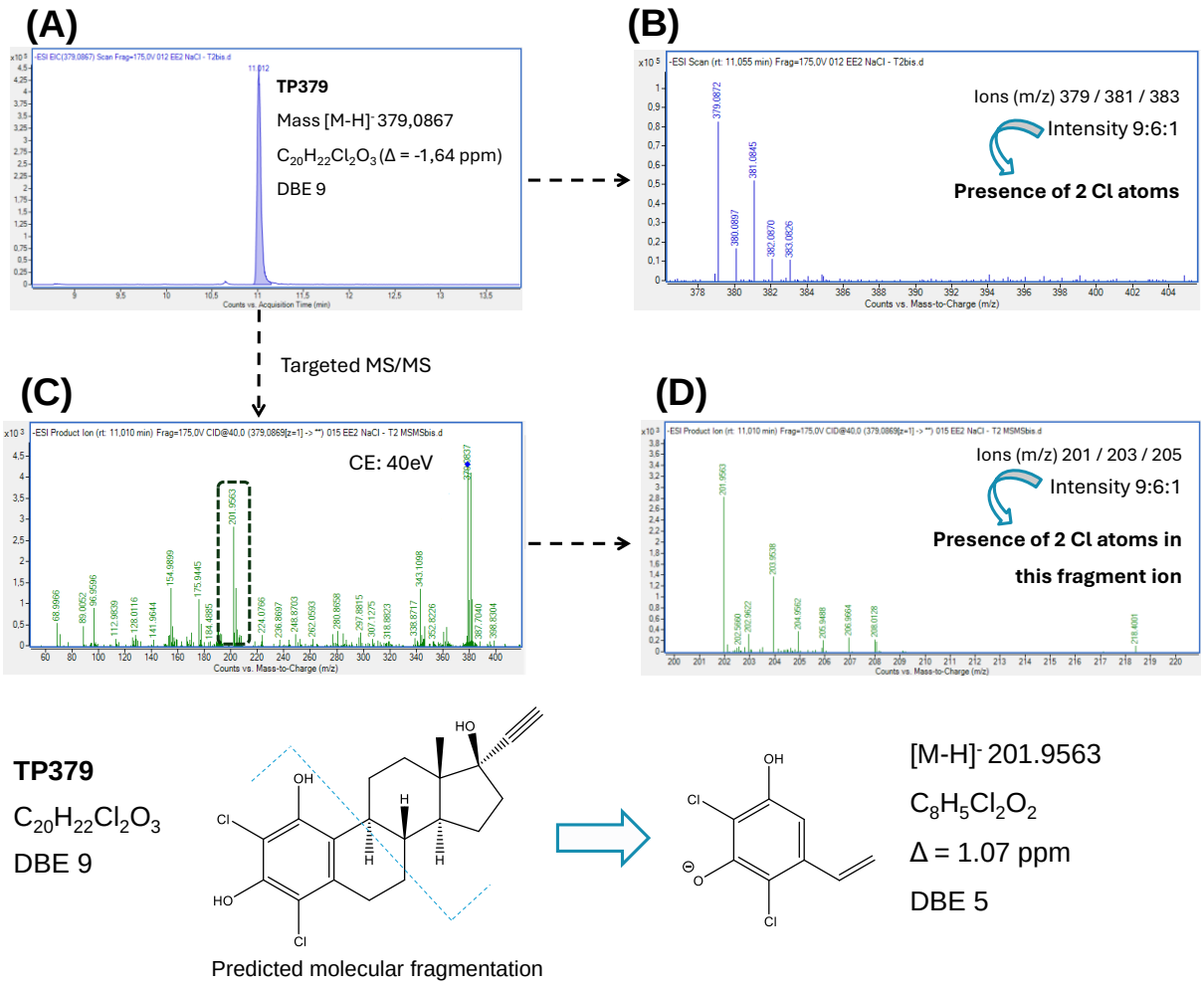

Figure 4.9 – Tentative structure elucidation workflow using TP379 as an example. **(A)** EIC of TP379. It is the TP with the highest signal intensity. **(B)** Spectra of TP379 showing typical isotopic pattern of 2 Cl atoms. **(C)** Fragmentation spectra of TP379. Focus on fragment 201. **(D)** Zoom on fragment 201. MSMS: tandem mass spectrometry; DBE: double bond equivalent.

Table 4.1 reports 22 TPs formed in the presence of Na_2SO_4, of which 17 were assigned a tentative structure. Most of these TPs had a higher molecular weight and lower retention time than EE2. This is in agreement with the addition of polar substituents, such as hydroxyl groups, that will lead to a lower retention on the reversed-phase stationary phase.

Fig. 4.10 shows the evolution of the TPs generated in the presence of Na_2SO_4 as a function of degradation time. In accordance with the obtained experimental data, the radicals mainly attacked the aromatic A-ring leading to its hydroxylation. The most abundant TP was TP312 which has a difference of 16 mass units with respect to EE2, indicating a hydroxylation of EE2. Semi-empirical calculations by Sun et al. (2010) showed that C2 is the most probable site of attack of the OH radicals, leading to an -OH attachment [260]. Therefore, TP312 is likely to be 2-OH-EE2. With a difference of 32 mass units with respect to EE2, TP328 has two additional hydroxyl groups on the A-ring with an unknown location. The formation of these TPs was also

reported for other types of AOPs, such as photocatalysis, *in situ* chemical oxidation (ISCO) and ozonation [260–262].

Moreover, based on the obtained product ion spectra, further direct attack of the radicals on the A-ring led to its oxidative cleavage. The resulting chemical structures displayed aromatic ring opening and the presence of hydroxyl, carbonyl and carboxyl groups (TP332, TP334, TP336, TP344a-c, TP360a-b). As can be seen in **Table 4.1**, fragment ions were detected at lower collision energies (10-20 eV), indicating the presence of C-C bonds that are energetically favorable for CID [147]. This is in contrast to the fragmentation of EE2 and TPs with an intact four fused ring structure that required higher collision energies to fragment (40-50 eV) [263]. Aromatic ring opening products are commonly produced in both $SO_4^{\bullet-}$ and •OH based oxidation of phenolic compounds [264]. Similar structures were found by Zhou et al. (2018) who reported the generation of TPs in the presence of peroxymonosulfate [261].

Nonetheless, the radicals also reacted with the ethinyl group leading to its detachment and a possible new conjugated double bond in the D-ring. This is the case for TP286 which despite having an extra hydroxylation on the A-ring, has a lower molecular weight than EE2 due to the loss of the ethinyl group (C_2H_2, 26 mass units). Further oxidation led to structures displaying aromatic ring opening (TP302a and TP302b). In accordance with the experimental data, a degradation pathway is proposed in **Fig. 4.11**.

Table 4.1 – List of TPs of EE2 formed during eAOP in the presence of Na_2SO_4.

Compound	RT (min)	Elemental formula	Measured m/z (Da)	Mass accuracy (Δ ppm)	DBE	Fragment ions (m/z)	Collision energy (eV)	Confidence level	Proposed structure	Match in literature
EE2	10.4	$C_{20}H_{24}O_2$	295.1700	-1.19	9	145.0644 159.0787 269.1505 199.1091	40 40 40 40	1	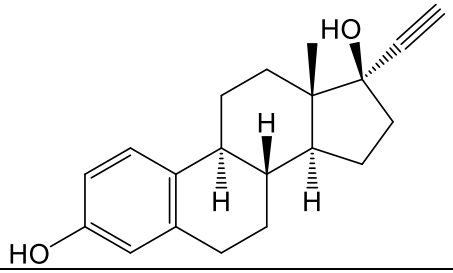	[265,266]
TP 286	8.8	$C_{18}H_{22}O_3$	285.1501	1.68	8	122.0387 108.0210	40 40	3	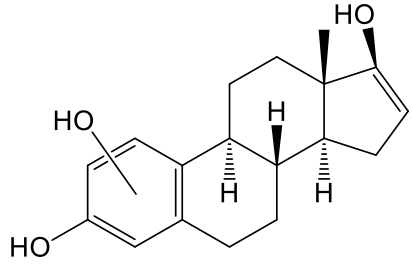	-
TP 294	10.4	$C_{20}H_{22}O_2$	293.1570	7.81	10	209.0968 195.0811	40 40	3	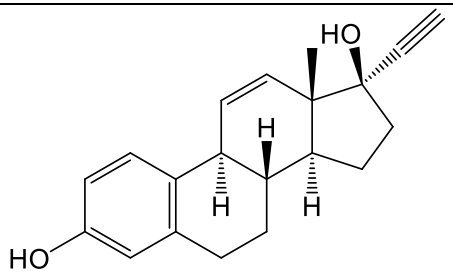	-

TP 302a	8.6	$C_{18}H_{22}O_4$	301.1442	-1.10	8	257.1558 231.1388	20 20	3	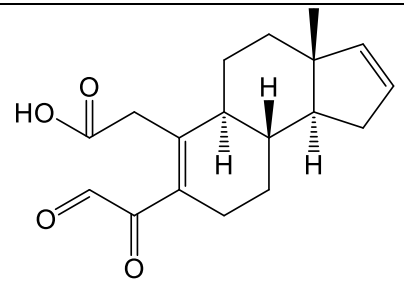	-
TP 302b	8.8					257.1558 231.1388	20 20	3	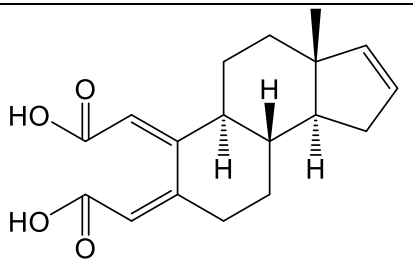	-
TP 302c	6.2					-		4	-	-
TP 310	9.5	$C_{20}H_{22}O_3$	309.1496	-0.06	10	119.0498 183.0119	50 40	3	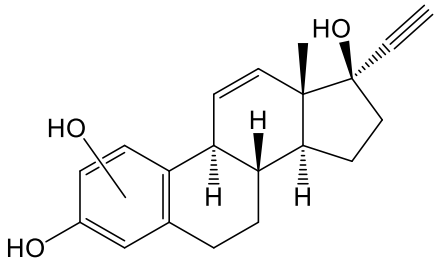	-
TP 312	8.8	$C_{20}H_{24}O_3$	311.1652	-0.22	9	285.1498 122.0361 108.0211	40 50 50	2b	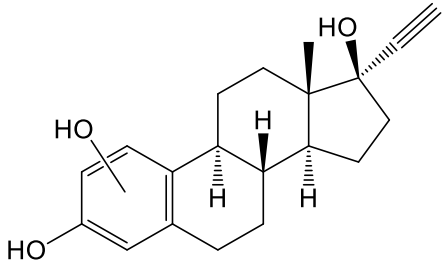	[260]

TP 326a	9.3	$C_{20}H_{22}O_4$	325.1446	0.21	10	299.1269 161.0601 159.0441	40 40 40	3	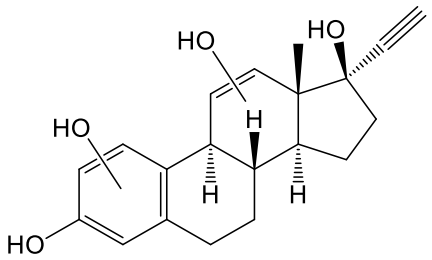	-
TP 326b	8.2					123.0488 237.0905	40 40	3	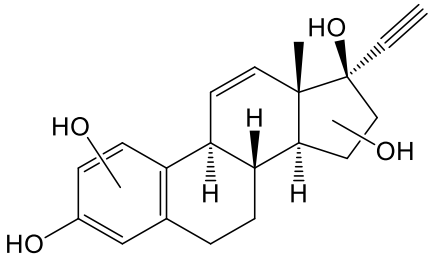	-
TP 328	9.1	$C_{20}H_{24}O_4$	327.161	2.49	9	299.1689 255.1780	40 40	2b	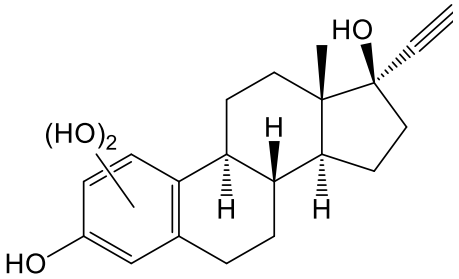	[261]
TP 332	7.4	$C_{19}H_{24}O_5$	331.1543	-2.40	8	287.1633 165.1309	10 20	2b	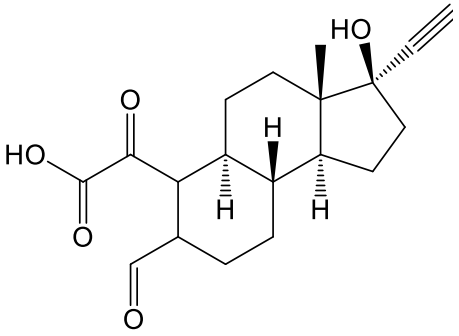	[261]

TP 334	5.8	$C_{18}H_{22}O_6$	333.1338	-1.68	8	289.1462 165.1277	20 20	3	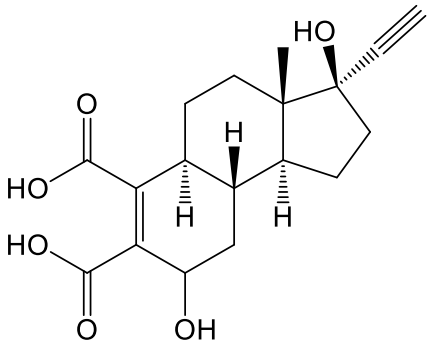	-
TP 336	5.4	$C_{18}H_{24}O_6$	335.1503	0.86	7	317.1376 291.1596 165.1274	10 10 20	3	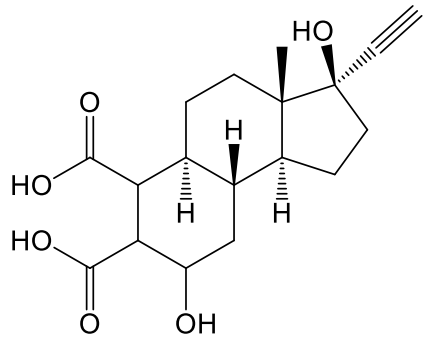	-
TP 344a	8.6	$C_{20}H_{24}O_5$	343.1559	2.33	9	291.1596 271.1670	20 20	3	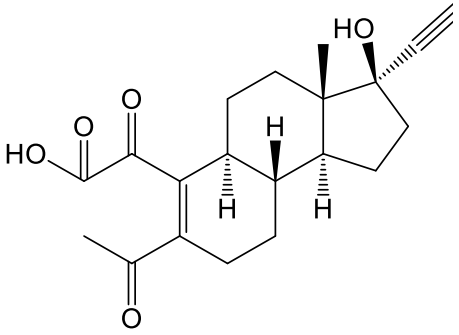	-

TP 344b	6.8					299.1655 273.1533	20 20	3	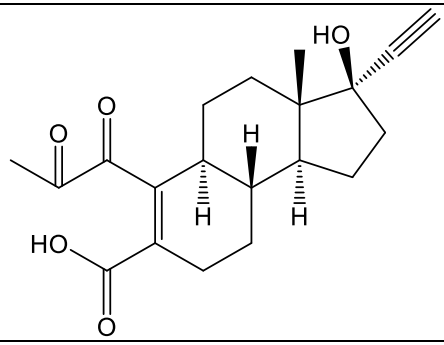	-
TP 344c	9.1					299.1640 285.1509	20 20	3	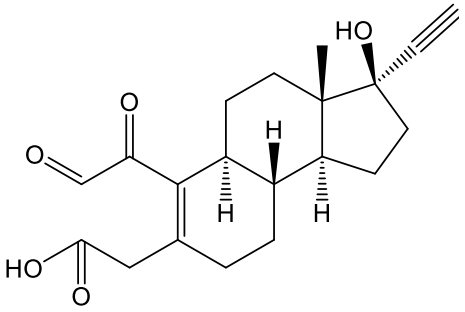	-
TP 360a	6.0	$C_{20}H_{24}O_6$	359.1497	-0.87	9	271.1642 72.9946 182.9388	20 20 20	2b	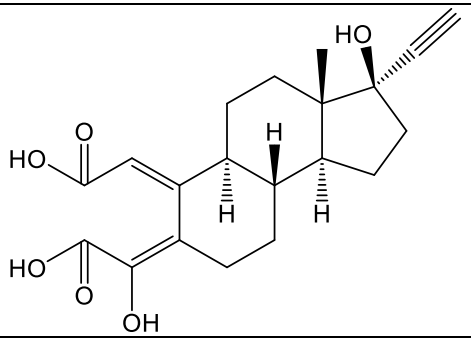	[261]

TP 360b	6.2					271.1633 315,1586 72.9929	20 20 20	2b	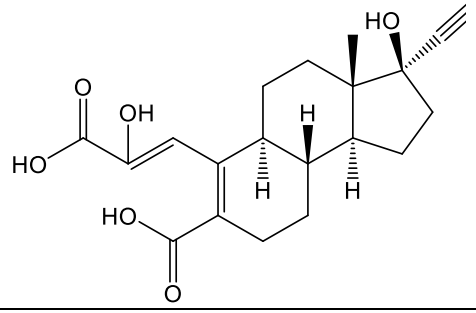	[261]
TP 360c	8.7					-	-	4	-	-
TP 378a	8.7					-	-	4	-	-
TP 378b	7.7	$C_{20}H_{26}O_7$	377.1601	-1.26	8	-	-	4	-	-
TP 378c	5.8					-		4	-	-

Legend: RT: retention time; DBE: double bond equivalent.

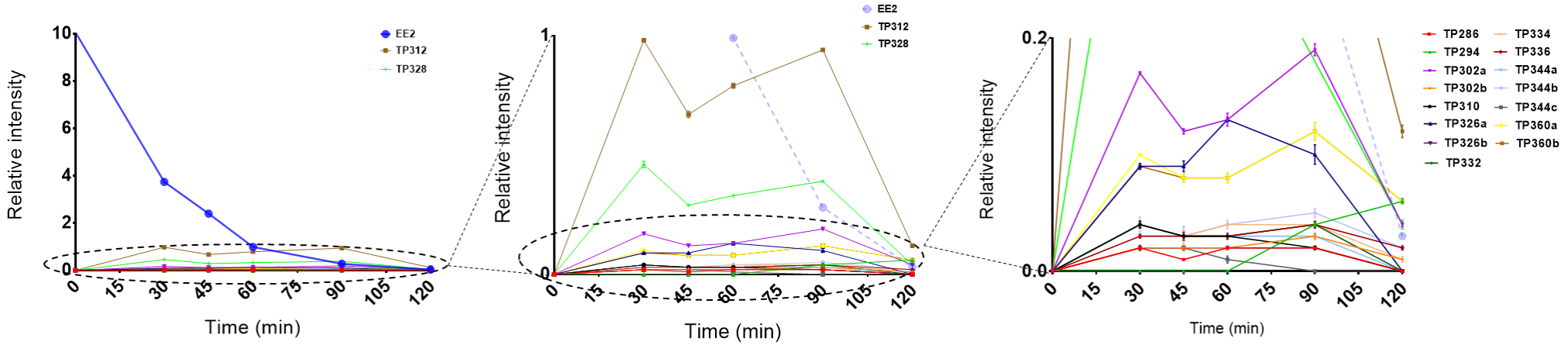

Figure 4.10 – Time course monitoring of TPs generated in the presence of Na_2SO_4. Relative intensity: AUC_{TP} / AUC_{IS}.

As can be seen in **Fig. 4.10**, the degradation profiles of the most relevant TPs exhibited an M-shaped pattern. After an initial increase from t= 0 to t= 30 min, the relative intensity of the TPs decreased from t= 30 to t= 45 min. Subsequently, the relative intensity increased again from t= 45 to t= 90 min, before decreasing until the end of the electrochemical degradation process. This pattern was consistently observed across multiple (repeated) measurements, while the EE2 degradation profile was as shown in **Fig. 4.2**. The cause for this M-shaped pattern is not clear. It is hypothesized that the reaction of •OH and $SO_4^{\bullet-}$ with the phenolic moiety led to the formation of hydroxycyclohexadienyl radicals (C_6H_6O•) via electron transfer and phenoxyl radicals (C_6H_5O•) via hydrogen abstraction [264,267]. The generation and recombination of these intermediate products could have led to the formation of carbon–carbon and carbon–oxygen dimerization products [264,268] and, in this way, reduced their relative intensity. The increase in relative intensity from t= 45 to t= 90 min could then have been caused by the dissociation of these dimers. Nevertheless, none of these presumed compounds was detected.

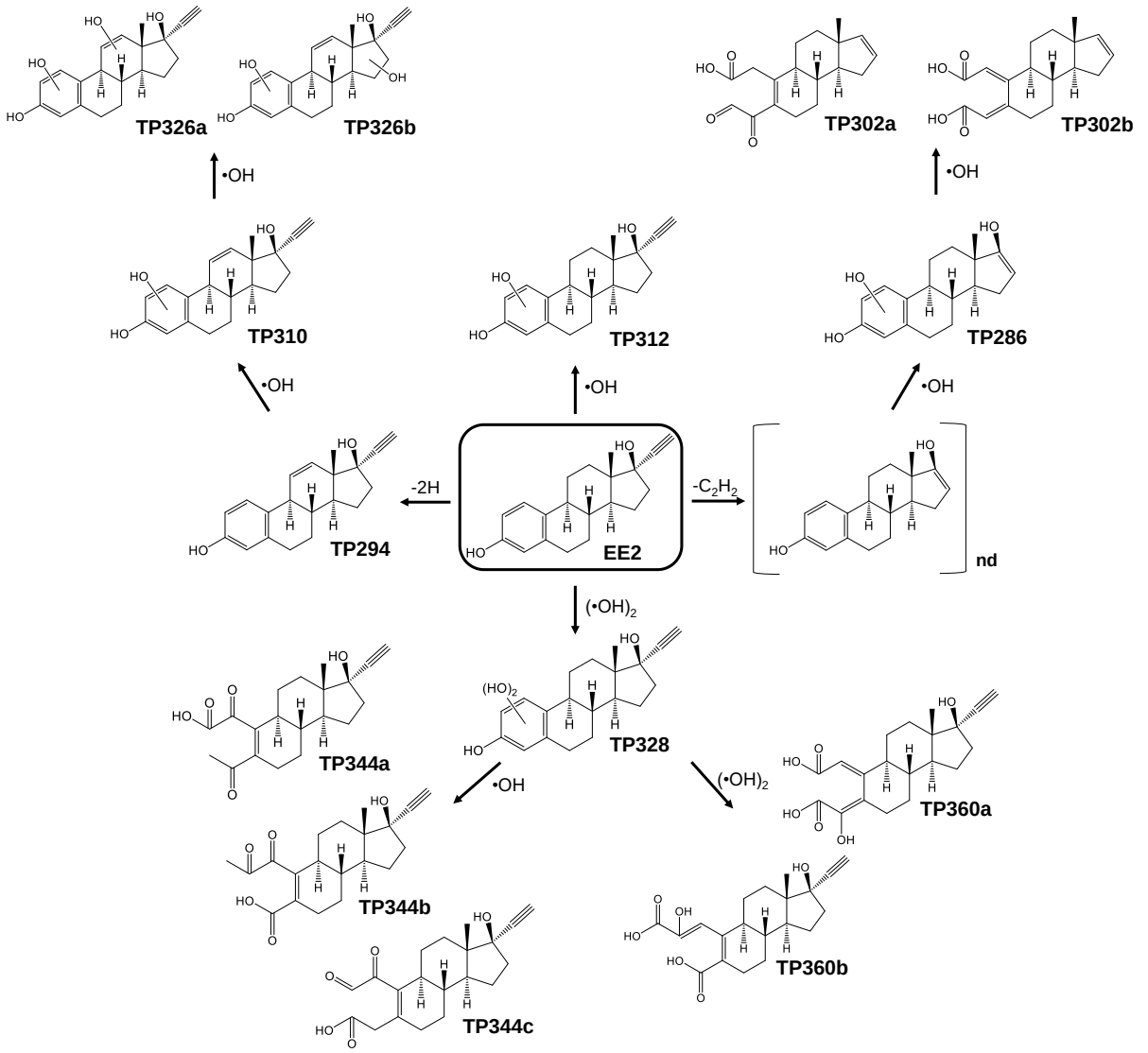

Figure 4.11 – Proposed degradation pathway of EE2 in the presence of Na_2SO_4. nd: not detected.

Table 4.2 shows 57 TPs formed in the presence of NaCl, of which 26 TPs were given a tentative chemical structure. The higher number of TPs generated in the presence of NaCl could be the result of the higher reactivity and the lower selectivity of the chlorine species [256,269]. The mass spectra of most of these TPs presented the typical isotopic pattern of ^{35}Cl / ^{37}Cl isotopes, confirming the halogenation of EE2. Based on the experimental data, it was deduced that chlorine species in combination with •OH reacted directly with the phenolic moiety. As shown in **Table 4.2**, several isomeric structures were formed due to the addition of oxygen and/or substitution of chlorine in the *ortho*, *meta* and *para* position. Moreover, the retention time of the halogenated TPs was higher than that of EE2. The halogenation of the A-ring is believed to decrease the polarity of the phenolic moiety, resulting in a higher retention on the reversed-phase column. This is consistent with the findings of Zhou et al. (2018) and Gervais et al. (2011) [261,270].

Nevertheless, the presence of NaCl did not only generate chlorinated TPs. The most abundant non-chlorinated TP was TP294. With regards to EE2, TP294 has two mass units less, one additional double bond equivalent (DBE) and the same chromatographic retention time, suggesting an additional conjugated double bond in the chemical structure. In accordance with the experimental data, it is believed that this compound was formed by the removal of two hydrogens from the aliphatic C-ring of EE2 via hydrogen abstraction. A similar structure was identified by Hwang et al. (2008) by the oxidation of EE2 with Mn (III) [271]. The authors confirmed that the extra double bond was situated between C9 and C11 by nuclear magnetic resonance (NMR). NMR was, however, not within the scope of the present study. Therefore, the exact position of the double bond could not be confirmed. Nevertheless, it is clear that the phenolic ring remained intact, conserving the estrogenicity of the parent compound. TP294 was generated at the start of the electrochemical process, and was detected from t= 1 min to t= 10 min, reaching its highest relative intensity at t= 2 min. Because of its high yield, TP294 was believed to be the main TP responsible for the higher relative HEq observed in **Fig. 4.8**. TP294 was also produced in the presence of Na_2SO_4, but to a much lower extent. In the presence of Na_2SO_4, TP294 was detected from t= 60 to t= 120 min of the electrochemical process, potentially contributing to the higher relative HEq in the later phase of the electrochemical process (**Fig. 4.7**). It is plausible that an extra double bond made this TP more susceptible to oxidation, making it an important intermediate. For example, TP328a-b ($C_{20}H_{21}ClO_2$) are the dehydrogenated counterparts of TP330a-b ($C_{20}H_{23}ClO_2$), and have an additional double bond. They have the same retention time and fragment ion (m/z 179, $C_{10}H_8ClO$), revealing the presence of a chlorine in the A-ring. However, the relative peak intensity of TP330a-b reached its maximum at t= 2 min, whereas for TP328a-b it was reached at t= 10 min. The later emergence of TP328a-b suggest that T294 was the intermediate compound.

Table 4.2 – List of TPs of EE2 formed during eAOP in the presence of NaCl.

Compound	RT (min)	Elemental formula	Measured m/z (Da)	Mass accuracy (Δ ppm)	DBE	Fragment ions (m/z)	Collision energy (eV)	Confidence level	Proposed structure	Match in literature
EE2	10.4	$C_{20}H_{24}O_2$	295.1700	-1.19	9	145.0644 159.0787 269.1505 199.1091	40 40 40 40	1	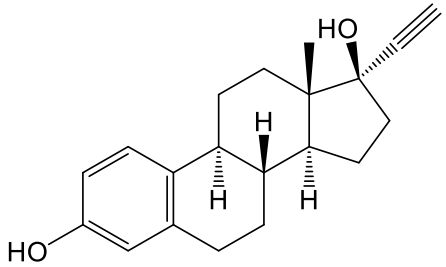	[265,266]
TP294	10.4	$C_{20}H_{22}O_2$	293.1542	-1.71	10	195.0808 209.0947 145.0650	40 40 50	3	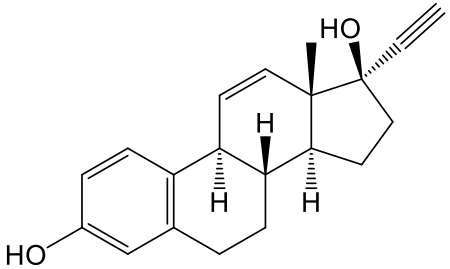	-
TP308a	9.9	$C_{20}H_{20}O_3$	307.1331	-2.82	11	209.0966 171.0813 119.0507	40 40 50	3	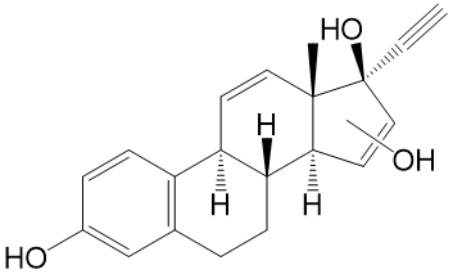	-
TP308b	9.5									

TP310	8.4	$C_{20}H_{22}O_3$	309.1509	0.91	10	211.0794 145.0657 107.0489	40 40 50	3	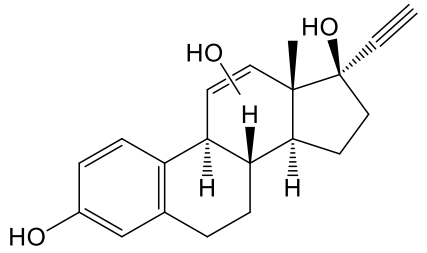	-
TP312	8.8	$C_{20}H_{24}O_3$	311.1651	-0.54	9	285.1490 122.0350 108.0206	40 50 50	2b	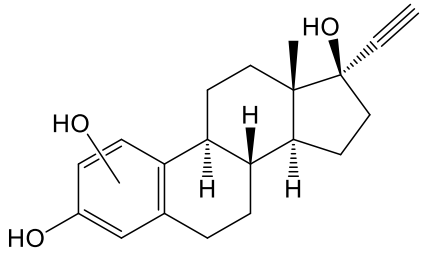	[260]
TP326a	9.3	$C_{20}H_{22}O_4$	325.1441	-1.33	10	299.1284 161.0595 159.0441	40 40 40	3	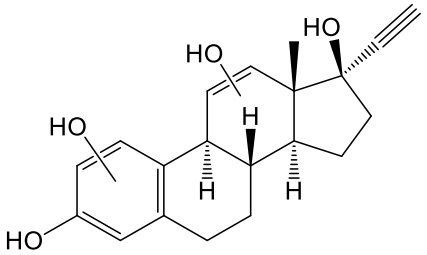	-
TP326b	8.2					307.1332 237.0920	20 40	3	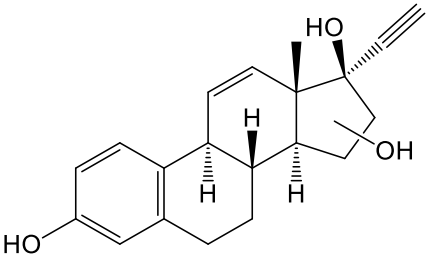	-
TP328a	11.1	$C_{20}H_{21}ClO_2$	327.1154	-1.01	10	229.0390	40	3		-

						179.0266	40			
TP328b	11.3								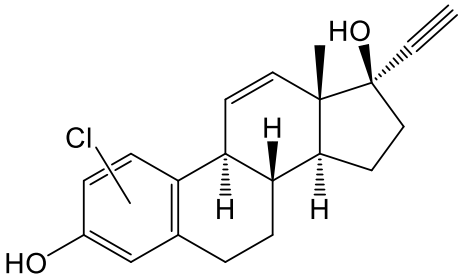	
TP330a	11.1	$C_{20}H_{23}ClO$	329.1313	-0.25	9	179.0250 233.0766	50 50	3	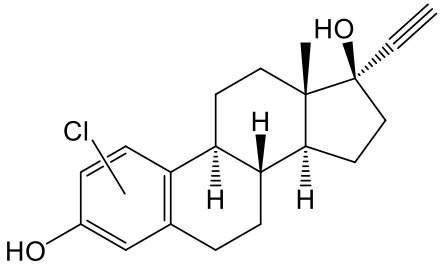	-
TP330b	11.3									
TP336a	11.3	$C_{18}H_{21}ClO_4$	335.1051	-1.37	8	-	-	4	-	-
TP336b	10.6						-			
TP342a	10.4	$C_{20}H_{22}O_5$	341.1401	1.91	10	-	-	4	-	-
TP342b	9					-	-	4	-	-
TP346a	10.1	$C_{20}H_{23}ClO_3$	345.1259	-1.14	9	327.1166 309.1514 167.9993	20 20 40	2b	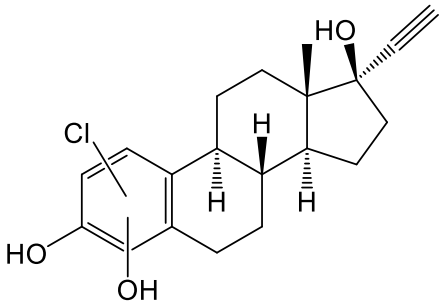	[261]
TP346b	9.9									
TP346c	9									
TP346d	8.7									
TP346e	9.6									
TP354	11.3	$C_{18}H_{20}Cl_2O_3$	353.0713	-1.05	8	-	-	4	-	-
TP356	10.6	$C_{18}H_{22}Cl_2O_3$	355.0869	-1.19	7	-	-	4	-	-

TP362	11.8	$C_{20}H_{20}Cl_2O_2$	361.0765	-0.71	10	263.0001 227.0031 174.9677	40 40 40	3	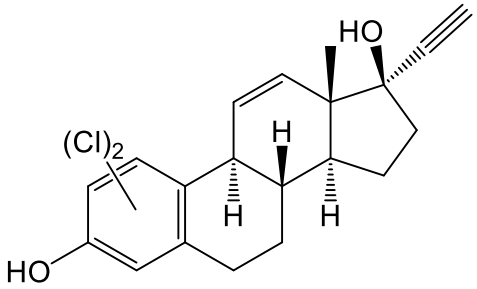	-
TP364	11.8	$C_{20}H_{22}Cl_2O_2$	363.0918	-1.67	9	212.9870 281.0528 174.9701	40 40 40	3	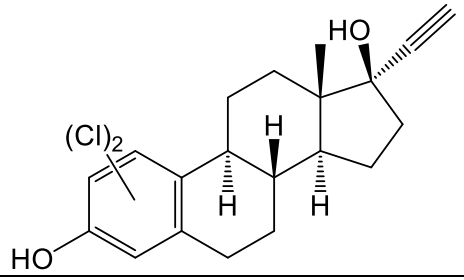	-
TP368a	11.9	$C_{19}H_{22}Cl_2O_3$	367.0864	-2.58	8	-	-	4	-	-
TP368b	11.5									
TP368c	11.4									
TP368d	10.9									
TP378	11.3	$C_{20}H_{20}Cl_2O_3$	377.0718	0.33	10	343.1105 203.9584	20 40	3	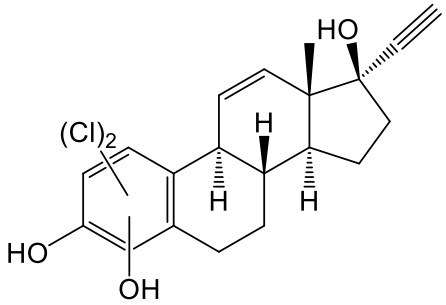	-
TP380a	11.0	$C_{20}H_{22}Cl_2O_3$	379.0873	-0.06	9	343.1100 201.9584	20 40	2b		[261]
TP380b	11.3									

TP380c	11.6					188.9509 154.9897	40 40		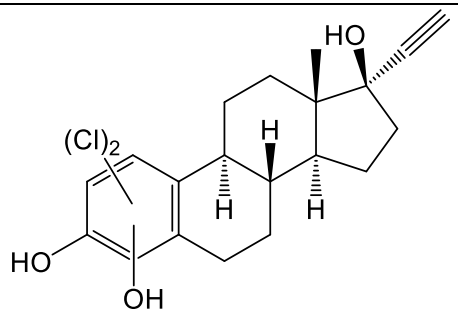	
TP380d	12.3					-		4	-	-
TP382	7.2	$C_{19}H_{20}Cl_2O_4$	381.0664	-0.49	9	-		4	-	-
TP394	11.4	$C_{20}H_{20}Cl_2O_4$	393.067	1.05	10	357,0893 201.9575 188.9512	20 40 40	3	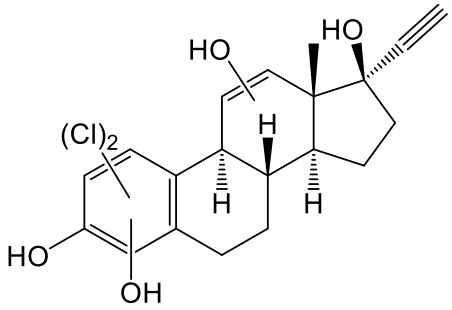	
TP398	9.3	$C_{19}H_{20}Cl_2O_5$	397.0615	-1.01	9	-	-	-	-	-
TP402a	12.6	$C_{19}H_{21}Cl_3O_3$	401.0481	-0.62	8	-	-	4	-	-
TP402b	12.3						-			
TP402c	12						-			
TP410	9.5	$C_{20}H_{20}Cl_2O_5$	409.0608	-1.71	10	-	-	4	-	-
TP412	9.5	$C_{20}H_{22}Cl_2O_5$	411.0794	4.45	9	-	-	4	-	-
TP414a	12.4	$C_{20}H_{21}Cl_3O_3$	413.0481	-0.61	9	377.0699 201.9583 188.9503	20 40 40	3		-

TP414b	13.1									
TP414c	12.1									
TP426	12.3	$C_{21}H_{24}Cl_2O_5$	425.092	-1.88	9	-	-	4	-	-
TP450	12.7	$C_{20}H_{22}Cl_4O_3$	449.0258	1.71	8	-	-	4	-	-
TP452	11.5	$C_{19}H_{20}Cl_4O_4$	451.0044	0.24	8	-	-	4	-	-
TP460a	12.4	$C_{21}H_{23}Cl_3O_5$	459.0532	-1.37	9	-	-	4	-	-
TP460b	13.1						-			
TP466a	12.4	$C_{20}H_{22}Cl_4O_4$	465.019	-2.02	8	-	-	4	-	-
TP466b	12.3						-			
TP466c	12.1						-			
TP483	13	$C_{20}H_{21}Cl_5O_3$	482.9845	-3.22	8	-	-	4	-	-
TP604a	11.6	$C_{40}H_{44}O_5$	603.3108	-1.32	19	-	-	4	-	-
TP604b	11.3						-			
TP604c	11.5						-			
TP706	10.4	$C_{40}H_{44}Cl_2O_7$	705.2392	0.1	18	-	-	4	-	-

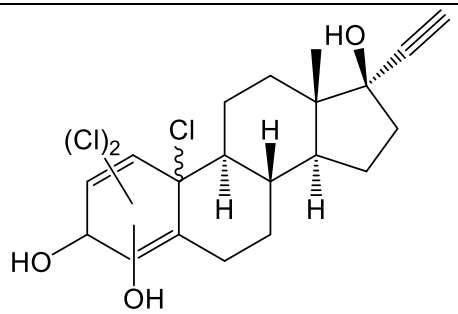

Legend: RT: retention time; DBE: double bond equivalent.

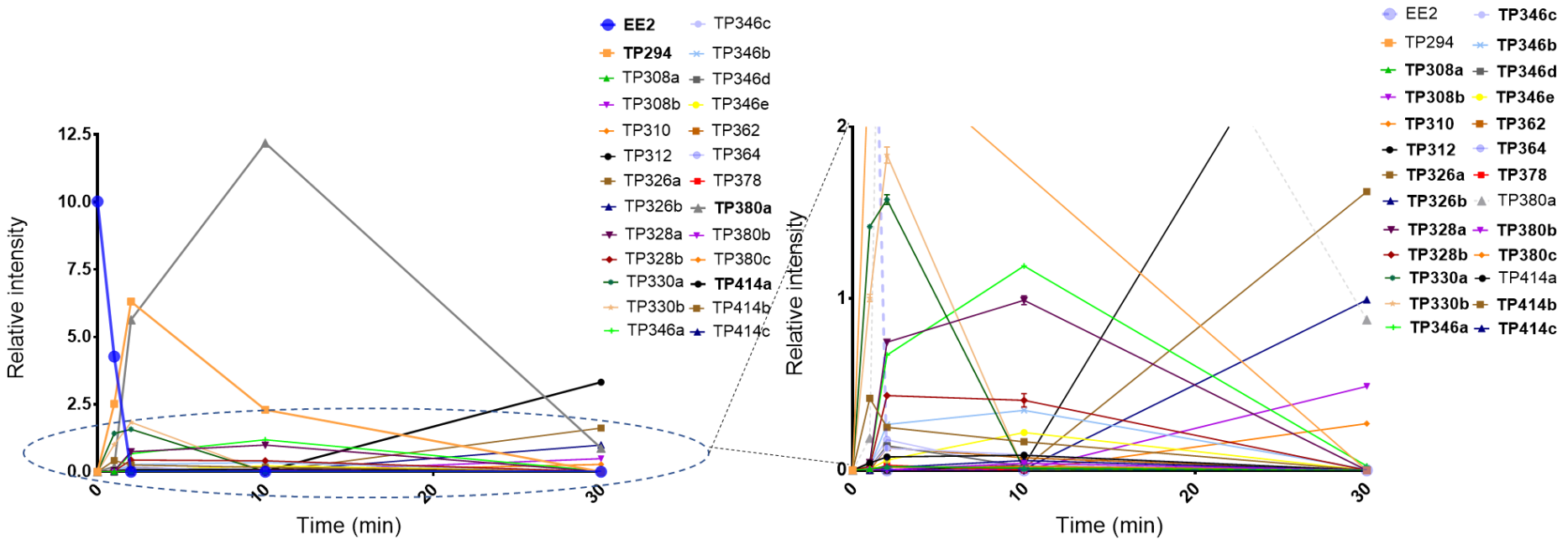

Figure 4.12 – Time course monitoring of TPs generated in the presence of NaCl. Relative intensity: AUC_{TP} / AUC_{IS}.

Fig. 4.12 shows the evolution of the TPs generated in the presence of NaCl as a function of time during the degradation experiment. In the early phase of the electrochemical process, TP330a-b and TP364 emerged via the electrophilic substitution of one and two Cl atoms on the A-ring, respectively. It is believed that these substitutions occurred mainly via *ortho* and *para* orientation on the phenolic moiety, in a reaction similar to the one described in previous works on the chlorination of E2 and EE2 [272–274]. Therefore, TP330a-b were likely 2-chloro-EE2 and 4-chloro-EE2, and TP364 2,4-dichloro-EE2. According to **Fig. 4.12**, TP364 was rapidly hydroxylated into TP380a, the most abundant TP in the presence of NaCl. The relative intensity of TP380a was notoriously high, reaching its maximum at t= 10 min. This outcome might be due to several factors: (i) TP380a is generated by the oxidation of more than one intermediate product leading to its higher yield; (ii) the chlorine substitution of the phenolic moiety increases its acidity, favoring deprotonation and hence detection in negative mode; (iii) as a more apolar compound, it is eluted with a more organic and volatile mobile phase, making the ionization process more efficient.

At the end of the electrochemical process, heavier and more halogenated TPs were formed. In accordance with the experimental data, a degradation pathway is proposed in **Fig. 4.13**.

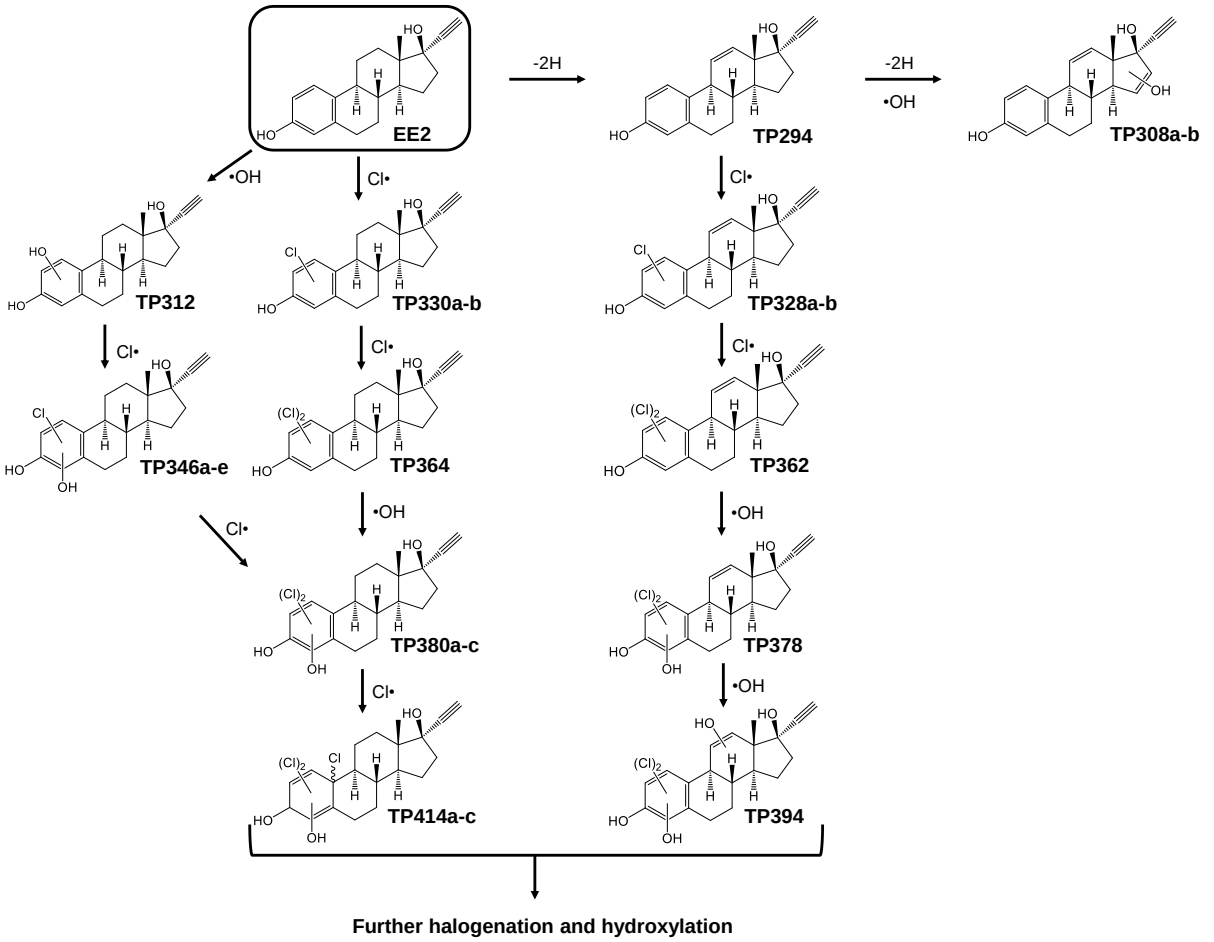

Figure 4.13 – Proposed degradation pathway of EE2 in the presence of NaCl.

By comparing the identified TPs formed in the presence of Na_2SO_4 and NaCl, it was found that only four TPs were commonly generated in both supporting electrolytes (TP294, TP312, TP326a-b), revealing the different oxidizing behaviors of the involved reactive species.
Despite the identification of several TPs, the structural elucidation of these compounds remained challenging due to a lack of reference standards and an exhaustive database. Moreover, the low intensity of the fragment ions and the occurrence of rearrangements after fragmentation, further complicated the structure elucidation [134,275].
Nevertheless, the experimental data clearly showed the formation of hydroxylated and/or halogenated TPs, as well as A-ring opening products during the eAOP. The oxidizing species generated in the presence of Na_2SO_4 and NaCl, readily attacked the phenolic A-ring, leading to its modification and partial cleavage. This greatly reduced the estrogenicity of the degraded samples as shown in **section 4.3.3**.

4.3.5. Application perspective of eAOP treatment technology

Although significant progress has been made on eAOP technologies over the past years, there is still insufficient knowledge of the reaction mechanisms producing TPs that could retain the biological activity of emerging pollutants. Therefore, a preliminary evaluation on their efficiency and safety is needed before any scale-up or hybridization of these processes can be done. This study aimed to address this research gap by chemically and biologically assessing the TPs generated in the presence of two prevalent electrolytes found in wastewater.
Despite the efficient removal of EE2 and the decrease in estrogenic activity observed during the eAOP experiments, the use of simple water matrices with high supporting electrolyte concentrations, to ensure sufficient conductivity, may not be directly applicable to treating (real) wastewater. This is due to the presence of scavengers, such as inorganic species and organic matter, in wastewater, that could lower the efficiency of the EE2 degradation, as well as the typically low conductivity of wastewater [276,277]. Furthermore, emerging pollutants are often present in mixtures in real-world scenarios, which can have diverse implications on the degradation efficiency and the toxicity. Nevertheless, the generation of potentially toxic compounds in these conditions should not be ruled out. As seen in **Figs. 4.10** and **4.12**, some of the TPs were still present in the final degraded samples (t= 120 min for Na_2SO_4 and t= 30 min for NaCl). Hydroxylated estrogens, mainly at position 4, have been reported to be carcinogenic [278–281]. Furthermore, despite the fact that the chlorination of EE2 leads to a reduction of its estrogenicity [282,283], the acute and chronic toxicity of some halogenated TPs has been reported to be higher than that of EE2 [261,284]. The decreased polarity caused by halogenation moreover increases the risk of bioaccumulation, making the generation of

these TPs a matter of concern. In addition, the presence of active chlorine may lead to the generation of perchlorates, chlorates and organochloride derivatives, which can be an impediment to the application of these eAOPs [257]. As the generation of transformation products (TPs) will lead to additional contaminants to consider in the WWTPs, the operational parameters of the WWTPs might have to be adapted in order to deal with this increasing load. To circumvent these drawbacks, the hybridization of AOPs might be an attractive solution. The combination of electrochemical oxidation with electrochemical reduction or photocatalytic processes may be a cutting-edge remediation for the removal of halogenated TPs [285–288]. Moreover, membrane technologies can be employed as a pre-treatment stage to concentrate emerging pollutants and increase salinity, which in turn can enhance the conductivity and efficiency of eAOPs [289].

Data on the full-scale application of electrochemical processes for water treatment remain scarce. However, studies have documented the use of these technologies on pilot-scale, serving as a bridge between lab-scale and full-scale set-ups [290,291]. Although a uniform current density, supplied through the electrodes, is key in determining the process efficiency, external factors such as flow dynamics, mechanical design, plumbing and operating parameters become more relevant for a full-scale operation of the process. A combined approach including the theoretical modelling of such electrochemical systems, coupled with the reactor configurations, electrode materials and the mechanical design of such large-scale set-ups could provide better insight into the industrial application and economics of eAOPs for wastewater treatment.

Nonetheless, fundamental studies, like the one reported here, remain a crucial first step when a new eAOP strategy is investigated, as they allow to identify optimal process conditions to achieve the desired treatment outcomes while minimizing any potential negative impacts. This is particularly relevant since the generation of powerful oxidants can lead to the production of toxic TPs that can pose a threat to the environment and human health. With robust and holistic analytical and biological tools available, potential adverse effects that might occur during water treatment can be identified and mitigated in an early stage.

4.4. Conclusions

In this study, the electrochemical degradation of EE2 using a BDD anode was assessed for the first time by an extensive chemical and biological characterization. The efficiency of the degradation process was evaluated by the relation between the analytically determined EE2 concentration and the HEq determined by the estrogenic tests. The quantification of EE2 in

degraded samples was performed using a validated UHPLC-QTOF-MS method. The ChgH-GFP medaka strain was used as a suitable biomonitoring model as indicated by its high sensitivity (GPF induction detected at 76 ng/L) and concentration-dependent responsiveness in the assessment of estrogenic activity. For both considered electrolytes, NaCl and Na_2SO_4, a high correlation between the removal of EE2 and the reduction of the HEq was observed. However, the detection of estrogenic activity in the final degraded samples suggested that the eradication of the sample estrogenicity was not complete, even though EE2 was no longer detected analytically. An untargeted LC-MS approach permitted the detection and tentative identification of several TPs. According to the experimental data, the radicals produced in the presence of Na_2SO_4 and NaCl reacted directly to the phenolic moiety, resulting in its alteration and partial cleavage. This significantly reduced or even neutralized the estrogenic potency of the generated TPs.

In conclusion, eAOP revealed to be a promising technology for the removal of EE2 in water. Nevertheless, special consideration needs to be given to the generation of potentially toxic transformation products before this technology can be implemented for real (waste)water treatment. This study demonstrates that the combination of analytical techniques and *in vivo* bioassays can provide a more comprehensive understanding of the environmental impact of pollutants and the effectiveness of remediation technologies.

CHAPTER 5

Electrochemical degradation of diclofenac generates unexpected thyroidogenic transformation products: Implications for environmental risk assessment

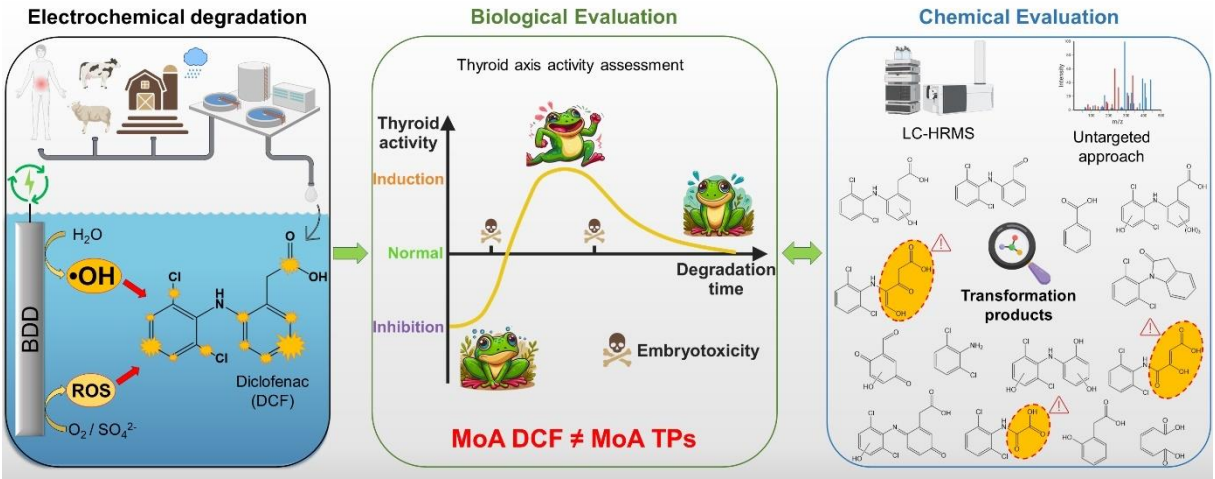

Adapted from: Rafael Reis, Rebecca Dhawle, Romain Girard, Zacharias Frontistis, Dionissios Mantzavinos, Peter de Witte, Deirdre Cabooter, David Du Pasquier, *Electrochemical degradation of diclofenac generates unexpected thyroidogenic transformation products: Implications for environmental risk assessment*. Journal of Hazardous Materials, 472 (2024) 134458.

5.1. Introduction

Non-steroidal anti-inflammatory drugs (NSAIDs) are most commonly used for their anti-inflammatory, antipyretic and analgesic properties [292]. In recent years, there has been a growing concern regarding their extensive consumption, leading to their widespread presence in the environment, and potential risks associated with their bioactivity and water toxicity [293]. Diclofenac (DCF), or 2-[2-(2,6-dichloroanilino)phenyl]acetic acid, is one of the most commonly prescribed NSAID due to its effectiveness to alleviate acute and chronic pain and treat inflammatory conditions [294]. First introduced in 1973, it is widely used in both human and veterinary medicine. It is estimated that over 1400 tons of DCF are annually consumed globally in human medicine alone [295].

As shown in **Fig. 5.1**, DCF possesses structural complexity due to its stereochemistry and the presence of multiple functional groups, allowing a wide range of interactions, reactivity and behavior during degradation or metabolic processes. DCF is mostly known for its inhibition of cyclooxygenase (COX). However, other modes of action (MoA) have been identified as well [296–298], resulting in an array of pharmacological and toxicological properties.

DCF has emerged as a significant environmental contaminant, due to its harmful presence in ecosystems [295,299,300]. It has been detected in groundwater at concentrations ranging in the hundreds of ng/L [301–304], in seawater at µg/L levels [305,306] and in drinking water in the range of a few ng/L [307–309], with possible direct implications for human health. The occurrence of DCF in the environment has been attributed to its elevated consumption, excretion of DCF and metabolites from humans and livestock, subsequent deconjugation of metabolites, and most importantly, its generally poor elimination in wastewater treatment plants (WWTPs) [299,300,310]. In many countries, the concentration of DCF in wastewater effluent reaches tens of µg/L [311–313]. The highest concentration of DCF ever detected was in Pakistan, where wastewater was reported to contain 836 µg/L [314]. WWTPs are moreover not only inefficient in removing DCF, but also its main metabolites. In German WWTP effluents, concentrations up to 1.7 µg/L, 0.86 µg/L and 0.66 µg/L were found for the main DCF metabolites 4'-hydroxydiclofenac (4′-OHD), 5-hydroxydiclofenac (5-OHD), and 4′-hydroxy diclofenac dehydrate (4′-OHDD), respectively, confirming that DCF metabolites are being introduced in the environment [315].

Electrochemical advanced oxidation processes (eAOPs) have gained significant interest as viable alternatives to conventional treatment methods for removing NSAIDs from wastewater [36,38]. These processes generate powerful reactive species, mainly hydroxyl radicals (•OH) that can effectively eliminate organic pollutants in wastewater [36]. The use of boron-doped diamond (BDD) electrodes for anodic oxidation leads to a high *in situ* •OH generation efficiency [227,316], enabling efficient degradation of NSAIDs.

Thanks to their electrophilic nature, •OH tend to react with the most electron-dense regions of the target molecules, such as aromatic rings or unsaturated bonds [293]. As NSAIDs commonly feature these electron-rich groups, the reaction with •OH predominantly occurs at those sites, leading to rapid degradation [293]. Nevertheless, in order to fully comprehend the feasibility of utilizing these processes for the destruction of NSAIDs, it is imperative to investigate the degradation mechanisms and assess the toxicity of the resulting transformation products (TPs). The identification of TPs generated during degradation processes, however, poses significant challenges due to their large numbers, frequently unknown chemical structures and low concentrations. In recent times, ultra high-performance liquid chromatography hyphenated to quadrupole time-of-flight mass spectrometry (UHPLC-QTOF-MS) has gained significant importance in environmental analysis [139]. This technique offers numerous advantages, such as a high sensitivity, high resolution, and high scan speed. This enables the screening of target compounds and provides the ability to analyze the structures of unidentified TPs in complex matrices.

The overarching goal of eAOPs is the breakdown of toxic organic pollutants. However, the removal of these pollutants does not necessarily imply the elimination of toxicity. If TPs are not completely mineralized, the toxicity of the treated wastewater may be equal to or even exceed that of the untreated wastewater, posing substantial risk to the aquatic environment [76,317]. Therefore, reliable biological tools are necessary to comprehend the toxicology properties of TPs. Several studies have reported the toxic effects of DCF and its metabolites on various organisms including animals, aquatic organisms and plants, via *in vitro* and *in vivo* methods [299,318]. Recent research indicated that even at low environmental concentrations (ng/L), DCF is toxic to aquatic organisms [319]. DCF was included in the first EU Watchlist and is a high prioritizing substance to monitor for its ecological risk in China [320,321].

In the last decade, several studies have revealed that NSAIDs, including DCF, also possess endocrine disrupting properties [322–326]. While the effects of endocrine disrupting chemicals (EDCs) are most commonly associated with estrogenic and androgenic disruptions, there is an increasing focus on other endocrine activities such as thyroid hormone (TH) signaling disruption. Thyroid disruption can stem from various MoA, such as the modified biosynthesis of TH, binding to transport proteins, alterations in TH metabolism and thyroid receptor (TR) agonism and antagonism [327]. *In vitro* studies, such as the thyroperoxidase (TPO) inhibition assay, transthyretin (TTR) displacement assay and thyroid hormone receptor beta (TRß) assay have been used to assess thyroid disruption [328]. Nevertheless, the use of these methods for hazard and risk assessment is currently constrained by their limited reliability. The full spectrum of MoA impacting the thyroid axis induced by a particular chemical can only be observed by employing *in vivo* models.

Thus far, the metamorphic process in anuran amphibians has been one of the primary *in vivo* models employed to investigate the actions of TH and, more recently, identify the impacts of TH disruption [329,330]. The high relevance of the model relies on the fact that metamorphosis is entirely controlled by TH signaling [107]. The fundamental mechanism of TH action is well conserved in both amphibians and mammals [102,106,331], implying that compounds affecting the thyroid system of amphibians can be considered as candidate thyroid-disrupting chemicals in mammals, including humans. *Xenopus laevis* is an attractive model to assess TH disturbance due to its rapid development, versatility and well-understood endocrine physiology [101,102]. The TH/bZIP-eGFP transgenic line of Xenopus possesses an integrated genetic construct in which a part of the promoter of the TH/bZIP gene is driving the expression of the enhanced green fluorescence protein (eGFP) gene. The portion of the TH/bZIP promoter containing thyroid responsive elements is notably activated by the endogenous hormone triiodothyronine (T3). Once this promotor is activated, the TH/bZIP gene expression is up-regulated in the brain and can be induced prematurely by exposing tadpoles to TH [332]. The TH/bZIP-GFP transgenic model has been shown to be capable of detecting disruption of the thyroid axis by environmentally relevant chemicals [333,334] and is hence a valuable tool for the comprehensive thyroid activity assessment of whole water samples. It is currently registered by the Organization for Economic Cooperation and Development (OECD) under the name Xenopus Eleutheroembryonic Thyroid Assay (XETA; OECD n°248, 2019) as test guideline for the detection of TH disrupting chemicals [335].

The main goal of this study was to comprehensively analyze the biological effects of DCF and its TPs generated by eAOP. For this purpose, DCF was electrochemically degraded in water using a BDD electrode. The generated TPs were monitored and tentatively identified by UHPLC-QTOF-MS. The acute toxicity and thyroidal activity of the degraded samples were assessed with the XETA bioassay. To the best of our knowledge, no other study has investigated in detail the thyroid disrupting effects of TPs that result from the degradation of EDCs by any AOP. By providing improved data for environmental risk assessment, this study will aid in developing a safe and sustainable use of eAOP for the removal of this widely used NSAID.

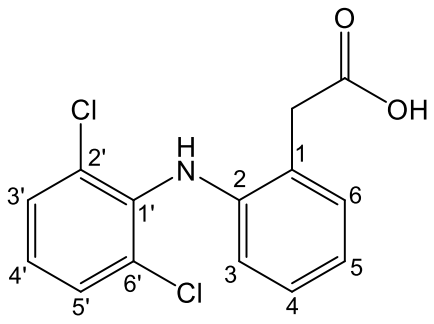

Fig. 5.1 – Chemical structure of diclofenac with carbon number annotation.

5.2. Materials & Methods

5.2.1. Chemicals

High purity (≥ 98%) diclofenac (DCF, $C_{14}H_{10}Cl_2NNaO_2$), 3,3′,5-triiodo-L-thyronine (T3, $C_{15}H_{11}I_3NNaO_4$) and 5,5-Dimethyl-1-pyrroline N-oxide (DMPO, $C_6H_{11}NO$) were purchased from Sigma (Steinheim, Germany). Diclofenac-$^{13}C_6$ (DCF-$^{13}C_6$, $^{13}C_6C_8H_{10}Cl_2NNaO_2$) was obtained from Toronto Research Chemicals (Toronto, Canada). Extra pure (≥ 99%) anhydrous sodium sulphate (Na_2SO_4) was bought from Merck KGaA (Darmstadt, Germany). Ultrapure water was obtained using a Milli-Q® system (18 M Ω/cm) from Merck (MA, USA). LC-MS-grade water and acetonitrile (ACN) were obtained from Fisher Chemicals (Loughborough, UK) and VWR chemicals (Rosny-sous-Bois, France), respectively. Tricaine methanesulfonate (MS222, $C_9H_{11}NO_2{\cdot}CH_4SO_3$) solution was prepared with the same mass of sodium bicarbonate and adjusted to pH 7.5–8.0. Glass-bottled Evian™ mineral water was used as the biological test medium and purchased from a local supplier (Evry, France).

5.2.2. Electrochemical degradation experiments

Electrochemical oxidation of DCF was conducted in a 200 mL plexiglass beaker. The anode was a BDD electrode (Boron/Carbon= 1000 ppm), active on one side, from Adamant Technologies SA (La-Chaux-de-Fond, Switzerland). The cathode was a 316L grade stainless steel plate. The active area of the electrodes was 16 cm^2. The electrodes were placed 2.5 cm away from each other and the solution was stirred continuously using a magnetic stirrer to facilitate mass transfer. The initial concentration of DCF was 50 mg/L, dissolved in ultrapure water. It is important to highlight that the concentration of DCF in the laboratory-scale experiments was significantly higher than what is typically found in the environment. This was necessary to adequately observe the formation of transformation products (TPs) and evaluate any variations in toxicity during this study, without requiring any extraction/pre-concentration procedure. The solution was stirred for 30 min to achieve equilibrium before the start of the electrochemical oxidation. 0.05 M Na_2SO_4 was used as supporting electrolyte and experiments were carried out at a current density of 21.8 mA/cm^2 according to preliminary experiments. Samples were electrochemically degraded for t= 30, t= 45, t= 120 and t= 300 min. Total organic carbon (TOC) measurements were performed using a Shimadzu TOC-LCSH analyzer (Kyoto, Japan). Hydroxyl radicals (•OH) were captured by 100 mM of DMPO and detected using a JEOL X310 electron paramagnetic resonance (EPR) spectrometer with the JEOL LC-12

aqueous flat cell. Detection conditions included a scanning time of 50 sec, resonance frequency of 9.83 GHz, microwave power of 10 mW, and sample volume of 100 µL.
High sample volumes were required for the biological experiments (150 mL). Therefore, a new experiment was conducted for each separate time point. For each experiment, a corresponding blank sample was generated that underwent the same eAOP process in the absence of DCF. Initial (t= 0 min) samples, with and without DCF, were collected non-electrolyzed directly from the bulk of the electrochemical cell. For each experiment, aliquots of 150 mL were collected for the XETA assay (see section 2.4) while 10 mL aliquots were collected for UHPLC-QTOF-MS analysis. All samples were frozen at -20°C for storage. Prior to UHPLC-QTOF-MS analysis, samples were thawed, filtered with regenerated cellulose filters (< 0.22 µm) and spiked with DCF-$^{13}C_6$ at a final concentration of 100 µg/L. DCF removal efficiency was calculated according to the following equation:

$$DCF\ removal\ (\%) = \left(\frac{C_0 - C_t}{C_0}\right) \times 100\% \qquad \textbf{(Eq. 5.1)}$$

Where C_0 is the DCF concentration at t= 0 min and C_t is the residual DCF concentration at time t.
The experimentally determined degradation of DCF was plotted against treatment time and fitted to a pseudo first-order rate equation:

$$\ln\left(\frac{C_t}{C_0}\right) = -k_{app}\, t \qquad \textbf{(Eq. 5.2)}$$

where *t* (min) is the treatment time and k_{app} is the apparent kinetic constant (min^{-1}).

5.2.3. UHPLC-QTOF-MS analysis

UHPLC-QTOF-MS analyses were carried out on an Agilent Infinity 1290 UHPLC system, equipped with a quaternary pump, an autosampler and a diode array detector (DAD) in combination with an Agilent 6530 QTOF-MS (Agilent Technologies, Waldbronn Germany). Separations were performed on a Zorbax RRHD Eclipse Plus ® Phenyl-Hexyl column (3.0 × 100 mm; particle size: 1.8 µm, Agilent Technologies) at room temperature. Ionization was performed in positive (ESI+) and negative (ESI-) electrospray ionization mode using Dual Agilent Jet Stream Technology. Ultimately, due to the existence of carboxyl and phenolic functional groups in multiple TPs, only data obtained in negative ionization mode were used. Collision induced dissociation (CID) experiments were conducted to obtain MS/MS fragmentation data.

Mobile phases were (A) LC-MS grade water with 5 mM ammonium acetate and (B) LC-MS grade ACN. The separation method started with a 2-min isocratic hold at 0% B, followed by a gradient from 0% to 80% B in 10 min. The mobile phase was then kept constant at 80% B for 2 min, returned to the initial composition of 0% B in 0.1 min and kept constant at 0% B for 8 min to re-equilibrate the column. The mobile phase flow rate and the injection volume were set at 0.5 mL/min and 5 µL, respectively. Each sample was analyzed in triplicate. The MS source was operated at a gas temperature of 300°C, a drying gas flow rate of 12 L/min, a nebulizer pressure of 40 psi and a sheath gas temperature and flow of 350°C and 11 L/min, respectively. The capillary voltage was set at 3500 V, the nozzle voltage at 0 V, the fragmentor and skimmer voltage at 75 and 65 V, respectively. The QTOF-MS was operated in 2 GHz Extended Dynamic Range mode. Purine (m/z 112.9855) and hexakis (m/z 1033.9881) were used as the external lock mass for real-time mass accuracy correction. MS and MS/MS spectra were collected at 5 and 1 spectra/s, respectively. Selected compounds for collision induced dissociation (CID) were fragmented with nitrogen gas at 10, 20 and 40 eV.

The method performance for DCF quantification was evaluated through verification of method specificity, linearity, limit of detection (LOD), lower limit of quantification (LLOQ) and matrix effects (ME). DCF working samples were prepared in LC-MS grade water. For the construction of calibration curves, 6 standard solutions with concentrations of 3, 20, 50, 200, 1000 and 5000 µg/L of DCF were prepared. To assess the matrix effects of the method, low (10 µg/L), medium (100 µg/L) and high (1000 µg/L) level quality control (QC) samples were prepared. DCF-$^{13}C_6$ was used as the internal standard (IS) at a concentration of 100 µg/L in each sample. The lower limit of quantification (LLOQ) was determined as the DCF concentration for which the signal to noise ratio (S/N) was at least 10:1 and the relative standard deviation (RSD) was less than 20%. The limit of detection (LOD) was determined as the lowest concentration of DCF for which the S/N was at least 3:1. The selectivity of the method was studied by analyzing ultrapure water and blank degraded samples (n= 6) to evaluate interferences with DCF or the IS. These samples were spiked with DCF at the LLOQ level and the IS and were compared with non-spiked samples. Matrix effects (MEs) were studied to evaluate possible interferences of the sample matrix with the ionization process. This was done by comparing the peak areas (the area under the curve or AUC) of DCF and the IS obtained in ultrapure water with the corresponding peak areas (AUC) in non-electrolyzed samples and degraded blank samples. All samples were spiked at the low, medium and high level of QC and with the IS (n= 3). MEs were calculated as follows (**Eq. 5.3**):

$$ME\ (\%) = \frac{\left(\frac{AUC_{DCF}}{AUC_{IS}}\right)_{Sample\ with\ matrix}}{\left(\frac{AUC_{DCF}}{AUC_{IS}}\right)_{Ultrapure\ water}} \times 100\% \qquad \textbf{(Eq. 5.3)}$$

MEs were considered not-significant if the results of the samples with matrix were within ± 15% of the obtained values in ultrapure water.

5.2.4. Identification and monitoring of transformation products

MassHunter and Profinder software (version 10.0, Agilent Technologies) were used for the quantification of DCF and to perform the structural elucidation of the TPs. An algorithm was employed to extract and identify peaks as features. The parameters used for the molecular feature extraction (MFE) are given in **Table S5.1** in the SI.

Following extraction from the chromatograms, only molecular features meeting the following criteria were considered: (i) molecular features were absent in the initial sample (t= 0 min) and in blank degraded samples; (ii) a single predicted molecular formula was obtained based on high mass accuracy (< 5 ppm), isotopic distribution, and similarity to the molecular formula of DCF ($C_{14}H_{11}Cl_2NO_2$); (iii) a change in intensity was observed across the duration of the electrochemical experiment, relative to the internal standard (DCF-$^{13}C_6$). Chemical structures and MS/MS fragments were generated using ChemDraw (version 21.0, PerkinElmer, Seer Green, UK). The calculation of the exact mass and LogD values was done with MarvinSketch (version 22.19, ChemAxon Ltd, Budapest, Hungary). TPs were classified by the identification confidence levels proposed by Schymanski et al. [156]. Level 1 was assigned to TPs with experimental data that aligned with a reference standard. TPs whose experimental data matched the exhaustive database were categorized as Level 2. Level 3 was designated for positional isomers. To monitor the evolution of TPs during the electrochemical oxidation process, peak areas of the TPs were normalized with respect to the peak area of DCF-$^{13}C_6$ at the corresponding time point.

5.2.5. XETA bioassay

The bioassay used in this study was adapted from the XETA OECD test guideline [335]. For each experimental group (see further below), 20 Nieuwkoop-Faber (NF) stage-45 tadpoles [336] were incubated in six-well plates containing 8 mL of exposure solution, with ten tadpoles per well. Exposure solutions were prepared in Evian water on the first day of the experiment, stored at 4 °C, and placed at room temperature 2 h before renewal, to equilibrate the temperature. Tadpoles were incubated for 48 h in the dark at a temperature of 26 °C, and exposure solutions were renewed after 24 h of incubation. At the end of the incubation period and before image capture, tadpoles were rinsed with Evian water, anesthetized in 200 mg/L of tricaine mesylate (MS222), and placed individually into black 96-well plates with conical wells

(Greiner Bio-One, Courtaboeuf, France). Two empty wells per line were used for the quantification of background fluorescence.

Tadpoles were manually positioned to expose the ventral side of the body, with the dorsal surface in contact with the bottom of the well and the head in the center of the well. An automatic imaging system, composed of a macrofluorescence stereomicroscope with band-pass GFP filters (excitation 475–495 nm, emission 495–545 nm) (Leica Microsystems, Wetzlar, Germany), a robotized platform (Märzhäuser Wetzlar, Wetzlar, Germany) and a high-resolution ORCA-AG camera (Hamamatsu Photonics, Hamamatsu City, Japan), was used to photograph each well. SimplePCI software (Hamamatsu Photonics) was used to quantify the mean pixel intensity of each well.

Each bioassay was conducted with three categories of experimental groups. The negative control group consisted of tadpoles incubated in Evian water, serving as a reference for the baseline fluorescence level of non-treated eleutheroembryos. The positive control groups consisted of eleutheroembryos incubated in Evian water containing 3.25, 6.5 and 16.25 µg/L of T3 to determine the level of fluorescence induced by T3 in a concentration-dependent manner. The third category of experimental group consisted of embryos exposed to electrochemically oxidized aqueous solutions of DCF diluted with Evian water. The sample pH was controlled and, if necessary, adjusted with HCl and NaOH to a value between 7.0 and 7.5. This group was used to determine fluorescence changes induced or inhibited by DCF and its TPs, with or without co-treatment of T3 (3.25 µg/L). As TH concentrations are residual at this larval stage [106], adding T3 to the test medium allowed the detection of compounds that affect T3 availability or antagonize the TR. Three independent experiments were performed on different days and the results were pooled for each condition. For a condition to be valid, embryo lethality had to be limited to 10% throughout the whole exposure time (48 h).

5.2.6. Statistical analysis

The measured fluorescence levels were processed in accordance with both the XETA test guideline and the OECD guidelines for the statistical analysis of eco-toxicology experiments. [249,335]. GraphPad Prism (version 10.1.0, GraphPad Software, La Jolla, CA, USA) was used for both statistical analysis and graph plotting. To normalize background fluorescence, the mean pixel intensity of empty wells was subtracted from the wells on a plate-by-plate basis. Prior statistical calculations, data trimming was performed by omitting in each run the highest and the lowest 10% of the fluorescence values for each experimental group. This was meant to remove values that result from missorted embryos for the bioassays (abnormal size or pigmentation), misplaced embryos on the 96-well plate, embryos dying after anaesthesia and

wells without embryos. The resulting values were then normalized to the mean of the negative control group and expressed as means ± standard error of the mean (SEM).

A bioassay was only considered valid if the fluorescence of the T3 - 3.25 µg/L control group was at least 20% higher compared to the negative control.

The distribution of fluorescence values in each experimental group was assessed using the D'Agostino and Pearson omnibus normality test. If all groups showed a normal distribution, a one-way ANOVA and Dunnett multi-comparison test were performed. In cases where one or more groups did not pass the normality test, a Kruskal-Wallis test with Dunn's multi-comparison test was used. All groups were compared to the appropriate control group: non-spiked degraded samples were compared with the negative control group, and T3-spiked samples were compared with the T3 - 3.25 µg/L control group. According to the XETA test guideline, a sample was considered thyroid-active in the case of a significant statistical difference and only if the mean fluorescence variation values exceeded ± 12% compared to the respective control and $p < 0.05$. This 12% threshold was based on experiments involving a range of thyroid-active and inactive compounds, aimed at minimizing the likelihood of false positive results [335,337].

5.2.7. Molecular docking

Molecular docking analysis was performed using the software Autodock Tools (version 1.5.7, The Scripps Research, USA) to verify the binding affinities of selected TPs with the thyroid receptor (TR). The TPs generated via ChemDraw were converted into PDB files using OpenBabel software [338]. Given the absence of available Xenopus TR conformations, human TR isoforms were selected in this study. It is important to note that the TR structure and ligand binding domain (LBD) are well conserved across vertebrates [339]. The isoforms of the human TRα ligand-binding domain (TRα-LBD, PDB ID: 4LNW, resolution: 1.90 Å) and TRβ-LBD (PDB ID: 3GWS, resolution: 2.20 Å) were obtained from the RCSB Protein Data Bank (http://www.rcsb.org/pdb). Prior to docking, the ligands and water molecules were removed from the crystal structure. Subsequently, polar hydrogens and Kollman charges were assigned to the receptor. The search algorithm chosen was the Lamarckian genetic algorithm (LGA), while the scoring algorithm was based on an empirical free energy function. Each independent docking simulation was configured with 200 runs of the genetic algorithm (GA), an average of 2,500,000 energy evaluations, and a maximum of 27,000 generations. The population size was set at 300, while the remaining parameters were maintained at their default settings. The conformation that resulted in the lowest binding energy was selected as the favorable conformation. The binding simulation of T3 was used as a positive control. The interactions between the ligand and the amino acid residues of the receptor were visualized using Biovia Discoverer Studio (version 21.1.0, Dassault Systems, Vélizy-Villacoublay, France).

5.3. Results & Discussion

5.3.1. UHPLC-QTOF-MS method validation

Under the specified UHPLC-QTOF-MS conditions, DCF and the IS ($^{13}C_6$-DCF) eluted at 8.6 min and exhibited sharp and well-defined peaks. **Fig. S5.1** illustrates typical extracted ion chromatograms of DCF and the IS at 100 µg/L in ultrapure water. In accordance with the obtained signal-to-noise ratios (S/N) and relative standard deviations (RSD), the LLOQ of DCF was determined at 3 µg/L (S/N= 11.3, RSD 11%), while the LOD was determined at 1 µg/L (S/N= 3.4, RSD 16%). Linearity was verified by constructing calibration curves (n= 6) for 6 calibration standards (3-20-50-200-1000-5000 µg/L). All calibration curves demonstrated highly satisfactory linearity ($R^2 \geq 0.9986$) (**Table S5.2**). Endogenous responses of blank degraded samples were lower than 1% of the DCF signal at the LLOQ level and of the IS (data not shown). Therefore, no substantial interference was detected between the sample matrix and the signals of DCF and the IS. Blank degraded samples and non-electrolyzed samples were used to assess matrix effects (MEs). These samples were spiked with DCF at three levels of QC (10, 100 and 1000 µg/L) and the IS at 100 µg/L. Peak areas obtained for these samples were compared with the corresponding peak areas in ultrapure water spiked with the molecules of interest at the same concentration. **Table S5.3** shows that MEs ranged from 97.1% to 108.4%, (RSDs ranging from 0.3% to 2.4%), indicating that the influence of the matrix of the degraded samples on the ionization process was not significant. These results demonstrate that the developed UHPLC-QTOF-MS method was suitable to detect and quantify the residual concentration of DCF in eAOP processed samples.

5.3.2. Electrochemical degradation of diclofenac

5.3.2.1. Removal of DCF

Boron Doped Diamond (BDD) electrodes, well-known for being non-active electrodes, exhibit an extremely high overpotential for oxygen evolution. This results in the direct generation of hydroxyl radicals (•OH) from water physisorbed on their surface [41–43,340] (**Eq. 5.4**):

$$BDD(H_2O) \rightarrow BDD(\bullet OH) + H^+ + e^- \quad \textbf{(Eq. 5.4)}$$

The variety of oxidant species that can be generated by BDD electrodes is extensive and depends on the composition of the water matrix.

In this study, Na_2SO_4 was chosen as the supporting electrolyte to ensure an adequate solution conductivity and sustain a stable current within the system. In addition, Na_2SO_4 is considered a relatively inert electrolyte, while the widely used NaCl has been correlated with the formation of potentially dangerous organochlorine compounds [257]. Although •OH and sulfate radicals ($SO_4^{\bullet-}$) are the main oxidants [40–42], several other oxidants such as $O_2^{\bullet-}$, H_2O_2 and O_3 are likely also produced [34,40–43]:

$$2\,{\bullet}OH \rightarrow H_2O_2 \quad \textbf{(Eq. 5.5)}$$

$$H_2O_2 \rightarrow O_2 + 2H^+ + 2e^- \quad \textbf{(Eq. 5.6)}$$

$$H_2O_2 + {\bullet}OH \rightarrow {\bullet}OH_2 + H_2O \quad \textbf{(Eq. 5.7)}$$

$$2SO_4^{2-} \rightarrow S_2O_8^{2-} + 2e^- \quad \textbf{(Eq. 5.8)}$$

$$3H_2O \rightarrow O_{3(g)} + 6H^+ + 6e^- \quad \textbf{(Eq. 5.9)}$$

eAOP experiments were conducted without pH control, to avoid possible interferences, at room temperature and without adding an •OH radical scavenger to quench the reaction, as this would pose problems for the biological tests. **Fig. 5.2A** shows the decrease in residual DCF concentration and the removal efficiency (calculated according to **Eq. 5.1**) in the presence of Na_2SO_4 as a function of degradation time. After a reaction time of 30 and 45 min, approximately one third and half of the initial concentration of DCF (50 mg/L) was removed, respectively. Furthermore, after two hours of treatment, roughly 6% of DCF remained in the degraded samples. Complete elimination of DCF was obtained after a treatment time of 300 min.

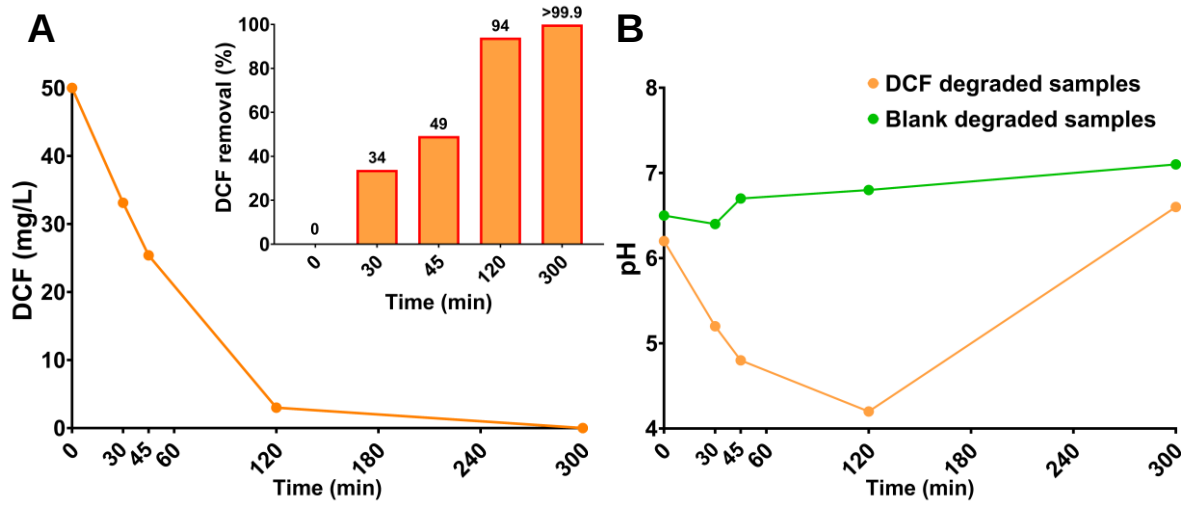

Fig. 5.2 – **(A)** Residual DCF concentration and relative removal (%) in the presence of Na_2SO_4 at t= 0, t= 30, t= 45, t= 120 and t= 300 min. $[DCF]_0$= 50 mg/L, $[Na_2SO_4]$= 0.05 M, j= 21.8 mA/cm2. DCF quantification was performed in triplicate. Mean ± standard deviation. **(B)** pH evolution of DCF and blank degraded samples during eAOP treatment. Note that error bars are too small to be visible.

The degradation of DCF followed pseudo-first order kinetics and according to **Eq. 5.2**, a straight line with R^2= 0.98 was obtained (**Fig. S5.2**). The apparent rate constant k_{app} for the degradation of DCF was calculated as 0.022 min^{-1} from the plot of ln (C_t/C_0) vs time in **Fig. S5.2**.

Despite the fact that the BDD, under the specific operating conditions, was able to degrade DCF in less than 300 min, the removal of total organic carbon (TOC) was significantly lower, reaching only 58% after 3 hours, as shown in **Fig. S5.3**. Brillas et al. examined the decomposition of DCF using BDD in a neutral medium (pH 6.5, 0.05 M KH_2PO_4 + 0.05 M Na_2SO_4 + NaOH) at 35°C and demonstrated that TOC removal decreased from 99% using 450 mA to 78% at 50 mA due to the lower production of reactive species [341]. However, the authors estimated a mineralization current efficiency (MCE) equal to 27% or even lower, mainly attributed to the increase of parasitic reactions at high current densities. The decrease in MCE over time indicated that the formed transformation products were more resistant to oxidation than the parent compound and the system was under mass transfer control. Therefore, from an engineering perspective, taking into account the low MCE, it is vital to assess the toxicity of the formed transformation products.

As shown in **Fig. 5.2B**, it was moreover observed that the pH-value of the degraded samples progressively decreased from pH= 6.2 at t= 0 min to pH= 4.2 at t= 120 min, whereas the pH of the blank degraded samples ranged between 6.4 to 6.8 within the same time period. This trend is consistent with previous work on the degradation of DCF using photo-Fenton processes, indicating the formation of acidic derivatives during the DCF degradation process [342]. Nevertheless, the pH-value at t= 300 min increased again to 6.5, indicating the longer degradation time allowed removing the generated acidic compounds.

5.3.2.2. Degradation mechanisms

Although the role of hydroxyl radicals (•OH) in the BDD-mediated electro-oxidation of persistent pollutants has already been demonstrated in several studies [41,42,340], an additional experiment was performed with the addition of 100 mM tert-butanol. This is a well-known •OH scavenger with a second-order reaction rate with hydroxyl radicals greater than 10^9. The obtained results are shown in **Fig. S5.4**. As expected, DCF removal was almost inhibited in the presence of tert-butanol, indicating the presence of •OH. To elucidate the formation process of •OH, an additional experiment employed 5,5-Dimethyl-1-pyrroline N-oxide (DMPO) as the spin trapping agent, with the analysis carried out using electron paramagnetic resonance spectroscopy. The results presented in **Fig. 5.3** confirm the formation of •OH in the system. While other reactive oxygen species (ROS) such as $SO_4^{\bullet-}$ and $O_2^{\bullet-}$ were

not detected, the generation of these, as well as other oxidants such as H_2O_2 and O_3 by the BDD electrode, cannot be fully excluded.

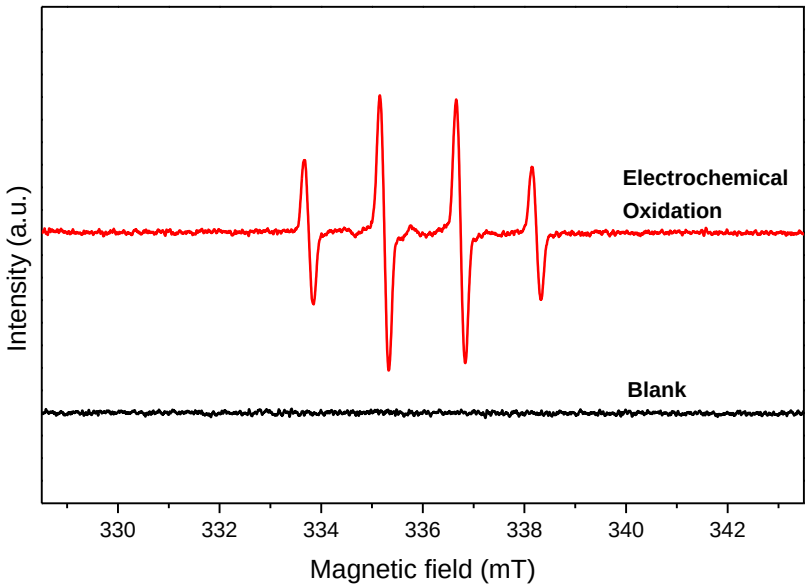

Fig. 5.3 – Spin-trapped (100 mM DMPO) CW-EPR spectra after 10 min of electrochemical oxidation over a BDD electrode in a sulfate electrolyte.

The identification of the main TPs generated during eAOP treatment was subsequently carried out to propose degradation pathways and obtain a better understanding of the effects of the TPs on the thyroidal activity. The primary TPs of DCF were tentatively identified via UHPLC-QTOF-MS, based on their accurate mass (*m*/*z*), isotopic pattern, MS/MS fragments and by verification with literature data. The structure elucidation of the detected TPs is summarized in **Table 5.1**. Isomeric structures for certain TPs were observed at different retention times (RT) and were annotated with lowercase letters. **Fig. 5.4** shows the evolution of the TPs generated in the presence of Na_2SO_4, as a function of degradation time.

According to the experimental data, various degradation pathways occurred during the electrochemical degradation of DCF. This can be attributed to the complex structure of DCF and the non-selective nature of the formed radicals. Hydroxylation, decarboxylation, formylation, dechlorination-hydroxylation, cyclization and C-N bond cleavage all occurred simultaneously.

The hydroxylation of DCF was confirmed by the presence of TPs whose chemical formula revealed an increase in one or more oxygen atoms with respect to the DCF formula, without changes in double bond equivalent (DBE) number. While the QTOF-MS does not provide sufficient information to determine the exact position of the -OH groups within the molecule, theoretical calculations revealed that the benzylic portion of DCF exhibits a greater reactivity compared to the chlorinated aromatic ring [343,344]. This suggests that •OH are more prone to attack the benzylic position.

Moreover, despite their higher susceptibility to attack due to the highest occupied molecular orbital (HOMO) coefficient, previous literature has suggested that C5 and C4' exhibit a different reactivity, with the latter showing a slightly lower reactivity. This was attributed to its proximity to electron-withdrawing chlorine atoms, hence reducing the electron density at that position [342,345]. The detection of hydroxylated compounds hence indicated that the initial degradation of DCF occurred through radical addition mainly on the benzylic aromatic ring, yielding primarily TP311a. The hydroxylation taking place on the benzylic ring increased the electron density at this site, enhancing its proclivity for subsequent hydroxylation and an eventual oxidative ring cleavage. The resulting intermediate products included open-ring compounds featuring an aliphatic side chain with hydroxyl, carbonyl and carboxyl groups (TP289, TP277, TP275, TP261a-b, TP259, TP247, and TP233). Nevertheless, it is plausible that the high generation of reactive species also increased the likelihood of reactions occurring at less favorable sites. This can explain the formation of TP311b, with the extra -OH group attached to the halogenated ring. Both TP311a and TP311b were further hydroxylated forming TP327, which was subsequently dehydrogenated to produce a quinone imine intermediate (TP325). As the electrochemical degradation progressed, further hydroxylation led to the formation of multi-hydroxylated TPs, such as TP333a-b and TP359a-d.

The process of decarboxylation was initiated through an electron transfer involving •OH and the carboxylic acid of DCF. This electron transfer led to the formation of a carboxylic radical, followed by the elimination of $-CO_2$ and an electron. The resulting aliphatic chain was subsequently oxidized leading to its hydroxylation (TP281) and formylation (TP265). As seen in **Table 5.1**, these compounds eluted later than DCF. This can be explained by the removal of the polar carboxylic moiety, resulting in a reduced polarity and increased retention on a reversed-phase LC column.

Cyclization of the DCF structure might have been caused by the strong intramolecular H-bonding interactions between the carboxylic oxygen and the amine hydrogen, resulting in the formation of oxindole derivatives (TP277o, TP293), which were rapidly oxidized.

Dechlorination-hydroxylation occurred in the initial phase of the degradation by the nucleophilic displacement of the chlorine atom by •OH, yielding TP276. As reported earlier, the release of chloride through DCF dehalogenation contributed to the decrease of the sample pH observed during the eAOP treatment [341,342].

C-N bond cleavage resulted from the addition of •OH at the ipso-position of the amino group. This led to the formation of 2,6-dichloroaniline (TP161), 2-hydroxyphenylacetic (TP152) and respective derivatives. In contrast to previous reports [346], no TPs resulting from the C-N cleavage of N and C1’ were detected. Therefore, no amino phenyl acetic derivatives were found.

Table 5.1 – List of TPs of DCF formed during eAOP.

Compound	RT (min)	Elemental formula	Measured m/z (Da)	Mass accuracy (Δ ppm)	DBE	Fragment ions (m/z)	Collision energy (eV)	Confidence level	Proposed structure
DCF	8.6	$C_{14}H_{11}Cl_2NO_2$	294.0097	-1.02	9	250.0187 214.0412 178.0636	10 20 40	1	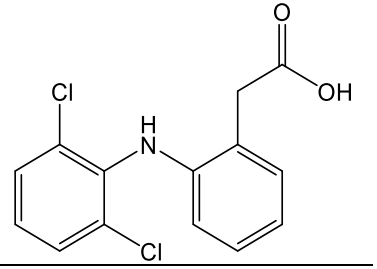
TP311a	7.9	$C_{14}H_{11}Cl_2NO_3$	310.004	-0.97	9	266.0153 230.0338 194.0638 166.0558	10 20 20 40	2	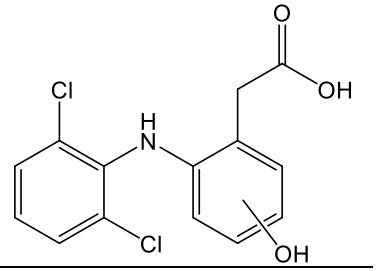
TP311b	7.6	$C_{14}H_{11}Cl_2NO_3$	310.004	-0.97	9	266.0149 230.0322 188.9363 166.0671	10 20 40 40	2	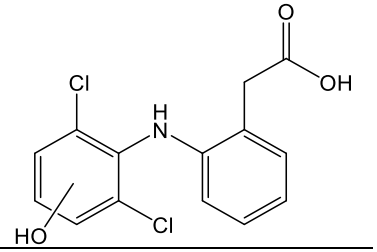
TP327	6.8	$C_{14}H_{11}Cl_2NO_4$	326.0003	3.37	9	282.0071 244.0160 160.9550	10 20 20	2	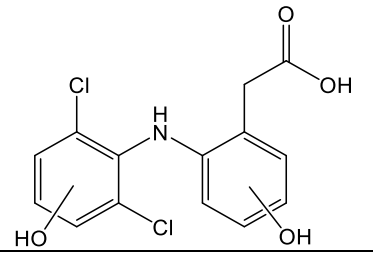

TP359a	6.5	$C_{14}H_{11}Cl_2NO_6$	357.9882	-2.51	9	299.9727 123.0079 109.0283	10 20 40	3	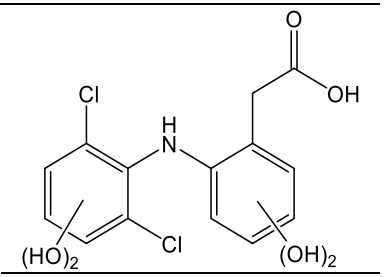
TP359b	6.3								
TP359c	5.9					297.9653 215.9975 127.9546	10 20 40		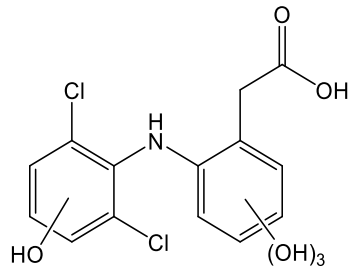
TP359d	5.5								
TP325	7.0	$C_{14}H_9Cl_2NO_4$	323.9837	0.31	10	279.9925 244.0155 134.0461	10 20 40	3	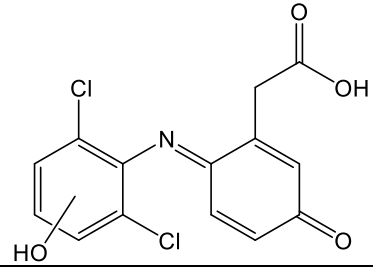
TP276	7.9	$C_{14}H_{12}ClNO_3$	276.0429	-1.45	9	232.0510 214.0062 186.0105	10 20 20	3	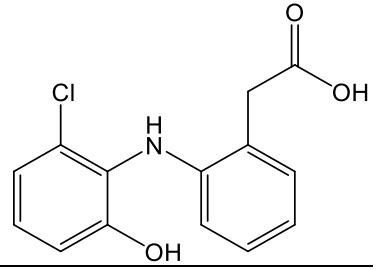

TP291	7.2	$C_{14}H_{10}ClNO_4$	290.0222	-1.38	10	246.0337 232.9204 196.9020	10 20 20	3	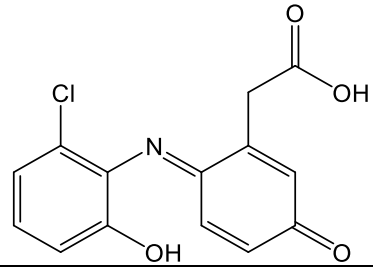
TP277o	10.2	$C_{14}H_9Cl_2NO$	275.9984	-1.45	10	242.0347 152.9999	10 40	3	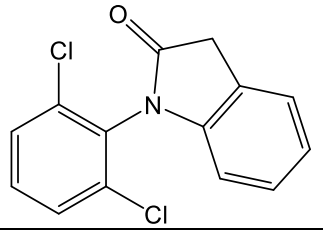
TP293	9.3	$C_{14}H_9Cl_2NO_2$	291.9935	-1.03	10	207.0760 176.0483	20 40	3	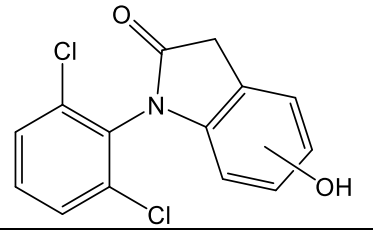
TP281	11.3	$C_{13}H_9Cl_2NO_2$	279.9929	-3.21	9	243.0077 216.0160	20 20	3	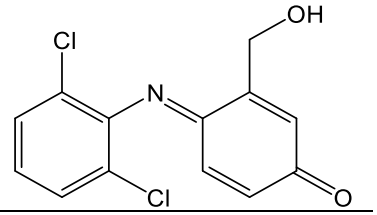
TP315	7.9	$C_{13}H_{11}Cl_2NO_4$	313.9989	-1.91	8	270.0088 232.0338 91.0186	10 20 40	3	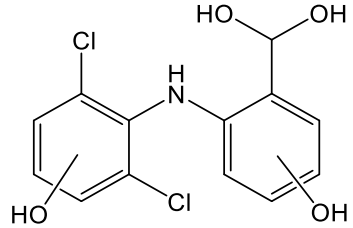

TP310	7.5	$C_{13}H_7Cl_2NO_4$	309.9691	3.87	10	273.9900 232.0331 43.9927	10 20	3	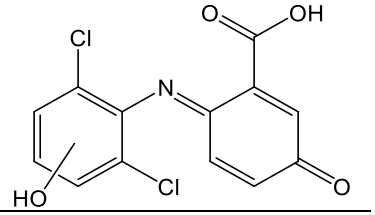
TP265	9.7	$C_{13}H_9Cl_2NO$	263.9981	-2.65	9	228.0218 194.0460 164.095	10 20 40	3	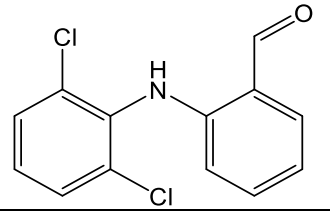
TP285a	11.0	$C_{12}H_9Cl_2NO_3$	283.9881	-2.11	8	249.0212 218.0150 179.0371	10 20 40	3	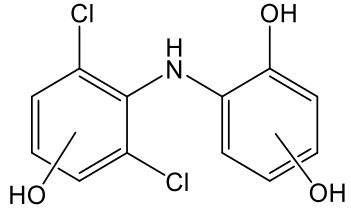
TP301	6.7	$C_{12}H_9Cl_2NO_4$	299.9834	-0.67	8	159.9704 123.9955	20 40	3	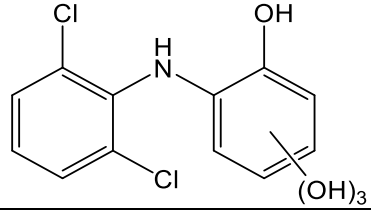
TP299	7.2	$C_{12}H_7Cl_2NO_4$	297.968	0.34	9	264.9985 216.9996 173.0120	10 20 40	3	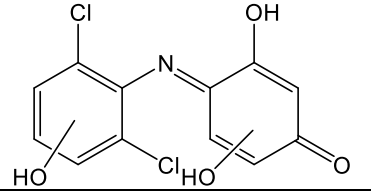

TP333a	6.1	$C_{12}H_9Cl_2NO_6$	331.9741	2.11	8	269.9716 159.9737 127.0019	20 40 40	3	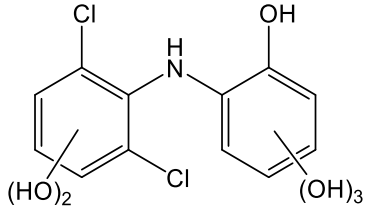
TP333b	6.9	$C_{12}H_9Cl_2NO_6$	331.9741	2.11	8	269.9695 188.9840 99.0107	20 40 40	3	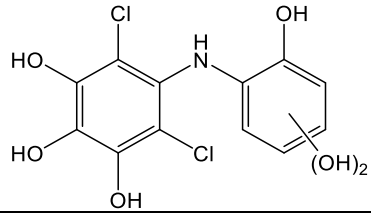
TP285b	7.4	$C_{11}H_5Cl_2NO_4$	283.9521	-0.70	9	211.9666 204.9672 68.9974	20 20 40	3	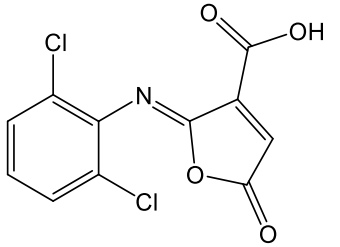
TP289	5.6	$C_{11}H_9Cl_2NO_4$	287.9831	-1.68	7	127.0027 159.9704 83.0139	10 20 20	3	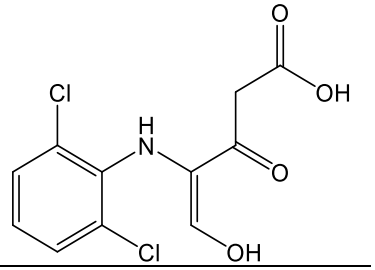

TP277	5.8	$C_{10}H_9Cl_2NO_4$	275.9829	-2.54	6	159.9740 103.0377 89.0220	20 20 20	3	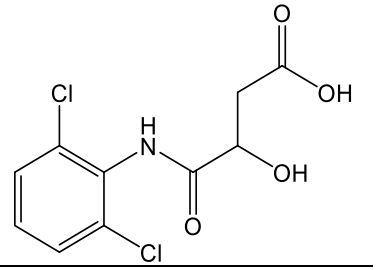
TP275	5.7	$C_{10}H_7Cl_2NO_4$	273.9672	-2.56	7	159.9731 87.0091	10 10	3	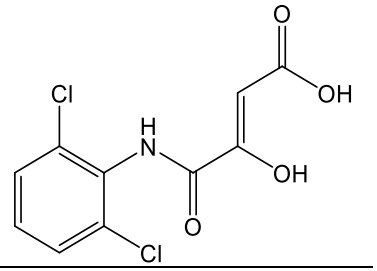
TP259	6.1	$C_{10}H_7Cl_2NO_3$	257.9716	-3.88	7	215.9969 82.9456	10 20	3	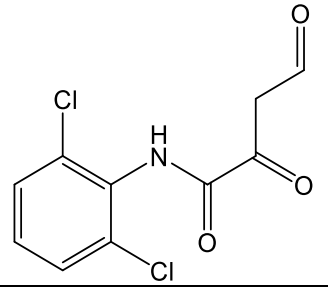
TP261a	6.0	$C_{10}H_9Cl_2NO_3$	259.9879	-3.08	6	159.9732 99.0087 73.0301	10 20 20	3	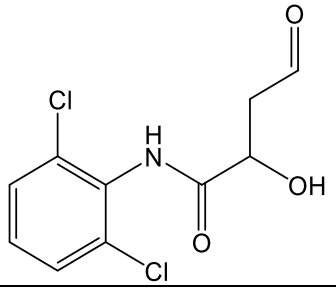

TP261b	6.4	$C_{10}H_9Cl_2NO_3$	259.9879	-3.08	6	215.9945 159.9731 132.0453	10 10 20	3	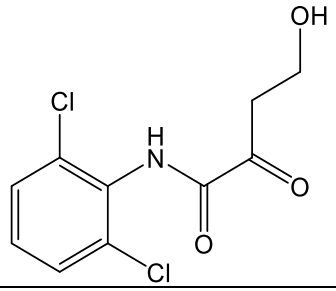
TP247	5.9	$C_9H_7Cl_2NO_3$	245.9723	-2.85	6	159.9703 112.9843 59.0156	10 20 40	3	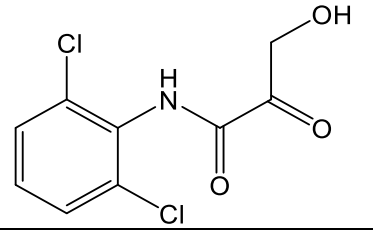
TP233	5.9	$C_8H_5Cl_2NO_3$	231.9569	-2.16	5	159.9707 154.9456	20 40	3	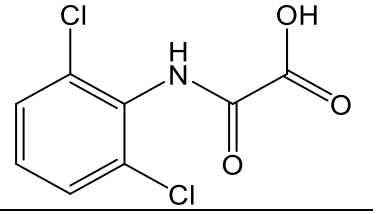
TP161	7.0	C6 H5 Cl2 N	159.9726	-3.13	4	123.9973 61.9889	10 20	1	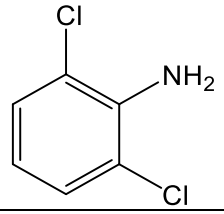
TP177	6.1	$C_6H_5Cl_2NO$	175.9671	-2.27	4	159.9724 140.9977	10 20	3	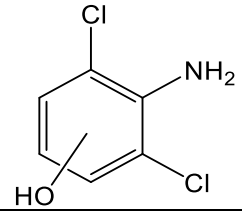

TP190	5.3	$C_6H_5Cl_2NO_3$	190.9317	4.71	5	176.8939 159.9703	10 20	3	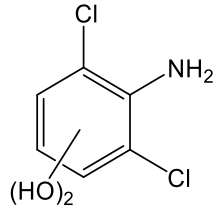
TP207	7.5	$C_6H_3Cl_2NO_3$	205.9408	-4.37	5	137.0250 44.9989	20 40	3	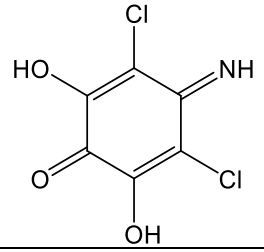
TP192	1.5	$C_6H_5ClO_5$	190.9757	2.09	4	172.9626 128.9726 84.9853	10 20 40	3	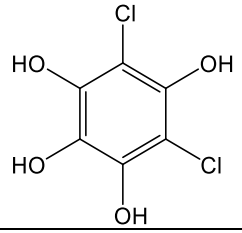
TP152a	5	$C_8H_8O_3$	151.0399	-1.32	5	107.0105 135.0441 59.0142	10 20 40	2	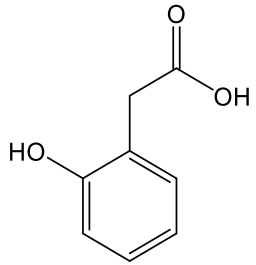

TP168	1.7	$C_8H_8O_4$	167.0418	-2.99	5	123.0437 108.0196 59.0145	10 20 40	3	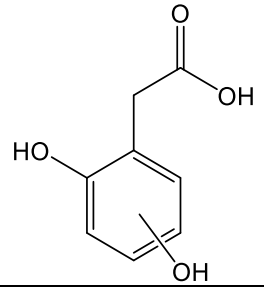
TP184	1.2	$C_8H_8O_5$	183.0295	-2.19	5	139.0378 121.0305 59.0153	10 20 40	3	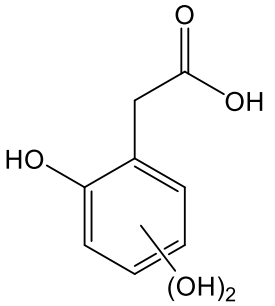
TP140	3.3	$C_7H_8O_3$	139.0397	-2.88	4	59.0146	40	3	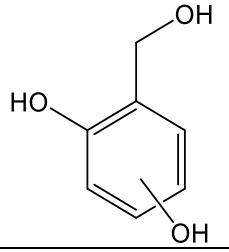
TP122	2.3	$C_7H_6O_2$	121.0295	-0.83	5	59.0151	40	2	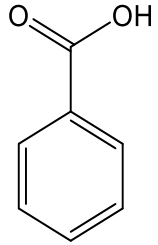

TP138a	1.8	$C_7H_6O_3$	137.0244	-4.38	5	93.0344 59.0142	20 40	2	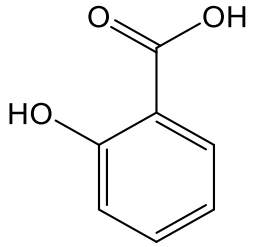
TP138b	7.0	$C_7H_6O_3$	137.0244	-4.38	5	108.0213 59.0133	20 40	3	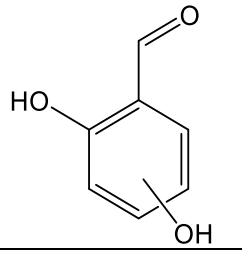
TP152b	7.3	$C_7H_4O_4$	151.003	-4.64	6	107.0463 59.0142	20 40	3	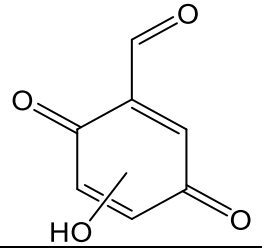
TP187	5.8	$C_7H_6ClNO_3$	185.9955	-4.30	5	143.9148 108.0078	10 20	3	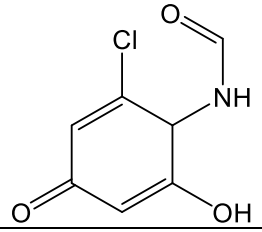
TP142	1.2	$C_6H_6O_4$	141.0187	-4.25	4	97.0253	10	3	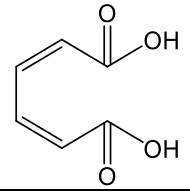

TP166	1.4	$C_4H_3ClO_5$	164.959	-3.76	3	119.9720 96.9612	10 10	3	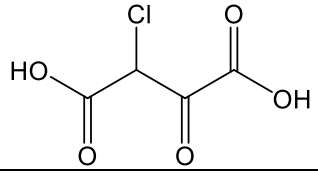
TP108	2.6	$C_3H_8O_4$	107.0348	-1.87	0	77.0345	10	3	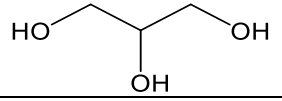

Legend: RT: retention time; DBE: double bond equivalent.

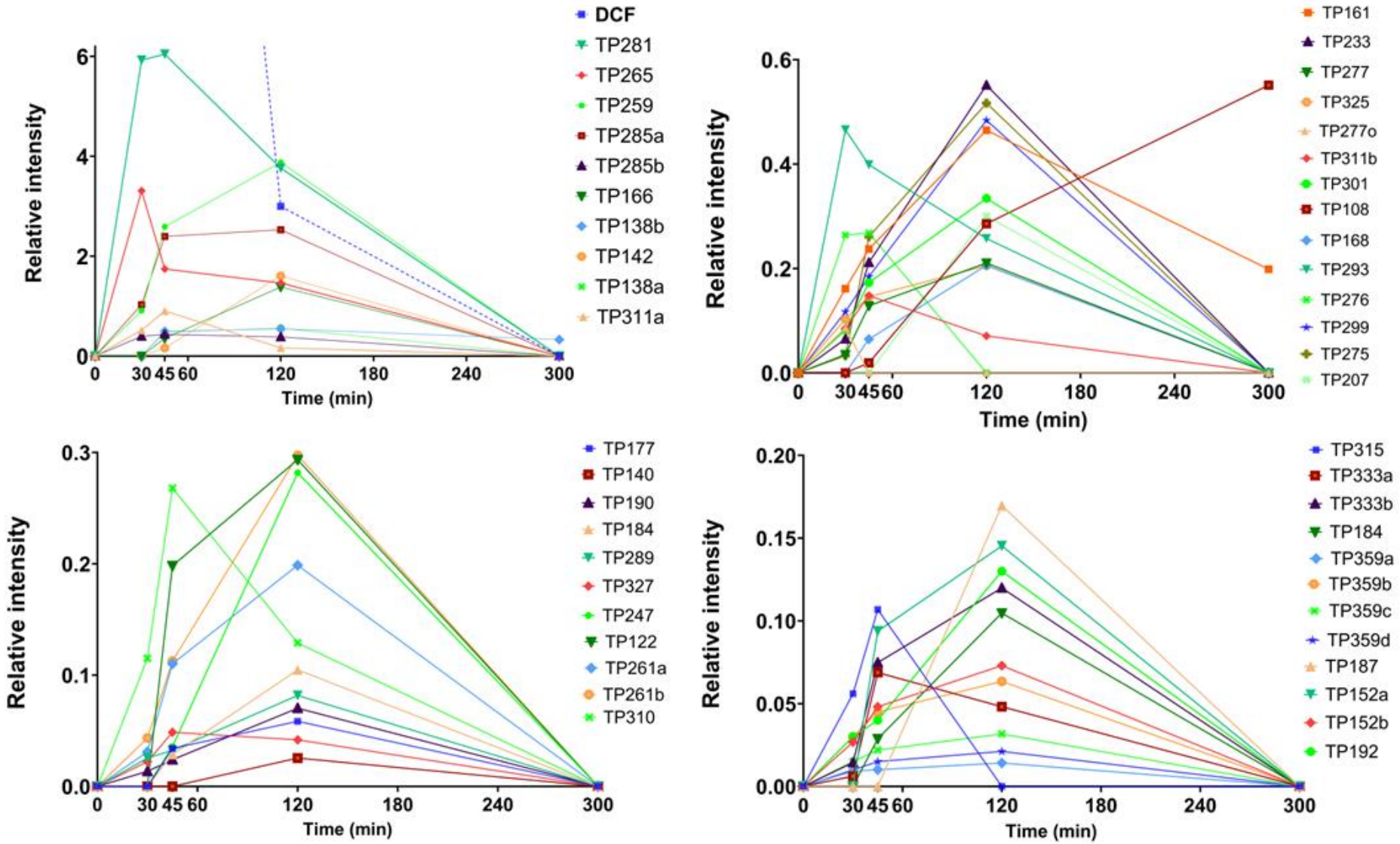

Figure 5.4 – Time course monitoring of TPs of DCF generated in the presence of Na_2SO_4.

Further oxidation by the reactive species resulted in the generation of organic acids, such as derivatives of benzoic and phenylacetic acid, and short chain organic acids through oxidative ring cleavage. The emergence of these acids at t= 120 min coincided with the lowest pH value observed during the eAOP treatment. The pH decrease during DCF degradation is consistent with previous publications on DCF degradation by photo-Fenton [342], ozonation [345] and sonication [347]. Finally, the neutral pH at t= 300 min can be explained by the removal of these organic acids and the deamination of the residual amino derivatives.

In accordance with the experimental data, the degradation pathways of DCF are proposed in **Fig. 5.5**.

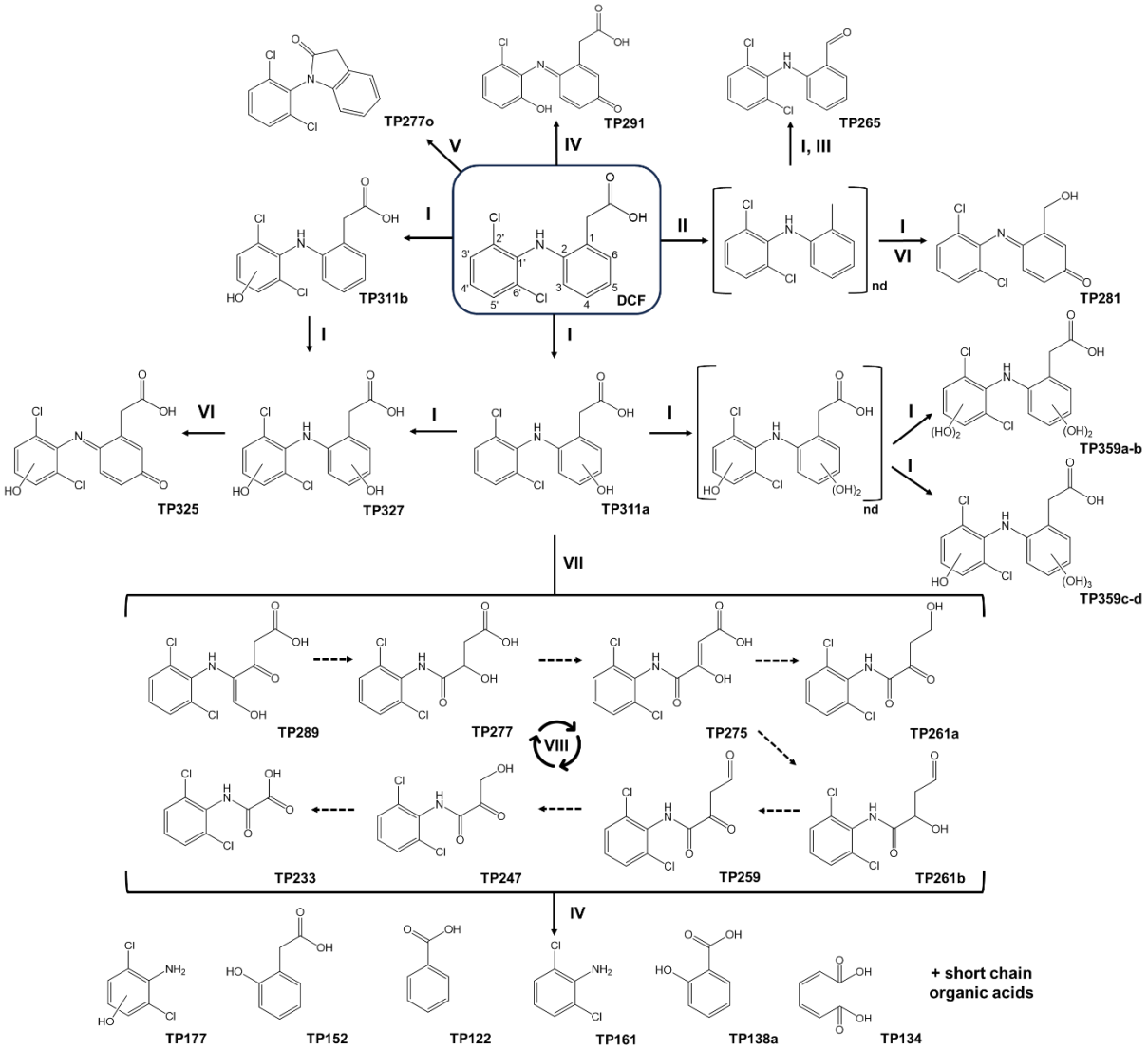

Fig. 5.5 – Proposed degradation pathways for diclofenac. **(I)** Hydroxylation **(II)** Decarboxylation **(III)** Formylation **(IV)** Dechlorination-oxidation **(V)** Cyclization **(VI)** Dehydrogenation **(VII)** Hydroxylation and oxidative ring cleavage **(VIII)** Oxidation and breakage of aliphatic side chain **(IV)** C-N cleavage and oxidative ring cleavage. nd: not detected.

5.3.3. Biological activity assessment

5.3.3.1. Thyroidal response

To detect any potential effects of DCF on the thyroidal system, an exposure study was carried out using the XETA. This bioassay involved transgenic *Xenopus laevis* tadpoles of the TH/bZIP-GFP line. **Fig. 5.6** represents a simplified diagram showing relevant features of the TH/bZIP-GFP transgenic line. Within this line, the promoter of the leucine zipper transcription factor TH/bZIP controls the expression of the GFP coding sequence. As a result, when thyroid hormone receptor (TR) activation occurs, the GFP signal is primarily detected in the head region, predominantly the brain [348].

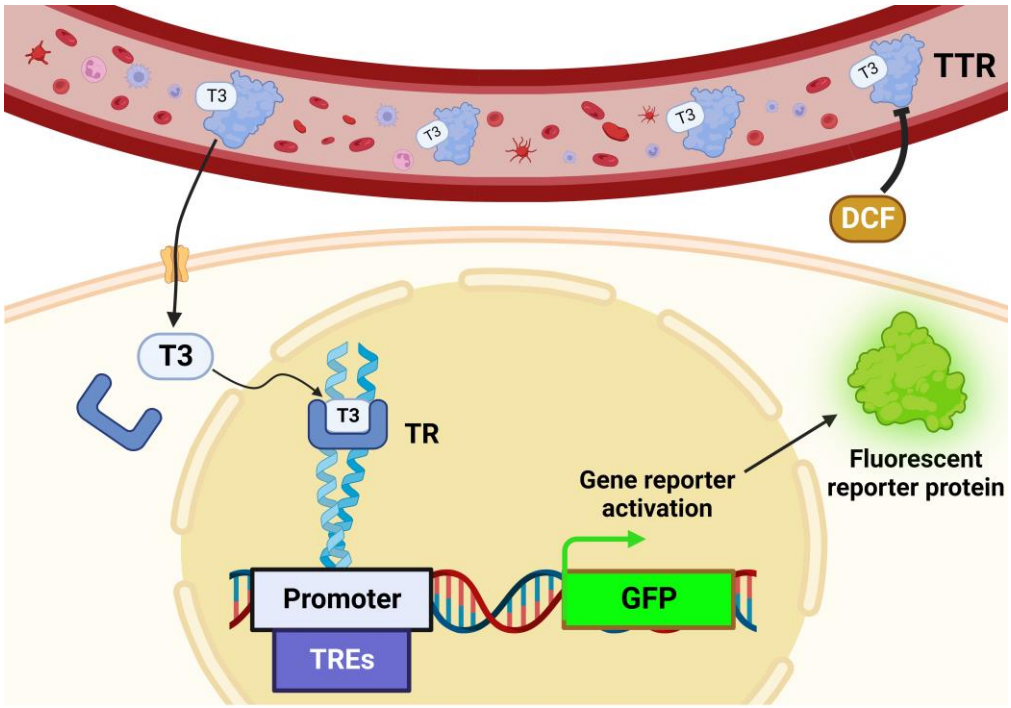

Figure 5.6 – Block diagram of XETA assay. Triiodothyronine (T3) is transported by the plasmatic transporter transthyretin (TTR) and enters the cell. In the nucleus, T3 binds to the thyroid receptor (TR) containing dimers, which bind to the promoter and other genomic thyroid receptor elements (TREs) to regulate gene transcription. The promoter induction will drive the expression of green fluorescent protein (GFP) in the brain. Diclofenac (DCF) is suspected to disrupt the transport of T3 through its attachment to TTR. Image created with BioRender.com

Fig. 5.7 gives a visual representation of the fluorescence signal of a non-treated eleutheroembryo and the fluorescence signal of a larva exposed to the highest T3 control sample (16.25 µg/L of T3).

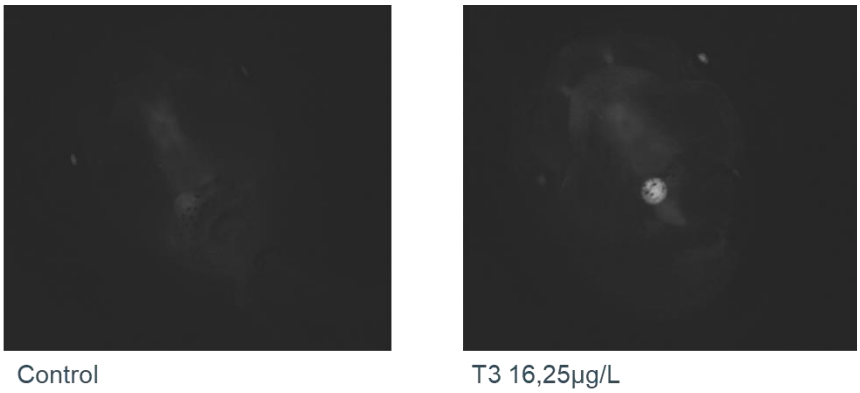

Figure 5.7 – Eleutheroembryos exposed to negative control (test medium) on the left and positive control (T3 – 16.25 µg/L) on the right. GFP is expressed in the brain.

To verify the biological activity of DCF over the thyroid axis of the TH/bZIP-GFP line, tadpoles were exposed to a range of DCF concentrations that covered the residual concentration after eAOP treatment, with and without co-treatment of T3.

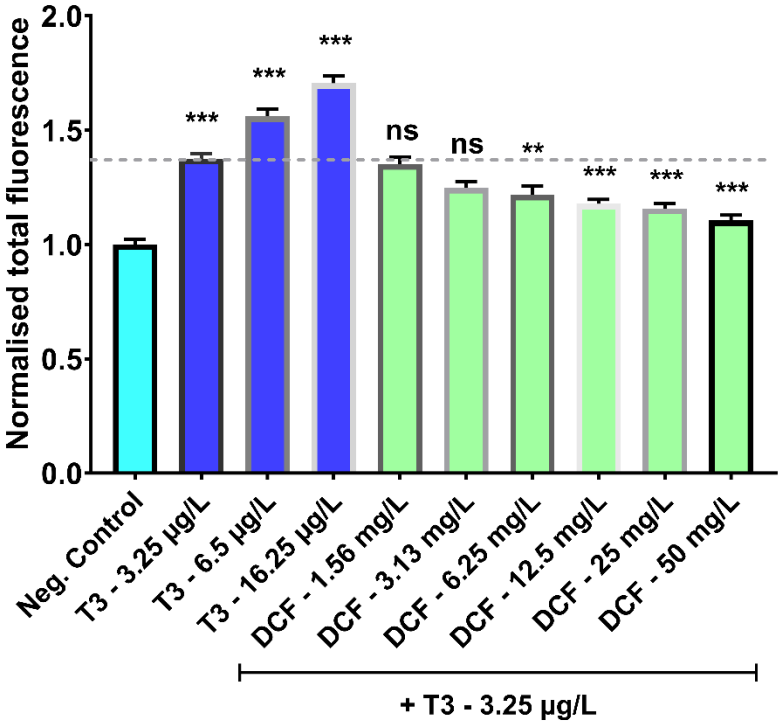

Fig. 1.8 – Fluorescence signal of eleutheroembryos exposed to the negative control (Neg. control), T3 at concentrations ranging between 3.25 – 16.25 µg/L, and DCF at concentrations ranging between 1.56 – 50 mg/L. DCF samples were spiked with T3 at 3.25 µg/L. Data shown are the mean of three independent experiments performed on different batches of eleutheroembryos (n= 20 for each experiment). Error bars represent the standard error of the mean. Statistical analysis with Kruskal-Wallis and Dunn's multicomparison test (negative control vs T3 3.25 – 16.25 µg/L and T3 3.25 µg/L vs DCF 1.56 – 50 mg/L), ns: non-significant, **p< 0.01 ***p< 0.001.

Fig. 5.8 reveals that in the presence of T3, a concentration dependent decrease in fluorescence was observed with increasing concentrations of DCF in the medium, becoming statistically significant at concentrations of 6.25 mg/L and above. In the absence of T3, however, no statistical significance with the negative control was found (**Fig. 5.9**), indicating that DCF is not an agonist of the TR. Furthermore, previous studies have demonstrated that exposure to 1 mg/L of DCF at earlier stages of *Xenopus laevis* embryonic development (NF 8.5) can lead to teratogenic effects [349,350]. However, no signs of teratogenesis were observed at NF 45 in this study, even with exposure to 50 mg/L of DCF. This observation is not surprising as most of the organogenesis is completed before stage NF 45.

The molecular mechanisms of TH disruption can be diverse. Previous studies revealed that exposure to DCF altered TH levels in fish [351,352] and rats [353]. Nevertheless, studies focusing on the potential thyroid disrupting effects of DCF have not been conducted in amphibians. One of the hypothetical disrupting mechanisms involves interference with TH plasmatic transport, primarily achieved by binding to transport proteins [354]. Transthyretin (TTR) is a major TH-binding protein in tadpoles of *Xenopus laevis* [355], with a higher affinity for T3 than T4 in amphibians [356,357]. EDCs binding to TTR modifies its apparent affinity for TH, which consequently can diminish cellular uptake and biological responses, and alter plasma TH homoeostasis [358]. Prior research studies have demonstrated that DCF exhibits significant binding affinity for the thyroxine pockets of TTR [359–361], which can lead to impaired active hormone delivery to target tissues. However, other disrupting mechanisms affecting the thyroid axis cannot be excluded.

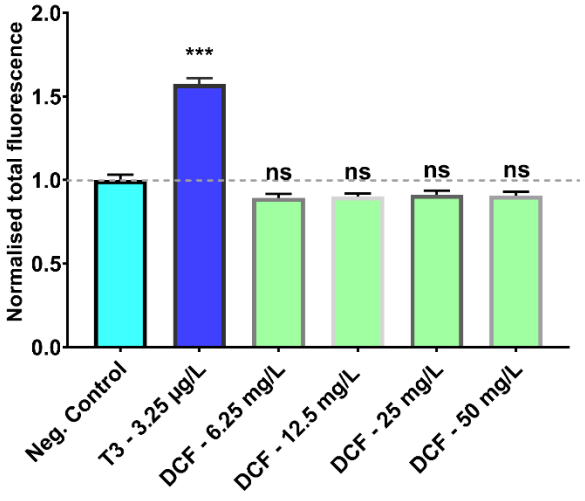

Figure 5.9 – Fluorescence of larvae exposed to negative control (Neg. control), T3 at 3.25 µg/L, and DCF at concentrations ranging between 6.25 – 50 mg/L Data shown are the mean of three independent experiments performed on different batches of eleutheroembryos (n= 20 for each experiment). Error bars represent the standard error of the mean. Statistical analysis with Kruskal-Wallis and Dunn's multicomparison test (negative control vs T3 3.25 µg/L and negative control vs DCF 6.25 – 50 mg/L), ns: non-significant, ***$p < 0.001$.

5.3.3.2. Evolution of thyroid axis activity in degraded samples

The main objective of implementing eAOP was to eradicate the thyroid disrupting activity in the sample by breaking down DCF into biologically inactive substances. Prior research indicated an increase in general toxicity for intermediately degraded samples when exposed to bacteria [362], algae [363,364] and daphnia [365]. However, it is important to note that various AOPs and experimental conditions might result in the formation of different TPs, which could confer distinct biological activities to the degraded samples. Additionally, sample biological activity may still persist even when the parent compound is no longer detected analytically [63,362,366].

Prior to the thyroid activity assessment of the degraded DCF samples, the thyroid activity of blank degraded samples was examined to verify the impact of their respective matrices on the thyroid system of the tadpoles. It was observed that non-electrolyzed (containing 0.05 M Na_2SO_4) and blank degraded samples were lethal to the eleutheroembryos after 24 hours of exposure. To address this, a series of dilutions were tested prior to the thyroid assessment. When samples were diluted by a factor of two with Evian water, no toxic signs were observed throughout the entire 48-hour bioassay. **Fig. S5.5** depicts the mean fluorescence of all time points for non-electrolyzed and blank degraded samples, either not-spiked or spiked with T3 at 3.25 µg/L. The level of fluorescence of all blank samples showed no statistically significant difference when compared to the corresponding control group, indicating no interaction between the matrix of the samples and the thyroid axis activity of the eleutheroembryos.

As discussed in section **3.3.1**, DCF possesses thyroidal activity only in the presence of T3. **Fig. 5.10A** reveals the thyroid activity of the degraded samples diluted two-fold with Evian water and spiked with T3 (3.25 µg/L). The initial (t= 0 min) sample had an inhibitory effect on the thyroid axis of the tadpoles, aligning with the results presented in **Fig. 5.8**. At t= 30 and t= 120 min, no GFP fluorescence data was obtained due to the occurrence of acute toxicity. Since these samples were tested at the same dilution factor as t= 0 min, this outcome indicates the generation of TPs that exert a greater toxicity than DCF.

The observed lethality at t= 30 min but not at t= 45 implies the emergence of toxic TPs at t= 30 that are rapidly oxidized. This is the case for TP277o, which features an oxindole moiety and has been documented to be very toxic for bacteria [367]. Nevertheless, it is very likely that the toxicity was caused by the increased hydrophobicity caused by the decarboxylation of DCF. This transformation was observed at the initial phase of the electrochemical process, evidenced by the emergence of TP265 at t= 30 min. While it is commonly assumed that oxidative treatment yields more polar TPs [48,368], the cleavage of polar functional groups by the reactive species can increase the hydrophobicity of intermediates, thereby increasing the risk of bioaccumulation and toxicity.

The lethality observed at t= 120 min might be attributed to the collective toxic effects of TPs. As seen in **Fig. 5.4**, most of the identified TPs have their highest concentration at this time point of the electrochemical process. Among these, TP325, TP281, TP299 and TP207 feature a quinone imine moiety in their structure. Compounds possessing quinone imines are considered to be highly reactive, capable of inducing cytotoxicity, immunotoxicity and carcinogenesis [369]. Moreover, C-N bond cleavage resulted in the generation and accumulation of derivatives of benzoic acid and dichloroaniline with toxic properties [370–372] and may have contributed to the overall toxicity of the degraded sample. Although the identification of multiple TPs was achieved, the correlation between the chemical data and the observed toxic effects remains challenging, mainly due to the scarcity of toxicity data on amphibians.

Unexpectedly, a significant induction of fluorescence was observed at t= 45 min compared to the control group (T3 – 3.25 µg/L). Based on the initial DCF concentration used for the eAOP treatment (50 mg/L), the 50% degradation of DCF at this time point (**Fig. 5.2A**) and the two-fold dilution with Evian water in this experimental condition, the residual DCF concentration (ca. 12.5 mg/L) remains inhibitory to the thyroid axis, as illustrated in **Fig. 5.8**. Therefore, the observation of a contrasting thyroid-stimulating effect strongly suggests the emergence of TPs that are thyroid-active and exert an opposed biological activity to that of DCF.

In order to mitigate the observed acute toxicity and, consequently, allow comparing the thyroidal activity of all degraded samples, the samples were subsequently diluted five-fold with Evian water, as shown in **Fig. 5.10B**. As illustrated, the pro-thyroid effect at t= 45 min was also observed at this higher dilution factor, further corroborating the fluorescence induction observed in **Fig. 5.10A**. Nevertheless, despite the eleutheroembryos surviving the entire bioassay exposure duration, no significant thyroid activity was apparent at t= 30 and t= 120 min. Likely, the excessive dilution was too high to verify any biological activity at these time points. Other dilution factors were not assessed due to the exhaustion of the degraded DCF samples for the thyroid activity assessment. From a molecular point of view, the DCF carboxylic group is very important to establish hydrogen bond interactions and to confer biological activity [373,374]. In the case of a hypothetical interaction with TTR, the attachment of DCF to its thyroxine binding pockets is mainly mediated by the carboxylate group [360]. Structure-relationship activity revealed that the loss of this carboxylate group greatly reduces DCF binding activity to TTR [359,360]. Therefore, the decarboxylation reaction observed at the initial phase of the electrochemical treatment might have contributed to the reduction of the DCF inhibitory activity on the thyroid axis. To further explore the biological activity of the DCF degraded samples, these samples were tested without spiking with T3. **Fig. 10C** demonstrates the thyroid activity of the degraded samples diluted five-fold with Evian water.

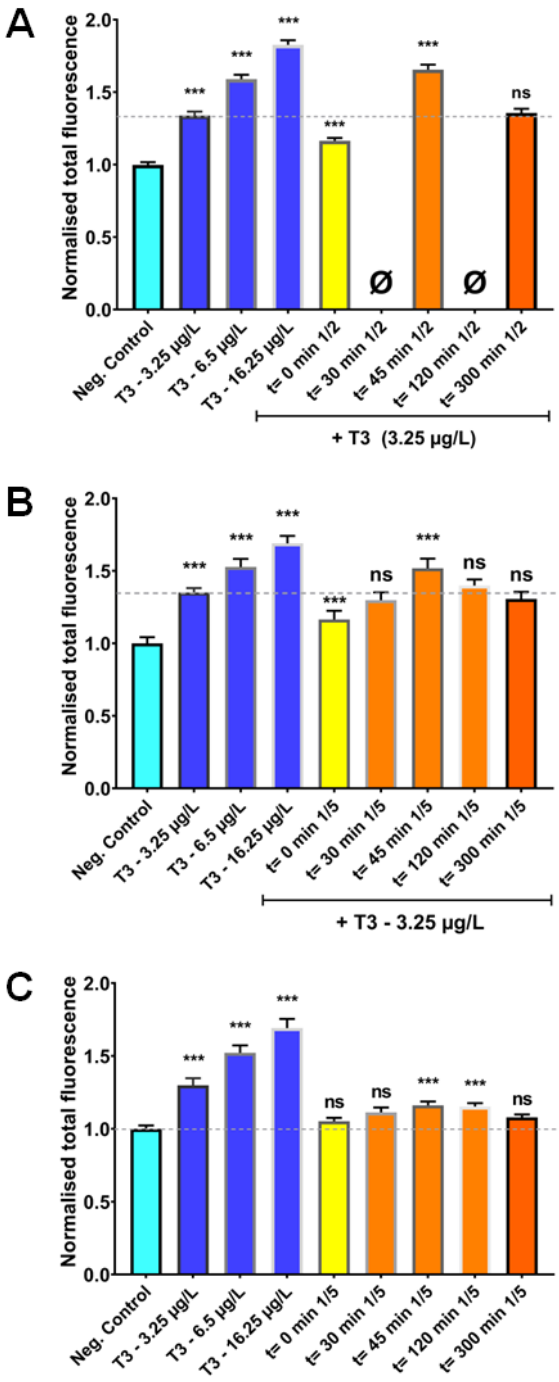

Fig. 5.10 – Fluorescence of tadpoles exposed to the negative control (Neg. control), T3 at concentrations ranging between 3.25 – 16.25 µg/L, initial (t= 0 min) and DCF degraded samples obtained at t= 30, t= 45, t= 120 and t= 300 min. **(A)** Initial and DCF degraded samples were diluted two-fold with Evian water (1/2) and spiked with T3 at 3.25 µg/L. No fluorescence values are shown for t= 30 and t= 120 due to the occurrence of lethality at these time points (Ø). **(B)** Initial and DCF degraded samples were diluted five-fold with Evian water (1/5) and spiked with T3 at 3.25 µg/L. **(C)** Initial and DCF degraded samples were diluted five-fold with Evian water (1/5) and not spiked with T3. Data shown are the mean of three independent experiments performed on different batches of eleutheroembryos (n= 20 per experiment). Error bars represent the SEM. Statistical analysis with Kruskal-Wallis and Dunn's multicomparison test (neg. control vs T3 3.25 – 16.25 µg/L, T3 3.25 µg/L vs spiked initial and DCF degraded samples, neg. control vs non-spiked initial and DCF degraded samples), ns: non-significant, ***$p < 0.001$.

As shown in this figure, the means of fluorescence increased compared to the negative control, becoming statistically significant at t= 45 min and t= 120. This suggests the emergence of TPs that trigger TH-like responses on the eleutheroembryos.

According to the results obtained with the XETA, it can be inferred that the observation of a thyroidogenic effect in samples either spiked or not with T3 at t= 45 min of the electrochemical treatment, strongly suggests that thyroid-active TPs possess a distinct MoA than DCF. Nevertheless, as XETA fluorescence data are indicative of the overall thyroid activity of degraded samples, it cannot be excluded that different TPs have different MoA, interacting in parallel at different sites of the thyroidal axis.

As can be seen in **Fig. 5.10**, irrespective of the dilution factor and the presence or absence of T3, the means of fluorescence of the final degraded sample (t= 300 min) were not statistically significant in comparison to the respective control group. Moreover, the tadpoles exposed to this sample did not exhibit any sign of acute toxicity. Consequently, these findings suggest that the total time set for DCF degradation was sufficient to break down toxic and thyroid-active TPs into compounds that do not exert significant biological impact on the eleutheroembryos.

5.3.3.3. Molecular docking

As seen in **Fig. 5.10C**, significant thyroid activity induction was observed when tadpoles were exposed to intermediately degraded samples (t= 45 and t= 120 min), in the absence of T3 hormonal spike. These tadpoles were exposed to the degraded samples during the NF stage 45 of their embryonic development, a stage at which the endogenous TH levels are residual [106,330]. Therefore, the thyroid-stimulating effect that occurred in the absence of any natural occurring TH, strongly suggests the presence of TPs that act as agonists of the TR.

In order to explore the underlying thyroid-stimulating effect on the eleutheroembryos, the interactions of selected test chemicals with TR isoforms were investigated using molecular docking analysis. As illustrated in **Fig. S5.6**, the interaction of T3 with TR isoforms showed that both benzene rings of T3 were mainly surrounded by hydrophobic residues such as alanine (Ala), methionine (Met), leucine (Leu), and isoleucine (Ile), establishing predominantly hydrophobic interactions. Furthermore, three hydrogen bonds were established between T3 and key hydrophilic amino acid residues arginine (Arg) and threonine (Thr) at the following sites: Arg228, Arg266, and Thr275 for TRα-LBD, and Arg282, Arg320, and Thr329 for TRβ-LBD. The binding energies were −11.37 for TRα-LBD and −11.97 kcal/mol for TRβ-LBD, indicating strong binding activities. The amino-proprionic side chain of T3 was moreover surrounded by electropositive and electroneutral residues. This suggests that the binding of a ligand containing a hydrophilic and an electronegative group is more likely to be favorable [375]. The identified open ring products (TP289, TP277, TP275, TP261a-b, TP259, TP247 and

TP233) possess an intact dichloroaniline moiety (supported by the presence of the fragment ion m/z 159 in **Table 5.1**) with a side chain containing electronegative groups such as hydroxyl, carbonyl and carboxyl groups. These structural features are shared with linuron, a thyroid eliciting compound verified by XETA in a previous study [337]. Given these similar characteristics, these TPs were selected for the simulation of the binding activity to the TR.
The binding energies computed for each chosen ligand through molecular docking simulation are shown in **Table 1. Fig. 5.11** illustrates the conformation of TP289 that had the highest binding score among the open ring products.

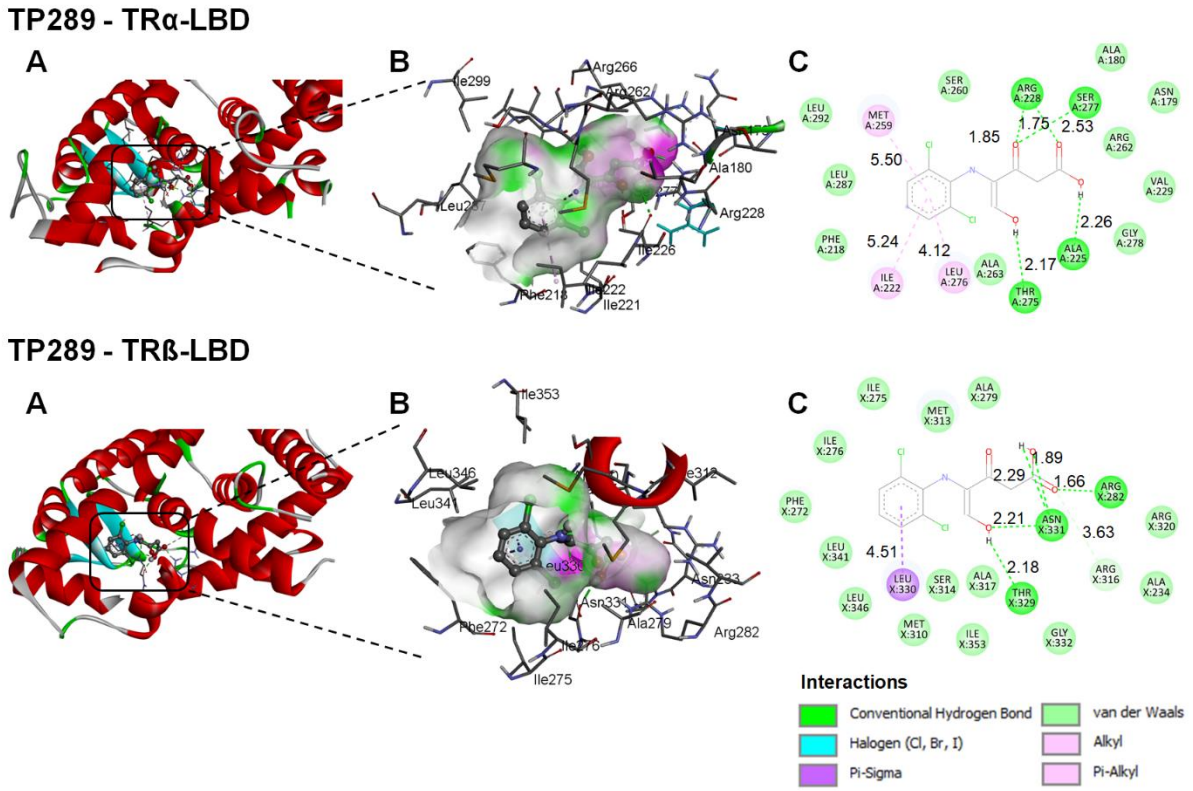

Fig. 5.11 – Binding simulation of TP289 to the TRα and TRβ LBDs using molecular docking analysis. **(A)** 3D visualization of TR with the LBD highlighted in the black box. **(B)** Representation of TR active site amino acid residues and ligand interactions with a hydrogen bond contour map. Purple and green indicate hydrogen bond donor and acceptor sites, respectively. **(C)** 2D diagrams illustrating the binding modes to the LBD in the most favorable conformation, with interaction distances shown in ångströms.

This TP emerged from the oxidative cleavage of the benzylic ring of DCF and the incorporation of hydroxyl and carbonyl groups in the resulting aliphatic chain (pathway VII – **Fig. 5.5**). This side chain of electronegative groups allowed four and three hydrogen bond interactions with the active pockets of TRα and TRß, respectively. This conferred binding energies of -9.37 kcal/mol for TRα and -8.17 kcal/mol for TRß, revealing a relatively strong binding activity in comparison with T3. The lower binding energy for TRα can be explained by the hydrogen bond

between a carbonyl group of the ligand and Ser277, a specific amino acid residue of TRα [376]. This can have implications for triggering a TH-like response since this TR isoform is predominantly expressed in premetamorphic tadpoles [377]. Likewise, all the selected TPs fit into the active pockets of TRα-LBD and TRβ-LBD in the correct orientation at their most favorable conformation (**Fig. S5.7** for TRα-LBD and **Fig. S5.8** for TRβ-LBD). From the data presented in **Table 5.2,** a pattern of diminished binding activity correlating with decreasing molecular weight of the tested compounds can be deduced. This can be attributed to the ongoing electrochemical degradation process, which resulted in the detachment of the functional groups responsible for interacting with the TR (pathway VIII - **Fig. 5.5**). Consequently, this detachment prevented the formation of hydrogen bond interactions essential for the TPs' binding activity and might have contributed to the normalization of the overall thyroid activity of the final degraded sample.

Table 5.2 – Binding energies of T3 and the open-ring TPs at the most favorable conformation to the TRα and TRß.

Ligand	TRα (kcal/mol)	TRß (kcal/mol)
T3	-11.37	-11.97
TP289	-9.37	-8.17
TP277	-8.27	-8.28
TP275	-7.64	-7.80
TP261a	-7.09	-7.46
TP261b	-7.63	-7.59
TP259	-6.84	-6.91
TP247	-5.97	-6.60
TP233	-6.03	-6.02

5.3.4. Implications and perspective on risk assessment of transformation products

Despite numerous studies reporting toxic and endocrine disrupting properties of pharmaceutically active compounds in the environment, there is currently no defined strategy to assess the environmental risk associated with TPs generated in advanced water treatment processes. TPs can present a significant risk when they are generated in large quantities, persist longer or exhibit greater toxicity compared to the parent compound [49]. Therefore, it is

essential to consider these TPs when conducting the environmental risk assessment for the degradation of the original compound, making the selection of the correct biological tool critical. Numerous bioassays can be employed to assess toxicity changes during advanced water treatment and verify the overall safety of these processes [76]. Nevertheless, it is often assumed that TPs share the same MoA as the parent compound and may collectively contribute in an additive or synergistic manner to the overall toxicity when found in mixtures. Consequently, numerous reports rely on *in vitro* assays that target the same MoA as the parent compound or use non-specific toxic tests. The latter include acute toxicity bioassays involving bacteria, with Microtox being the primary example, as well as biotests using *Daphnia magna*, assessments of algae growth, and the use of *in silico* tools such as ECOSAR.

As demonstrated in this study, even slight alterations in the molecular structure, such as the decarboxylation of DCF, can significantly alter the chemical and biological properties of the resulting TPs.

This becomes particularly relevant in the context of advanced water treatment such as eAOPs, wherein the high generation of non-selective reactive species like •OH can lead to the formation of a diverse array of TPs through unpredictable degradation pathways. In such instances, certain TPs may acquire new toxicophores that give rise to a specific but different MoA, potentially posing risk to non-targeted organisms. This risk may go unnoticed if the particular bioassay used in the toxicity evaluation is unable to detect this distinct MoA.

To address this challenge, a viable approach involves the use of whole organism testing such as eleutheroembryos. These organisms are valuable tools in the assessment of complex environmental samples as they can screen multiple MoAs. They aid in assessing complex samples that may contain EDCs and their respective TPs that potentially interact with any given endocrine axis [67]. Furthermore, this approach offers an advantage over *in vitro* assays as it incorporates essential biological processes such as absorption, distribution, metabolism and excretion (ADME), thus delivering a holistic understanding of how electrochemically induced chemical changes could affect more complex organisms. Moreover, since the endocrine signaling pathways are highly conserved across vertebrate taxa [83], *in vivo* vertebrate models can play a critical role in assessing the endocrine activity of EDCs, generated TPs, and their potential risks on human health.

The limitations of this study can be attributed to the lack of authentic reference standards which would not only allow the structural confirmation of TPs, but also to verify their respective biological activity on XETA. Additionally, while offering greater realism and representation of living organisms, *in vivo* models pose challenges in precisely identifying the MoA due to their inherent complexity and potential interferences from other chemical and biological factors. While beyond the scope of this study, further research should focus on the application of eAOPs in more complex samples to verify the influence of the matrix on the generation of TPs,

and their associated toxicity. Despite these drawbacks, the observation of a contrasting thyroid system activity between non-treated samples and intermediately degraded samples clearly indicates that generated TPs have a distinct MoA. Such outcome would certainly be overlooked if an *in vitro* assay that assesses the MoA of the parent compound, such as the TTR binding assay, was used to evaluate the degradation of DCF. As a result, in the preliminary evaluation of AOPs, it is recommended to employ a battery of bioassays, starting with *in vivo* toxicity assessment. This approach would enable the exploration of a broader spectrum of MoAs at the initial stage and simplify the process of choosing suitable *in vitro* assay(s) to confirm the MoA of bioactive TPs.

5.4. Conclusions

For the first time, this study revealed that DCF has a thyroid activity in amphibians. To mitigate this endocrine activity, this EDC was electrochemically degraded for the purpose of its abatement into biologically inert compounds.

As the electrochemical degradation of DCF was carried out, an observed increase in toxicity indicated potential risks associated with the incomplete removal by eAOPs due to the production of intermediates possessing a higher toxicity than the original compound. Moreover, an unexpected pro-thyroid effect was observed, inferring that thyroid-active TPs possess distinct MoAs compared to the parent compound. These TPs induced a pro-thyroid response even in the presence of a residual DCF concentration that previously revealed to inhibit the thyroid function. It is hypothesized that this pro-thyroid effect was caused by TPs that were generated through the oxidative cleavage of the benzylic ring of DCF. This transformation gave rise to an aliphatic side chain with electronegative groups that potentially allowed the interaction with the LBD of the TR, triggering a TH-like response. However, despite the hypotheses proposed in this study, the molecular mechanisms of acute toxicity and thyroid disruption warrant further investigation. Nevertheless, a prolonged degradation duration eradicated the toxic and thyroid activity effects caused by DCF and its TPs, highlighting the potential of eAOPs as a promising remediation technology for DCF removal in water.

In conclusion, this study revealed that the radical transformation of organic pollutants by eAOPs can produce TPs with unpredictable chemical and biological features, potentially posing risks to the environment and public health. This highlights the need for holistic and reliable chemical and biological tools for the assessment of the efficiency and safety of these novel remediation technologies. Moreover, the present findings clearly indicate the importance and necessity to incorporate *in vivo* bioassays that are able to screen multiple MoAs. This should guide the decision-making process for conducting higher-level assays to identify

potential adverse effects on toxic and endocrine-related endpoints. On the other hand, future work must also focus on environmental samples and examine the role of different water constituents, such as chlorides, that potentially can affect the degradation mechanism and thus the observed toxicity.

CHAPTER 6

General Discussion & Perspectives



The quality of water and its effects on ecosystems and human health pose significant challenges worldwide. Although the oxidative treatment of water can address numerous issues associated with hygiene and micropollutants, ensuring that none of the transformation products (TPs) formed during oxidative treatment exhibit toxicity is extremely challenging. The mineralization of micropollutants, which is the simplest way to ensure loss of toxicity, is cost-prohibitive for typical treatment conditions and often accompanied by the production of high concentrations of disinfection by-products (DBPs). Consequently, oxidative treatment introduces another compromise: balancing the removal of micropollutants against the potential adverse effects of creating toxic TPs and DBPs. These risks can be minimized through a rigorous approach that considers reaction kinetics, identifies TPs, and assesses toxicological effects. Consequently, it is crucial to enhance our comprehension of the mechanisms behind the generation of TPs and their possible toxicity. However, the task of identifying and predicting TPs resulting from a wide range of emerging micropollutants (EMs) due to oxidative treatment remains a significant hurdle.

This PhD thesis focused on the combination of advanced analytical techniques and biological tools to thoroughly assess the electro-degradation of common EMs, aiming to reduce the knowledge gap regarding the formation mechanisms of TPs and their related toxicity. The subsequent sections provide an overview of the various research dimensions of this thesis.

6.1. Feasibility of electrochemical advanced oxidation processes

In recent years, there has been a growing interest in the use of electrochemical processes for the treatment of polluted waters. These methods are valued for their versatility and ability to break down a broad spectrum of pollutants at ambient temperature and pressure without waste production. Despite their numerous advantages over conventional and other AOPs, there are still many obstacles to overcome, such as mass transfer limitations, the high energy demand, undesired side reactions and the generation of toxic by-products [378,379]. Therefore, the efficiency and safety of eAOPs needs to be thoroughly assessed before they are implemented for water treatment.

The applied experimental conditions for the degradation of 17α-ethinylestradiol (EE2) in **Chapter 4** and diclofenac (DCF) in **Chapter 5** allowed the complete removal of these EMs from water. Despite this, it is important to highlight that these studies were carried out using simple water matrices with high supporting electrolyte concentrations to ensure sufficient conductivity. Such experimental conditions may not be directly applicable to treat (real)

wastewater. This is due to the typically low conductivity of wastewater and the presence of scavengers, such as inorganic species and organic matter, that could greatly lower the efficiency of EMs degradation [276,277].

In real-world scenarios, dissolved organic matter (DOM) consumes the majority of the oxidative agents [379–381]. This consumption is largely attributed to the oxidation of phenolic components within DOM, that are present at concentrations higher than the concentration of micropollutants in natural and treated waters [379,382]. The consequences are the loss of oxidative capacity and the formation of organic and inorganic DBPs. When DOM reacts with hydroxyl radicals (•OH), it results in the creation of oxygen-rich DBPs such as aldehydes, ketones, and carboxylic acids at much higher concentrations than the residual concentration of micropollutants post-treatment [383,384]. As a result, these oxygen-rich byproducts may have a greater impact on the toxicity and biological effects of treated waters than the micropollutants and respective TPs themselves. Furthermore, EMs are often present in mixtures in real-world scenarios, which can have diverse implications on the degradation efficiency and the toxicity. As the generation of TPs will lead to additional contaminants to consider in WWTPs, the operational parameters of the WWTPs might have to be adapted in order to deal with this increasing load.

Very importantly, the widespread occurrence of halide ions such as chloride and bromide in natural waters and wastewater, leads to the inevitable formation of halogenated organic by-products during electrochemical treatment [385,386]. Halogenated TPs can be more hydrophobic than the parent compounds (PCs), posing a considerable health risk. Similarly, the generation of inorganic chlorate, perchlorate, and bromate is a critical concern, as these species are suspected to be carcinogenic and mutagenic [387]. Perchlorate is formed through the oxidation of chlorate at the anode surface and primarily at highly oxidizing boron doped diamond (BDD) anodes [257]. Previous research indicated that the formation of chlorine, chlorate, or perchlorate is a concern at applied current densities ranging from 50 to 300 A/m² [378]. The degradation of EE2 in **Chapter 4** and DCF in **Chapter 5** were conducted within these current densities. It is likely that the observed lethality of medaka fish exposed to the degraded samples with sodium chloride (NaCl) were caused by these chlorine species. Moreover, electro-degradation experiments were conducted with 0.025 M of NaCl to investigate the influence of chloride ions in the abatement of DCF. The treated samples proved too toxic for effective toxicity assessment, with observed lethality in tadpoles shortly after exposure. This toxicity might be attributed to the formation of organochloride compounds, as well as toxic chlorates and perchlorates produced by the BDD anode. This toxicity is a matter of concern since perchlorate has been found in both surface and groundwater and is considered an EM due to its potential to disrupt the synthesis of maternal thyroid hormones during pregnancy [388]. Although lowering the current densities at BDD anodes can be a

strategy to mitigate perchlorate formation, operating at current densities below 50 A/m² might compromise oxidation efficiency by limiting the charge transfer and decrease •OH production [378]. Moreover, completely avoiding chlorine formation is challenging, as the chlorine evolution reaction has a lower overpotential compared to the oxygen evolution reaction [378,389].

The aforementioned drawbacks can be circumvented through the hybridization of eAOPs with other remediation technologies. Membrane technologies can be employed as a pre-treatment to concentrate micropollutants and increase salinity, which in turn can enhance the conductivity and efficiency of eAOPs [289]. Moreover, the combination of electrochemical oxidation with electrochemical reduction or photocatalytic processes may be a cutting-edge remediation for the removal of halogenated TPs [285–288]. Other removal methods such as adsorption to activated carbon may be effective, depending on the water source composition and the applied treatment [390,391]. Additionally, various treatment techniques, including ion-exchange, membrane filtration, and microbial, chemical, and electrochemical reduction, have been explored for removing chlorate, perchlorate, and bromate, though further development is necessary for their widespread application [378,392,393].

It should be emphasized that assessing the feasibility of eAOPs in real world applications requires scaling-up these processes. However, data on the full-scale application of electrochemical processes for water treatment remain limited [36,394]. The challenge in scaling up these remediation technologies lies on the fact that it requires significantly more than merely increasing the volume that is used in lab-scale experiments [30]. Although a uniform current density, supplied through the electrodes, is key in determining the process efficiency, external factors such as flow dynamics, mechanical design, plumbing, materials, construction details and operating parameters become more relevant for a full-scale operation of these processes [30]. Moreover, the economic viability of eAOPs in terms of set-up costs and energy consumption for electrochemical cell operation at large scale should be evaluated [36]. Nevertheless, studies have documented the successful use of these technologies on pilot-scale, serving as a bridge between lab-scale and full-scale set-ups [36,290]. Moreover, a combined approach including the theoretical modelling of such electrochemical systems, coupled with the reactor configurations, electrode materials and mechanical design of such large-scale set-ups could provide better insight into the industrial application and economics of eAOPs for wastewater treatment [395].

Nonetheless, the described mechanistic studies on the degradation of EE2 and DCF in **Chapter 4** and **5** remain a crucial first step when a new eAOP strategy is investigated, as they allow to identify optimal process conditions to achieve the desired treatment outcomes while minimizing any potential negative impacts. This is particularly relevant since the generation of

powerful non-selective oxidants can lead to the production of toxic TPs that can pose a threat to the environment and human health.

6.2. Technological advancement in analyzing EMs and respective TPs

The generation of highly reactive radical species has attracted significant interest for the removal of a wide variety of EMs from water. Beyond the successful abatement of pollutants, it is becoming increasingly important to identify the TPs generated during these processes to accurately assess their environmental impact. The full structural elucidation of TPs requires advanced analytical methods that combine high separation efficiency with a maximum of structural information.

6.2.1. Multidimensional liquid chromatography for the separation of transformation products

Recent developments in two-dimensional liquid chromatography (2D-LC) have showcased its effectiveness in analyzing environmental samples that cannot be fully characterized by conventional one-dimensional liquid chromatography (1D-LC) methods [119,396]. However, performing 2D-LC analysis with dedicated commercial instrumentation can still be cost prohibitive for many academic and private laboratories.

The goal of **Chapter 3** was to make a comparison between an in-house developed 2D-LC setup and a commercially available 2D-LC instrument, based on experimental differences, in addition to more general differences, including cost price, flexibility, and ease of operation. To achieve this, the separation of 28 representative pharmaceuticals and pesticides displaying a large polarity range was compared on both setups. The use of HILIC in the first dimension (^{1}D) and RPLC in the second dimension (^{2}D) is one of the most frequently employed combinations because of the high orthogonality of this combination, which has been enhanced by the development of multiple modulation techniques to minimize the solvent incompatibility between both dimensions [123,396]. In this chapter, different strategies to deal with the mobile phase incompatibility between HILIC and RPLC were investigated in detail on both setups. For the commercial 2D-LC instrument, the strategy used was active solvent modulation (ASM) and in-line mixing modulation (ILMM), while for the in-house developed setup, a combination of restriction capillaries and a trap column was used.

The selective comprehensive 2D-LC (sLC × LC) approach, only possible on the commercial setup, provided the best peak shapes and recoveries for all 28 compounds. On the other hand,

due to the large volume of strong ^{1}D eluent transferred to the ^{2}D, the LC-LC approach was not capable of retaining paracetamol on the ^{2}D on both systems, and the peaks of early eluting compounds such as caffeine, ticlopidine and sulfamethoxazole were broadened.

For later eluting compounds, there were no significant differences between the instruments in terms of peak shapes and recoveries. Regarding the overall analysis time, sLC × LC took the longest to separate all 28 compounds, whereas the LC-LC approach on the commercial instrument took 30 min versus 45 min on the in-house developed system. This difference was attributed to the commercial system being equipped with two binary pumps, allowing for simultaneous ^{1}D and ^{2}D separations, unlike the in-house system that is equipped with a single quaternary pump. It should be noted, however, that the simultaneous separation and analysis of both dimensions is only possible when using non-destructive detectors, such as diode array detector (DAD). If a destructive detector such as a mass spectrometer (MS) is used, and if detection in both dimensions is required, the separation in both dimensions needs to be sequential, as was the case for the in-house developed setup.

Generally, the choice between an in-house developed and commercial system for 2D-LC, whether it is a single heart-cut or comprehensive, depends on the sample complexity, the analytical objectives and the available budget.

The more expensive commercial 2D-LC setup is equipped with valves with multiple sample loops and allows analysts to conduct 2D-LC separations in a variety of formats, such as single LC-LC, multiple LC-LC (mLC-LC), sLC × LC, and comprehensive (LC × LC) 2D-LC. To address issues related to the incompatibility of mobile phases, commercially available instruments offer several strategies, with ASM standing out as a particularly noteworthy solution. Additionally, in combination with dedicated software, these systems facilitate a broad spectrum of applications in a user-friendly manner, thereby making the 2D-LC approachable for analysts with varying levels of experience.

For less complex samples and stricter budgets, the use of the in-house developed system in **Chapter 3** can be a more cost-effective alternative. This system was implemented using a modified 1D-LC setup, requiring only one quaternary pump and no specialized software, significantly lowering operational costs. The current configuration of this system enables the analysis of both polar and non-polar compounds within a single chromatographic run. This in-house developed system could be used for the analysis of the samples described in **Chapter 4** and **5**. The electro-degradation of EE2 and DCF resulted in the incorporation of multiple polar functional groups such as hydroxyl, carbonyl, and carboxylic groups, increasing the polarity of the resulting TPs. As seen in **Table 5.1**, TPs of DCF such as TP184, TP168 and TP138a eluted nearly in the void volume of the RPLC column, indicating that more polar TPs were likely formed during the electro-degradation of DCF, but were not retained on the RPLC column.

Consequently, employing an orthogonal retention mechanism such as HILIC could retain these highly hydrophilic TPs.

However, while the in-house developed system can effectively separate a broad polarity range of substances as verified in **Chapter 3,** the loss of certain compounds (e.g., paracetamol) is a critical disadvantage for comprehensive chemical analysis. The application of the in-house developed setup in its current configuration could imply the loss of relevant EMs and TPs and compromise the correlation with toxicity data. While this compound loss also occurred in the LC-LC approach on the commercial system, this system has the advantage that sLC × LC is readily accessible, offering a feasible solution to this problem. While the in-house developed system offers the flexibility to further customize it by adding extra components (valves, columns, sample loops) to meet analytical needs, it is important to carefully consider the bulkiness and practicality of the resulting setup before proceeding with further development and validation of such solutions. Additionally, in-house developed setups are less user-friendly, require manual configuration and a careful monitoring of chromatographic runs, which can be time consuming and laborious. Regardless, analyzing more complex samples, such as real wastewater whether treated by eAOPs or not, the necessity for a higher peak capacity makes the LCxLC method, exclusive to commercial instruments, the more suitable option.

Finally, it is important to highlight that the detailed comparison of the in-house developed and commercial systems described in **Chapter 3** was carried out using a clean sample matrix containing selected compounds at concentrations significantly higher than those typically found in the environment. Although the used sample was representative for the wide polarity range that is characteristic for environmental samples, it does not accurately reflect their complexity, which often involve a multitude of unknown compounds at low concentrations. Under these conditions, sensitive instrumentation capable of delivering extensive structural information, like mass spectrometry (MS), becomes necessary. This, however, involves further adaptation of the chromatographic settings to obtain an optimal MS ionization efficiency. Moreover, other types of samples that encompass a broader range of compound classes could impact the performance differences between in-house and commercially available systems.

6.2.2. High resolution-mass spectrometry for the structural elucidation of TPs

The capacity to identify unknown compounds through accurate mass measurements and the structural information provided by fragmentation spectra, makes high-resolution mass spectrometry (HRMS) one of the most powerful tools for detecting and identifying TPs of EMs. A total of 79 TPs of EE2 (**Chapter 4**) and 43 TPs of DCF (**Chapter 5**) were monitored and

tentatively identified, reflecting the non-selective nature of the radicals involved in the degradation of these EMs. However, it is precisely this non-selective nature of the oxidizing species that makes the identification and structural elucidation of TPs challenging, as it leads to the formation of a plethora of new, unidentified compounds that are not documented in existing databases or literature. While non-target screening strategies have been developed to enable the identification of unknown molecules, prioritizing relevant chemical features is essential. This approach allows to focus the intensive and complex identification and confirmation processes towards the unidentified analytes that are most significant from an environmental perspective.

During the search for TPs, efforts were made to annotate chemical features through suspect screening. However, most features remain unannotated due to their absence in reference databases, highlighting the major limitation of the suspect screening method: its reliance on compounds listed within reference databases for annotation. Furthermore, isobaric interferences can arise due to the presence of dehydrogenated TPs resulting from hydrogen-abstraction reactions by •OH. These TPs share similar physicochemical properties which can render chromatographic separation unfeasible. In case these TPs are chlorinated or undergo chlorination, their simultaneous elution can cause overlapping isotopic mass signals, thereby complicating chemical interpretation.

Tandem MS (MS/MS) fragmentation data play a key role in obtaining higher confidence in the molecular structure of TPs. This data can be verified by matching with spectral library, providing a strong indication for the structure of the annotated compound. However, this approach presupposes the existence of a comprehensive spectral library, which is frequently not the case. Furthermore, rearrangement reactions following MS/MS fragmentation, particularly for steroid hormones [275], add another layer of complexity. Consequently, the task of identifying completely unknown compounds becomes more difficult, necessitating manual analysis of fragmentation patterns, a process that is both complex and time-consuming.

Currently, research into the identification of TPs and the development of related workflows is still in its nascent stages. There remains a noticeable absence of specific, automated workflows designed for suspect and non-target analysis that fully leverage the capabilities of HRMS instruments. Effective workflows require exclusion criteria and robust filtering methods to prioritize peaks accurately and to eliminate both false positives and negatives. There is also a need for improved *in silico* fragmentation models that can accurately predict fragments for each ionization mode in accordance with specific rules. Nevertheless, there are continuous improvements in both instrumentation and software, which are becoming more comprehensive and easier to use [149,397].

An integrated approach should incorporate prediction models that can identify TPs from a wide array of radical-driven transformation reactions, such as those involving •OH, and automatically incorporate these predictions into suspect screening processes.

Furthermore, non-target screening should extend beyond the identification of the most intense peaks to also include those of greatest relevance based on ecotoxicological data. Moreover, the development of a universal retention time prediction model that is simple to calibrate and can accommodate both neutral and ionic compounds would greatly improve data analysis. Consequently, the creation of new computational tools for toxicity prediction or their integration with high-throughput toxicity testing methods would be highly beneficial.

However, definite identification can only be performed by using reference standards, which, in most cases, is not possible since these are not commercially available. Additional and supplementary orthogonal techniques such as ion mobility spectrometry (IMS) and nuclear magnetic resonance (NMR) could contribute to the structure elucidation of unknown TPs. NMR stands out as a powerful instrument that provides comprehensive molecular insights that allow the structure elucidation of TPs [398]. Its major drawbacks are the low sensitivity and the need for sample purity [398], which is problematic when several TPs are present at low concentrations in complex matrices. This highlights that, despite the demands for a robust identification process, sample preparation techniques should not be forgotten and should definitely be integrated in the analytical workflow. It is clear, however, that sample preparation is very challenging in order to capture the wide range of polarities of TPs and to take full advantage of the analytical instruments while, at the same time, eliminating interfering matrix components [397,399].

6.3. Integrating *in vivo* assessment in the toxicity profiling of TPs

The overarching goal of AOPs is the breakdown of toxic organic pollutants into biologically inert compounds. However, the removal of these pollutants does not necessarily imply the elimination of toxicity. If the resulting TPs are not completely mineralized, the toxicity of the treated wastewater may be equal to or even exceed that of the untreated wastewater, posing substantial risk to the aquatic environment. This risk increases if the biological tool used for toxic assessment is not suitable for this purpose. Ideally, the toxicity evaluation should involve of a battery of bioassays that cover all the toxic modes of action (MoAs) of EMs found in environmental samples or in wastewater. However, screening all toxic MoAs is currently out of reach.

Regardless of the approach taken to assess the environmental risk of TPs, it is always necessary to careful select bioassays that can monitor the toxicity during the degradation processes and that are appropriate for the selected compounds. Each EM and corresponding TPs have a unique structure and can behave differently.

As of now, the assessment of toxicity changes during degradation processes primarily relies on general toxicity. The bioluminescent marine bacterium *Vibrio fischeri* (Microtox®) alongside with predictive QSAR models such as ECOSAR are among the most common tools for their simplicity and high-throughput [75,76,87]. However, the Microtox® test might not be sensitive enough to detect toxicity [87,400]. Moreover, it is incapable of detecting any kind of specific toxicity, such as endocrine disruption. Furthermore, predictive QSAR models depend on reliable data, which can be limited and fail to consider the combined effects of compounds in treated samples [75].

Numerous bioassays have been developed and can be employed to assess toxicity changes during advanced water treatment and verify the overall safety of these processes [76]. When selecting a bioassay, it is often assumed that TPs differ from their PCs by only slight modifications of their molecular structure and therefore retain the toxicophore, leading to the same toxic MoA [49]. It is moreover assumed that these changes regard the addition of polar functional groups such as hydroxyl groups, resulting in more polar compounds with less potential to bioaccumulate and hence less toxicity [401]. However, even minor structural modifications can significantly change the chemical and biological properties of the resulting TPs. This was the case of the chlorination of EE2 and the decarboxylation of DCF. As discussed in the respective chapters, both reactions may have contributed to the loss of biological activity. However, they also lead to a decrease in polarity of the TPs, rendering them more toxic.

A key finding of this thesis was the first-time identification of TPs generated by advanced oxidative treatment that possess a different toxic MoA compared to the original compound (**Chapter 5**). This demonstrates that these novel remediation techniques are able to significantly modify the molecular structure of TPs, potentially introducing new toxicophores that lead to a specific but distinct MoA. The detection of an opposite biological effect in the intermediate degraded samples was made possible only through the use of an *in vivo* model capable of identifying multiple MoAs. Certainly, this unexpected biological activity would have been missed using an *in vitro* assay that assesses the same MoA as the parent compound.

Research literature indicates that TPs generated by AOPs that are more toxic than their PCs are rather the exception than the norm [49,402]. However, it is important to note that there have been no comprehensive studies that combine the structural elucidation of TPs through LC-HRMS and toxicity profiling with *in vivo* models, which can detect multiple MoAs. Considering the unexpected findings presented in **Chapter 5**, it is plausible that other AOPs

may have produced TPs with different and potentially more dangerous toxic MoAs that have remained undetected due to the lack of suitable biological tools. Therefore, in the preliminary evaluation of AOPs, it is advisable to employ a battery of bioassays, starting with *in vivo* toxicity assessment that would enable the exploration of a broader spectrum of MoAs.

Despite the benefits that *in vivo* models hold over *in vitro* and *in silico* approaches, the low-throughput and tighter regulations governing the use of living animals in ecotoxicity assessments make *in vivo* models less appealing for the toxicity evaluation of TPs.

To address this challenge, a viable approach involves the use of whole organism testing such as eleutheroembryos. As discussed in **Chapter 1**, bioassays based on eleuthero-embryonic life stages are ethical and are considered to be in line with the 3R's principles of replacement, reduction, and refinement [403]. Moreover, they cover a broader range of MoAs, which is crucial for accurately measuring endocrine disruption. By nature, endocrine hormones are produced in one tissue or gland and act distantly in a different tissue [404]. This complexity makes it challenging for a single cell culture line to encompass all possible MoAs, which can include changes in hormone synthesis, transport, metabolism, excretion, and receptor binding. Currently, only *in vivo* assays are capable of fully addressing these essential aspects of endocrine signaling. Moreover, since the endocrine signaling pathways are highly conserved across vertebrate taxa [83], *in vivo* vertebrate models such as fish and amphibians can play a critical role in assessing the endocrine activity of EDCs, generated TPs, and their potential risks on human health.

It is important to recognize that the use of embryos of fish and amphibians is more costly than employing cell culture lines or computational tools. Furthermore, the development and validation of embryonic assays require dedicated facilities and equipment, expert handling, extensive maintenance, combined with limited regulatory acceptance [67]. Moreover, these *in vivo* assays can only inform on the potential for a test substance to interact directly or indirectly with an endocrine axis via various mechanisms [67]. Therefore, in the evaluation of toxicity evolution during AOPs, these *in vivo* assays should be complemented with mechanistical *in vitro* studies to confirm the MoA of bioactive TPs. Moreover, computation tools such as the molecular docking simulation used in **Chapter 5** can be complementary to aid in the delineation of a nuclear receptor-mediated activity exerted by TPs.

6.4. Environmental risk assessment of transformation products

Numerous studies have documented the toxic and endocrine-disrupting effects of EMs in the environment [405]. However, there is currently no established strategy to evaluate the

environmental risks posed by TPs produced in advanced water treatment processes. TPs can present a significant risk when they are generated in large quantities, persist longer or exhibit greater toxicity compared to the PC [49]. As discussed in **Chapter 1**, there are two main approaches to conduct the environmental risk assessment (ERA) of TPs: exposure-driven approach and effect-driven analysis (EDA).

Previously, remediation strategies employed selective oxidants such as ozone, chlorine, and chlorine dioxide, which only reacted with a limited number of functional groups within a target compound resulting in a few major TPs [406]. The ERA of these TPs was conducted by an exposure-driven approach, wherein the most intense TPs were classified as “major TPs” and considered relevant for risk assessment. These TPs were distinguished and singled out for identification according to their occurrence followed by assessments of their environmental fate and (eco)toxicity testing.

However, recent remediation technologies are based on the production of radicals characterized by a lower selectivity which can interact with a broader range of functional groups, potentially resulting in a "combinatorial explosion" of TPs [407]. This scenario was exemplified by the degradation of EE2 (**Chapter 4**) and DCF (**Chapter 5**) in this thesis, where a significant number of TPs were monitored and identified, including various structural isomers. Given the overwhelming number of transformation pathways and products, a comprehensive risk assessment for all TPs is not feasible. In this scenario, EDA, which applies a tiered approach directed by toxicity evolution, is the most suitable approach to reach the more relevant TPs for ecotoxicity. Nevertheless, since a comprehensive chemical and biological analysis through EDA remains laborious and time-consuming, most studies that evaluate the toxicity of TPs generated by low selective oxidizing species, still use the exposure-driven approach. Furthermore, in most cases, the toxicity assessment relies on simpler bacterial assays or predictive QSAR models [76,402].

In this thesis, the assessment of toxicity and endocrine disruption of TPs from EE2 and DCF was conducted by EDA. While the toxicity evolution during the degradation of EE2 roughly paralleled its degradation kinetics, this was not the case for DCF. Indeed, with EDA, the observation of an unexpected thyroidogenic effect in the intermediately degraded samples allowed directing the research efforts towards the identification of the relevant TPs that were responsible for this biological effect (**Chapter 5**). Throughout these investigations, it became evident that it is imperative to establish a clear distinction between the concepts of “major TPs” and “relevant TPs”.

Firstly, the prevalent categorization of TPs into "major" and "minor" can be misleading. According to OECD Testing Guideline 316, which addresses the phototransformation of chemicals in water via direct photolysis, major TPs are defined as those that constitute at least 10% of the applied test chemical in any individual sample at any sampling time [408]. Further

studies that propose strategies to assess the ERA of TPs follow this definition [49,409]. However, this assumes that the MS ionization efficiency of the TP in question is equivalent to that of the PC. This assumption can be flawed since during degradation, the oxidative agents can modify or even cleave the functional group responsible for the ionization site of the resulting TP. Consequently, the observation of a diminished MS signal intensity might also be an indication of an inefficient ionization of the TP, leading to an underestimation of its concentration.

From a biological perspective, disregarding so-called "minor TPs" could compromise the accuracy of the toxicity assessment. Frequently, studies using an exposure-driven methodology focus on a selected few of the most intense TPs for QSAR analysis, assigning overall sample toxicity based on these selected compounds. However, for MoA that involve a specific target, such as interactions with estrogen or thyroid receptors, the toxicity exerted by TPs may adhere to the Pareto principle, where a small number of compounds are responsible for the majority of the toxic effects. This is because only a small number of TPs will have the correct conformation that allows to effectively bind to the receptor and trigger a biological response. Moreover, a compound with a high affinity for the ligand-binding domain (LBD) of a receptor will require a lower effective concentration (EC) to elicit a toxic response, potentially contributing to a higher overall sample toxicity despite its lower concentration.

This can be evidenced by the thyroid disruption evaluation of the TPs of DCF in **Chapter 5**. TP289 resulted from the oxidative cleavage of the benzylic ring of DCF, and is one of the least intense TPs detected during the chemical analysis (**Fig. 5.4**). Moreover, it is more polar than its parent compound, since it elutes earlier from the RPLC column (**Table 5.1**), which suggests it has less capacity to bioaccumulate and exert toxicity. Using an exposure-driven approach, TP289 would be considered as “minor” for its low intensity signal and most likely not considered relevant for ecotoxicity. However, employing an effect-based approach enabled the identification of TP289 as having the highest binding affinity to the thyroid receptor, that could explain the thyroid-stimulating effect observed in the intermediately degraded samples (**Fig 5.10**). This TP is thus considered relevant for the observed pro-thyroid activity despite its relatively low intensity. Therefore, the EDA used in this thesis revealed to be a strong approach to assess the toxicity of TPs.

It is important to acknowledge that uncertainties remain in assessing the hazardous effects of TPs due to the extreme scarcity of acute and chronic data and the potential disparity between experimental and real environmental conditions. To date, the toxicological profiles of TPs have not been as thoroughly characterized as their PCs. Furthermore, the antagonistic and synergistic effects of mixtures containing PCs and their numerous TPs will require further exploration to enable a precise risk assessment.

Although EDA offers a comprehensive methodology for assessing the toxicity of TPs, it can be a complex and time and resource-intensive process [61]. Identifying possible toxicants in a high-throughput manner has been one of the main bottlenecks of EDA. Confirmation of annotated compounds is still required which can be a laborious process. Also, unannotated features that were selected as a result of the workflow may require further investigation applying nontarget screening techniques, which requires powerful analytical instruments that are not within reach of many laboratories.

While currently the combination of advanced analytical techniques with reliable bioassays provides the best approach for the ERA of PCs and their TP mixtures, such approach needs expertise from different fields in order to get reliable and meaningful results.

6.5. Future perspectives

Given that typically more than 99% of oxidant reagents are consumed by DOM and inorganic substances [406], there is a significant challenge in electrochemical wastewater treatment, highlighting the need for careful consideration in the development of further treatment systems. Furthermore, while it is crucial to assess the toxicity of TPs resulting from the degradation of EMs, controlling the formation of DBPs, such as chlorate, perchlorate, and other halogenated derivatives, is equally essential. To tackle these challenges, conducting bench-scale studies with authentic (waste)water samples represents a pivotal next step. Furthermore, combining eAOPs with other remediation technologies should be considered to ensure a wide range of applications and reduce the risks associated with relying solely on electrochemical treatments. These studies must be complemented with a comprehensive chemical and biological assessment during oxidation processes to capture a thorough understanding of the treatment impacts of real samples. Furthermore, the majority of contaminants in wastewater are found at low concentration, meaning their electrochemical reactivity is predominantly hindered by mass transfer limitations [378]. This highlights the critical need for shifting research efforts towards authentic conditions prevalent in wastewater treatment scenarios, where the concentrations of contaminants are substantially lower. Doing so will ensure that further research is more aligned with practical challenges faced in electrochemical wastewater treatment.

The use of robust and comprehensive analytical and biological tools will enable the early identification and mitigation of potential adverse effects arising during water treatment processes. High-efficiency chromatographic techniques coupled to HRMS are increasingly being considered as a cornerstone in environmental research. Further development of these methods should ensure that every step of the analytical process incorporates the multi-residue

approach. This is essential for the effective analysis of a range of substances that exhibit diverse physical and chemical properties. Essential steps in the analytical workflow should include proper sample preparation techniques, chromatographic separation, ionization, accurate mass measurement and data-processing algorithms for both the screening of thousands of compounds simultaneously in a given sample and to identify new substances generated during wastewater treatment or in the environment.

LC and more specifically multidimensional chromatography remains one of the most important aspects of method development since a proper separation facilitates identification and can reduce matrix interferences, serving as a robust technique for environmental analysis. The combination with HILIC offers a compelling alternative alongside established RPLC methods for separating polar compounds, necessary to analyze hydrophilic TPs. Despite the focus of this thesis on important EMs such as pharmaceuticals and pesticides, further studies should also include other classes of EMs such as personal care products, industrial chemicals, microplastics, nanoparticles and biological agents. Thus, exploring additional retention mechanisms, such as ion exchange and size exclusion chromatography should be integrated into these studies to broaden the scope and enhance the effectiveness of environmental analyses.

The future of identifying relevant TPs in a high-throughput manner involves tiered approaches that use HRMS, additional complementary techniques, and sophisticated software tools. The deployment of LC-HRMS-based analytical methods and data processing tools has enabled the identification of hundreds of EMs and oxidative TPs. At present, the analysis of these data sets is quite constrained, highlighting the need for a better connection between mechanistic studies and toxicity databases.

While the importance of mechanistic studies of EMs' oxidation reactions is important, the research focus should shift from selected EMs to fundamental research on specific functional groups. This can be applied to micropollutants sharing similar chemical structures, thereby extending findings across a broader spectrum of EMs present in environmental matrices. For example, research could extend beyond estrogen steroid hormones to include phenolic compounds that interact with the estrogen receptor. Likewise, pathway prediction platforms have recently been developed for •OH and for ozone reactions [410,411]. This allows an interpretation of results from nontarget analyses of oxidation processes and a rapid screening of possible TPs for potentially toxic structures. However, the identification of toxicophores as indicators of specific modes of action needs further scrutiny. As MoA are species-dependent [412], future developments in this field should account for species-specific toxicophores.

Integrating *in vivo*, *in vitro*, and *in silico* tools could enhance our understanding of the key pathways involved in the toxicological activation of micropollutants in the water cycle. The use of quantum chemical computations, along with the potential application of statistical tools like

machine learning, holds significant promise when combined with experimental studies to improve predictions of reaction kinetics and product formation. This comprehensive approach could effectively complement the assessment of the overall environmental risks of TPs of emerging EMs in both natural and engineered settings. However, it is important to recognize that each predictive model carries its own level of uncertainty, and combining them could increase the overall uncertainty in the final risk assessment. Therefore, a robust risk assessment should rely on thorough toxicity testing and precise quantification using chemical standards.

6.6. General conclusion

The non-selectivity of AOPs for water treatment towards EMs presents both a potential benefit and a significant challenge, and is an inherent aspect of oxidation treatments. Nevertheless, micropollutants are not fully mineralized during oxidation but transformed to a multitude of TPs, which, in some cases, are more toxic than the PCs. Furthermore, the ubiquitous matrix components reduce the treatment efficiency during oxidation and may lead to unintended consequences, such as toxic DBPs. Considering the complex nature and variability of water sources, along the trade-offs associated with the use of powerful radical oxidants, it is clear that neither a single oxidant nor a single remediation technology can be universally applied for all treatment purposes.

Ensuring that the benefits of advanced oxidative treatment outweigh its risks is challenging, as these risks cannot be completely eliminated. However, they can be significantly reduced through a comprehensive multidisciplinary assessment. Such assessments should cover several critical areas in the abatement of micropollutants, including (i) kinetics of the transformation reactions of EMs, (ii) kinetics and mechanisms of TPs formation, (iii) assessment of biological effects/toxicology and fate of TPs. By doing so, it is possible to develop more effective, safer, and environmentally friendly electrochemical treatment systems, thereby enhancing the sustainability and safety of water resources. This holistic strategy guarantees that advancements in the field are both practical and beneficial for addressing the complexities of modern wastewater treatment.

Supporting Information



Supporting information of Chapter 3

Table S3.1 – Compounds used in this study with their stock solvents and concentrations in the stock and working solutions. The Log D values at pH 3.0 were predicted by Marvin Sketch software.

#	Compound	Sample stock solvent	Concentration stock solution (mg mL^{-1})	Concentration working solution (µg mL^{-1})	Log D (pH = 3.0)
1	Bezafibrate	EtOH	2	10	3.93
2	Amitrole	H_2O	20	400	-0.67
3	Iopromide	H_2O	10	10	-0.44
4	Lidocaine	EtOH	10	200	-0.63
5	Trimethoprim	MeOH	2	20	-0.19
6	Propranolol	H_2O	5	100	-0.66
7	Imipramine	H_2O	20	10	0.78
8	Escilatopram	MeOH	2	100	0.26
9	Paroxetine	EtOH	10	100	-0.09
10	Venlafaxine	MeOH	2	200	-0.76
11	Pipamperone	H_2O	2	20	-4.66
12	Codeine	H_2O	20	100	-2.16
13	Atenolol	H_2O	10	200	-2.82
14	Paracetamol	MeOH	10	20	0.91
15	Cafeine	H_2O	2	40	-0.55
16	Ticlopidine	H_2O	20	200	0.83
17	Sulfamethoxazole	EtOH	5	20	0.75
18	Carbamazepine	ACN	5	40	2.77
19	Oxazepam	EtOH	2	20	2.92
20	Lorazepam	EtOH	2	20	3.53
21	Diazepam	EtOH	2	20	2.81
22	Ketoprofen	EtOH	10	20	3.56
23	Cilostazol	MeOH	2	20	3.31
24	Diclofenac sodium	EtOH	5	40	4.22
25	Ibuprofen	ACN	10	400	3.84
26	Metolachlor	EtOH	10	400	3.45
27	Progesterone	EtOH	10	40	4.15
28	(4-)Nonylphenol	MeOH	5	400	5.74

Table S3.2 – Peak widths for the 1D-RPLC chromatogram in **Figure 3.4**, obtained on the in-house developed setup (compound numbers correspond to the compounds in **Table S3.1**).

Compound	Peak width (s)
14	0.020
15	0.019
16	0.037
17	0.023
18	0.022
19	0.022
20	0.023
21	0.023
22	0.023
23	0.024
24	0.023
25	0.025
26	0.027
27	0.026
28	0.025

Table S3.3 – Influence of sample loop volume and flush times on recoveries and peak widths obtained in the in-house developed setup. Dilution factor: 74 (compound numbers as in **Table S3.1**).

Sample loop volume (µL)	100		150		183	
Flush time	**1.2**	**1.5**	**1.2**	**1.5**	**1.2**	**1.5**
Compound	**Recovery (%)**					
14	/	/	/	/	/	/
15	96.2	98.5	91.5	95.5	95.5	78.3
16	98.4	99.4	100.4	105.0	101.8	114.0
17	98.2	99.9	99.6	104.2	101.6	108.2
18	96.4	99.2	97.7	104.0	97.8	105.8
19	95.6	103.0	100.4	107.0	100.9	108.4
20	89.8	102.3	109.9	105.1	94.1	102.7
21	94.7	102.8	96.5	105.3	103.0	106.9
22	94.2	96.6	92.2	100.1	91.8	103.6
23	99.3	97.5	99.0	101.1	105.6	104.4
24	104.9	105.9	96.7	106.6	107.1	105.6
25	91.3	91.9	91.3	92.0	89.8	88.8
26	98.7	99.5	99.5	103.6	95.0	97.7
27	99.5	100.1	100.6	104.2	102.0	107.4
28	103.1	102.6	106.0	107.3	101.5	109.3
Compound	**Peak width (s)**					
14	/	/	/	/	/	/
15	0.034	0.035	0.038	0.038	0.037	0.030
16	0.039	0.037	0.043	0.042	0.049	0.048
17	0.030	0.029	0.03	0.03	0.032	0.030
18	0.023	0.022	0.021	0.02	0.023	0.021
19	0.022	0.022	0.021	0.02	0.023	0.020
20	0.022	0.022	0.021	0.02	0.023	0.021
21	0.022	0.022	0.019	0.019	0.021	0.020
22	0.023	0.023	0.021	0.02	0.023	0.022
23	0.024	0.024	0.021	0.021	0.024	0.022
24	0.023	0.023	0.021	0.021	0.023	0.022
25	0.025	0.024	0.023	0.023	0.025	0.024
26	0.027	0.026	0.025	0.025	0.027	0.026
27	0.025	0.024	0.023	0.023	0.025	0.024
28	0.025	0.024	0.022	0.022	0.024	0.023

Table S3.4 – Peak widths of 1D-RPLC chromatogram in **Figure 3.7**, obtained on the commercial 2D-LC setup (compound numbers correspond to the compounds in **Table S3.1**).

Compound	Peak width (s)
14	0.015
15	0.014
16	0.026
17	0.017
18	0.016
19	0.016
20	0.018
21	0.016
22	0.017
23	0.018
24	0.017
25	0.018
26	0.020
27	0.020
28	0.021

Table S3.5 – Comparison of recoveries and peak widths obtained for the different compounds and for different dilution factors (DFs) in the HILIC-RPLC setup on the commercial 2D-LC system. Four different DFs (5, 10, 22, and 64) were investigated (compound numbers as in **Table S3.1**).

DF	No ASM	5	10	22	64
Compound			**Recovery (%)**		
14	/	/	/	/	/
15	/	/	/	84.8	81.6
16	/	113.9	116.6	112.8	107.8
17	/	90.5	92.6	90.5	83.9
18	/	100.2	102.0	98.4	93.7
19	/	101.7	103.0	99.2	94.1
20	/	103.5	107.0	104.0	107.9
21	/	93.8	93.8	91.7	85.3
22	/	94.2	95.1	91.6	85.4
23	/	97.9	98.7	95.5	90.4
24	/	92.9	92.4	89.8	84.6
25	52.2	100.6	99.9	98.0	92.9
26	96.6	103.2	104.2	101.0	96.2
27	88.2	101.3	102.0	99.1	94.6
28	84.2	87.1	89.5	87.7	85.3
Compound			**Peak width (s)**		
14	/	/	/	/	/
15	/	/	/	0.051	0.047
16	/	0.031	0.042	0.024	0.024
17	/	0.027	0.027	0.028	0.039
18	/	0.022	0.017	0.017	0.016
19	/	0.017	0.017	0.017	0.015
20	/	0.017	0.017	0.018	0.017
21	/	0.016	0.017	0.015	0.016
22	/	0.017	0.016	0.016	0.016
23	/	0.018	0.018	0.017	0.018
24	/	0.017	0.017	0.017	0.017
25	0.0267	0.018	0.018	0.018	0.018
26	0.028	0.02	0.02	0.019	0.020
27	0.019	0.019	0.018	0.019	0.019
28	0.02	0.019	0.019	0.020	0.020

Table S3.6 – Comparison of recoveries and peak widths obtained for the different compounds in the HILIC-RPLC setup, with Jet Weaver (JW) mixer (100 µL) and with or without ASM on the commercial 2D-LC system (compound numbers correspond to the compounds in **Table S3.1**).

DF	No ASM	22
Compound	**Recovery (%)**	
14	/	/
15	14.9	85.4
16	47.9	112.2
17	89.8	89.8
18	102.8	99.7
19	107.4	105.9
20	103.1	103.1
21	93.5	92.1
22	94.0	91.8
23	98.2	96.3
24	94.2	90.7
25	100.6	97.4
26	103.5	101.0
27	102.0	99.3
28	84.8	83.6
Compound	**Peak width (s)**	
14	/	/
15	0.036	0.052
16	0.025	0.024
17	0.057	0.027
18	0.042	0.016
19	0.037	0.016
20	0.033	0.016
21	0.024	0.016
22	0.023	0.016
23	0.027	0.018
24	0.018	0.017
25	0.018	0.018
26	0.020	0.02
27	0.019	0.019
28	0.020	0.020

Table S3.7 – Comparison of recoveries and peak widths obtained for the different compounds in the sHILIC × RPLC setup on the commercial 2D-LC system (compound numbers as in **Table S3.1**).

DF	No ASM	10
Compound	**Recovery (%)**	
14	22.4	89.5
15	26.0	28.1
16	42.9	111.1
17	80.5	88.1
18	94.5	100.2
19	92.6	96.0
20	95.7	101.8
21	97.1	99.6
22	87.5	92.7
23	96.0	94.2
24	90.2	95.5
25	99.9	98.0
26	101.0	99.5
27	97.2	97.8
28	91.8	87.1
Compound	**Peak width (s)**	
14	0.026	0.052
15	0.023	0.018
16	0.019	0.023
17	0.032	0.017
18	0.024	0.015
19	0.025	0.016
20	0.023	0.016
21	0.029	0.018
22	0.029	0.016
23	0.022	0.017
24	0.021	0.02
25	0.019	0.018
26	0.021	0.02
27	0.02	0.019
28	0.019	0.02

Table S3.8 – Comparison of recoveries and peak widths obtained for the different compounds in the sHILIC × RPLC setup, with Jet Weaver mixer (100 µL) and with or without ASM on the commercial 2D-LC system (compound numbers correspond to the compounds in **Table S3.1**).

DF	No ASM	10
Compound	**Recovery (%)**	
14	82.3	87.3
15	84.2	88.9
16	112.2	112.8
17	85.7	88.8
18	98.9	99.2
19	97.6	97.9
20	106.6	107.5
21	98.1	98.1
22	92.3	92.3
23	95.2	95.0
24	88.9	88.5
25	98.0	97.4
26	100.2	99.5
27	97.8	98.3
28	88.9	84.8
Compound	**Peak width (s)**	
14	0.06	0.065
15	0.019	0.018
16	0.024	0.023
17	0.019	0.018
18	0.015	0.015
19	0.015	0.015
20	0.016	0.016
21	0.018	0.018
22	0.016	0.016
23	0.017	0.017
24	0.016	0.018
25	0.017	0.017
26	0.02	0.02
27	0.018	0.018
28	0.02	0.02

Supporting information of Chapter 4

Table S4.1 – Parameters of molecular features extraction (MFE).

Parameter	Description
RT range (min)	2-15
m/z range (Da)	50 - 1000
Minimum height (counts)	1000
Adducts	$[M-H]^-$ $[M+F]^-$ $[M-H_2O]^-$
RT tolerance (min)	± 0.3 min
Mass tolerance (ppm)	± 7
Isotope model	Common organic model
Quality score (MFE)	> 70

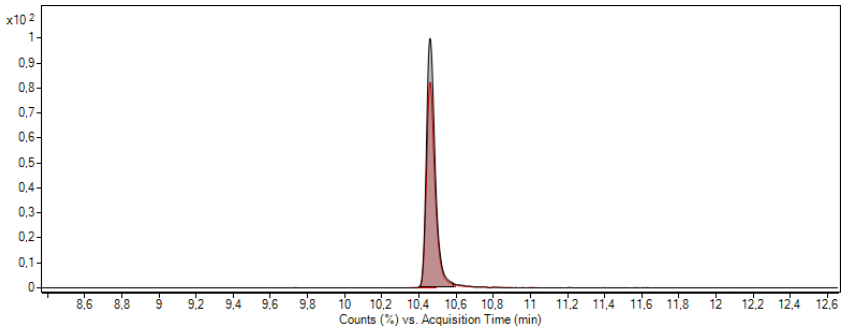

Figure S4.1 – Extracted ion chromatogram of EE2 (black peak, 10.43 min, m/z 295.1704) and EE2-$^{13}C_2$ (red peak, 10.42 min, m/z 297.1771) in ultrapure water at 500 µg/L. y-axis: relative count numbers to the highest peak.

Table S4.2 – Linearity data of 6 replicates.

Replicate	Slope	Intercept	Regression coefficient (R^2)
1	0.001803	0.002804	0.9990
2	0.001793	0.003623	0.9992
3	0.001877	0.003646	0.9970
4	0.001716	0.003193	0.9989
5	0.001641	0.003068	0.9986
6	0.001698	0.03990	0.9978

Table S4.3 – Matrix effect in blank degraded samples (mean ± relative standard deviation; n= 3).

Blank degraded samples with Na_2SO_4		Blank degraded samples with NaCl	
Target concentration (µg/L)	**Matrix Effect (%)**	**Target concentration (µg/L)**	**Matrix Effect (%)**
t= 0 min		**t= 0 min**	
20	99.4 ± 2.1	20	99.7 ± 1.2
250	98.2 ± 0.6	250	97.6 ± 0.3
2500	101.2 ± 0.2	2500	103.4 ± 0.8
t= 30 min		**t= 1 min**	
20	95.2 ± 1.4	20	95.1 ± 1.1
250	98.4 ± 1.6	250	94.2 ± 1.2
2500	100.6 ± 1.5	2500	91.9 ± 0.9
t= 45 min		**t= 2 min**	
20	95.7 ± 1.3	20	90.1 ± 2.5
250	97.9 ± 0.8	250	93.1 ± 1.3
2500	101.8 ± 0.3	2500	92.3 ± 2.7
t= 60 min		**t= 10 min**	
20	104.5 ± 1.9	20	87.9 ± 2.5
250	102.2 ± 2.5	250	88.5 ± 1.3
2500	101.2 ± 0.3	2500	89.8 ± 2.7
t= 90 min		**t= 30 min**	
20	93.2 ± 0.5	20	87.2 ± 1.5
250	94.9 ± 1.8	250	86.4 ± 1.1
2500	102.3 ± 0.2	2500	88.6 ± 0.9
t= 120 min			
20	95.6 ± 1.1		
250	94.8 ± 1.8		
2500	104.1 ± 0.4		

Table S4.4 – Accuracy and precision of EE2 analysis.

Target Concentration (µg/L)	Level	Intra-day precision (%RSD, n= 6)	Intra-day accuracy (n= 6)	Inter-day precision (%RSD, n= 18)	Inter-day accuracy (n= 18)
10	LLOQ	5.9	105.0	8.1	110.6
20	Low QC	1.6	106.9	6.5	109.5
250	Medium QC	1.0	102.7	6.2	102.3
2500	High QC	1.3	97.0	8.1	103.7

LLOQ: Lower limit of quantification
QC: Quality control
RSD: Relative standard deviation

Table S4.5 – Dilution integrity test (n= 5). Initial working solution 1.6-fold ULOQ (8000 µg/L).

Target Concentration (µg/L)	Dilution factor	Precision (%RSD, n= 5)	Accuracy (n= 5)
800	10	0.9	103.8
80	100	2.1	106.4
16	500	4.9	113.8

RSD: Relative standard deviation

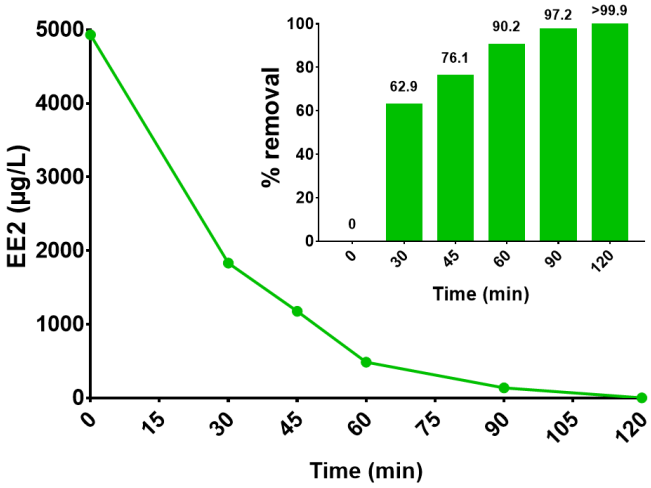

Figure S4.2 – Residual EE2 concentration and relative removal ($[EE2]_{t= x\ min}$ / $[EE2]_0$, %) in the presence of Na_2SO_4 at t= 0, t= 30, t= 45, t= 60, t= 90 and t= 120 min. $[EE2]_0$= 5000 µg/L, $[Na_2SO_4]$= 0.05 M, j= 12.5 mA/cm^2. EE2 quantification was performed in triplicate. Mean ± standard deviation.

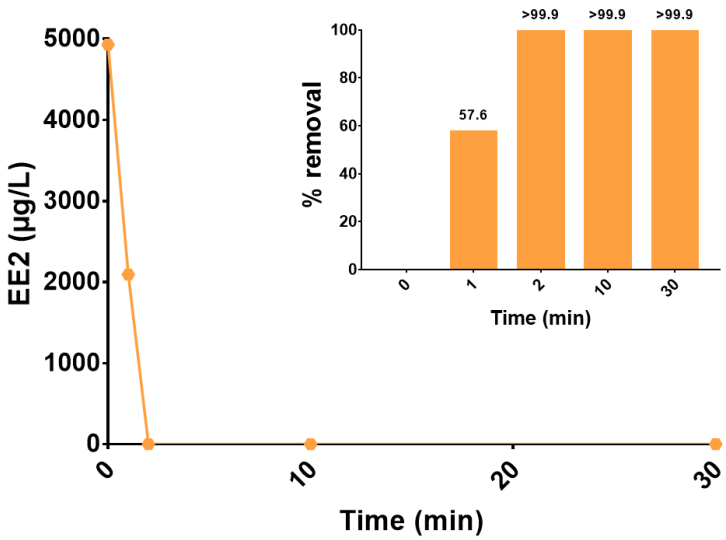

Figure S4.3 – Residual EE2 concentration and relative removal ($[EE2]_{t= x\ min}$ / $[EE2]_0$, %) in the presence of NaCl at t= 0, t= 1, t= 2, t= 10 and t= 30 min. $[EE2]_0$= 5000 µg/L, [NaCl]= 0.025 M, j= 3.125 mA/cm2. EE2 quantification was performed in triplicate. Mean ± standard deviation.

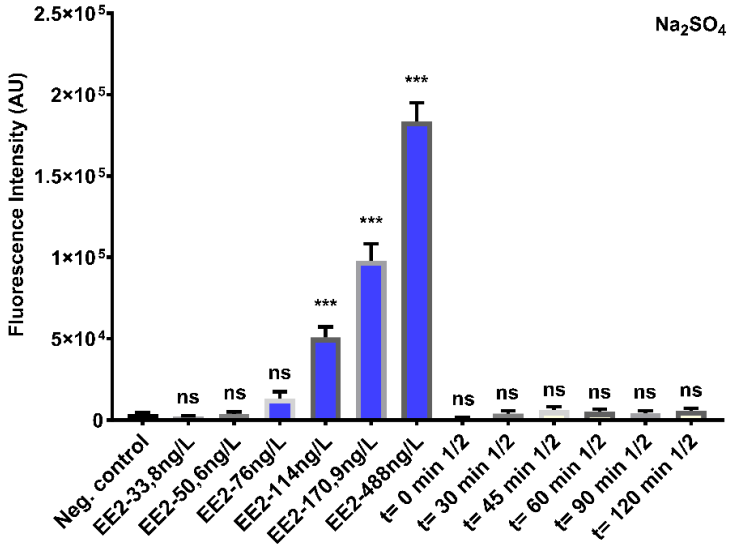

Figure S4.4 – Fluorescence of larvae exposed to negative control (Neg. control), EE2 at concentrations ranging between 33.8 - 488ng/L, un-electrolyzed (t= 0 min) sample and blank degraded samples obtained at t= 30, t= 45, t= 60, t= 90, t= 120 min in the presence of Na_2SO_4 at 0.05 M. Un-electrolyzed and blank degraded samples were 2-fold diluted. Data are shown are the mean of three experiments. Error bars represent the standard error of the mean. Statistical analysis with Kruskal-Wallis and Dunn's multicomparison test (negative control vs EE2 33.8-488 ng/L and negative control vs initial and blank degraded samples), ns: non-significant *p < 0.05, **p < 0.01, and ***p < 0.001.

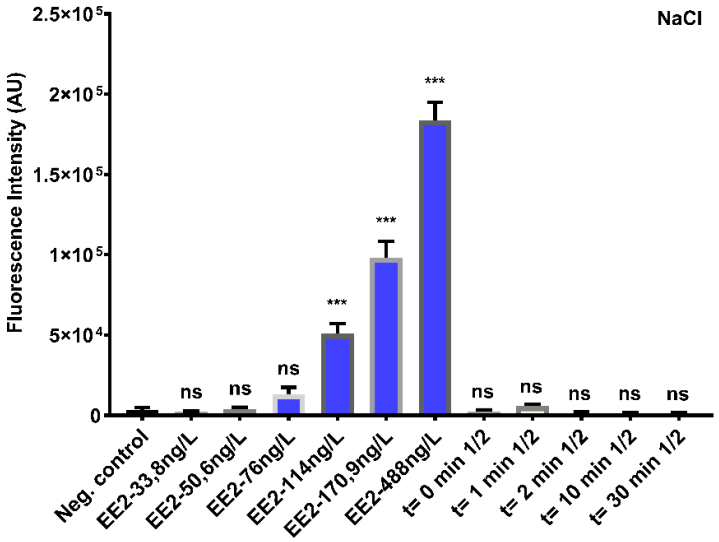

Figure S4.5 – Fluorescence of larvae exposed to negative control (Neg. control), EE2 at concentrations ranging between 33.8 - 488 ng/L, un-electrolyzed (t= 0 min) sample and blank degraded samples obtained at t= 1, t= 2, t= 10 and t= 30 min in the presence of NaCl at 0.025 M. Un-electrolyzed and blank degraded sample were two-fold diluted (1/2). Data are shown are the mean of three experiments. Error bars represent the standard error of the mean. Statistical analysis with Kruskal-Wallis and Dunn's multicomparison test (negative control vs EE2 33.8-488 ng/L and negative control vs initial and blank degraded samples), ns: non-significant *p < 0.05, **p < 0.01, and ***p < 0.001.

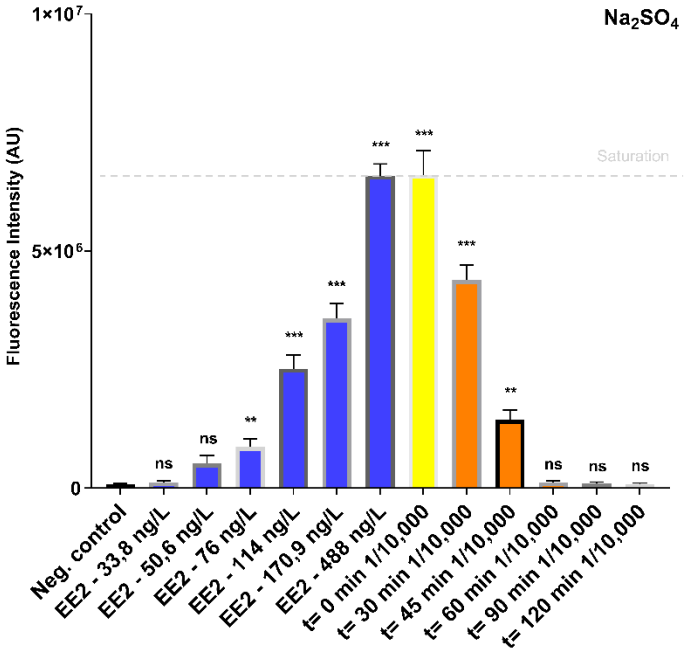

Figure S4.6 – Fluorescence of larvae exposed to negative control (Neg. control), EE2 at concentration ranging between 33.8 - 488 ng/L, initial (t= 0 min) and EE2 degraded samples obtained at t= 30, t= 45, t= 60, t= 90 min and t= 120 min in the presence of Na_2SO_4 at 0.05 M. Initial and EE2 degraded samples were diluted 10,000-fold (1/10,000). Data shown are the mean of three experiments. Error bars represent the standard error of the mean. Statistical analysis with Kruskal-Wallis and Dunn's multicomparison test (neg. control vs EE2 33.8 – 488 ng/L and neg. control vs initial and EE2 degraded samples), ns: non-significant *p < 0.05, **p < 0.01, and ***p < 0.001.

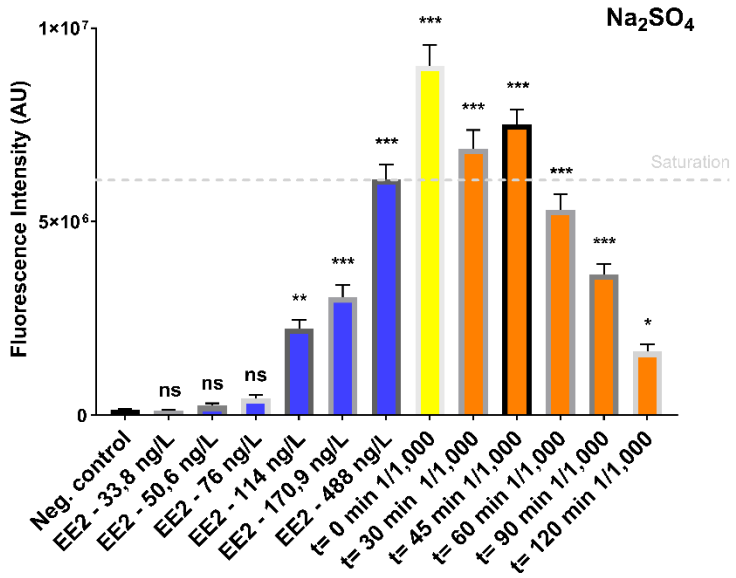

Figure S4.7 – Fluorescence of larvae exposed to negative control (Neg. control), EE2 at concentration ranging between 33.8 - 488 ng/L, initial (t= 0 min) and EE2 degraded samples obtained at t= 30, t= 45, t= 60, t= 90 min and t= 120 min in the presence of Na_2SO_4 at 0.05 M. Initial and EE2 degraded samples were diluted 1,000-fold (1/1,000). Data shown are the mean of three experiments. Error bars represent the standard error of the mean. Statistical analysis with Kruskal-Wallis and Dunn's multicomparison test (neg. control vs EE2 33.8 – 488 ng/L and neg. control vs initial and EE2 degraded samples), ns: non-significant *p < 0.05, **p < 0.01, and ***p < 0.001.

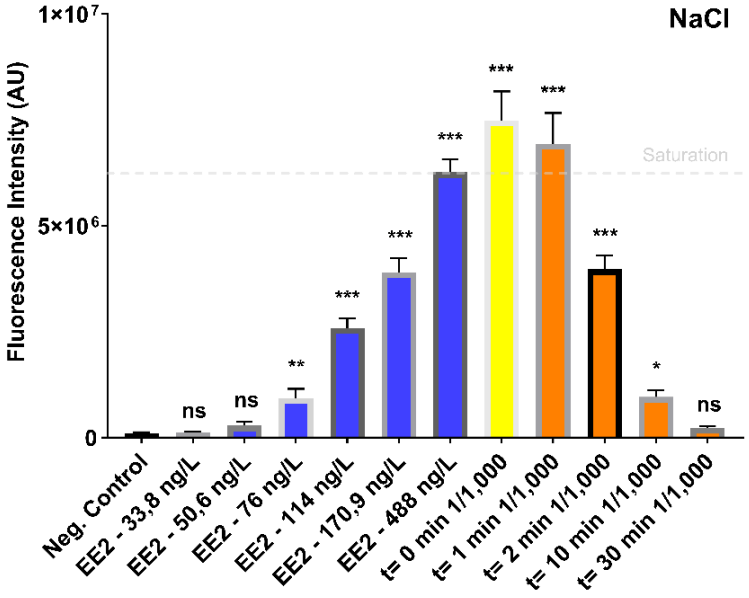

Figure S4.8 – Fluorescence of larvae exposed to negative control (Neg. control), EE2 at concentration ranging between 33.8 - 488 ng/L, initial (t= 0 min) and EE2 degraded samples obtained at t= 1, t= 2, t= 10 and t= 30 min in the presence of NaCl 0.025 M. Initial and EE2 degraded samples were diluted 1,000-fold (1/1,000). Data shown are the mean of 3 experiments. Error bars represent the standard error of the mean. Statistical analysis with Kruskal-Wallis and Dunn's multicomparison test (neg. control vs EE2 33.8 – 488 ng/L and neg. control vs initial and EE2 degraded samples), ns: non-significant *p < 0.05, **p < 0.01, and ***p < 0.001.

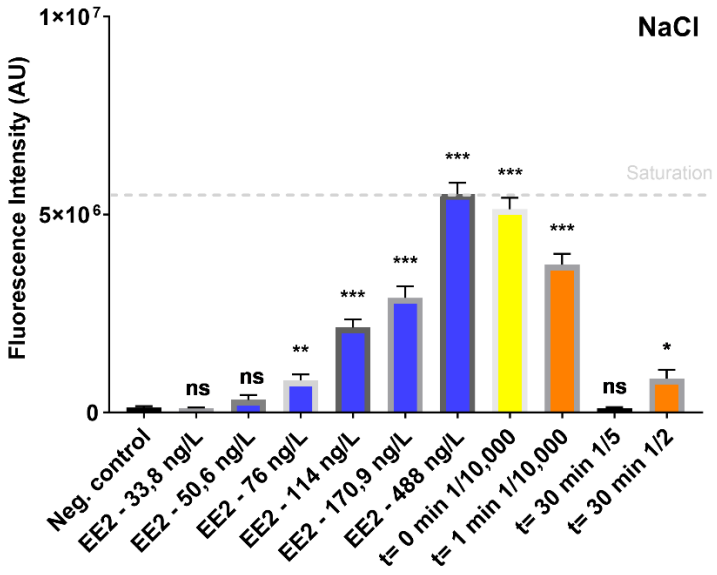

Figure S4.8 – Fluorescence of fry exposed to negative control (Neg. control), EE2 at concentrations ranging between 33.8 - 488 ng/L, initial (t= 0 min) sample and EE2 degraded samples obtained at t= 1, and t= 30 min in the presence of NaCl at 0.025 M. t= 0 and t= 1 min samples were diluted 10.000-fold (1/10,000). t= 30 min were diluted 5 (1/5) and 2-fold (1/2). Data are shown are the mean of three experiments. Error bars represent the standard error of the mean. Statistical analysis with Kruskal-Wallis and Dunn's multicomparison test (negative control vs EE2 33.8-488 ng/L and negative control vs initial and blank degraded samples), ns: non-significant *p < 0.05, **p < 0.01, and ***p < 0.001.

Supporting information of Chapter 5

Table S5.1 – Parameters of molecular features extraction (MFE).

Parameter	Description
RT range (min)	1-15
m/z range (Da)	50 - 1000
Minimum height (counts)	1000
Adducts	$[M-H]^-$ $[M+CHCOO]^-$ $[M-H_2O]^-$
RT tolerance (min)	± 0.3 min
Mass tolerance (ppm)	± 5
Isotope model	Common organic model
Quality score (MFE)	> 70

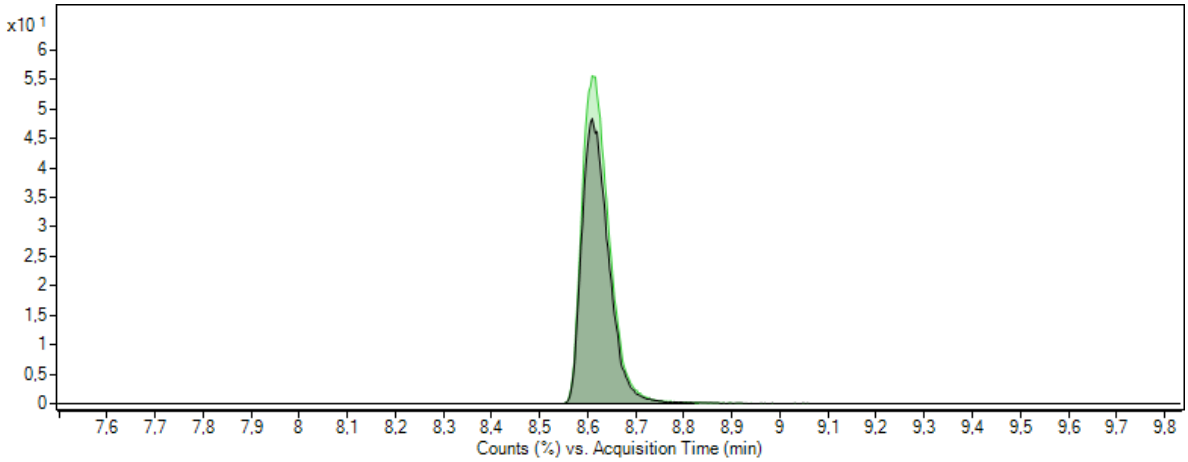

Figure S5.1 – Extracted ion chromatogram of DCF (green peak, 8.61 min, m/z 294.0094) and DCF-$^{13}C_6$ (black peak, 8.61 min, m/z 300.0295) in ultrapure water at 100 µg/L. y-axis: relative count numbers to the highest peak.

Table S5.2 – Linearity data of 6 replicates of calibration curves.

Replicate	Slope	Intercept	Regression coefficient (R^2)
1	0.001024	0.01512	0.9982
2	0.001187	0.00983	0.9997
3	0.001063	0.01275	0.9998
4	0.001171	0.01060	0.9999
5	0.001241	0.00868	0.9986
6	0.001198	0.00990	0.9987

Table S5.3 – Matrix effect in blank degraded samples at different time points (t) of degradation (mean ± relative standard deviation; n= 3).

Blank degraded samples with Na_2SO_4	
Target concentration (µg/mL)	**Matrix Effect (%)**
t = 0 min	
10	108.4 ± 2.2
100	98.2 ± 0.8
1000	101.8 ± 0.4
t = 30 min	
10	106.5 ± 2.4
100	98.0 ± 1.6
1000	103.8 ± 0.7
t = 45 min	
10	102.8 ± 1.7
100	97.2 ± 0.7
1000	102.6 ± 0.3
t = 120 min	
10	107.7 ± 2.0
100	103.7 ± 0.7
1000	98.1 ± 0.3
t = 300 min	
10	108.7 ± 1.6
100	97.1 ± 1.4
1000	104.6 ± 0.6

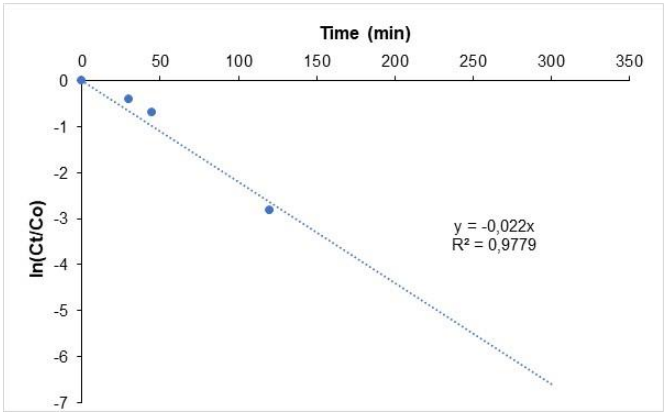

Figure S5.2 – Degradation kinetics of DCF.

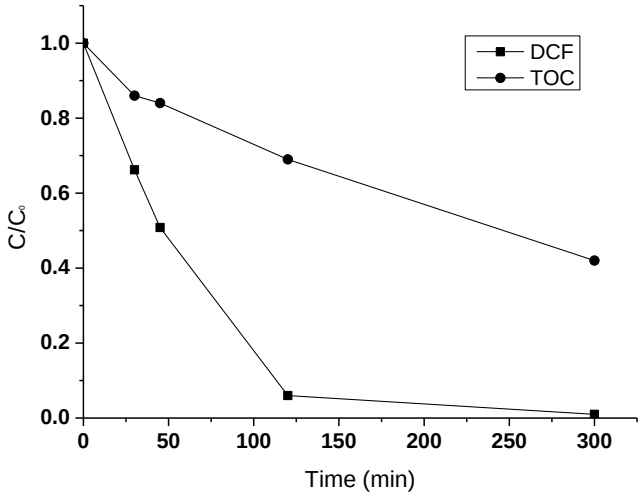

Figure S5.3 – TOC and DCF removal. Experimental conditions: $[DCF]_0$= 50 mg/L, $[Na_2SO_4]$= 0.05 M, j= 21.8 mA/cm^2.

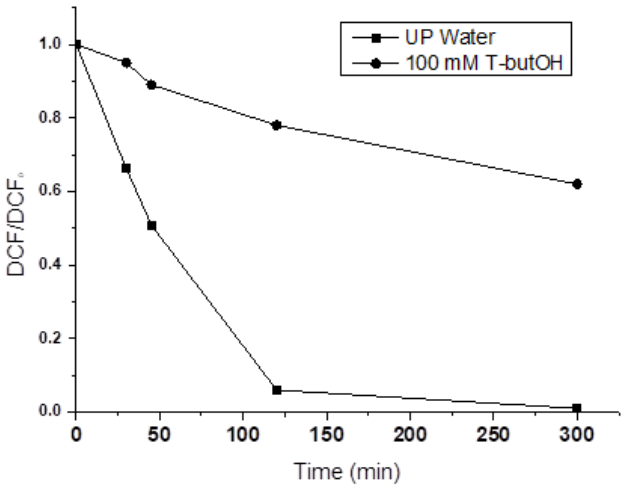

Figure S5.4 – Effect of radicals scavengers. Experimental conditions: $[DCF]_0$= 50 mg/L, $[Na_2SO_4]$= 0.05 M, [t-butOH]= 100mM, j= 21.8 mA/cm^2.

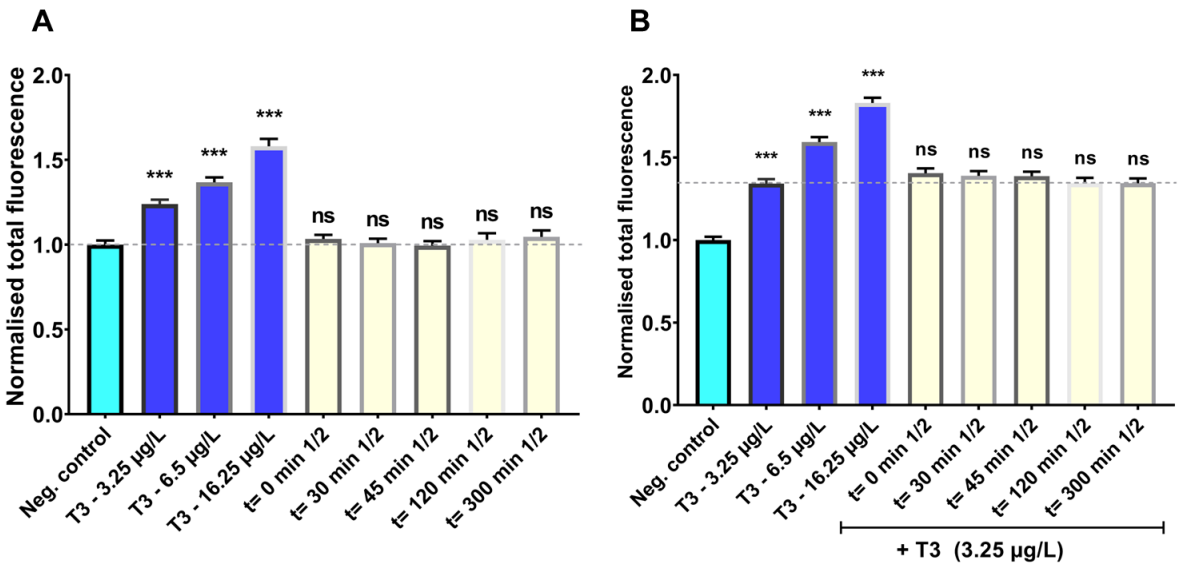

Figure S5.5 – Fluorescence of tadpoles exposed to negative control, T3 at concentrations ranging between 3.25 - 16.25 µg/L, non-electrolyzed (t= 0 min) and blank degraded samples obtained at t= 30, t= 45, t= 120 and t= 300 min. **(A)** Non-electrolyzed and blank degraded samples were diluted two-fold with Evian water. **(B)** Non-electrolyzed and blank degraded samples were diluted two-fold with Evian water and spiked with T3 at 3.25 µg/L. Data shown are the mean of three independent experiments performed on different batches of eleutheroembryos (n= 20 for each experiment). Error bars represent the standard error of the mean. Statistical analysis with Kruskal-Wallis and Dunn's multicomparison test (negative control vs T3 3.25 – 16.25 µg/L, negative control vs non-spiked initial and blank degraded samples, negative control vs spiked initial and blank degraded samples), ns: non-significant ***p < 0.001.

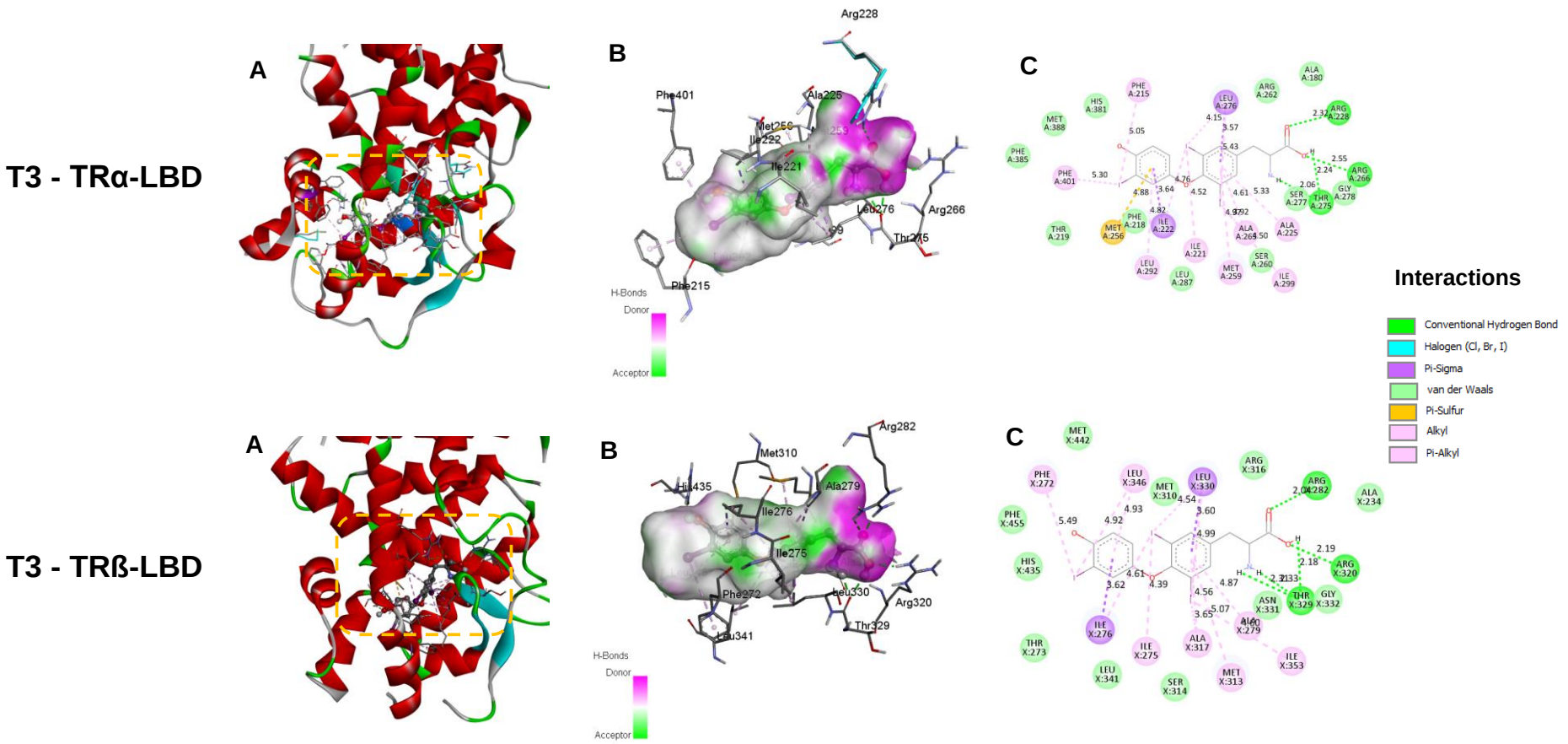

Figure S5.6 – Simulation of T3 binding to TRα and TRβ LBDs using molecular docking analysis. **(A)** 3D visualization of TR with the LBD highlighted in the orange box. **(B)** Representation of TR active site amino acid residues and ligand interactions with a hydrogen bond contour map. Purple and green indicate hydrogen bond donor and acceptor sites, respectively. **(C)** 2D diagrams illustrating the binding modes to the LBD in the most favorable conformation, with interaction distances shown in ångström.

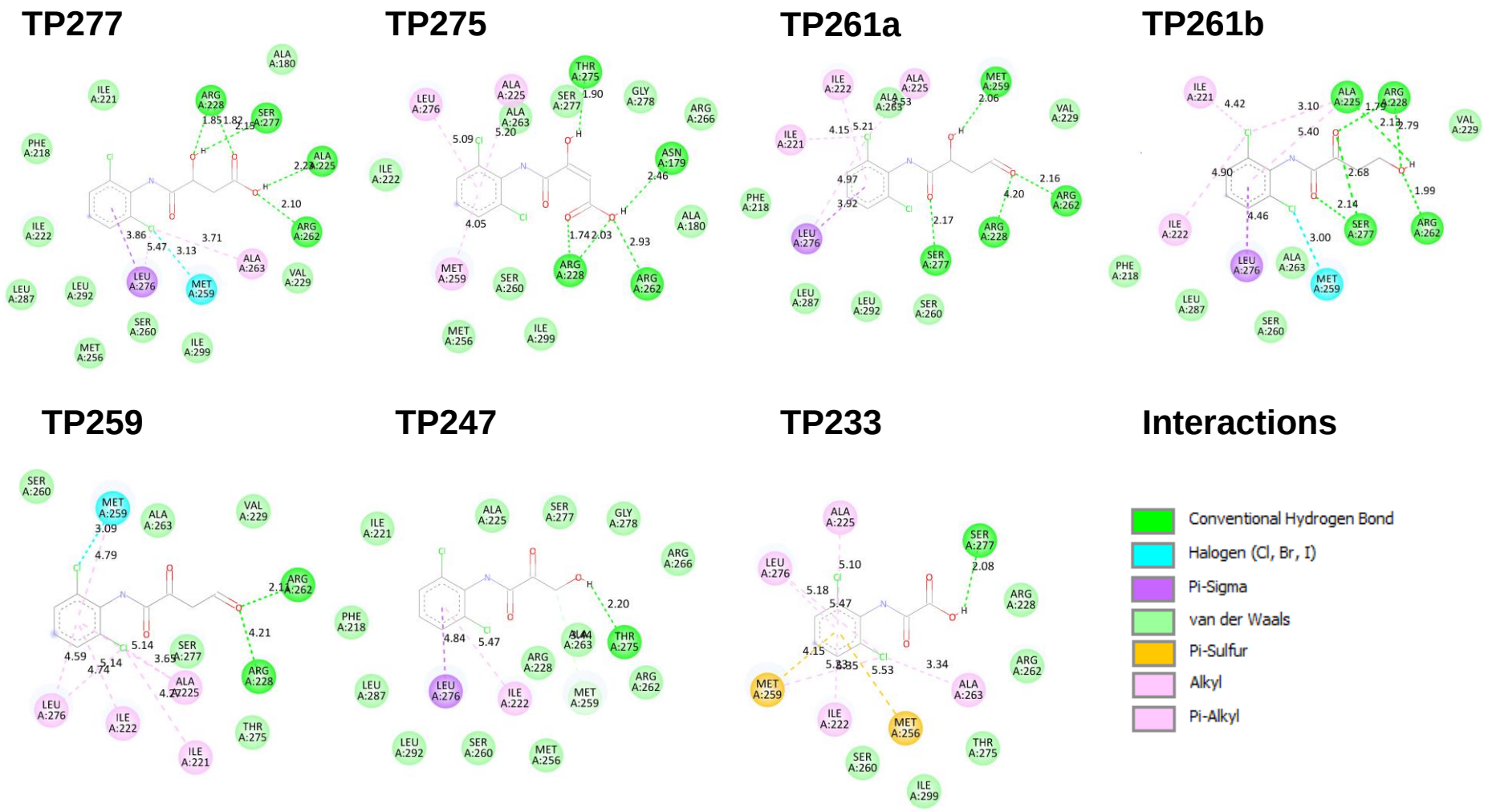

Figure S5.7 – 2D diagram illustrating the binding modes of the chosen TPs to the TRα-LBD at the most favorable conformation as simulated by molecular docking. Interaction distances are presented in ångström.

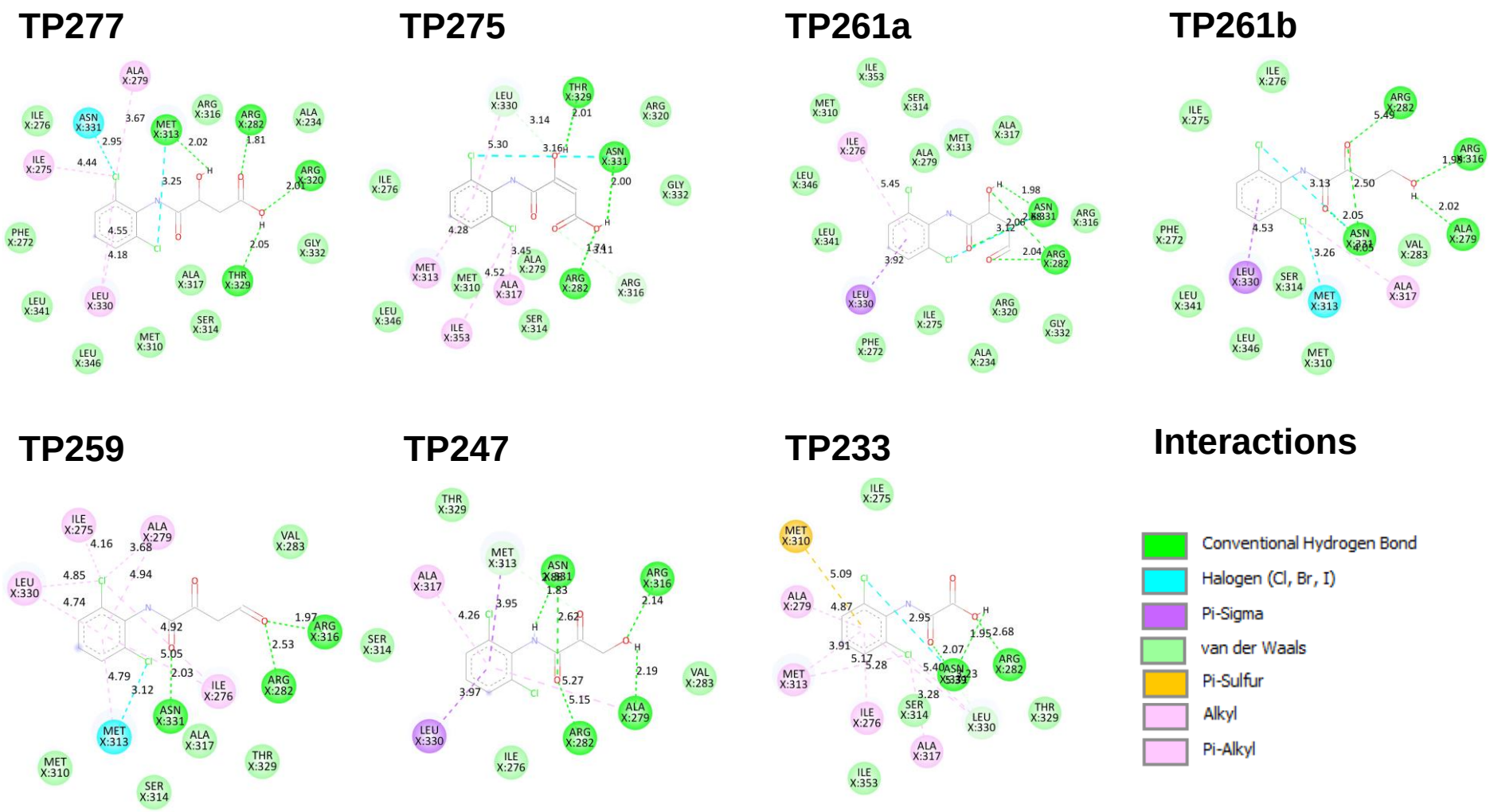

Figure S5.8 – 2D diagram illustrating the binding modes of the chosen TPs to the TRß-LBD at the most favorable conformation as simulated by molecular docking. Interaction distances are presented in angstrom.

References



[1] H. Oy, West Anatolian mining in early bronze age (3000-2000 BC), Journal of Ancient History and Archaeology 4 (2017). https://doi.org/10.14795/j.v4i2.219.

[2] K. Hess, A. Hauptmann, H. Wright, R. Whallon, Evidence of fourth millennium BC silver production at Fatmalı-Kalecik, East Anatolia, Metallurgica Antiqua 8 (1998) 112–122.

[3] S.W. Merkel, Evidence for the widespread use of dry silver ore in the Early Islamic period and its implications for the history of silver metallurgy, J Archaeol Sci 135 (2021) 105478. https://doi.org/https://doi.org/10.1016/j.jas.2021.105478.

[4] Y. Erel, R. Pinhasi, A. Coppa, A. Ticher, O. Tirosh, L. Carmel, Lead in Archeological Human Bones Reflecting Historical Changes in Lead Production, Environ Sci Technol 55 (2021) 14407–14413. https://doi.org/10.1021/acs.est.1c00614.

[5] EPA, Contaminants of Emerging Concern including Pharmaceuticals and Personal Care Products, United States Environmental Protection Agency (2015).

[6] W. Selmi, S. Selmi, J. Teller, C. Weber, E. Rivière, D.J. Nowak, Prioritizing the provision of urban ecosystem services in deprived areas, a question of environmental justice, Ambio 50 (2021) 1035–1046. https://doi.org/10.1007/s13280-020-01438-1.

[7] N. Morin-Crini, E. Lichtfouse, G. Liu, V. Balaram, A.R.L. Ribeiro, Z. Lu, F. Stock, E. Carmona, M.R. Teixeira, L.A. Picos-Corrales, J.C. Moreno-Piraján, L. Giraldo, C. Li, A. Pandey, D. Hocquet, G. Torri, G. Crini, Worldwide cases of water pollution by emerging contaminants: a review, Environ Chem Lett 20 (2022) 2311–2338. https://doi.org/10.1007/s10311-022-01447-4.

[8] Y. Luo, W. Guo, H.H. Ngo, L.D. Nghiem, F.I. Hai, J. Zhang, S. Liang, X.C. Wang, A review on the occurrence of micropollutants in the aquatic environment and their fate and removal during wastewater treatment, Sci. Total Environ. 473–474 (2014) 619–641. https://doi.org/10.1016/j.scitotenv.2013.12.065.

[9] A. Müller, H. Österlund, J. Marsalek, M. Viklander, The pollution conveyed by urban runoff: A review of sources, Science of the Total Environment 709 (2020) 136125. https://doi.org/10.1016/j.scitotenv.2019.136125.

[10] A. Majumder, B. Gupta, A.K. Gupta, Pharmaceutically active compounds in aqueous environment: A status, toxicity and insights of remediation, Environ Res 176 (2019) 108542. https://doi.org/10.1016/j.envres.2019.108542.

[11] H. Wang, H. Xi, L. Xu, M. Jin, W. Zhao, H. Liu, Ecotoxicological effects, environmental fate and risks of pharmaceutical and personal care products in the water environment: A review, Science of The Total Environment 788 (2021) 147819. https://doi.org/https://doi.org/10.1016/j.scitotenv.2021.147819.

[12] M. la Farré, S. Pérez, L. Kantiani, D. Barceló, Fate and toxicity of emerging pollutants, their metabolites and transformation products in the aquatic environment, TrAC - Trends in Analytical Chemistry 27 (2008) 991–1007. https://doi.org/10.1016/j.trac.2008.09.010.

[13] U.S. McKnight, J.J. Rasmussen, B. Kronvang, P.J. Binning, P.L. Bjerg, Sources, occurrence and predicted aquatic impact of legacy and contemporary pesticides in streams, Environmental Pollution 200 (2015) 64–76. https://doi.org/10.1016/j.envpol.2015.02.015.

[14] V.M. Pathak, V.K. Verma, B.S. Rawat, B. Kaur, N. Babu, A. Sharma, S. Dewali, M. Yadav, R. Kumari, S. Singh, A. Mohapatra, V. Pandey, N. Rana, J.M. Cunill, Current status of pesticide effects on environment, human health and it's eco-friendly management as bioremediation: A comprehensive review, Front Microbiol 13 (2022) 962619. https://doi.org/10.3389/fmicb.2022.962619.

References

[15] N. Narwal, D. Katyal, N. Kataria, P.K. Rose, S.G. Warkar, A. Pugazhendhi, S. Ghotekar, K.S. Khoo, Emerging micropollutants in aquatic ecosystems and nanotechnology-based removal alternatives: A review, Chemosphere 341 (2023) 139945. https://doi.org/10.1016/j.chemosphere.2023.139945.

[16] M. Dubey, S. Mohapatra, V.K. Tyagi, S. Suthar, A.A. Kazmi, Occurrence, fate, and persistence of emerging micropollutants in sewage sludge treatment, Environmental Pollution 273 (2021) 116515. https://doi.org/10.1016/j.envpol.2021.116515.

[17] D. Hering, A. Borja, J. Carstensen, L. Carvalho, M. Elliott, C.K. Feld, A.S. Heiskanen, R.K. Johnson, J. Moe, D. Pont, A.L. Solheim, W. van de Bund, The European Water Framework Directive at the age of 10: A critical review of the achievements with recommendations for the future, Science of the Total Environment 408 (2010) 4007–4019. https://doi.org/10.1016/j.scitotenv.2010.05.031.

[18] G. Crini, E. Lichtfouse, Advantages and disadvantages of techniques used for wastewater treatment, Environ Chem Lett 17 (2019) 145–155. https://doi.org/10.1007/s10311-018-0785-9.

[19] EU, Directive 2013/39/EU of the European Parliament and of the Council of 12 August 2013 amending Directives 2000/60/ECand 2008/105/EC as regards priority substances in the field of water policy, Official Journal of the European Union 226 (2013).

[20] E. Simon, A. Duffek, C. Stahl, M. Frey, M. Scheurer, J. Tuerk, L. Gehrmann, S. Könemann, K. Swart, P. Behnisch, D. Olbrich, F. Brion, S. Aït-Aïssa, R. Pasanen-Kase, I. Werner, E.L.M. Vermeirssen, Biological effect and chemical monitoring of Watch List substances in European surface waters: Steroidal estrogens and diclofenac – Effect-based methods for monitoring frameworks, Environ Int 159 (2022) 107033. https://doi.org/10.1016/j.envint.2021.107033.

[21] COMMISSION IMPLEMENTING DECISION (EU) 2022/1307 of 22 July 2022 establishing a watch list of substances for Union-wide monitoring in the field of water policy pursuant to Directive 2008/105/EC of the European Parliament and of the Council, Official Journal of the European Union 197 (2022) 117–120.

[22] S.F. Ahmed, M. Mofijur, S. Nuzhat, A.T. Chowdhury, N. Rafa, M.A. Uddin, A. Inayat, T.M.I. Mahlia, H.C. Ong, W.Y. Chia, P.L. Show, Recent developments in physical, biological, chemical, and hybrid treatment techniques for removing emerging contaminants from wastewater, J Hazard Mater 416 (2021) 125912. https://doi.org/10.1016/j.jhazmat.2021.125912.

[23] I. Lozano, C.J. Pérez-Guzmán, A. Mora, J. Mahlknecht, C.L. Aguilar, P. Cervantes-Avilés, Pharmaceuticals and personal care products in water streams: Occurrence, detection, and removal by electrochemical advanced oxidation processes, Science of the Total Environment 827 (2022) 154348. https://doi.org/10.1016/j.scitotenv.2022.154348.

[24] A. Jelic, M. Gros, A. Ginebreda, R. Cespedes-Sánchez, F. Ventura, M. Petrovic, D. Barcelo, Occurrence, partition and removal of pharmaceuticals in sewage water and sludge during wastewater treatment, Water Res 45 (2011) 1165–1176. https://doi.org/10.1016/j.watres.2010.11.010.

[25] C. Burzio, J. Ekholm, O. Modin, P. Falås, O. Svahn, F. Persson, T. van Erp, D.J.I. Gustavsson, B.M. Wilén, Removal of organic micropollutants from municipal wastewater by aerobic granular sludge and conventional activated sludge, J Hazard Mater 438 (2022) 129528. https://doi.org/10.1016/j.jhazmat.2022.129528.

[26] L. Rizzo, C. Manaia, C. Merlin, T. Schwartz, C. Dagot, M.C. Ploy, I. Michael, D. Fatta-Kassinos, Urban wastewater treatment plants as hotspots for antibiotic resistant bacteria and genes spread into the environment: A review, Science of the Total Environment 447 (2013) 345–360. https://doi.org/10.1016/j.scitotenv.2013.01.032.

[27] L. Paredes, F. Omil, J.M. Lema, M. Carballa, What happens with organic micropollutants during UV disinfection in WWTPs? A global perspective from laboratory to full-scale, J Hazard Mater 342 (2018) 670–678. https://doi.org/10.1016/j.jhazmat.2017.08.075.

[28] Y. Lee, D. Gerrity, M. Lee, S. Gamage, A. Pisarenko, R.A. Trenholm, S. Canonica, S.A. Snyder, U. Von Gunten, Organic Contaminant Abatement in Reclaimed Water by UV/H2O2 and a Combined Process Consisting of O3/H2O2 Followed by UV/H2O2: Prediction of Abatement Efficiency, Energy Consumption, and Byproduct Formation, Environ Sci Technol 50 (2016) 3809–3819. https://doi.org/10.1021/acs.est.5b04904.

[29] C. Comninellis, A. Kapalka, S. Malato, S.A. Parsons, I. Poulios, D. Mantzavinos, Advanced oxidation processes for water treatment: Advances and trends for R&D, Journal of Chemical Technology and Biotechnology 83 (2008) 769–776. https://doi.org/10.1002/jctb.1873.

[30] R. Dewil, D. Mantzavinos, I. Poulios, M.A. Rodrigo, New perspectives for Advanced Oxidation Processes, J Environ Manage 195 (2017) 93–99. https://doi.org/10.1016/j.jenvman.2017.04.010.

[31] D.B. Miklos, C. Remy, M. Jekel, K.G. Linden, J.E. Drewes, U. Hübner, Evaluation of advanced oxidation processes for water and wastewater treatment – A critical review, Water Res 139 (2018) 118–131. https://doi.org/https://doi.org/10.1016/j.watres.2018.03.042.

[32] K. Dhangar, M. Kumar, Tricks and tracks in removal of emerging contaminants from the wastewater through hybrid treatment systems: A review, Science of the Total Environment 738 (2020) 140320. https://doi.org/10.1016/j.scitotenv.2020.140320.

[33] D. Kanakaraju, B.D. Glass, M. Oelgemöller, Advanced oxidation process-mediated removal of pharmaceuticals from water: A review, J Environ Manage 219 (2018) 189–207. https://doi.org/10.1016/j.jenvman.2018.04.103.

[34] S. Feijoo, X. Yu, M. Kamali, L. Appels, R. Dewil, Generation of oxidative radicals by advanced oxidation processes (AOPs) in wastewater treatment: a mechanistic, environmental and economic review, Rev Environ Sci Biotechnol 22 (2023) 205–248. https://doi.org/10.1007/s11157-023-09645-4.

[35] J.A. Khan, M. Sayed, S. Khan, N.S. Shah, D.D. Dionysiou, G. Boczkaj, Advanced oxidation processes for the treatment of contaminants of emerging concern, in: Contaminants of Emerging Concern in Water and Wastewater: Advanced Treatment Processes, 2020: pp. 299–365. https://doi.org/10.1016/B978-0-12-813561-7.00009-2.

[36] F.C. Moreira, R.A.R. Boaventura, E. Brillas, V.J.P. Vilar, Electrochemical advanced oxidation processes: A review on their application to synthetic and real wastewaters, Appl Catal B 202 (2017) 217–261. https://doi.org/10.1016/j.apcatb.2016.08.037.

[37] I. Sirés, E. Brillas, M.A. Oturan, M.A. Rodrigo, M. Panizza, Electrochemical advanced oxidation processes: Today and tomorrow. A review, Environmental Science and Pollution Research 21 (2014) 8336–8367. https://doi.org/10.1007/s11356-014-2783-1.

[38] L. Feng, E.D. van Hullebusch, M.A. Rodrigo, G. Esposito, M.A. Oturan, Removal of residual anti-inflammatory and analgesic pharmaceuticals from aqueous systems by electrochemical advanced oxidation processes. A review, Chem Eng J 228 (2013) 944–964. https://doi.org/10.1016/j.cej.2013.05.061.

[39] M. Panizza, G. Cerisola, Direct and mediated anodic oxidation of organic pollutants, Chem Rev 109 (2009) 6541–6569. https://doi.org/10.1021/cr9001319.

[40] H. Qiu, P. Fan, X. Li, G. Hou, Electrochemical degradation of DCF by boron-doped diamond anode: Degradation mechanism, pathways and influencing factors, Water Sci Technol 84 (2021) 431–444. https://doi.org/10.2166/wst.2021.231.

[41] S.O. Ganiyu, C.A. Martínez-Huitle, Nature, Mechanisms and Reactivity of Electrogenerated Reactive Species at Thin-Film Boron-Doped Diamond (BDD) Electrodes During Electrochemical Wastewater Treatment, ChemElectroChem 6 (2019) 2379–2392. https://doi.org/10.1002/celc.201900159.

[42] C.A. Martínez-Huitle, S. Ferro, Electrochemical oxidation of organic pollutants for the wastewater treatment: Direct and indirect processes, Chem Soc Rev 35 (2006) 1324–1340. https://doi.org/10.1039/b517632h.

[43] Y. Einaga, Boron-Doped Diamond Electrodes: Fundamentals for Electrochemical Applications, Acc Chem Res 55 (2022) 3605–3615. https://doi.org/10.1021/acs.accounts.2c00597.

[44] A. Kapałka, G. Fóti, C. Comninellis, The importance of electrode material in environmental electrochemistry. Formation and reactivity of free hydroxyl radicals on boron-doped diamond electrodes, Electrochim Acta 54 (2009) 2018–2023. https://doi.org/10.1016/j.electacta.2008.06.045.

[45] A. V. Karim, P.V. Nidheesh, M.A. Oturan, Boron-doped diamond electrodes for the mineralization of organic pollutants in the real wastewater, Curr Opin Electrochem 30 (2021) 100855. https://doi.org/10.1016/j.coelec.2021.100855.

[46] G. Divyapriya, P. V. Nidheesh, Electrochemically generated sulfate radicals by boron doped diamond and its environmental applications, Curr Opin Solid State Mater Sci 25 (2021) 100921. https://doi.org/https://doi.org/10.1016/j.cossms.2021.100921.

[47] J. Maculewicz, D. Kowalska, K. Świacka, M. Toński, P. Stepnowski, A. Białk-Bielińska, J. Dołżonek, Transformation products of pharmaceuticals in the environment: Their fate, (eco)toxicity and bioaccumulation potential, Science of the Total Environment 802 (2022). https://doi.org/10.1016/j.scitotenv.2021.149916.

[48] D. Zahn, P. Mucha, V. Zilles, A. Touffet, H. Gallard, T.P. Knepper, T. Frömel, Identification of potentially mobile and persistent transformation products of REACH-registered chemicals and their occurrence in surface waters, Water Res 150 (2019) 89–96. https://doi.org/10.1016/j.watres.2018.11.042.

[49] B.I. Escher, K. Fenner, Recent Advances in Environmental Risk Assessment of Transformation Products, Environ Sci Technol 45 (2011) 3835–3847. https://doi.org/10.1021/es1030799.

[50] D. Zahn, H.P.H. Arp, K. Fenner, A. Georgi, J. Hafner, S.E. Hale, J. Hollender, T. Letzel, E.L. Schymanski, G. Sigmund, T. Reemtsma, Should Transformation Products Change the Way We Manage Chemicals?, Environ Sci Technol 58 (2024) 7710–7718. https://doi.org/10.1021/acs.est.4c00125.

[51] C.J. Sinclair, A.B.A. Boxall, Assessing the ecotoxicity of pesticide transformation products, Environ Sci Technol 37 (2003) 4617–4625. https://doi.org/10.1021/es030038m.

[52] A.P. Toolaram, K. Kümmerer, M. Schneider, Environmental risk assessment of anti-cancer drugs and their transformation products: A focus on their genotoxicity characterization-state of knowledge and short comings, Mutat Res Rev Mutat Res 760 (2014) 18–35. https://doi.org/10.1016/j.mrrev.2014.02.001.

[53] J.C. Amiard, C. Amiard-Triquet, Conventional Risk Assessment of Environmental Contaminants, in: Aquatic Ecotoxicology: Advancing Tools for Dealing with Emerging Risks, 2015: pp. 25–49. https://doi.org/10.1016/B978-0-12-800949-9.00002-4.

[54] EMEA, Guideline on the environmental risk assessment of medicinal products for human use, European Medicines Agency 44 (2006).

[55] E.S. Committee, Guidance to develop specific protection goals options for environmental risk assessment at EFSA, in relation to biodiversity and ecosystem services, EFSA Journal 14 (2016) e04499. https://doi.org/https://doi.org/10.2903/j.efsa.2016.4499.

[56] E. Lewis, REGULATION (EC) No 1907/2006 OF THE EUROPEAN PARLIAMENT AND OF THE COUNCIL, Official Journal of the European Union (2018).

[57] M. Wright-Walters, C. Volz, E. Talbott, D. Davis, An updated weight of evidence approach to the aquatic hazard assessment of Bisphenol A and the derivation a new predicted no effect concentration (Pnec) using a non-parametric methodology, Science of the Total Environment 409 (2011) 676–685. https://doi.org/10.1016/j.scitotenv.2010.07.092.

[58] P.M. Chapman, J.R. Elphick, Critical predicted no effect concentrations (PNECs) should not be based on a single toxicity test, Environ Toxicol Chem 34 (2015) 1088–1090. https://doi.org/10.1002/etc.2897.

[59] B.I. Escher, N. Bramaz, J.F. Mueller, P. Quayle, S. Rutishauser, E.L.M. Vermeirssen, Toxic equivalent concentrations (TEQs) for baseline toxicity and specific modes of action as a tool to improve interpretation of ecotoxicity testing of environmental samples, Journal of Environmental Monitoring 10 (2008) 612–621. https://doi.org/10.1039/b800949j.

[60] S. Zhou, S. Peng, W. Brack, J.A. Doering, T.B. Seiler, H. Hollert, Bioanalytical equivalents and relative potencies for predicting the biological effects of mixtures, Science of the Total Environment 763 (2021) 143030. https://doi.org/10.1016/j.scitotenv.2020.143030.

[61] W. Brack, S. Ait-Aissa, R.M. Burgess, W. Busch, N. Creusot, C. Di Paolo, B.I. Escher, L. Mark Hewitt, K. Hilscherova, J. Hollender, H. Hollert, W. Jonker, J. Kool, M. Lamoree, M. Muschket, S. Neumann, P. Rostkowski, C. Ruttkies, J. Schollee, E.L. Schymanski, T. Schulze, T.B. Seiler, A.J. Tindall, G. De Aragão Umbuzeiro, B. Vrana, M. Krauss, Effect-directed analysis supporting monitoring of aquatic environments - an in-depth overview, Science of the Total Environment 544 (2016) 1073–1118. https://doi.org/10.1016/j.scitotenv.2015.11.102.

[62] P. Välitalo, N. Perkola, T.B. Seiler, M. Sillanpää, J. Kuckelkorn, A. Mikola, H. Hollert, E. Schultz, Estrogenic activity in Finnish municipal wastewater effluents, Water Res 88 (2016) 740–749. https://doi.org/10.1016/j.watres.2015.10.056.

[63] R. Reis, R. Dhawle, D. Du Pasquier, A.J. Tindall, Z. Frontistis, D. Mantzavinos, P. de Witte, D. Cabooter, Electrochemical degradation of 17α-ethinylestradiol: Transformation products, degradation pathways and in vivo assessment of estrogenic activity, Environ Int 176 (2023) 107992. https://doi.org/https://doi.org/10.1016/j.envint.2023.107992.

[64] B. Jarošová, L. Bláha, J.P. Giesy, K. Hilscherová, What level of estrogenic activity determined by in vitro assays in municipal waste waters can be considered as safe?, Environ Int 64 (2014) 98–109. https://doi.org/10.1016/j.envint.2013.12.009.

[65] F.D.L. Leusch, P.A. Neale, A. Hebert, M. Scheurer, M.C.M. Schriks, Analysis of the sensitivity of in vitro bioassays for androgenic, progestagenic, glucocorticoid, thyroid and estrogenic activity: Suitability for drinking and environmental waters, Environ Int 99 (2017) 120–130. https://doi.org/10.1016/j.envint.2016.12.014.

[66] L.M. Schuijt, F.-J. Peng, S.J.P. van den Berg, M.M.L. Dingemans, P.J. Van den Brink, (Eco)toxicological tests for assessing impacts of chemical stress to aquatic ecosystems: Facts, challenges, and future, Science of The Total Environment 795 (2021) 148776. https://doi.org/https://doi.org/10.1016/j.scitotenv.2021.148776.

[67] C.A. Mitchell, N. Burden, M. Bonnell, M. Hecker, T.H. Hutchinson, M. Jagla, C.A. LaLone, L. Lagadic, S.G. Lynn, B. Shore, Y. Song, S.M. Vliet, J.R. Wheeler, M.R. Embry, New Approach

Methodologies for the Endocrine Activity Toolbox: Environmental Assessment for Fish and Amphibians, Environ Toxicol Chem (2023) 757–777. https://doi.org/10.1002/etc.5584.

[68] L. Bajard, O. Adamovsky, K. Audouze, K. Baken, R. Barouki, J.B. Beltman, A. Beronius, E.C. Bonefeld-Jørgensen, G. Cano-Sancho, M.L. de Baat, F. Di Tillio, M.F. Fernández, R.E. FitzGerald, C. Gundacker, A.F. Hernández, K. Hilscherova, S. Karakitsios, E. Kuchovska, M. Long, M. Luijten, S. Majid, P. Marx-Stoelting, V. Mustieles, C.K. Negi, D. Sarigiannis, S. Scholz, I. Sovadinova, R. Stierum, S. Tanabe, K.E. Tollefsen, A.D. van den Brand, C. Vogs, M. Wielsøe, C. Wittwehr, L. Blaha, Application of AOPs to assist regulatory assessment of chemical risks – Case studies, needs and recommendations, Environ Res 217 (2023) 114650. https://doi.org/10.1016/j.envres.2022.114650.

[69] J. Tannenbaum, B.T. Bennett, Russell and Burch's 3Rs then and now: The need for clarity in definition and purpose, Journal of the American Association for Laboratory Animal Science 54 (2015) 120–132.

[70] OECD, Guidance document on the validation and international acceptance of new or updated test methods for hazard assessment, in: Series on Testing and Assessment, 2005.

[71] K.A. Magurany, X. Chang, R. Clewell, S. Coecke, E. Haugabrooks, S. Marty, A pragmatic framework for the application of new approach methodologies in one health toxicological risk assessment, Toxicological Sciences 192 (2023) 155–177. https://doi.org/10.1093/toxsci/kfad012.

[72] I. Cattaneo, M.C. Astuto, M. Binaglia, Y. Devos, J.L.C.M. Dorne, A. Fernandez Agudo, A. Fernandez Dumont, P. Garcia-Vello, G.E.N. Kass, A. Lanzoni, A.K.D. Liem, M. Panzarea, K. Paraskevopulos, J.M. Parra Morte, J. V. Tarazona, A. Terron, Implementing New Approach Methodologies (NAMs) in food safety assessments: Strategic objectives and actions taken by the European Food Safety Authority, Trends Food Sci Technol 133 (2023) 277–290. https://doi.org/10.1016/j.tifs.2023.02.006.

[73] P. Pastorino, M. Prearo, D. Barceló, Ethical principles and scientific advancements: In vitro, in silico, and non-vertebrate animal approaches for a green ecotoxicology, Green Analytical Chemistry 8 (2024) 100096. https://doi.org/https://doi.org/10.1016/j.greeac.2024.100096.

[74] M. Schneider, J.L. Pons, G. Labesse, W. Bourguet, In silico predictions of endocrine disruptors properties, Endocrinology (United States) 160 (2019) 2709–2716. https://doi.org/10.1210/en.2019-00382.

[75] M. Voigt, M. Jaeger, In silico and in vivo ecotoxicity—QSAR-based predictions and experimental assays for the aquatic environment, in: QSAR in Safety Evaluation and Risk Assessment, 2023: pp. 495–509. https://doi.org/10.1016/B978-0-443-15339-6.00018-7.

[76] J. Wang, S. Wang, Toxicity changes of wastewater during various advanced oxidation processes treatment: An overview, J Clean Prod 315 (2021) 128202. https://doi.org/10.1016/j.jclepro.2021.128202.

[77] G. Patlewicz, N. Jeliazkova, R.J. Safford, A.P. Worth, B. Aleksiev, An evaluation of the implementation of the Cramer classification scheme in the Toxtree software, SAR QSAR Environ Res 19 (2008) 495–524. https://doi.org/10.1080/10629360802083871.

[78] G. Piir, I. Kahn, A.T. García-Sosa, S. Sild, P. Ahte, U. Maran, Best practices for QSAR model reporting: Physical and chemical properties, ecotoxicity, environmental fate, human health, and toxicokinetics endpoints, Environ Health Perspect 126 (2018) 126001. https://doi.org/10.1289/EHP3264.

[79] S.J. Belfield, J.W. Firman, S.J. Enoch, J.C. Madden, K. Erik Tollefsen, M.T.D. Cronin, A review of quantitative structure-activity relationship modelling approaches to predict the toxicity of mixtures, Computational Toxicology 25 (2023) 100251. https://doi.org/10.1016/j.comtox.2022.100251.

[80] S.D. Walker, S. McEldowney, Molecular docking: A potential tool to aid ecotoxicity testing in environmental risk assessment of pharmaceuticals, Chemosphere 93 (2013) 2568–2577. https://doi.org/10.1016/j.chemosphere.2013.09.074.

[81] X.-Y. Meng, H.-X. Zhang, M. Mezei, M. Cui, Molecular Docking: A Powerful Approach for Structure-Based Drug Discovery, Current Computer Aided-Drug Design 7 (2012) 146–157. https://doi.org/10.2174/157340911795677602.

[82] M. Kenda, M.S. Dolenc, Computational study of drugs targeting nuclear receptors, Molecules 25 (2020). https://doi.org/10.3390/molecules25071616.

[83] M.E. McArdle, E.L. Freeman, J.P. Staveley, L.S. Ortego, K.K. Coady, L. Weltje, A. Weyers, J.R. Wheeler, A.J. Bone, Critical Review of Read-Across Potential in Testing for Endocrine-Related Effects in Vertebrate Ecological Receptors, Environ Toxicol Chem 39 (2020) 739–753. https://doi.org/10.1002/etc.4682.

[84] E. Yuriev, M. Agostino, P.A. Ramsland, Challenges and advances in computational docking: 2009 in review, Journal of Molecular Recognition 24 (2011) 149–164. https://doi.org/10.1002/jmr.1077.

[85] A. V. Sadybekov, V. Katritch, Computational approaches streamlining drug discovery, Nature 616 (2023) 673–685. https://doi.org/10.1038/s41586-023-05905-z.

[86] B. Escher, F. Leusch, Bioanalytical Tools in Water Quality Assessment, Water Intelligence Online 10 (2011). https://doi.org/10.2166/9781780400778.

[87] M. Abbas, M. Adil, S. Ehtisham-ul-Haque, B. Munir, M. Yameen, A. Ghaffar, G.A. Shar, M. Asif Tahir, M. Iqbal, Vibrio fischeri bioluminescence inhibition assay for ecotoxicity assessment: A review, Science of the Total Environment 626 (2018) 1295–1309. https://doi.org/10.1016/j.scitotenv.2018.01.066.

[88] S. Parvez, C. Venkataraman, S. Mukherji, A review on advantages of implementing luminescence inhibition test (Vibrio fischeri) for acute toxicity prediction of chemicals, Environ Int 32 (2006) 265–268. https://doi.org/10.1016/j.envint.2005.08.022.

[89] A.K. Jain, D. Singh, K. Dubey, R. Maurya, S. Mittal, A.K. Pandey, Models and Methods for In Vitro Toxicity, in: In Vitro Toxicol, 2018: pp. 45–65. https://doi.org/10.1016/B978-0-12-804667-8.00003-1.

[90] E. Madorran, A. Stožer, S. Bevc, U. Maver, In vitro toxicity model: Upgrades to bridge the gap between preclinical and clinical research, Bosn J Basic Med Sci 20 (2020) 157–168. https://doi.org/10.17305/bjbms.2019.4378.

[91] S.J. Sturla, A.R. Boobis, R.E. Fitzgerald, J. Hoeng, R.J. Kavlock, K. Schirmer, M. Whelan, M.F. Wilks, M.C. Peitsch, Systems toxicology: From basic research to risk assessment, Chem Res Toxicol 27 (2014) 314–329. https://doi.org/10.1021/tx400410s.

[92] European Parliament Council of the European Union, Directive 2010/63/EU of the European Parliament and of the Council of 22 September 2010 on the protection of animals used for scientific purposes Text with EEA relevance, Official Journal of the European Union 53 (2010).

[93] K. Howe, M.D. Clark, C.F. Torroja, J. Torrance, C. Berthelot, M. Muffato, J.E. Collins, S. Humphray, K. McLaren, L. Matthews, S. McLaren, I. Sealy, M. Caccamo, C. Churcher, C. Scott, J.C. Barrett, R. Koch, G.J. Rauch, S. White, W. Chow, B. Kilian, L.T. Quintais, J.A. Guerra-

Assunção, Y. Zhou, Y. Gu, J. Yen, J.H. Vogel, T. Eyre, S. Redmond, R. Banerjee, J. Chi, B. Fu, E. Langley, S.F. Maguire, G.K. Laird, D. Lloyd, E. Kenyon, S. Donaldson, H. Sehra, J. Almeida-King, J. Loveland, S. Trevanion, M. Jones, M. Quail, D. Willey, A. Hunt, J. Burton, S. Sims, K. McLay, B. Plumb, J. Davis, C. Clee, K. Oliver, R. Clark, C. Riddle, D. Eliott, G. Threadgold, G. Harden, D. Ware, B. Mortimer, G. Kerry, P. Heath, B. Phillimore, A. Tracey, N. Corby, M. Dunn, C. Johnson, J. Wood, S. Clark, S. Pelan, G. Griffiths, M. Smith, R. Glithero, P. Howden, N. Barker, C. Stevens, J. Harley, K. Holt, G. Panagiotidis, J. Lovell, H. Beasley, C. Henderson, D. Gordon, K. Auger, D. Wright, J. Collins, C. Raisen, L. Dyer, K. Leung, L. Robertson, K. Ambridge, D. Leongamornlert, S. McGuire, R. Gilderthorp, C. Griffiths, D. Manthravadi, S. Nichol, G. Barker, S. Whitehead, M. Kay, J. Brown, C. Murnane, E. Gray, M. Humphries, N. Sycamore, D. Barker, D. Saunders, J. Wallis, A. Babbage, S. Hammond, M. Mashreghi-Mohammadi, L. Barr, S. Martin, P. Wray, A. Ellington, N. Matthews, M. Ellwood, R. Woodmansey, G. Clark, J. Cooper, A. Tromans, D. Grafham, C. Skuce, R. Pandian, R. Andrews, E. Harrison, A. Kimberley, J. Garnett, N. Fosker, R. Hall, P. Garner, D. Kelly, C. Bird, S. Palmer, I. Gehring, A. Berger, C.M. Dooley, Z. Ersan-Ürün, C. Eser, H. Geiger, M. Geisler, L. Karotki, A. Kirn, J. Konantz, M. Konantz, M. Oberländer, S. Rudolph-Geiger, M. Teucke, K. Osoegawa, B. Zhu, A. Rapp, S. Widaa, C. Langford, F. Yang, N.P. Carter, J. Harrow, Z. Ning, J. Herrero, S.M.J. Searle, A. Enright, R. Geisler, R.H.A. Plasterk, C. Lee, M. Westerfield, P.J. De Jong, L.I. Zon, J.H. Postlethwait, C. Nüsslein-Volhard, T.J.P. Hubbard, H.R. Crollius, J. Rogers, D.L. Stemple, The zebrafish reference genome sequence and its relationship to the human genome, Nature 496 (2013) 498–503. https://doi.org/10.1038/nature12111.

[94] R. Silva Brito, A. Canedo, D. Farias, T.L. Rocha, Transgenic zebrafish (Danio rerio) as an emerging model system in ecotoxicology and toxicology: Historical review, recent advances, and trends, Science of the Total Environment 848 (2022) 157665. https://doi.org/10.1016/j.scitotenv.2022.157665.

[95] B. Bauer, A. Mally, D. Liedtke, Zebrafish embryos and larvae as alternative animal models for toxicity testing, Int J Mol Sci 22 (2021). https://doi.org/10.3390/ijms222413417.

[96] OECD, Test No. 236: Fish Embryo Acute Toxicity (FET) Test., OECD Guidelines for the Testing of Chemicals, Section 2, OECD Publishing (2013).

[97] D. Wlodkowic, M. Jansen, High-throughput screening paradigms in ecotoxicity testing: Emerging prospects and ongoing challenges, Chemosphere 307 (2022) 135929. https://doi.org/10.1016/j.chemosphere.2022.135929.

[98] S. Padilla, J. Cowden, D.E. Hinton, B. Yuen, S. Law, S.W. Kullman, R. Johnson, R.C. Hardman, K. Flynn, D.W.T. Au, Use of Medaka in toxicity testing, Curr Protoc Toxicol (2009) Chapter 1:Unit1.10. https://doi.org/10.1002/0471140856.tx0110s39.

[99] A.K. Dasmahapatra, C.B. Williams, A. Myla, S.K. Tiwary, Paul.B. Tchounwou, A systematic review of the evaluation of endocrine-disrupting chemicals in the Japanese medaka (Oryzias latipes) fish, Frontiers in Toxicology 5 (2023) 1272368. https://www.frontiersin.org/articles/10.3389/ftox.2023.1272368.

[100] O. Lee, J.M. Green, C.R. Tyler, Transgenic fish systems and their application in ecotoxicology, Crit Rev Toxicol 45 (2015) 124–141. https://doi.org/10.3109/10408444.2014.965805.

[101] J. Gao, W. Shen, Xenopus in revealing developmental toxicity and modeling human diseases, Environ Pollut 268 (2021) 115809. https://doi.org/10.1016/j.envpol.2020.115809.

[102] D.R. Buchholz, Xenopus metamorphosis as a model to study thyroid hormone receptor function during vertebrate developmental transitions, Mol Cell Endocrinol 459 (2017) 64–70. https://doi.org/10.1016/j.mce.2017.03.020.

[103] J. Robitaille, N.D. Denslow, B.I. Escher, H.G. Kurita-Oyamada, V. Marlatt, C.J. Martyniuk, L. Navarro-Martín, R. Prosser, T. Sanderson, V. Yargeau, V.S. Langlois, Towards regulation of Endocrine Disrupting chemicals (EDCs) in water resources using bioassays – A guide to developing a testing strategy, Environ Res 205 (2022) 112483. https://doi.org/10.1016/j.envres.2021.112483.

[104] D.J. Fort, S. Degitz, J. Tietge, L.W. Touart, The hypothalamic-pituitary-thyroid (HPT) axis in frogs and its role in frog development and reproduction, Crit Rev Toxicol 37 (2007) 117–161. https://doi.org/10.1080/10408440601123545.

[105] J.B. Fini, S. Le Mével, K. Palmier, V.M. Darras, I. Punzon, S.J. Richardson, M.S. Clerget-Froidevaux, B.A. Demeneix, Thyroid hormone signaling in the Xenopus laevis embryo is functional and susceptible to endocrine disruption, Endocrinology 153 (2012) 5068–5081. https://doi.org/10.1210/en.2012-1463.

[106] J.D. Furlow, E.S. Neff, A developmental switch induced by thyroid hormone: Xenopus laevis metamorphosis, Trends Endocrinol Metab 17 (2006) 40–47. https://doi.org/10.1016/j.tem.2006.01.007.

[107] Y. Shi, Amphibian Metamorphosis: From Morphology to Molecular Biology, Wiley-Liss, New York, 2000.

[108] M. Horb, M. Wlizla, A. Abu-Daya, S. McNamara, D. Gajdasik, T. Igawa, A. Suzuki, H. Ogino, A. Noble, M. Nicolas, T. Lafond, D. Boujard, Y. Audic, B. Guillet, A. Kashiwagi, K. Kashiwagi, N. Suzuki, I. Tazawa, H. Ochi, N. Furuno, M. Takase, K. Nakajima, H. Hanada, I. Miura, A. Kurabayashi, T. Kato, K. Sato, K. Takebayashi-Suzuki, H. Yoshida, J. Robert, C. James-Zorn, M. Guille, Xenopus resources: Transgenic, inbred and mutant animals, training opportunities, and web-based support, Front Physiol 10 (2019) 387. https://doi.org/10.3389/fphys.2019.00387.

[109] Y.A. Yu, K. Oberg, G. Wang, A.A. Szalay, Visualization of molecular and cellular events with green fluorescent proteins in developing embryos: A review, Luminescence 18 (2003) 1–18. https://doi.org/10.1002/bio.701.

[110] N. Burden, M.R. Embry, T.H. Hutchinson, S.G. Lynn, S.K. Maynard, C.A. Mitchell, F. Pellizzato, F. Sewell, K.L. Thorpe, L. Weltje, J.R. Wheeler, Investigating endocrine-disrupting properties of chemicals in fish and amphibians: Opportunities to apply the 3Rs, Integr Environ Assess Manag 18 (2022) 442–458. https://doi.org/10.1002/ieam.4497.

[111] V. Pérez-Fernández, L. Mainero Rocca, P. Tomai, S. Fanali, A. Gentili, Recent advancements and future trends in environmental analysis: Sample preparation, liquid chromatography and mass spectrometry, Anal Chim Acta 983 (2017) 9–41. https://doi.org/10.1016/j.aca.2017.06.029.

[112] Y. Picó, D. Barceló, Transformation products of emerging contaminants in the environment and high-resolution mass spectrometry: A new horizon, Anal Bioanal Chem 407 (2015) 6257–6273. https://doi.org/10.1007/s00216-015-8739-6.

[113] M.W. Dong, K. Zhang, Ultra-high-pressure liquid chromatography (UHPLC) in method development, TrAC - Trends in Analytical Chemistry 63 (2014) 21–30. https://doi.org/10.1016/j.trac.2014.06.019.

[114] HPLC Columns, Theory, Technology, and Practice, Instrum Sci Technol 26 (1998). https://doi.org/10.1080/10739149808001913.

[115] P. Žuvela, M. Skoczylas, J. Jay Liu, T. Baczek, R. Kaliszan, M.W. Wong, B. Buszewski, Column Characterization and Selection Systems in Reversed-Phase High-Performance Liquid Chromatography, Chem Rev 119 (2019) 3674–3729. https://doi.org/10.1021/acs.chemrev.8b00246.

[116] M. Yabré, L. Ferey, I.T. Somé, K. Gaudin, Greening reversed-phase liquid chromatography methods using alternative solvents for pharmaceutical analysis, Molecules 23 (2018). https://doi.org/10.3390/molecules23051065.

[117] B. Buszewski, S. Noga, Hydrophilic interaction liquid chromatography (HILIC)-a powerful separation technique, Anal Bioanal Chem 402 (2012) 231–247. https://doi.org/10.1007/s00216-011-5308-5.

[118] J. Bernal, A.M. Ares, J. Pól, S.K. Wiedmer, Hydrophilic interaction liquid chromatography in food analysis, J Chromatogr A 1218 (2011) 7438–7452. https://doi.org/10.1016/j.chroma.2011.05.004.

[119] R.M.B.O. Duarte, P.F. Brandão, A.C. Duarte, Multidimensional chromatography in environmental analysis: Comprehensive two-dimensional liquid versus gas chromatography, J Chromatogr A 1706 (2023) 464288. https://doi.org/10.1016/j.chroma.2023.464288.

[120] D.R. Stoll, P.W. Carr, Two-Dimensional Liquid Chromatography: A State of the Art Tutorial, Anal Chem 89 (2017) 519–531. https://doi.org/10.1021/acs.analchem.6b03506.

[121] Z. Liu, D.G. Patterson, M.L. Lee, Geometric Approach to Factor Analysis for the Estimation of Orthogonality and Practical Peak Capacity in Comprehensive Two-Dimensional Separations, Anal Chem 67 (1995) 3840–3845. https://doi.org/10.1021/ac00117a004.

[122] B.W.J. Pirok, A.F.G. Gargano, P.J. Schoenmakers, Optimizing separations in online comprehensive two-dimensional liquid chromatography, J Sep Sci 41 (2018) 68–98. https://doi.org/10.1002/jssc.201700863.

[123] I. Caño-Carrillo, B. Gilbert-López, L. Montero, A.B. Martínez-Piernas, J.F. García-Reyes, A. Molina-Díaz, Comprehensive and heart-cutting multidimensional liquid chromatography-mass spectrometry and its applications in food analysis, Mass Spectrom Rev (2023) 1–41. https://doi.org/10.1002/mas.21843.

[124] K. Horváth, J. Fairchild, G. Guiochon, Optimization strategies for off-line two-dimensional liquid chromatography, J Chromatogr A 1216 (2009) 2511–2518. https://doi.org/10.1016/j.chroma.2009.01.064.

[125] P. Česla, J. Křenková, Fraction transfer process in on-line comprehensive two-dimensional liquid-phase separations, J Sep Sci 40 (2017) 109–123. https://doi.org/10.1002/jssc.201600921.

[126] F. Cacciola, P. Donato, D. Sciarrone, P. Dugo, L. Mondello, Comprehensive liquid chromatography and other liquid-based comprehensive techniques coupled to mass spectrometry in food analysis, Anal Chem 89 (2017) 414–429. https://doi.org/10.1021/acs.analchem.6b04370.

[127] B.W.J. Pirok, D.R. Stoll, P.J. Schoenmakers, Recent Developments in Two-Dimensional Liquid Chromatography: Fundamental Improvements for Practical Applications, Anal Chem 91 (2019) 240–263. https://doi.org/10.1021/acs.analchem.8b04841.

[128] S.R. Groskreutz, M.M. Swenson, L.B. Secor, D.R. Stoll, Selective comprehensive multi-dimensional separation for resolution enhancement in high performance liquid chromatography. Part I: Principles and instrumentation, J Chromatogr A 1228 (2012) 31–40. https://doi.org/10.1016/j.chroma.2011.06.035.

[129] S. Chapel, S. Heinisch, Strategies to circumvent the solvent strength mismatch problem in online comprehensive two-dimensional liquid chromatography, J Sep Sci 45 (2022) 7–26. https://doi.org/10.1002/jssc.202100534.

[130] D. Li, C. Jakob, O. Schmitz, Practical considerations in comprehensive two-dimensional liquid chromatography systems (LCxLC) with reversed-phases in both dimensions, Anal Bioanal Chem 407 (2015) 153–167. https://doi.org/10.1007/s00216-014-8179-8.

[131] Y. Chen, J. Li, O.J. Schmitz, Development of an At-Column Dilution Modulator for Flexible and Precise Control of Dilution Factors to Overcome Mobile Phase Incompatibility in Comprehensive Two-Dimensional Liquid Chromatography, Anal Chem 91 (2019) 10251–10257. https://doi.org/10.1021/acs.analchem.9b02391.

[132] S. Chapel, F. Rouvière, S. Heinisch, Comparison of existing strategies for keeping symmetrical peaks in on-line Hydrophilic Interaction Liquid Chromatography x Reversed-Phase Liquid Chromatography despite solvent strength mismatch, J Chromatogr A 1642 (2021) 462001. https://doi.org/10.1016/j.chroma.2021.462001.

[133] D.R. Stoll, K. Shoykhet, P. Petersson, S. Buckenmaier, Active Solvent Modulation: A Valve-Based Approach to Improve Separation Compatibility in Two-Dimensional Liquid Chromatography, Anal Chem 89 (2017) 9260–9267. https://doi.org/10.1021/acs.analchem.7b02046.

[134] L. Ma, S.R. Yates, A review on structural elucidation of metabolites of environmental steroid hormones via liquid chromatography–mass spectrometry, TrAC - Trends Anal. Chem. 109 (2018) 142–153. https://doi.org/10.1016/j.trac.2018.10.007.

[135] D.X. Li, L. Gan, A. Bronja, O.J. Schmitz, Gas chromatography coupled to atmospheric pressure ionization mass spectrometry (GC-API-MS): Review, Anal Chim Acta 891 (2015) 43–61. https://doi.org/10.1016/j.aca.2015.08.002.

[136] E. De Hoffmann, V. Stroobant, Mass spectrometry: principles and applications, John Wiley & Sons, 2007.

[137] H. Awad, M.M. Khamis, A. El-Aneed, Mass spectrometry, review of the basics: Ionization, Appl Spectrosc Rev 50 (2015) 158–175. https://doi.org/10.1080/05704928.2014.954046.

[138] M. Farré, L. Kantiani, M. Petrovic, S. Pérez, D. Barceló, Achievements and future trends in the analysis of emerging organic contaminants in environmental samples by mass spectrometry and bioanalytical techniques, J Chromatogr A 1259 (2012) 86–99. https://doi.org/10.1016/j.chroma.2012.07.024.

[139] V. Leendert, H. Van Langenhove, K. Demeestere, Trends in liquid chromatography coupled to high-resolution mass spectrometry for multi-residue analysis of organic micropollutants in aquatic environments, TrAC - Trends Anal. Chem. 67 (2015) 192–208. https://doi.org/10.1016/j.trac.2015.01.010.

[140] M. Krauss, H. Singer, J. Hollender, LC-high resolution MS in environmental analysis: From target screening to the identification of unknowns, Anal Bioanal Chem 397 (2010) 943–951. https://doi.org/10.1007/s00216-010-3608-9.

[141] F. Gosetti, E. Mazzucco, M.C. Gennaro, E. Marengo, Contaminants in water: non-target UHPLC/MS analysis, Environ Chem Lett 14 (2016) 51–65. https://doi.org/10.1007/s10311-015-0527-1.

[142] A. Kaufmann, Combining UHPLC and high-resolution MS: A viable approach for the analysis of complex samples?, TrAC Trends in Analytical Chemistry 63 (2014) 113–128. https://doi.org/https://doi.org/10.1016/j.trac.2014.06.025.

[143] X. Fang, J. Xie, S. Chu, Y. Jiang, Y. An, C. Li, X. Gong, R. Zhai, Z. Huang, C. Qiu, X. Dai, Quadrupole-Linear Ion Trap Tandem Mass Spectrometry System for Clinical Biomarker Analysis, Engineering 16 (2022) 56–64. https://doi.org/10.1016/j.eng.2020.10.021.

[144] C. Li, S. Chu, S. Tan, X. Yin, Y. Jiang, X. Dai, X. Gong, X. Fang, D. Tian, Towards Higher Sensitivity of Mass Spectrometry: A Perspective From the Mass Analyzers, Front Chem 9 (2021). https://doi.org/10.3389/fchem.2021.813359.

[145] J. Wang, M.E. Pursell, A. DeVor, O. Awoyemi, S.J. Valentine, P. Li, Portable mass spectrometry system: instrumentation, applications, and path to 'omics analysis, Proteomics 22 (2022). https://doi.org/10.1002/pmic.202200112.

[146] J. Urban, N.K. Afseth, D. Štys, Fundamental definitions and confusions in mass spectrometry about mass assignment, centroiding and resolution, TrAC - Trends in Analytical Chemistry 53 (2014) 126–136. https://doi.org/10.1016/j.trac.2013.07.010.

[147] A.R. Johnson, E.E. Carlson, Collision-Induced Dissociation Mass Spectrometry: A Powerful Tool for Natural Product Structure Elucidation, Anal Chem 87 (2015) 10668–10678. https://doi.org/10.1021/acs.analchem.5b01543.

[148] A.G. Brenton, A.R. Godfrey, Accurate mass measurement: Terminology and treatment of data, J Am Soc Mass Spectrom 21 (2010) 1821–1835. https://doi.org/10.1016/j.jasms.2010.06.006.

[149] A.A. Bletsou, J. Jeon, J. Hollender, E. Archontaki, N.S. Thomaidis, Targeted and non-targeted liquid chromatography-mass spectrometric workflows for identification of transformation products of emerging pollutants in the aquatic environment, TrAC - Trends in Analytical Chemistry 66 (2015) 32–44. https://doi.org/10.1016/j.trac.2014.11.009.

[150] T. Ruan, P. Li, H. Wang, T. Li, G. Jiang, Identification and Prioritization of Environmental Organic Pollutants: From an Analytical and Toxicological Perspective, Chem Rev 123 (2023) 10584–10640. https://doi.org/10.1021/acs.chemrev.3c00056.

[151] E.L. Schymanski, A.J. Williams, Open Science for Identifying "Known Unknown" Chemicals, Environ Sci Technol 51 (2017) 5357–5359. https://doi.org/10.1021/acs.est.7b01908.

[152] S. Alseekh, A. Aharoni, Y. Brotman, K. Contrepois, J. D'Auria, J. Ewald, J. C. Ewald, P.D. Fraser, P. Giavalisco, R.D. Hall, M. Heinemann, H. Link, J. Luo, S. Neumann, J. Nielsen, L. Perez de Souza, K. Saito, U. Sauer, F.C. Schroeder, S. Schuster, G. Siuzdak, A. Skirycz, L.W. Sumner, M.P. Snyder, H. Tang, T. Tohge, Y. Wang, W. Wen, S. Wu, G. Xu, N. Zamboni, A.R. Fernie, Mass spectrometry-based metabolomics: a guide for annotation, quantification and best reporting practices, Nat Methods 18 (2021) 747–756. https://doi.org/10.1038/s41592-021-01197-1.

[153] J. Hollender, E.L. Schymanski, H.P. Singer, P.L. Ferguson, Nontarget Screening with High Resolution Mass Spectrometry in the Environment: Ready to Go?, Environ Sci Technol 51 (2017) 11505–11512. https://doi.org/10.1021/acs.est.7b02184.

[154] P. Hajeb, L. Zhu, R. Bossi, K. Vorkamp, Sample preparation techniques for suspect and non-target screening of emerging contaminants, Chemosphere 287 (2022) 132306. https://doi.org/10.1016/j.chemosphere.2021.132306.

[155] M. Pourchet, L. Debrauwer, J. Klanova, E.J. Price, A. Covaci, N. Caballero-Casero, H. Oberacher, M. Lamoree, A. Damont, F. Fenaille, J. Vlaanderen, J. Meijer, M. Krauss, D. Sarigiannis, R. Barouki, B. Le Bizec, J.P. Antignac, Suspect and non-targeted screening of chemicals of emerging concern for human biomonitoring, environmental health studies and support to risk assessment: From promises to challenges and harmonisation issues, Environ Int 139 (2020) 105545. https://doi.org/10.1016/j.envint.2020.105545.

[156] E.L. Schymanski, J. Jeon, R. Gulde, K. Fenner, M. Ruff, H.P. Singer, J. Hollender, Identifying small molecules via high resolution mass spectrometry: Communicating confidence, Environ Sci Technol 48 (2014) 2097–2098. https://doi.org/10.1021/es5002105.

[157] A. Celma, J. V. Sancho, E.L. Schymanski, D. Fabregat-Safont, M. Ibáñez, J. Goshawk, G. Barknowitz, F. Hernández, L. Bijlsma, Improving Target and Suspect Screening High-Resolution Mass Spectrometry Workflows in Environmental Analysis by Ion Mobility Separation, Environ Sci Technol 54 (2020) 15120–15131. https://doi.org/10.1021/acs.est.0c05713.

[158] I. Pugajeva, L.E. Ikkere, M. Jansons, I. Perkons, V. Sukajeva, V. Bartkevics, Two-dimensional liquid chromatography - mass spectrometry as an effective tool for assessing a wide range of pharmaceuticals and biomarkers in wastewater-based epidemiology studies, J Pharm Biomed Anal 205 (2021) 114295. https://doi.org/https://doi.org/10.1016/j.jpba.2021.114295.

[159] N. Muhammad, F. Wang, Q. Subhani, Q. Zhao, M.A. Qadir, H. Cui, Y. Zhu, Comprehensive two-dimensional ion chromatography (2D-IC) coupled to a post-column photochemical fluorescence detection system for determination of neonicotinoids (imidacloprid and clothianidin) in food samples, RSC Adv 8 (2018) 9277–9286. https://doi.org/10.1039/C7RA12555K.

[160] M. Iguiniz, S. Heinisch, Two-dimensional liquid chromatography in pharmaceutical analysis. Instrumental aspects, trends and applications, J Pharm Biomed Anal 145 (2017) 482–503. https://doi.org/https://doi.org/10.1016/j.jpba.2017.07.009.

[161] A.S. Fernández, P. Rodríguez-González, L. Álvarez, M. García, H.G. Iglesias, J.I. García Alonso, Multiple heart-cutting two dimensional liquid chromatography and isotope dilution tandem mass spectrometry for the absolute quantification of proteins in human serum, Anal Chim Acta 1184 (2021) 339022. https://doi.org/https://doi.org/10.1016/j.aca.2021.339022.

[162] L.S. Roca, A.F.G. Gargano, P.J. Schoenmakers, Development of comprehensive two-dimensional low-flow liquid-chromatography setup coupled to high-resolution mass spectrometry for shotgun proteomics, Anal Chim Acta 1156 (2021) 338349. https://doi.org/https://doi.org/10.1016/j.aca.2021.338349.

[163] M. Grübner, A. Dunkel, F. Steiner, T. Hofmann, Systematic Evaluation of Liquid Chromatography (LC) Column Combinations for Application in Two-Dimensional LC Metabolomic Studies, Anal Chem 93 (2021) 12565–12573. https://doi.org/10.1021/acs.analchem.1c01857.

[164] F. Yuan, S. Kim, X. Yin, X. Zhang, I. Kato, Integrating two-dimensional gas and liquid chromatography-mass spectrometry for untargeted colorectal cancer metabolomics: A proof-of-principle study, Metabolites 10 (2020). https://doi.org/10.3390/metabo10090343.

[165] G. Groeneveld, B.W.J. Pirok, P.J. Schoenmakers, Perspectives on the future of multi-dimensional platforms, Faraday Discuss 218 (2019) 72–100. https://doi.org/10.1039/C8FD00233A.

[166] J. Feng, Q. Zhong, J. Kuang, J. Liu, T. Huang, T. Zhou, Simultaneous Analysis of the Metabolome and Lipidome Using Polarity Partition Two-Dimensional Liquid Chromatography–Mass Spectrometry, Anal Chem 93 (2021) 15192–15199. https://doi.org/10.1021/acs.analchem.1c03905.

[167] N. Abdulhussain, S. Nawada, P. Schoenmakers, Latest Trends on the Future of Three-Dimensional Separations in Chromatography, Chem Rev 121 (2021) 12016–12034. https://doi.org/10.1021/acs.chemrev.0c01244.

[168] T.H. Walter, R.W. Andrews, Recent innovations in UHPLC columns and instrumentation, TrAC Trends in Analytical Chemistry 63 (2014) 14–20. https://doi.org/https://doi.org/10.1016/j.trac.2014.07.016.

[169] R. Hayes, A. Ahmed, T. Edge, H. Zhang, Core–shell particles: Preparation, fundamentals and applications in high performance liquid chromatography, J Chromatogr A 1357 (2014) 36–52. https://doi.org/https://doi.org/10.1016/j.chroma.2014.05.010.

[170] H. Zou, X. Huang, M. Ye, Q. Luo, Monolithic stationary phases for liquid chromatography and capillary electrochromatography, J Chromatogr A 954 (2002) 5–32. https://doi.org/https://doi.org/10.1016/S0021-9673(02)00072-9.

[171] M. Beccaria, D. Cabooter, Current developments in LC-MS for pharmaceutical analysis, Analyst 145 (2020) 1129–1157. https://doi.org/10.1039/C9AN02145K.

[172] J.C. Giddings, Two-dimensional separations: concept and promise, Anal Chem 56 (1984) 1258A-1270A. https://doi.org/10.1021/ac00276a003.

[173] K. Arena, F. Mandolfino, F. Cacciola, P. Dugo, L. Mondello, Multidimensional liquid chromatography approaches for analysis of food contaminants, J Sep Sci 44 (2021) 17–34. https://doi.org/https://doi.org/10.1002/jssc.202000754.

[174] G. Groeneveld, M.N. Dunkle, M. Pursch, E.P.C. Mes, P.J. Schoenmakers, A.F.G. Gargano, Investigation of the effects of solvent-mismatch and immiscibility in normal-phase × aqueous reversed-phase liquid chromatography, J Chromatogr A 1665 (2022) 462818. https://doi.org/https://doi.org/10.1016/j.chroma.2022.462818.

[175] S. Knoll, T. Rösch, C. Huhn, Trends in sample preparation and separation methods for the analysis of very polar and ionic compounds in environmental water and biota samples, Anal Bioanal Chem 412 (2020) 6149–6165. https://doi.org/10.1007/s00216-020-02811-5.

[176] G. Loos, K. Shoykhet, M. Dittmann, D. Cabooter, Restriction capillaries as an innovative mixing unit for intermediate mobile phase exchange in multidimensional analysis, J Chromatogr A 1497 (2017) 70–80. https://doi.org/https://doi.org/10.1016/j.chroma.2017.03.036.

[177] A.G. Atanasov, S.B. Zotchev, V.M. Dirsch, I.E. Orhan, M. Banach, J.M. Rollinger, D. Barreca, W. Weckwerth, R. Bauer, E.A. Bayer, M. Majeed, A. Bishayee, V. Bochkov, G.K. Bonn, N. Braidy, F. Bucar, A. Cifuentes, G. D'Onofrio, M. Bodkin, M. Diederich, A.T. Dinkova-Kostova, T. Efferth, K. El Bairi, N. Arkells, T.-P. Fan, B.L. Fiebich, M. Freissmuth, M.I. Georgiev, S. Gibbons, K.M. Godfrey, C.W. Gruber, J. Heer, L.A. Huber, E. Ibanez, A. Kijjoa, A.K. Kiss, A. Lu, F.A. Macias, M.J.S. Miller, A. Mocan, R. Müller, F. Nicoletti, G. Perry, V. Pittalà, L. Rastrelli, M. Ristow, G.L. Russo, A.S. Silva, D. Schuster, H. Sheridan, K. Skalicka-Woźniak, L. Skaltsounis, E. Sobarzo-Sánchez, D.S. Bredt, H. Stuppner, A. Sureda, N.T. Tzvetkov, R.A. Vacca, B.B. Aggarwal, M. Battino, F. Giampieri, M. Wink, J.-L. Wolfender, J. Xiao, A.W.K. Yeung, G. Lizard, M.A. Popp, M. Heinrich, I. Berindan-Neagoe, M. Stadler, M. Daglia, R. Verpoorte, C.T. Supuran, the I.N.P.S. Taskforce, Natural products in drug discovery: advances and opportunities, Nat Rev Drug Discov 20 (2021) 200–216. https://doi.org/10.1038/s41573-020-00114-z.

[178] A.D. Southam, H. Pursell, G. Frigerio, A. Jankevics, R.J.M. Weber, W.B. Dunn, Characterization of Monophasic Solvent-Based Tissue Extractions for the Detection of Polar Metabolites and Lipids Applying Ultrahigh-Performance Liquid Chromatography–Mass Spectrometry Clinical Metabolic Phenotyping Assays, J Proteome Res 20 (2021) 831–840. https://doi.org/10.1021/acs.jproteome.0c00660.

[179] Y. Chen, L. Montero, J. Luo, J. Li, O.J. Schmitz, Application of the new at-column dilution (ACD) modulator for the two-dimensional RP×HILIC analysis of Buddleja davidii, Anal Bioanal Chem 412 (2020) 1483–1495. https://doi.org/10.1007/s00216-020-02392-3.

[180] S. Bieber, G. Greco, S. Grosse, T. Letzel, RPLC-HILIC and SFC with Mass Spectrometry: Polarity-Extended Organic Molecule Screening in Environmental (Water) Samples, Anal Chem 89 (2017) 7907–7914. https://doi.org/10.1021/acs.analchem.7b00859.

[181] S. CHAPEL, F. Rouvière, V. Peppermans, G. Desmet, S. Heinisch, A comprehensive study on the phenomenon of total breakthrough in liquid chromatography, J Chromatogr A 1653 (2021) 462399. https://doi.org/https://doi.org/10.1016/j.chroma.2021.462399.

[182] Y. Chen, L. Montero, O.J. Schmitz, Advance in on-line two-dimensional liquid chromatography modulation technology, TrAC Trends in Analytical Chemistry 120 (2019) 115647. https://doi.org/https://doi.org/10.1016/j.trac.2019.115647.

[183] M.R. Filgueira, Y. Huang, K. Witt, C. Castells, P.W. Carr, Improving Peak Capacity in Fast Online Comprehensive Two-Dimensional Liquid Chromatography with Post-First-Dimension Flow Splitting, Anal Chem 83 (2011) 9531–9539. https://doi.org/10.1021/ac202317m.

[184] M. Iguiniz, E. Corbel, N. Roques, S. Heinisch, Quantitative aspects in on-line comprehensive two-dimensional liquid chromatography for pharmaceutical applications, Talanta 195 (2019) 272–280. https://doi.org/https://doi.org/10.1016/j.talanta.2018.11.030.

[185] M. Sarrut, F. Rouvière, S. Heinisch, Theoretical and experimental comparison of one dimensional versus on-line comprehensive two dimensional liquid chromatography for optimized sub-hour separations of complex peptide samples, J Chromatogr A 1498 (2017) 183–195. https://doi.org/https://doi.org/10.1016/j.chroma.2017.01.054.

[186] C.M. Willemse, M.A. Stander, J. Vestner, A.G.J. Tredoux, A. de Villiers, Comprehensive Two-Dimensional Hydrophilic Interaction Chromatography (HILIC) × Reversed-Phase Liquid Chromatography Coupled to High-Resolution Mass Spectrometry (RP-LC-UV-MS) Analysis of Anthocyanins and Derived Pigments in Red Wine, Anal Chem 87 (2015) 12006–12015. https://doi.org/10.1021/acs.analchem.5b03615.

[187] S. Tang, C.J. Venkatramani, Resolving Solvent Incompatibility in Two-Dimensional Liquid Chromatography with In-Line Mixing Modulation, Anal Chem 94 (2022) 16142–16150. https://doi.org/10.1021/acs.analchem.2c03572.

[188] A.F.G. Gargano, M. Duffin, P. Navarro, P.J. Schoenmakers, Reducing Dilution and Analysis Time in Online Comprehensive Two-Dimensional Liquid Chromatography by Active Modulation, Anal Chem 88 (2016) 1785–1793. https://doi.org/10.1021/acs.analchem.5b04051.

[189] J.-L. Cao, L.-J. Ma, S.-P. Wang, Y. Deng, Y.-T. Wang, P. Li, J.-B. Wan, Comprehensively qualitative and quantitative analysis of ginsenosides in Panax notoginseng leaves by online two-dimensional liquid chromatography coupled to hybrid linear ion trap Orbitrap mass spectrometry with deeply optimized dilution and modulation system, Anal Chim Acta 1079 (2019) 237–251. https://doi.org/https://doi.org/10.1016/j.aca.2019.06.040.

[190] A. Martín-Ortiz, A.I. Ruiz-Matute, M.L. Sanz, F.J. Moreno, M. Herrero, Separation of di- and trisaccharide mixtures by comprehensive two-dimensional liquid chromatography. Application to prebiotic oligosaccharides, Anal Chim Acta 1060 (2019) 125–132. https://doi.org/https://doi.org/10.1016/j.aca.2019.01.040.

[191] M. Muller, A.G.J. Tredoux, A. de Villiers, Application of Kinetically Optimised Online HILIC × RP-LC Methods Hyphenated to High Resolution MS for the Analysis of Natural Phenolics, Chromatographia 82 (2019) 181–196. https://doi.org/10.1007/s10337-018-3662-6.

[192] J.-L. Cao, S.-S. Wang, H. Hu, C.-W. He, J.-B. Wan, H.-X. Su, Y.-T. Wang, P. Li, Online comprehensive two-dimensional hydrophilic interaction chromatography×reversed-phase liquid chromatography coupled with hybrid linear ion trap Orbitrap mass spectrometry for the analysis of phenolic acids in Salvia miltiorrhiza, J Chromatogr A 1536 (2018) 216–227. https://doi.org/https://doi.org/10.1016/j.chroma.2017.09.041.

[193] H. Tian, J. Xu, Y. Xu, Y. Guan, Multidimensional liquid chromatography system with an innovative solvent evaporation interface, J Chromatogr A 1137 (2006) 42–48. https://doi.org/https://doi.org/10.1016/j.chroma.2006.10.005.

[194] E. Fornells, B. Barnett, M. Bailey, E.F. Hilder, R.A. Shellie, M.C. Breadmore, Evaporative membrane modulation for comprehensive two-dimensional liquid chromatography, Anal Chim Acta 1000 (2018) 303–309. https://doi.org/https://doi.org/10.1016/j.aca.2017.11.053.

[195] F. Erni, R.W. Frei, Two-dimensional column liquid chromatographic technique for resolution of complex mixtures, J Chromatogr A 149 (1978) 561–569. https://doi.org/https://doi.org/10.1016/S0021-9673(00)81011-0.

[196] M.M. Bushey, J.W. Jorgenson, Automated instrumentation for comprehensive two-dimensional high-performance liquid chromatography of proteins, Anal Chem 62 (1990) 161–167. https://doi.org/10.1021/ac00201a015.

[197] 2D-LC, 1290 Infinity II 2D-LC System | Agilent, (n.d.).

[198] Superior HPLC testing, 1260 Infinity II LC System | Agilent, (n.d.).

[199] M. Pardon, S. Chapel, P. de Witte, D. Cabooter, Optimizing transfer and dilution processes when using active solvent modulation in on-line two-dimensional liquid chromatography, Anal Chim Acta 1252 (2023) 341040. https://doi.org/https://doi.org/10.1016/j.aca.2023.341040.

[200] S. Deridder, G. Desmet, K. Broeckhoven, Numerical investigation of band spreading generated by flow-through needle and fixed loop sample injectors, J Chromatogr A 1552 (2018) 29–42. https://doi.org/https://doi.org/10.1016/j.chroma.2018.04.001.

[201] A. Moussa, T. Lauer, D. Stoll, G. Desmet, K. Broeckhoven, Modelling of analyte profiles and band broadening generated by interface loops used in multi-dimensional liquid chromatography, J Chromatogr A 1659 (2021) 462578. https://doi.org/https://doi.org/10.1016/j.chroma.2021.462578.

[202] D.J. Lapworth, N. Baran, M.E. Stuart, R.S. Ward, Emerging organic contaminants in groundwater: A review of sources, fate and occurrence, Environmental Pollution 163 (2012). https://doi.org/10.1016/j.envpol.2011.12.034.

[203] A.Z. Aris, A.S. Shamsuddin, S.M. Praveena, Occurrence of 17α-ethynylestradiol (EE2) in the environment and effect on exposed biota: A review, Environ Int 69 (2014). https://doi.org/10.1016/j.envint.2014.04.011.

[204] P. Matthiessen, D. Arnold, A.C. Johnson, T.J. Pepper, T.G. Pottinger, K.G.T. Pulman, Contamination of headwater streams in the United Kingdom by oestrogenic hormones from livestock farms, Science of the Total Environment 367 (2006). https://doi.org/10.1016/j.scitotenv.2006.02.007.

[205] S. Liu, G.G. Ying, L.J. Zhou, R.Q. Zhang, Z.F. Chen, H.J. Lai, Steroids in a typical swine farm and their release into the environment, Water Res 46 (2012). https://doi.org/10.1016/j.watres.2012.04.006.

[206] Y. Zuo, K. Zhang, S. Zhou, Determination of estrogenic steroids and microbial and photochemical degradation of 17α-ethinylestradiol (EE2) in lake surface water, a case study, Environmental Sciences: Processes and Impacts 15 (2013). https://doi.org/10.1039/c3em00239j.

[207] K.M. Lai, K.L. Johnson, M.D. Scrimshaw, J.N. Lester, Binding of waterborne steroid estrogens to solid phases in river and estuarine systems, Environ Sci Technol 34 (2000). https://doi.org/10.1021/es9912729.

[208] M.S. Perkins, R. Louw-du Toit, D. Africander, A comparative characterization of estrogens used in hormone therapy via estrogen receptor (ER)-α and -β, Journal of Steroid Biochemistry and Molecular Biology 174 (2017). https://doi.org/10.1016/j.jsbmb.2017.07.022.

[209] R.M. Blair, H. Fang, W.S. Branham, B.S. Hass, S.L. Dial, C.L. Moland, W. Tong, L. Shi, R. Perkins, D.M. Sheehan, The estrogen receptor relative binding affinities of 188 natural and xenochemicals: Structural diversity of ligands, Toxicological Sciences 54 (2000). https://doi.org/10.1093/toxsci/54.1.138.

[210] J.S. Denny, M.A. Tapper, P.K. Schmieder, M.W. Hornung, K.M. Jensen, G.T. Ankley, T.R. Henry, Comparison of relative binding affinities of endocrine active compounds to fathead minnow and rainbow trout estrogen receptors, Environ Toxicol Chem 24 (2005). https://doi.org/10.1897/04-595R.1.

[211] S.C. Tilton, C.M. Foran, W.H. Benson, Relationship between ethinylestradiol-mediated changes in endocrine function and reproductive impairment in Japanese medaka (Oryzias latipes), Environ Toxicol Chem 24 (2005). https://doi.org/10.1897/04-016R.1.

[212] J.P. Nash, D.E. Kime, L.T.M. Van der Ven, P.W. Wester, F. Brion, G. Maack, P. Stahlschmidt-Allner, C.R. Tyler, Long-term exposure to environmental concentrations of the pharmaceutical ethynylestradiol causes reproductive failure in fish, Environ Health Perspect 112 (2004). https://doi.org/10.1289/ehp.7209.

[213] M.J. Tsai, B.W. O'Malley, Molecular mechanisms of action of steroid/thyroid receptor superfamily members, Annu Rev Biochem 63 (1994) 451–486. https://doi.org/10.1146/annurev.bi.63.070194.002315.

[214] A.M. Brzozowski, A.C.W. Pike, Z. Dauter, R.E. Hubbard, T. Bonn, O. Engström, L. Öhman, G.L. Greene, J.Å. Gustafsson, M. Carlquist, Molecular basis of agonism and antagonism in the oestrogen receptor, Nature 389 (1997). https://doi.org/10.1038/39645.

[215] Z. Tang, Z. hua Liu, H. Wang, Z. Dang, Y. Liu, A review of 17α-ethynylestradiol (EE2) in surface water across 32 countries: Sources, concentrations, and potential estrogenic effects, J Environ Manage 292 (2021). https://doi.org/10.1016/j.jenvman.2021.112804.

[216] C. Grandclément, I. Seyssiecq, A. Piram, P. Wong-Wah-Chung, G. Vanot, N. Tiliacos, N. Roche, P. Doumenq, From the conventional biological wastewater treatment to hybrid processes, the evaluation of organic micropollutant removal: a review, Water Res 111 (2017) 297–317.

[217] M. Klaic, F. Jirsa, 17α-Ethinylestradiol (EE2): concentrations in the environment and methods for wastewater treatment – an update, RSC Adv. 12 (2022) 12794–12805. https://doi.org/10.1039/D2RA00915C.

[218] J. Wang, S. Wang, Removal of pharmaceuticals and personal care products (PPCPs) from wastewater: A review, J Environ Manage 182 (2016). https://doi.org/10.1016/j.jenvman.2016.07.049.

[219] Z. Zhang, H. Zhu, X. Wen, X. Si, Degradation behavior of 17α-ethinylestradiol by ozonation in the synthetic secondary effluent, Journal of Environmental Sciences 24 (2012). https://doi.org/10.1016/S1001-0742(11)60749-3.

[220] S. Larcher, G. Delbès, B. Robaire, V. Yargeau, Degradation of 17α-ethinylestradiol by ozonation - Identification of the by-products and assessment of their estrogenicity and toxicity, Environ Int 39 (2012). https://doi.org/10.1016/j.envint.2011.09.008.

[221] M. Guedes Maniero, D. Maia Bila, M. Dezotti, Degradation and estrogenic activity removal of 17β-estradiol and 17α-ethinylestradiol by ozonation and O3/H2O2, Science of the Total Environment 407 (2008). https://doi.org/10.1016/j.scitotenv.2008.08.011.

[222] Z. Frontistis, V.M. Daskalaki, E. Hapeshi, C. Drosou, D. Fatta-Kassinos, N.P. Xekoukoulotakis, D. Mantzavinos, Photocatalytic (UV-A/TiO 2) degradation of 17α- ethynylestradiol in

environmental matrices: Experimental studies and artificial neural network modeling, J Photochem Photobiol A Chem 240 (2012). https://doi.org/10.1016/j.jphotochem.2012.05.007.

[223] G. Li Puma, V. Puddu, H.K. Tsang, A. Gora, B. Toepfer, Photocatalytic oxidation of multicomponent mixtures of estrogens (estrone (E1), 17β-estradiol (E2), 17α-ethynylestradiol (EE2) and estriol (E3)) under UVA and UVC radiation: Photon absorption, quantum yields and rate constants independent of photon absorption, Appl Catal B 99 (2010). https://doi.org/10.1016/j.apcatb.2010.05.015.

[224] Z. Pan, E.A. Stemmler, H.J. Cho, W. Fan, L.A. LeBlanc, H.H. Patterson, A. Amirbahman, Photocatalytic degradation of 17α-ethinylestradiol (EE2) in the presence of TiO2-doped zeolite, J Hazard Mater 279 (2014). https://doi.org/10.1016/j.jhazmat.2014.06.040.

[225] K. López-Velázquez, M. Villanueva-Rodríguez, G. Mejía-González, D. Herrera-López, Removal of 17α-ethinylestradiol and caffeine from wastewater by UASB-Fenton coupled system, Environmental Technology (United Kingdom) 42 (2021). https://doi.org/10.1080/09593330.2020.1740799.

[226] Y. He, H. Lin, Z. Guo, W. Zhang, H. Li, W. Huang, Recent developments and advances in boron-doped diamond electrodes for electrochemical oxidation of organic pollutants, Sep Purif Technol 212 (2019). https://doi.org/10.1016/j.seppur.2018.11.056.

[227] B. Marselli, J. Garcia-Gomez, P.-A. Michaud, M.A. Rodrigo, Ch. Comninellis, Electrogeneration of Hydroxyl Radicals on Boron-Doped Diamond Electrodes, J Electrochem Soc 150 (2003) 79–83. https://doi.org/10.1149/1.1553790.

[228] A. Dirany, I. Sirés, N. Oturan, M.A. Oturan, Electrochemical abatement of the antibiotic sulfamethoxazole from water, Chemosphere 81 (2010). https://doi.org/10.1016/j.chemosphere.2010.08.032.

[229] E. Grilla, M.E. Taheri, K. Miserli, D. Venieri, I. Konstantinou, D. Mantzavinos, Degradation of dexamethasone in water using BDD anodic oxidation and persulfate: reaction kinetics and pathways, Journal of Chemical Technology and Biotechnology 96 (2021). https://doi.org/10.1002/jctb.6833.

[230] Z. Miao, M.L. Brusseau, K.C. Carroll, C. Carreón-Diazconti, B. Johnson, Sulfate reduction in groundwater: Characterization and applications for remediation, Environ Geochem Health 34 (2012). https://doi.org/10.1007/s10653-011-9423-1.

[231] D. Abiriga, L.S. Vestgarden, H. Klempe, Groundwater contamination from a municipal landfill: Effect of age, landfill closure, and season on groundwater chemistry, Science of the Total Environment 737 (2020). https://doi.org/10.1016/j.scitotenv.2020.140307.

[232] O. Lefebvre, R. Moletta, Treatment of organic pollution in industrial saline wastewater: A literature review, Water Res 40 (2006). https://doi.org/10.1016/j.watres.2006.08.027.

[233] Z. Frontistis, C. Brebou, D. Venieri, D. Mantzavinos, A. Katsaounis, BDD anodic oxidation as tertiary wastewater treatment for the removal of emerging micro-pollutants, pathogens and organic matter, Journal of Chemical Technology and Biotechnology 86 (2011). https://doi.org/10.1002/jctb.2669.

[234] H.A. Nájera-Aguilar, R.F. Gutiérrez-Hernández, R.G. De Los Santos, C. García-Lara, R. Méndez-Novelo, M.N. Rojas-Valencia, Degradation of gestodene (GES)-17A-ethinylestradiol (EE2) mixture by electrochemical oxidation, J Water Health 14 (2016). https://doi.org/10.2166/wh.2016.104.

[235] G. Loos, T. Scheers, K. Van Eyck, A. Van Schepdael, E. Adams, B. Van der Bruggen, D. Cabooter, R. Dewil, Electrochemical oxidation of key pharmaceuticals using a boron doped

diamond electrode, Sep Purif Technol 195 (2018) 184–191. https://doi.org/10.1016/j.seppur.2017.12.009.

[236] X. Chen, S.H. Cheng, M. Kinoshita, P.A. de Witte, J. Liu, D. Hinton, T. Braunbeck, I. Cotgreave, D. Schlenk, Z. Gong, H. El-Nezami, K.C. Ho, K.F. Chan, S. Xu, P.Y. Yiu, H. Zhang, D. Wu, Y.S. Chan, A. Ny, J. Maes, Pre-validation of choriogenin H transgenic medaka eleutheroembryos as a quantitative estrogenic activity test method, Anal Biochem 629 (2021). https://doi.org/10.1016/j.ab.2021.114311.

[237] P. Spirhanzlova, M. Leleu, A. Sébillot, G.F. Lemkine, T. Iguchi, B.A. Demeneix, A.J. Tindall, Oestrogen reporter transgenic medaka for non-invasive evaluation of aromatase activity, Comp. Biochem. Physiol. Part - C: Toxicol. Pharmacol. 179 (2016) 64–71. https://doi.org/10.1016/j.cbpc.2015.08.011.

[238] Z. Zeng, T. Shan, Y. Tong, S.H. Lam, Z. Gong, Development of estrogen-responsive transgenic medaka for environmental monitoring of endocrine disrupters, Environ Sci Technol 39 (2005). https://doi.org/10.1021/es050728l.

[239] K. Kurauchi, Y. Nakaguchi, M. Tsutsumi, H. Hori, R. Kurihara, S. Hashimoto, R. Ohnuma, Y. Yamamoto, S. Matsuoka, S. Kawai, T. Hirata, M. Kinoshita, In vivo visual reporter system for detection of estrogen-like substances by transgenic medaka, Environ Sci Technol 39 (2005) 2762–2768. https://doi.org/10.1021/es0486465.

[240] A. Yamaguchi, K. Kato, K. Arizono, N. Tominaga, Induction of the estrogen-responsive genes encoding choriogenin H and L in the liver of male medaka (Oryzias latipes) upon exposure to estrogen receptor subtype-selective ligands, Journal of Applied Toxicology 35 (2015). https://doi.org/10.1002/jat.3063.

[241] M. Bondesson, R. Hao, C.Y. Lin, C. Williams, J.Å. Gustafsson, Estrogen receptor signaling during vertebrate development, Biochim. Biophys. Acta - Gene Regul. 1849 (2015) 142–151. https://doi.org/10.1016/j.bbagrm.2014.06.005.

[242] M.C. Campos-Mañas, S.M. Cuevas, I. Ferrer, E.M. Thurman, J.A. Sánchez-Pérez, A. Agüera, Determination of dextromethorphan and dextrorphan solar photo-transformation products by LC/Q-TOF-MS: Laboratory scale experiments and real water samples analysis, Environmental Pollution 265 (2020). https://doi.org/10.1016/j.envpol.2020.114722.

[243] K. Chen, X. Liu, X. Wu, J. Xu, F. Dong, Y. Zheng, The degradation dynamics and rapid detection of thiacloprid and its degradation products in water and soil by UHPLC-QTOF-MS, Chemosphere 263 (2021). https://doi.org/10.1016/j.chemosphere.2020.127960.

[244] G.P. Black, G. He, M.S. Denison, T.M. Young, Using Estrogenic Activity and Nontargeted Chemical Analysis to Identify Contaminants in Sewage Sludge, Environ Sci Technol 55 (2021). https://doi.org/10.1021/acs.est.0c07846.

[245] J.C.F. Law, Y. Huang, C.H. Chow, T.K. Lam, K.S.Y. Leung, Comparative physicochemical properties and toxicity of organic UV filters and their photocatalytic transformation products, Environmental Pollution 286 (2021). https://doi.org/10.1016/j.envpol.2021.117551.

[246] N. Zwart, W. Jonker, R. ten Broek, J. de Boer, G. Somsen, J. Kool, T. Hamers, C.J. Houtman, M.H. Lamoree, Identification of mutagenic and endocrine disrupting compounds in surface water and wastewater treatment plant effluents using high-resolution effect-directed analysis, Water Res 168 (2020). https://doi.org/10.1016/j.watres.2019.115204.

[247] C.J. Houtman, R. ten Broek, Y. van Oorschot, D. Kloes, R. van der Oost, M. Rosielle, M.H. Lamoree, High resolution effect-directed analysis of steroid hormone (ant)agonists in surface

and wastewater quality monitoring, Environ Toxicol Pharmacol 80 (2020). https://doi.org/10.1016/j.etap.2020.103460.

[248] European Medicines Agency, European Medicines Agency, Guideline on bioanalytical method validation, Reference Number EMEA/CHMP/EWP/192217/2009 (2012).

[249] OECD, OECD Series on Testing and Assessment n° 54 Current Approaches in the Statistical Analysis of Ecotoxicity Data: a Guidance To Application ENV/JM/MONO(2006)18, n.d.

[250] A. Shareef, M.J. Angove, J.D. Wells, B.B. Johnson, Aqueous solubilities of estrone, 17β-estradiol, 17α- ethynylestradiol, and bisphenol A, J Chem Eng Data 51 (2006). https://doi.org/10.1021/je050318c.

[251] A. Farhat, J. Keller, S. Tait, J. Radjenovic, Assessment of the impact of chloride on the formation of chlorinated by-products in the presence and absence of electrochemically activated sulfate, Chemical Engineering Journal 330 (2017). https://doi.org/10.1016/j.cej.2017.08.033.

[252] R. Dhawle, Z. Frontistis, D. Mantzavinos, Electrochemical Oxidation of Anastrozole over a BDD Electrode: Role of Operating Parameters and Water Matrix, Processes 10 (2022). https://doi.org/10.3390/pr10112391.

[253] N. Pueyo, M.P. Ormad, N. Miguel, P. Kokkinos, A. Ioannidi, D. Mantzavinos, Z. Frontistis, Electrochemical oxidation of butyl paraben on boron doped diamond in environmental matrices and comparison with sulfate radical-AOP, J Environ Manage 269 (2020). https://doi.org/10.1016/j.jenvman.2020.110783.

[254] Z. Frontistis, D. Mantzavinos, S. Meriç, Degradation of antibiotic ampicillin on boron-doped diamond anode using the combined electrochemical oxidation - Sodium persulfate process, J Environ Manage 223 (2018). https://doi.org/10.1016/j.jenvman.2018.06.099.

[255] Y. Ning, K. Li, Z. Zhao, D. Chen, Y. Li, Y. Liu, Q. Yang, B. Jiang, Simultaneous electrochemical degradation of organophosphorus pesticides and recovery of phosphorus: Synergistic effect of anodic oxidation and cathodic precipitation, J Taiwan Inst Chem Eng 125 (2021). https://doi.org/10.1016/j.jtice.2021.06.039.

[256] Y. Lei, X. Lei, P. Westerhoff, X. Zhang, X. Yang, Reactivity of Chlorine Radicals (Cl•and Cl2•-) with Dissolved Organic Matter and the Formation of Chlorinated Byproducts, Environ Sci Technol 55 (2021). https://doi.org/10.1021/acs.est.0c05596.

[257] S. Garcia-Segura, J. Keller, E. Brillas, J. Radjenovic, Removal of organic contaminants from secondary effluent by anodic oxidation with a boron-doped diamond anode as tertiary treatment, J Hazard Mater 283 (2015) 551–557. https://doi.org/10.1016/j.jhazmat.2014.10.003.

[258] P. Niziński, A. Błażewicz, J. Kończyk, R. Michalski, Perchlorate – Properties, toxicity and human health effects: An updated review, Rev Environ Health 36 (2021) 199–222. https://doi.org/10.1515/reveh-2020-0006.

[259] D.J. Van Wijk, S.G.M. Kroon, I.C.M. Garttener-Arends, Toxicity of chlorate and chlorite to selected species of algae, bacteria, and fungi, Ecotoxicol Environ Saf 40 (1998) 206–211. https://doi.org/10.1006/eesa.1998.1685.

[260] W. Sun, S. Li, J. Mai, J. Ni, Initial photocatalytic degradation intermediates/pathways of 17α-ethynylestradiol: Effect of pH and methanol, Chemosphere 81 (2010) 92–99. https://doi.org/10.1016/j.chemosphere.2010.06.051.

[261] Y. Zhou, J. Jiang, Y. Gao, S.Y. Pang, J. Ma, J. Duan, Q. Guo, J. Li, Y. Yang, Oxidation of steroid estrogens by peroxymonosulfate (PMS) and effect of bromide and chloride ions: Kinetics,

products, and modeling, Water Res 138 (2018) 56–66. https://doi.org/10.1016/j.watres.2018.03.045.

[262] K.M. Vieira, C.C. Nascentes, R. Augusti, Ozonation of ethinylestradiol in aqueous-methanolic solution: Direct monitoring by electrospray ionization mass spectrometry, J Braz Chem Soc 21 (2010). https://doi.org/10.1590/S0103-50532010000500004.

[263] O.J. Pozo, P. Van Eenoo, K. Deventer, S. Grimalt, J. V. Sancho, F. Hernández, F.T. Delbeke, Collision-induced dissociation of 3-keto anabolic steroids and related compounds after electrospray ionization. Considerations for structural elucidation, Rapid Communications in Mass Spectrometry 22 (2008). https://doi.org/10.1002/rcm.3823.

[264] T. Olmez-Hanci, I. Arslan-Alaton, Comparison of sulfate and hydroxyl radical based advanced oxidation of phenol, Chemical Engineering Journal 224 (2013). https://doi.org/10.1016/j.cej.2012.11.007.

[265] E. Vulliet, L. Wiest, R. Baudot, M.F. Grenier-Loustalot, Multi-residue analysis of steroids at sub-ng/L levels in surface and ground-waters using liquid chromatography coupled to tandem mass spectrometry, J Chromatogr A 1210 (2008). https://doi.org/10.1016/j.chroma.2008.09.034.

[266] P. Labadie, E.M. Hill, Analysis of estrogens in river sediments by liquid chromatography-electrospray ionisation mass spectrometry. Comparison of tandem mass spectrometry and time-of-flight mass spectrometry, J Chromatogr A 1141 (2007). https://doi.org/10.1016/j.chroma.2006.12.045.

[267] Q. Mei, J. Sun, D. Han, B. Wei, Z. An, X. Wang, J. Xie, J. Zhan, M. He, Sulfate and hydroxyl radicals-initiated degradation reaction on phenolic contaminants in the aqueous phase: Mechanisms, kinetics and toxicity assessment, Chemical Engineering Journal 373 (2019). https://doi.org/10.1016/j.cej.2019.05.095.

[268] T. Miyazaki, Y. Katsumura, M. Lin, Y. Muroya, H. Kudo, M. Taguchi, M. Asano, M. Yoshida, Radiolysis of phenol in aqueous solution at elevated temperatures, Radiation Physics and Chemistry 75 (2006). https://doi.org/10.1016/j.radphyschem.2005.09.009.

[269] L. Wojnárovits, J. Wang, L. Chu, E. Takács, Rate constants of chlorine atom reactions with organic molecules in aqueous solutions, an overview, Environmental Science and Pollution Research 29 (2022) 55492–55513. https://doi.org/10.1007/s11356-022-20807-9.

[270] G. Gervais, E. Bichon, J.P. Antignac, F. Monteau, G. Leroy, L. Barritaud, M. Chachignon, V. Ingrand, P. Roche, B. Le Bizec, Differential global profiling as a new analytical strategy for revealing micropollutant treatment by-products: Application to ethinylestradiol and chlorination water treatment, Chemosphere 83 (2011) 1553–1559. https://doi.org/10.1016/j.chemosphere.2011.01.027.

[271] S. Hwang, D.I. Lee, C.H. Lee, I.S. Ahn, Oxidation of 17α-ethinylestradiol with Mn(III) and product identification, J Hazard Mater 155 (2008) 334–341. https://doi.org/10.1016/j.jhazmat.2007.11.115.

[272] K. Moriyama, H. Matsufuji, M. Chino, M. Takeda, Identification and behavior of reaction products formed by chlorination of ethynylestradiol, Chemosphere 55 (2004). https://doi.org/10.1016/j.chemosphere.2003.11.045.

[273] Y. Lee, U. Von Gunten, Transformation of 17#-ethinylestradiol during water chlorination: Effects of bromide on kinetics, products, and transformation pathways, Environ Sci Technol 43 (2009). https://doi.org/10.1021/es8023989.

[274] J. Hu, S. Cheng, T. Aizawa, Y. Terao, S. Kunikane, Products of Aqueous Chlorination of 17β-Estradiol and Their Estrogenic Activities, Environ Sci Technol 37 (2003). https://doi.org/10.1021/es034324+.

[275] F. Guan, L.R. Soma, Y. Luo, C.E. Uboh, S. Peterman, Collision-induced dissociation pathways of anabolic steroids by electrospray ionization tandem mass spectrometry, J Am Soc Mass Spectrom 17 (2006) 477–489. https://doi.org/10.1016/j.jasms.2005.11.021.

[276] A.R. Lado Ribeiro, N.F.F. Moreira, G. Li Puma, A.M.T. Silva, Impact of water matrix on the removal of micropollutants by advanced oxidation technologies, Chemical Engineering Journal 363 (2019). https://doi.org/10.1016/j.cej.2019.01.080.

[277] F.E. Titchou, H. Zazou, H. Afanga, J. El Gaayda, R. Ait Akbour, P.V. Nidheesh, M. Hamdani, An overview on the elimination of organic contaminants from aqueous systems using electrochemical advanced oxidation processes, Journal of Water Process Engineering 41 (2021). https://doi.org/10.1016/j.jwpe.2021.102040.

[278] J. Russo, M.H. Lareef, G. Balogh, S. Guo, I.H. Russo, Estrogen and its metabolites are carcinogenic agents in human breast epithelial cells, Journal of Steroid Biochemistry and Molecular Biology 87 (2003). https://doi.org/10.1016/S0960-0760(03)00390-X.

[279] V.K. Turan, R.I. Sanchez, J.J. Li, S.A. Li, K.R. Reuhl, P.E. Thomas, A.H. Conney, M.A. Gallo, F.C. Kauffman, S. Mesia-Vela, The effects of steroidal estrogens in ACI rat mammary carcinogenesis: 17β-estradiol, 2-hydroxyestradiol, 4-hydroxyestradiol, 16α-hydroxyestradiol, and 4-hydroxyestrone, Journal of Endocrinology 183 (2004). https://doi.org/10.1677/joe.1.05802.

[280] J.G. Liehr, M.J. Ricci, 4-Hydroxylation of estrogens as marker of human mammary tumors, Proc Natl Acad Sci U S A 93 (1996). https://doi.org/10.1073/pnas.93.8.3294.

[281] H.K. Bhat, G. Calaf, T.K. Hei, T. Loya, J. V. Vadgama, Critical role of oxidative stress in estrogen-induced carcinogenesis, Proc Natl Acad Sci U S A 100 (2003). https://doi.org/10.1073/pnas.0437929100.

[282] B.C. Lee, M. Kamata, Y. Akatsuka, M. Takeda, K. Ohno, T. Kamei, Y. Magara, Effects of chlorine on the decrease of estrogenic chemicals, Water Res 38 (2004). https://doi.org/10.1016/j.watres.2003.10.010.

[283] Y. Lee, B.I. Escher, U. Von Gunten, Efficient removal of estrogenic activity during oxidative treatment of waters containing steroid estrogens, Environ Sci Technol 42 (2008). https://doi.org/10.1021/es7023302.

[284] F.P. Chaves, G. Gomes, A. Della-Flora, A. Dallegrave, C. Sirtori, E.M. Saggioro, D.M. Bila, Comparative endocrine disrupting compound removal from real wastewater by UV/Cl and UV/H2O2: Effect of pH, estrogenic activity, transformation products and toxicity, Science of the Total Environment 746 (2020). https://doi.org/10.1016/j.scitotenv.2020.141041.

[285] J. Radjenović, M.J. Farré, Y. Mu, W. Gernjak, J. Keller, Reductive electrochemical remediation of emerging and regulated disinfection byproducts, Water Res 46 (2012). https://doi.org/10.1016/j.watres.2011.12.042.

[286] G. Hurwitz, P. Pornwongthong, S. Mahendra, E.M.V. Hoek, Degradation of phenol by synergistic chlorine-enhanced photo-assisted electrochemical oxidation, Chemical Engineering Journal 240 (2014). https://doi.org/10.1016/j.cej.2013.11.087.

[287] J.T. Petroff, A.H. Nguyen, A.J. Porter, F.D. Morales, M.P. Kennedy, D. Weinstein, H. El Nazer, R.D. McCulla, Enhanced photocatalytic dehalogenation of aryl halides by combined poly-p-phenylene (PPP) and TiO2 photocatalysts, J Photochem Photobiol A Chem 335 (2017). https://doi.org/10.1016/j.jphotochem.2016.11.024.

[288] Y. Wang, Y. Wei, W. Song, C. Chen, J. Zhao, Photocatalytic Hydrodehalogenation for the Removal of Halogenated Aromatic Contaminants, ChemCatChem 11 (2019). https://doi.org/10.1002/cctc.201801222.

[289] Z. Pan, C. Song, L. Li, H. Wang, Y. Pan, C. Wang, J. Li, T. Wang, X. Feng, Membrane technology coupled with electrochemical advanced oxidation processes for organic wastewater treatment: Recent advances and future prospects, Chemical Engineering Journal 376 (2019). https://doi.org/10.1016/j.cej.2019.01.188.

[290] P. Ma, H. Ma, S. Sabatino, A. Galia, O. Scialdone, Electrochemical treatment of real wastewater. Part 1: Effluents with low conductivity, Chemical Engineering Journal 336 (2018). https://doi.org/10.1016/j.cej.2017.11.046.

[291] N. Klidi, F. Proietto, F. Vicari, A. Galia, S. Ammar, A. Gadri, O. Scialdone, Electrochemical treatment of paper mill wastewater by electro-Fenton process, Journal of Electroanalytical Chemistry 841 (2019). https://doi.org/10.1016/j.jelechem.2019.04.022.

[292] S. Wongrakpanich, A. Wongrakpanich, K. Melhado, J. Rangaswami, A comprehensive review of non-steroidal anti-inflammatory drug use in the elderly, Aging Dis 9 (2018) 143–150. https://doi.org/10.14336/AD.2017.0306.

[293] T.L. da Silva, C.S.D. Costa, M.G.C. da Silva, M.G.A. Vieira, Overview of non-steroidal anti-inflammatory drugs degradation by advanced oxidation processes, J Clean Prod 346 (2022) 131226. https://doi.org/10.1016/j.jclepro.2022.131226.

[294] T.J. Gan, Diclofenac: an update on its mechanism of action and safety profile, Curr Med Res Opin 26 (2010) 1715–1731. https://doi.org/10.1185/03007995.2010.486301.

[295] V. Acuña, A. Ginebreda, J.R. Mor, M. Petrovic, S. Sabater, J. Sumpter, D. Barceló, Balancing the health benefits and environmental risks of pharmaceuticals: Diclofenac as an example, Environ Int 85 (2015) 327–333. https://doi.org/10.1016/j.envint.2015.09.023.

[296] R. Altman, B. Bosch, K. Brune, P. Patrignani, C. Young, Advances in NSAID development: Evolution of diclofenac products using pharmaceutical technology, Drugs 75 (2015) 859–877. https://doi.org/10.1007/s40265-015-0392-z.

[297] T.J. Gan, Diclofenac: An update on its mechanism of action and safety profile, Curr Med Res Opin 26 (2010) 1715–1731. https://doi.org/10.1185/03007995.2010.486301.

[298] P. Sathishkumar, K. Mohan, R.A.A. Meena, M. Balasubramanian, L. Chitra, A.R. Ganesan, T. Palvannan, S.K. Brar, F.L. Gu, Hazardous impact of diclofenac on mammalian system: Mitigation strategy through green remediation approach, J Hazard Mater 419 (2021) 126135. https://doi.org/10.1016/j.jhazmat.2021.126135.

[299] L. Lonappan, S.K. Brar, R.K. Das, M. Verma, R.Y. Surampalli, Diclofenac and its transformation products: Environmental occurrence and toxicity - A review, Environ Int 96 (2016) 127–138. https://doi.org/10.1016/j.envint.2016.09.014.

[300] P. Sathishkumar, R.A.A. Meena, T. Palanisami, V. Ashokkumar, T. Palvannan, F.L. Gu, Occurrence, interactive effects and ecological risk of diclofenac in environmental compartments and biota - a review, Sci Total Environ 698 (2020) 134057. https://doi.org/10.1016/j.scitotenv.2019.134057.

[301] M.C. Lu, Y.Y. Chen, M.R. Chiou, M.Y. Chen, H.J. Fan, Occurrence and treatment efficiency of pharmaceuticals in landfill leachates, Waste Manage 55 (2016) 257–264. https://doi.org/10.1016/j.wasman.2016.03.029.

[302] P. Branchet, N. Ariza Castro, H. Fenet, E. Gomez, F. Courant, D. Sebag, J. Gardon, C. Jourdan, B. Ngounou Ngatcha, I. Kengne, E. Cadot, C. Gonzalez, Anthropic impacts on Sub-Saharan urban water resources through their pharmaceutical contamination (Yaoundé Center Region, Cameroon), Sci Total Environ 660 (2019) 886–898. https://doi.org/10.1016/j.scitotenv.2018.12.256.

[303] C. Carrara, C.J. Ptacek, W.D. Robertson, D.W. Blowes, M.C. Moncur, E. Sverko, S. Backus, Fate of pharmaceutical and trace organic compounds in three septic system plumes, Ontario, Canada, Environ Sci Technol 42 (2008) 2805–2811. https://doi.org/10.1021/es070344q.

[304] G. Teijon, L. Candela, K. Tamoh, A. Molina-Díaz, A.R. Fernández-Alba, Occurrence of emerging contaminants, priority substances (2008/105/CE) and heavy metals in treated wastewater and groundwater at Depurbaix facility (Barcelona, Spain), Sci Total Environ 408 (2010) 3584–3595. https://doi.org/10.1016/j.scitotenv.2010.04.041.

[305] A.M. Ali, H.T. Rønning, W.M. Al Arif, R. Kallenborn, R. Kallenborn, Occurrence of pharmaceuticals and personal care products in effluent-dominated Saudi Arabian coastal waters of the Red Sea, Chemosphere 175 (2017) 505–513. https://doi.org/10.1016/j.chemosphere.2017.02.095.

[306] A. Togola, H. Budzinski, Multi-residue analysis of pharmaceutical compounds in aqueous samples, J Chromatogr A 1177 (2008) 150–158. https://doi.org/10.1016/j.chroma.2007.10.105.

[307] E. Vulliet, C. Cren-Olivé, Screening of pharmaceuticals and hormones at the regional scale, in surface and groundwaters intended to human consumption, Environ Pollut 159 (2011) 2929–2934. https://doi.org/10.1016/j.envpol.2011.04.033.

[308] D. Simazaki, R. Kubota, T. Suzuki, M. Akiba, T. Nishimura, S. Kunikane, Occurrence of selected pharmaceuticals at drinking water purification plants in Japan and implications for human health, Water Res 76 (2015) 187–200. https://doi.org/10.1016/j.watres.2015.02.059.

[309] E. Carmona, V. Andreu, Y. Picó, Occurrence of acidic pharmaceuticals and personal care products in Turia River Basin: From waste to drinking water, Sci Total Environ 484 (2014) 53–63. https://doi.org/10.1016/j.scitotenv.2014.02.085.

[310] N. Vieno, M. Sillanpää, Fate of diclofenac in municipal wastewater treatment plant - A review, Environ Int 69 (2014) 28–39. https://doi.org/10.1016/j.envint.2014.03.021.

[311] S. Sari, G. Ozdemir, C. Yangin-Gomec, G.E. Zengin, E. Topuz, E. Aydin, E. Pehlivanoglu-Mantas, D. Okutman Tas, Seasonal variation of diclofenac concentration and its relation with wastewater characteristics at two municipal wastewater treatment plants in Turkey, J Hazard Mater 272 (2014) 155–164. https://doi.org/10.1016/j.jhazmat.2014.03.015.

[312] J. Kapelewska, U. Kotowska, J. Karpińska, D. Kowalczuk, A. Arciszewska, A. Świrydo, Occurrence, removal, mass loading and environmental risk assessment of emerging organic contaminants in leachates, groundwaters and wastewaters, Microchem J 137 (2018) 292–301. https://doi.org/10.1016/j.microc.2017.11.008.

[313] F.O. Agunbiade, B. Moodley, Occurrence and distribution pattern of acidic pharmaceuticals in surface water, wastewater, and sediment of the Msunduzi River, Kwazulu-Natal, South Africa, Environ Toxicol Chem 35 (2016) 36–46. https://doi.org/10.1002/etc.3144.

[314] M. Ashfaq, K. Nawaz Khan, M. Saif Ur Rehman, G. Mustafa, M. Faizan Nazar, Q. Sun, J. Iqbal, S.I. Mulla, C.P. Yu, Ecological risk assessment of pharmaceuticals in the receiving environment of pharmaceutical wastewater in Pakistan, Ecotoxicol Environ Saf 136 (2017) 31–39. https://doi.org/10.1016/j.ecoenv.2016.10.029.

[315] D. Stülten, S. Zühlke, M. Lamshöft, M. Spiteller, Occurrence of diclofenac and selected metabolites in sewage effluents, Sci Total Environ 405 (2008) 310–316. https://doi.org/10.1016/j.scitotenv.2008.05.036.

[316] C. Kuang, G. Zeng, Y. Zhou, Y. Wu, D. Li, Y. Wang, C. Li, Integrating anodic sulfate activation with cathodic H2O2 production/activation to generate the sulfate and hydroxyl radicals for the degradation of emerging organic contaminants, Water Res 229 (2023). https://doi.org/10.1016/j.watres.2022.119464.

[317] D. Fatta-Kassinos, M.I. Vasquez, K. Kümmerer, Transformation products of pharmaceuticals in surface waters and wastewater formed during photolysis and advanced oxidation processes - Degradation, elucidation of byproducts and assessment of their biological potency, Chemosphere 85 (2011) 693–709. https://doi.org/10.1016/j.chemosphere.2011.06.082.

[318] B. Bonnefille, E. Gomez, F. Courant, A. Escande, H. Fenet, Diclofenac in the marine environment: A review of its occurrence and effects, Mar Pollut Bull 131 (2018) 496–506. https://doi.org/10.1016/j.marpolbul.2018.04.053.

[319] M.K. Fontes, P.K. Gusso-Choueri, L.A. Maranho, D.M. de S. Abessa, W.A. Mazur, B.G. de Campos, L.L. Guimarães, M.S. de Toledo, D. Lebre, J.R. Marques, A.A. Felicio, A. Cesar, E.A. Almeida, C.D.S. Pereira, A tiered approach to assess effects of diclofenac on the brown mussel Perna perna: A contribution to characterize the hazard, Water Res 132 (2018) 361–370. https://doi.org/10.1016/j.watres.2017.12.077.

[320] J. Guo, S. Liu, L. Zhou, B. Cheng, Q. Li, Prioritizing pharmaceuticals based on environmental risks in the aquatic environment in China, J Environ Manage 278 (2021) 111479. https://doi.org/10.1016/j.jenvman.2020.111479.

[321] Y. Li, L. Zhang, X. Liu, J. Ding, Ranking and prioritizing pharmaceuticals in the aquatic environment of China, Sci Total Environ 658 (2019) 333–342. https://doi.org/10.1016/j.scitotenv.2018.12.048.

[322] D.M. Kristensen, S. Mazaud-Guittot, P. Gaudriault, L. Lesné, T. Serrano, K.M. Main, B. Jégou, Analgesic use-prevalence, biomonitoring and endocrine and reproductive effects, Nat Rev Endocrinol 12 (2016) 381–393. https://doi.org/10.1038/nrendo.2016.55.

[323] G.S. Branco, R.G. Moreira, M.I. Borella, M. de P. Camargo, M. Muñoz-Peñuela, A.D.O. Gomes, C.E. Tolussi, Nonsteroidal anti-inflammatory drugs act as endocrine disruptors in Astyanax lacustris (Teleostei: Characidae) reproduction: An ex vivo approach, Aquat Toxicol 232 (2021) 105767. https://doi.org/10.1016/j.aquatox.2021.105767.

[324] N.J. Efosa, W. Kleiner, W. Kloas, F. Hoffmann, Diclofenac can exhibit estrogenic modes of action in male Xenopus laevis, and affects the hypothalamus-pituitary-gonad axis and mating vocalizations, Chemosphere 173 (2017) 69–77. https://doi.org/10.1016/j.chemosphere.2017.01.030.

[325] K. Ji, X. Liu, S. Lee, S. Kang, Y. Kho, J.P. Giesy, K. Choi, Effects of non-steroidal anti-inflammatory drugs on hormones and genes of the hypothalamic-pituitary-gonad axis, and reproduction of zebrafish, J Hazard Mater 254–255 (2013). https://doi.org/10.1016/j.jhazmat.2013.03.036.

[326] I. Klopčič, T. Markovič, I. Mlinarič-Raščan, M. Sollner Dolenc, Endocrine disrupting activities and immunomodulatory effects in lymphoblastoid cell lines of diclofenac, 4-hydroxydiclofenac and paracetamol, Toxicol Lett 294 (2018) 95–104. https://doi.org/10.1016/j.toxlet.2018.05.022.

[327] G.A. Brent, Mechanisms of thyroid hormone action, J Clin Invest 122 (2012) 3035–3043. https://doi.org/10.1172/JCI60047.

[328] P.D. Noyes, K.P. Friedman, P. Browne, J.T. Haselman, M.E. Gilbert, M.W. Hornung, S. Barone, K.M. Crofton, S.C. Laws, T.E. Stoker, S.O. Simmons, J.E. Tietge, S.J. Degitz, Evaluating chemicals for thyroid disruption: Opportunities and challenges with in Vitro testing and adverse outcome pathway approaches, Environ Health Perspect 127 (2019). https://doi.org/10.1289/EHP5297.

[329] J.R. Tata, Amphibian metamorphosis as a model for the developmental actions of thyroid hormone, Mol Cell Endocrinol 246 (2006) 10–20. https://doi.org/10.1016/j.mce.2005.11.024.

[330] A.A. Thambirajah, E.M. Koide, J.J. Imbery, C.C. Helbing, Contaminant and environmental influences on thyroid hormone action in amphibian metamorphosis, Front Endocrinol (Lausanne) 10 (2019). https://doi.org/10.3389/fendo.2019.00276.

[331] B.J. Mengeling, Y. Wei, L.N. Dobrawa, M. Streekstra, J. Louisse, V. Singh, L. Singh, P.J. Lein, H. Wulff, A.J. Murk, J.D. Furlow, A multi-tiered, in vivo, quantitative assay suite for environmental disruptors of thyroid hormone signaling, Aquat Toxicol 190 (2017) 1–10. https://doi.org/10.1016/j.aquatox.2017.06.019.

[332] R.J. Denver, S. Pavgi, Y.B. Shi, Thyroid hormone-dependent gene expression program for Xenopus neural development, J Biol Chem 272 (1997) 8179–8188. https://doi.org/10.1074/jbc.272.13.8179.

[333] J.B. Fini, B.B. Mughal, S. Le Mével, M. Leemans, M. Lettmann, P. Spirhanzlova, P. Affaticati, A. Jenett, B.A. Demeneix, Human amniotic fluid contaminants alter thyroid hormone signalling and early brain development in Xenopus embryos, Sci Rep 7 (2017) 43786. https://doi.org/10.1038/srep43786.

[334] F.D.L. Leusch, N.H. Aneck-Hahn, J.A.E. Cavanagh, D. Du Pasquier, T. Hamers, A. Hebert, P.A. Neale, M. Scheurer, S.O. Simmons, M. Schriks, Comparison of in vitro and in vivo bioassays to measure thyroid hormone disrupting activity in water extracts, Chemosphere 191 (2018) 868–875. https://doi.org/10.1016/j.chemosphere.2017.10.109.

[335] TG 248: Xenopus Eleutheroembryonic Thyroid Assay (XETA), OECD, 2019. https://doi.org/10.1787/a13f80ee-en.

[336] N. Zahn, C. James-Zorn, V.G. Ponferrada, D.S. Adams, J. Grzymkowski, D.R. Buchholz, N.M. Nascone-Yoder, M. Horb, S.A. Moody, P.D. Vize, A.M. Zorn, Normal Table of Xenopus development: a new graphical resource, Development (Cambridge) 149 (2022) dev200356. https://doi.org/10.1242/dev.200356.

[337] P. Spirhanzlova, B. De Groef, F.E. Nicholson, S.V.H. Grommen, G. Marras, A. Sébillot, B.A. Demeneix, S. Pallud-Mothré, G.F. Lemkine, A.J. Tindall, D. Du Pasquier, Using short-term bioassays to evaluate the endocrine disrupting capacity of the pesticides linuron and fenoxycarb, Comp Biochem Physiol C Toxicol Pharmacol 200 (2017) 52–58. https://doi.org/10.1016/j.cbpc.2017.06.006.

[338] N.M. O'Boyle, M. Banck, C.A. James, C. Morley, T. Vandermeersch, G.R. Hutchison, Open Babel: An Open chemical toolbox, J Cheminform 3 (2011). https://doi.org/10.1186/1758-2946-3-33.

[339] R.L. Wagner, B.R. Huber, A.K. Shiau, A. Kelly, S.T. Cunha Lima, T.S. Scanlan, J.W. Apriletti, J.D. Baxter, B.L. West, R.J. Fletterick, Hormone selectivity in thyroid hormone receptors, Mol Cell Endocrinol 15 (2001) 398–410. https://doi.org/10.1210/mend.15.3.0608.

[340] A. Kapałka, G. Fóti, C. Comninellis, Kinetic modelling of the electrochemical mineralization of organic pollutants for wastewater treatment, J Appl Electrochem 38 (2008) 7–16. https://doi.org/10.1007/s10800-007-9365-6.

[341] E. Brillas, S. Garcia-Segura, M. Skoumal, C. Arias, Electrochemical incineration of diclofenac in neutral aqueous medium by anodic oxidation using Pt and boron-doped diamond anodes, Chemosphere 79 (2010) 605–612. https://doi.org/10.1016/j.chemosphere.2010.03.004.

[342] L.A. Pérez-Estrada, S. Malato, W. Gernjak, A. Agüera, E.M. Thurman, I. Ferrer, A.R. Fernández-Alba, Photo-fenton degradation of diclofenac: Identification of main intermediates and degradation pathway, Environ Sci Technol 39 (2005) 8300–8306. https://doi.org/10.1021/es050794n.

[343] J. Yang, G. Lv, T. Li, S. Sun, X. Sun, Theoretical insight into the degradation of diclofenac by hydroxyl and sulfate radicals in aqueous-phase: Mechanisms, kinetics and eco-toxicity, J Environ Chem Eng 10 (2022) 108311. https://doi.org/10.1016/j.jece.2022.108311.

[344] S. Agopcan Cinar, A. Ziylan-Yavaş, S. Catak, N.H. Ince, V. Aviyente, Hydroxyl radical-mediated degradation of diclofenac revisited: a computational approach to assessment of reaction mechanisms and by-products, Environ Sci Pollut Res Int 24 (2017) 18458–18469. https://doi.org/10.1007/s11356-017-9482-7.

[345] M.M. Sein, M. Zedda, J. Tuerk, T.C. Schmidt, A. Golloch, C. Von Sonntag, Oxidation of diclofenac with ozone in aqueous solution, Environ Sci Technol 42 (2008) 6656–6662. https://doi.org/10.1021/es8008612.

[346] X. Zhao, Y. Hou, H. Liu, Z. Qiang, J. Qu, Electro-oxidation of diclofenac at boron doped diamond: Kinetics and mechanism, Electrochim Acta 54 (2009) 4172–4179. https://doi.org/10.1016/j.electacta.2009.02.059.

[347] J. Hartmann, P. Bartels, U. Mau, M. Witter, W. v. Tümpling, J. Hofmann, E. Nietzschmann, Degradation of the drug diclofenac in water by sonolysis in presence of catalysts, Chemosphere 70 (2008) 453–461. https://doi.org/10.1016/j.chemosphere.2007.06.063.

[348] J.B. Fini, S. Le Mevel, N. Turque, K. Palmier, D. Zalko, J.P. Cravedi, B.A. Demeneix, An in vivo multiwell-based fluorescent screen for monitoring vertebrate thyroid hormone disruption, Environ Sci Technol 41 (2007) 5908–5914. https://doi.org/10.1021/es0704129.

[349] J.P. Chae, M.S. Park, Y.S. Hwang, B.H. Min, S.H. Kim, H.S. Lee, M.J. Park, Evaluation of developmental toxicity and teratogenicity of diclofenac using Xenopus embryos, Chemosphere 120 (2015) 52–58. https://doi.org/10.1016/j.chemosphere.2014.05.063.

[350] J.D. Cardoso-Vera, H. Islas-Flores, N. SanJuan-Reyes, E.I. Montero-Castro, M. Galar-Martínez, S. García-Medina, A. Elizalde-Velázquez, O. Dublán-García, L.M. Gómez-Oliván, Comparative study of diclofenac-induced embryotoxicity and teratogenesis in Xenopus laevis and Lithobates catesbeianus, using the frog embryo teratogenesis assay: Xenopus (FETAX), Sci Total Environ 574 (2017) 467–475. https://doi.org/10.1016/j.scitotenv.2016.09.095.

[351] M. Saravanan, J.H. Hur, N. Arul, M. Ramesh, Toxicological effects of clofibric acid and diclofenac on plasma thyroid hormones of an Indian major carp, Cirrhinus mrigala during short and long-term exposures, Environ Toxicol Pharmacol 38 (2014) 948–958. https://doi.org/10.1016/j.etap.2014.10.013.

[352] H. Wang, F. Dong, Y. Zhao, S. Fu, H. Zhao, S. Liu, W. Zhang, F. Hu, Exposure to diclofenac alters thyroid hormone levels and transcription of genes involved in the hypothalamic–pituitary–thyroid axis in zebrafish embryos/larvae, Comp Biochem Physiol C Toxicol Pharmacol 257 (2022) 109335. https://doi.org/10.1016/j.cbpc.2022.109335.

[353] T.K. Motawi, S.A. Ahmed, N.A. El-Boghdady, N.S. Metwally, N.N. Nasr, Protective effects of betanin against paracetamol and diclofenac induced neurotoxicity and endocrine disruption in rats, Biomarkers 24 (2019) 645–651. https://doi.org/10.1080/1354750X.2019.1642958.

[354] M. Boas, U. Feldt-Rasmussen, K.M. Main, Thyroid effects of endocrine disrupting chemicals, Mol Cell Endocrinol 355 (2012) 240–248. https://doi.org/10.1016/j.mce.2011.09.005.

[355] A. Ishihara, N. Nishiyama, Y. Makita, K. Yamauchi, The genomic structure and the expression profile of the Xenopus laevis transthyretin gene, Gene 510 (2012) 126–132. https://doi.org/10.1016/j.gene.2012.09.002.

[356] P. Prapunpoj, K. Yamauchi, N. Nishiyama, S.J. Richardson, G. Schreiber, Evolution of structure, ontogeny of gene expression, and function of Xenopus laevis transthyretin, Am J Physiol Regul Integr Comp Physiol 279 (2000) R2026–R2041. https://doi.org/10.1152/ajpregu.2000.279.6.r2026.

[357] A. Ishihara, N. Nishiyama, S.I. Sugiyama, K. Yamauchi, The effect of endocrine disrupting chemicals on thyroid hormone binding to Japanese quail transthyretin and thyroid hormone receptor, Gen Comp Endocrinol 134 (2003) 36–43. https://doi.org/10.1016/S0016-6480(03)00197-7.

[358] K. Miyata, K. Ose, Thyroid hormone-disrupting effects and the amphibian metamorphosis assay, J Toxicol Pathol 25 (2012) 1–9. https://doi.org/10.1293/tox.25.1.

[359] T. Klabunde, H.M. Petrassi, V.B. Oza, P. Raman, J.W. Kelly, J.C. Sacchettini, Rational design of potent human transthyretin amyloid disease inhibitors, Nat Struct Biol 7 (2000) 312–321. https://doi.org/10.1038/74082.

[360] V.B. Oza, C. Smith, P. Raman, E.K. Koepf, H.A. Lashuel, H.M. Petrassi, K.P. Chiang, E.T. Powers, J. Sachettinni, J.W. Kelly, Synthesis, structure, and activity of diclofenac analogues as transthyretin amyloid fibril formation inhibitors, J Med Chem 45 (2002) 321–332. https://doi.org/10.1021/jm010257n.

[361] J.M. Weiss, P.L. Andersson, J. Zhang, E. Simon, P.E.G. Leonards, T. Hamers, M.H. Lamoree, Tracing thyroid hormone-disrupting compounds: Database compilation and structure-activity evaluation for an effect-directed analysis of sediment, Anal Bioanal Chem 407 (2015) 5625–5634. https://doi.org/10.1007/s00216-015-8736-9.

[362] H. Yu, E. Nie, J. Xu, S. Yan, W.J. Cooper, W. Song, Degradation of Diclofenac by Advanced Oxidation and Reduction Processes: Kinetic Studies, Degradation Pathways and Toxicity Assessments, Water Res 47 (2013) 1909–1918. https://doi.org/10.1016/j.watres.2013.01.016.

[363] T. Schulze, S. Weiss, E. Schymanski, P.C. von der Ohe, M. Schmitt-Jansen, R. Altenburger, G. Streck, W. Brack, Identification of a phytotoxic photo-transformation product of diclofenac using effect-directed analysis, Environ Pollut 158 (2010) 1461–1466. https://doi.org/10.1016/j.envpol.2009.12.032.

[364] M. Schmitt-Jansen, P. Bartels, N. Adler, R. Altenburger, Phytotoxicity assessment of diclofenac and its phototransformation products, in: Anal Bioanal Chem, 2007: pp. 1389–1396. https://doi.org/10.1007/s00216-006-0825-3.

[365] A. Achilleos, E. Hapeshi, N.P. Xekoukoulotakis, D. Mantzavinos, D. Fatta-Kassinos, Factors affecting diclofenac decomposition in water by UV-A/TiO2 photocatalysis, Chem Eng J 161 (2010) 53–59. https://doi.org/10.1016/j.cej.2010.04.020.

[366] X. Lu, Y. Shao, N. Gao, J. Chen, Y. Zhang, H. Xiang, Y. Guo, Degradation of diclofenac by UV-activated persulfate process: Kinetic studies, degradation pathways and toxicity assessments, Ecotoxicol Environ Saf 141 (2017) 139–147. https://doi.org/10.1016/j.ecoenv.2017.03.022.

[367] A. Ziylan, S. Dogan, S. Agopcan, R. Kidak, V. Aviyente, N.H. Ince, Sonochemical degradation of diclofenac: Byproduct assessment, reaction mechanisms and environmental considerations, Environ Sci Pollut Res Int 21 (2014) 5929–5939. https://doi.org/10.1007/s11356-014-2514-7.

[368] A.B.A. Boxall, C.J. Sinclair, K. Fenner, D. Kolpin, S.J. Maund, When synthetic chemicals degrade in the environment, Environ Sci Technol 38 (2004) 368A-375A.

[369] I. Klopčič, M.S. Dolenc, Chemicals and Drugs Forming Reactive Quinone and Quinone Imine Metabolites, Chem Res Toxicol 32 (2019) 1–34. https://doi.org/10.1021/acs.chemrestox.8b00213.

[370] Y. Kamaya, Y. Fukaya, K. Suzuki, Acute toxicity of benzoic acids to the crustacean Daphnia magna, Chemosphere 59 (2005) 255–261. https://doi.org/10.1016/j.chemosphere.2004.11.003.

[371] M.H. Keshavarz, F. Gharagheizi, A. Shokrolahi, S. Zakinejad, Accurate prediction of the toxicity of benzoic acid compounds in mice via oral without using any computer codes, J Hazard Mater 237–238 (2012) 79–101. https://doi.org/10.1016/j.jhazmat.2012.07.048.

[372] M. Matejczyk, P. Ofman, K. Dąbrowska, R. Świsłocka, W. Lewandowski, The study of biological activity of transformation products of diclofenac and its interaction with chlorogenic acid, J Environ Sci (China) 91 (2020) 128–141. https://doi.org/10.1016/j.jes.2020.01.022.

[373] S.W. Rowlinson, J.R. Kiefer, J.J. Prusakiewicz, J.L. Pawlitz, K.R. Kozak, A.S. Kalgutkar, W.C. Stallings, R.G. Kurumbail, L.J. Marnett, A Novel Mechanism of Cyclooxygenase-2 Inhibition Involving Interactions with Ser-530 and Tyr-385, J Biol Chem 278 (2003) 45763–45769. https://doi.org/10.1074/jbc.M305481200.

[374] C.A. Rouzer, L.J. Marnett, Structural and Chemical Biology of the Interaction of Cyclooxygenase with Substrates and Non-Steroidal Anti-Inflammatory Drugs, Chem Rev 120 (2020) 7592–7641. https://doi.org/10.1021/acs.chemrev.0c00215.

[375] F.F. Wang, W. Yang, Y.H. Shi, X.R. Cheng, G.W. Le, Structure-based approach for the study of thyroid hormone receptor binding affinity and subtype selectivity, J Biomol Struct Dyn 34 (2016) 2251–2267. https://doi.org/10.1080/07391102.2015.1113384.

[376] S. Borngraeber, M.J. Budny, G. Chiellini, S.T. Cunha-Lima, M. Togashi, P. Webb, J.D. Baxter, T.S. Scanlan, R.J. Fletterick, Ligand selectivity by seeking hydrophobicity in thyroid hormone receptor, Proc Natl Acad Sci U S A 100 (2003) 15358–15363. https://doi.org/10.1073/pnas.2136689100.

[377] K. Nakajima, I. Tazawa, Y.B. Shi, A unique role of thyroid hormone receptor β in regulating notochord resorption during Xenopus metamorphosis, Gen Comp Endocrinol 277 (2019) 66–72. https://doi.org/10.1016/j.ygcen.2019.03.006.

[378] J. Radjenovic, D.L. Sedlak, Challenges and Opportunities for Electrochemical Processes as Next-Generation Technologies for the Treatment of Contaminated Water, Environ Sci Technol 49 (2015) 11292–11302. https://doi.org/10.1021/acs.est.5b02414.

[379] U. Von Gunten, Oxidation Processes in Water Treatment: Are We on Track?, Environ Sci Technol 52 (2018) 5062–5075. https://doi.org/10.1021/acs.est.8b00586.

[380] M.S. Elovitz, U. Von Gunten, H.P. Kaiser, The influence of dissolved organic matter character on ozone decomposition rates and Rct, ACS Symposium Series 761 (2000) 248–269. https://doi.org/10.1021/bk-2000-0761.ch016.

[381] J.A. Leenheer, J.P. Croué, Characterizing aquatic dissolved organic matter, Environ Sci Technol 37 (2003) 18A-26A.

[382] M. Aeschbacher, C. Graf, R.P. Schwarzenbach, M. Sander, Antioxidant properties of humic substances, Environ Sci Technol 46 (2012) 4916–4925. https://doi.org/10.1021/es300039h.

[383] M. Bourgin, B. Beck, M. Boehler, E. Borowska, J. Fleiner, E. Salhi, R. Teichler, U. von Gunten, H. Siegrist, C.S. McArdell, Evaluation of a full-scale wastewater treatment plant upgraded with

ozonation and biological post-treatments: Abatement of micropollutants, formation of transformation products and oxidation by-products, Water Res 129 (2018) 486–498. https://doi.org/10.1016/j.watres.2017.10.036.

[384] C.K. Remucal, E. Salhi, N. Walpen, U. von Gunten, Molecular-Level Transformation of Dissolved Organic Matter during Oxidation by Ozone and Hydroxyl Radical, Environ Sci Technol 54 (2020) 10351–10360. https://doi.org/10.1021/acs.est.0c03052.

[385] J.M. Barazesh, C. Prasse, D.L. Sedlak, Electrochemical Transformation of Trace Organic Contaminants in the Presence of Halide and Carbonate Ions, Environ Sci Technol 50 (2016) 10143–10152. https://doi.org/10.1021/acs.est.6b02232.

[386] X.F. Li, W.A. Mitch, Drinking Water Disinfection Byproducts (DBPs) and Human Health Effects: Multidisciplinary Challenges and Opportunities, Environ Sci Technol 52 (2018) 1681–1689. https://doi.org/10.1021/acs.est.7b05440.

[387] M.E.H. Bergmann, A.S. Koparal, T. Iourtchouk, Electrochemical Advanced oxidation processes, formation of halogenate and perhalogenate species: A critical review, Crit Rev Environ Sci Technol 44 (2014) 348–390. https://doi.org/10.1080/10643389.2012.718948.

[388] K.S. Kumar, S. Kavitha, K. Parameswari, A. Sakunthala, P. Sathishkumar, Environmental occurrence, toxicity and remediation of perchlorate – A review, Chemosphere 311 (2023) 137017. https://doi.org/10.1016/j.chemosphere.2022.137017.

[389] G.O.S. Santos, K.I.B. Eguiluz, G.R. Salazar-Banda, C. Sáez, M.A. Rodrigo, Understanding the electrolytic generation of sulfate and chlorine oxidative species with different boron-doped diamond anodes, Journal of Electroanalytical Chemistry 857 (2020) 113756. https://doi.org/10.1016/j.jelechem.2019.113756.

[390] J.P. Gutkoski, E.E. Schneider, C. Michels, How effective is biological activated carbon in removing micropollutants? A comprehensive review, J Environ Manage 349 (2024) 119434. https://doi.org/https://doi.org/10.1016/j.jenvman.2023.119434.

[391] Y. Ling, M.J. Klemes, L. Xiao, A. Alsbaiee, W.R. Dichtel, D.E. Helbling, Benchmarking Micropollutant Removal by Activated Carbon and Porous β-Cyclodextrin Polymers under Environmentally Relevant Scenarios, Environ Sci Technol 51 (2017) 7590–7598. https://doi.org/10.1021/acs.est.7b00906.

[392] Y. Xie, L. Ren, X. Zhu, X. Gou, S. Chen, Physical and chemical treatments for removal of perchlorate from water–A review, Process Safety and Environmental Protection 116 (2018) 180–198. https://doi.org/https://doi.org/10.1016/j.psep.2018.02.009.

[393] J.G. Russel, V. Thulasiraman, R.R. Nair, S.C. Ravindran, U.N.S. Hareesh, K. Bhaskaran, A novel bio-physical approach for perchlorate contaminated well water treatment, Environmental Advances 4 (2021) 100058. https://doi.org/https://doi.org/10.1016/j.envadv.2021.100058.

[394] D. Seibert, C.F. Zorzo, F.H. Borba, R.M. de Souza, H.B. Quesada, R. Bergamasco, A.T. Baptista, J.J. Inticher, Occurrence, statutory guideline values and removal of contaminants of emerging concern by Electrochemical Advanced Oxidation Processes: A review, Science of the Total Environment 748 (2020) 141527. https://doi.org/10.1016/j.scitotenv.2020.141527.

[395] R. Fu, P.S. Zhang, Y.X. Jiang, L. Sun, X.H. Sun, Wastewater treatment by anodic oxidation in electrochemical advanced oxidation process: Advance in mechanism, direct and indirect oxidation detection methods, Chemosphere 311 (2023) 136993. https://doi.org/10.1016/j.chemosphere.2022.136993.

[396] R.S. van den Hurk, M. Pursch, D.R. Stoll, B.W.J. Pirok, Recent trends in two-dimensional liquid chromatography, TrAC - Trends in Analytical Chemistry 166 (2023) 117166. https://doi.org/10.1016/j.trac.2023.117166.

[397] J. Hollender, E.L. Schymanski, L. Ahrens, N. Alygizakis, F. Béen, L. Bijlsma, A.M. Brunner, A. Celma, A. Fildier, Q. Fu, P. Gago-Ferrero, R. Gil-Solsona, P. Haglund, M. Hansen, S. Kaserzon, A. Kruve, M. Lamoree, C. Margoum, J. Meijer, S. Merel, C. Rauert, P. Rostkowski, S. Samanipour, B. Schulze, T. Schulze, R.R. Singh, J. Slobodnik, T. Steininger-Mairinger, N.S. Thomaidis, A. Togola, K. Vorkamp, E. Vulliet, L. Zhu, M. Krauss, NORMAN guidance on suspect and non-target screening in environmental monitoring, Environ Sci Eur 35 (2023) 75. https://doi.org/10.1186/s12302-023-00779-4.

[398] A.J. Simpson, M.J. Simpson, R. Soong, Environmental Nuclear Magnetic Resonance Spectroscopy: An Overview and a Primer, Anal Chem 90 (2018) 628–639. https://doi.org/10.1021/acs.analchem.7b03241.

[399] P. Hajeb, L. Zhu, R. Bossi, K. Vorkamp, Sample preparation techniques for suspect and non-target screening of emerging contaminants, Chemosphere 287 (2022) 132306. https://doi.org/https://doi.org/10.1016/j.chemosphere.2021.132306.

[400] J. Radjenović, M. Petrović, D. Barceló, Complementary mass spectrometry and bioassays for evaluating pharmaceutical-transformation products in treatment of drinking water and wastewater, TrAC - Trends in Analytical Chemistry 28 (2009) 562–580. https://doi.org/10.1016/j.trac.2009.02.006.

[401] D. Zahn, H.P.H. Arp, K. Fenner, A. Georgi, J. Hafner, S.E. Hale, J. Hollender, T. Letzel, E.L. Schymanski, G. Sigmund, T. Reemtsma, Should Transformation Products Change the Way We Manage Chemicals?, Environ Sci Technol 58 (2024) 7710–7718. https://doi.org/10.1021/acs.est.4c00125.

[402] A. Sharma, J. Ahmad, S.J.S. Flora, Application of advanced oxidation processes and toxicity assessment of transformation products, Environ Res 167 (2018) 223–233. https://doi.org/10.1016/j.envres.2018.07.010.

[403] N. Burden, M.R. Embry, T.H. Hutchinson, S.G. Lynn, S.K. Maynard, C.A. Mitchell, F. Pellizzato, F. Sewell, K.L. Thorpe, L. Weltje, J.R. Wheeler, Investigating endocrine-disrupting properties of chemicals in fish and amphibians: Opportunities to apply the 3Rs, Integr Environ Assess Manag 18 (2022) 442–458. https://doi.org/10.1002/ieam.4497.

[404] M.A. La Merrill, L.N. Vandenberg, M.T. Smith, W. Goodson, P. Browne, H.B. Patisaul, K.Z. Guyton, A. Kortenkamp, V.J. Cogliano, T.J. Woodruff, L. Rieswijk, H. Sone, K.S. Korach, A.C. Gore, L. Zeise, R.T. Zoeller, Consensus on the key characteristics of endocrine-disrupting chemicals as a basis for hazard identification, Nat Rev Endocrinol 16 (2020) 45–57. https://doi.org/10.1038/s41574-019-0273-8.

[405] H. Zhang, N. Shen, Y. Li, C. Hu, P. Yuan, Source, transport, and toxicity of emerging contaminants in aquatic environments: A review on recent studies, Environmental Science and Pollution Research 30 (2023) 121420–121437. https://doi.org/10.1007/s11356-023-30869-y.

[406] U. von Gunten, Oxidation processes and me, Water Res 253 (2024) 121148. https://doi.org/https://doi.org/10.1016/j.watres.2024.121148.

[407] D. Minakata, U. von Gunten, Predicting Transformation Products during Aqueous Oxidation Processes: Current State and Outlook, Environ Sci Technol 57 (2023) 18410–18419. https://doi.org/10.1021/acs.est.3c04086.

[408] OECD, OECD Guideline for the Testing of Chemicals No. 316. Phototransformation of Chemicals in Water – Direct Photolysis, OECD Guideline for the Testing of Chemicals (2008).

[409] A. Michel, D. Armbruster, A. Benz-Birck, N. Deppermann, R. Doetzer, M. Flörs, M. Frericks, S. Li, S. Gebler, T. Schröder, W. Seitz, Proposal for a tiered approach to evaluate the risk of transformation products formed from pesticide residues during drinking water treatment, Environ Sci Eur 34 (2022). https://doi.org/10.1186/s12302-022-00688-y.

[410] M. Lee, L.C. Blum, E. Schmid, K. Fenner, U. von Gunten, A computer-based prediction platform for the reaction of ozone with organic compounds in aqueous solution: kinetics and mechanisms, Environ Sci Process Impacts 19 (2017) 465–476. https://doi.org/10.1039/C6EM00584E.

[411] P.R. Tentscher, M. Lee, U. von Gunten, Micropollutant Oxidation Studied by Quantum Chemical Computations: Methodology and Applications to Thermodynamics, Kinetics, and Reaction Mechanisms, Acc Chem Res 52 (2019) 605–614. https://doi.org/10.1021/acs.accounts.8b00610.

[412] A. Kienzler, M.G. Barron, S.E. Belanger, A. Beasley, M.R. Embry, Mode of Action (MOA) Assignment Classifications for Ecotoxicology: An Evaluation of Approaches, Environ Sci Technol 51 (2017) 10203–10211. https://doi.org/10.1021/acs.est.7b02337.

Scientific Acknowledgements

Funding agency

This PhD project was funded by the European Union's EU Framework Program for Research and Innovation Horizon 2020 [Grant Agreement No 861369, 2019, innoveox.eu].

Scientific contributions

In **Chapter 3**, I was responsible for the conceptualization, data curation, formal analysis, investigation, methodology, and the writing of the original draft. Marie Pardon and I contributed equally to the work presented in this chapter.

In **Chapter 4**, I was responsible for the conceptualization, methodology, validation, investigation, formal analysis, data curation, visualization, and the writing of the original draft.

In **Chapter 5,** I was responsible for the conceptualization, visualization, validation, software, methodology, investigation, formal analysis, data curation, and the writing of the original draft.

I carried out all the research literature work necessary for **Chapter 1** and **Chapter 6**, as well as the writing and editing of this PhD thesis.

The image illustrated on the cover of this PhD manuscript was created with BioRender.com.

The images presented in **Chapter** 1 (page 1), **Chapter 2** (page 37), **Chapter 6** (page 155), **Supporting Information** (page 173) and **References** (page 199) were generated using DALL·E, an image generation tool developed by OpenAI.

Curriculum Vitae

INFO & CONTACT

Name: Rafael Teixeira dos Reis

Birthday: 23/04/1992

Place of birth: Sion (Switzerland)

Address: 3000 Leuven

LinkedIn: linkedin.com/in/rafaeltreis/

Orcid ID: 0000-0002-3693-1718

e-mail: rafaelreis234@gmail.com

WORK EXPERIENCE

- **MARIE CURIE EARLY-STAGE RESEARCHER | KU LEUVEN | 2020 – 2024**

Marie Skłodowska Curie InnovEOX project

Laboratory for Pharmaceutical Analysis, KU Leuven, Belgium

- **Visiting Researcher (research secondment**) | University of Patras, Greece | 08/2022 – 10/2022
- **Visiting Researcher (research secondment**) | Watchfrog, France | 08/2022 – 10/2022

- **RESEARCH INTERN | L'ORÉAL, SA | 02/2019 - 08/2019 (6 MONTHS)**

- **PHARMACIST | PUBLIC HOSPITALS OF PARIS | 2016 – 2019**

- **ERASMUS+ INTERN | PUBLIC HOSPITALS OF PARIS | 01/2016 – 05/2016 (5 MONTHS)**

EDUCATION

- **PhD STUDENT | PHARMACEUTICAL SCIENCES | KU LEUVEN | 2024**

PhD thesis: Combining advanced LC-MS techniques and in vivo models for the holistic assessment of the electrochemical degradation of emerging micropollutants.

- **RESEARCH MASTER | ANALYTICAL CHEMISTRY | UNIVERSITY OF PARIS-SACLAY | 2019**

Master thesis: Exploration of pollutant metabolism using reconstructed skin models.

- **MASTER'S DEGREE | PHARMACEUTICAL SCIENCES | UNIVERSITY OF PORTO | 2015**

FELLOWSHIPS & RECOGNITIONS

- Nominated for best presentation award (SETAC)
- Marie Skłodowska-Curie Fellowship | 2020
- Erasmus + fellowship | 2016

COURSES

- Laboratory Animal Science - KU Leuven
- Matlab - Supercalculator - KU Leuven

LANGUAGES

Native: Portuguese

Fully proficient: English and French

Intermediate: Spanish

Beginner: Dutch and German

SCIENTIFIC OUTPUTS

- **Peer-reviewed journal manuscripts**

- **Rafael Reis**, et al., *Electrochemical degradation of diclofenac generates unexpected thyroidogenic transformation products: implications for environmental risk assessment*. Journal of Hazardous Materials, 472, 2024.

- Marie Pardon, **Rafael Reis**, et al., *Detailed comparison of in-house developed and commercially available heart-cutting and selective comprehensive two-dimensional liquid chromatography systems*. Journal of Chromatography A, 1713, 2024.

- **Rafael Reis**, et al., *Electrochemical degradation of 17α-ethinylestradiol: Transformation products, degradation pathways and in vivo assessment of estrogenic activity*. Environment International, 176, 2023.

- **Rafael Reis**, et al., *Liquid chromatography-tandem mass spectrometric assay for therapeutic drug monitoring of the EGFR inhibitors afatinib, erlotinib and osimertinib, the ALK inhibitor*

crizotinib and the VEGFR inhibitor nintedanib in human plasma from non-small cell lung cancer patients. Journal of Pharmaceutical and Biomedical Analysis, 158, 2018.

- Magalie Chartier, Salma Tannous, Nadia Benturquia, Laurence Labat, **Rafael Reis**, et al., *Baclofen-induced neuro-respiratory toxicity in the rat: Contribution of tolerance and characterization of withdrawal syndrome*. Toxicological Sciences, 164, 2018.

- Lorry Hachon, **Rafael Reis**, et al., *Morphine and metabolites plasma levels following administration of sustained release morphine in Roux-en-Y gastric bypass subjects versus matched control subjects*. Surgery for Obesity and Related Diseases, 13, 2017.

- **Scientific conferences**

- **Rafael Reis**, et al., *Combining LC-HRMS and in vivo models to assess unexpected thyroid-active transformation products from the degradation of diclofenac*. Society of Environmental Toxicology and Chemistry (SETAC) Europe 34th Annual Meeting, Sevilla, Spain, 5-9 May 2024.

- **Rafael Reis**, et al., *UHPLC-HRMS for the analysis of electrochemical degradation products of 17α-ethinylestradiol (EE2) and biological assessment of their estrogenic activity*. 33rd Internation Symposium on Chromatography, Budapest, Hungary, 18-22 Sep 2022.

- **Rafael Reis**, et al., *Development of a heart cutting 2D-LC method for the analysis of emerging micropollutants in wastewater*. 17th International Symposium on Hyphenated Techniques in Chromatography and Separation Technology, Ghent, Belgium, 17-20 May 2022.

- **Rafael Reis**, et al., *Simultaneous cocktail phenotyping of CYP450-mediated drug metabolism in patients with inappropriate response to psychotropic drugs*, Congress of the French Society of Pharmacology and Therapeutics, 12-14 June 2018.

- **Dissemination activities**

- InnovEOX Blogpost: Pharmaceuticals in the waters - September 2020

- InnovEOX Podcast #1: Introduction to InnovEOX - September 2021

- InnovEOX Podcast #4: Endocrine Disruption assessment at WatchFrog - September 2022

CONFLICT OF INTEREST

I declare that I have no known competing financial interests or personal relationships that could have appeared to influence the work reported in this PhD thesis.